

**Experimental and Theoretical Studies on Reversible
Deactivation Radical Polymerization of
N-arylitaconimides with Methyl Methacrylate**

THESIS

Submitted in partial fulfilment
of the requirements for the degree of

DOCTOR OF PHILOSOPHY

by

CHETANA ANAND DEOGHARE

Under the Supervision of

Dr. RASHMI CHAUHAN

and

Co-Supervision of

Dr. RAGHU NATH BEHERA



BITS Pilani
Pilani | Dubai | Goa | Hyderabad

**BIRLA INSTITUTE OF TECHNOLOGY AND SCIENCE
PILANI (RAJASTHAN) INDIA**

2018

**BIRLA INSTITUTE OF TECHNOLOGY AND SCIENCE
PILANI (RAJASTHAN)**

CERTIFICATE

This is to certify that the thesis entitled “**Experimental and Theoretical Studies on Reversible Deactivation Radical Polymerization of *N*-arylitacconimides with Methyl Methacrylate**” submitted by **Chetana Anand Deoghare**, ID. No. **2010PHXF0435G**, for award of Ph. D. of the Institute embodies original work done by her under our supervision.

Rashmi

Signature of the Supervisor:

Name: **Dr. RASHMI CHAUHAN**

Designation: Assistant Professor, Department of Chemistry

Date: **14/03/18**

R. Behera

Signature of the Co-Supervisor:

Name: **Dr. RAGHU NATH BEHERA**

Designation: Associate Professor, Department of Chemistry

Date: **14/03/2018**

ABSTRACT

Approximately 60% of synthetic polymers are currently prepared via free radical polymerization processes. The conventional free radical polymerization methods offer poor control over the molecular weight with broad polydispersity index (PDI) making difficult to synthesize the polymers with desirable architectures. These limitations can be overcome by using reversible deactivation radical polymerization (RDRP) methods which is commonly known as 'controlled'/ 'living' radical polymerization. The "itaconimides" are the members of imide (-CO-NH-CO-) family with reactive exocyclic double bond and easily obtained from the renewable resource viz. D-glucose. In literature, the work has been done on the copolymerization of *N*-arylitaconimides (NAI) and methyl methacrylate (MMA) mostly using conventional free radical polymerization methods. The resultant 'random' copolymers showed enhanced glass transition temperature and thermal stability as compared to poly(methyl methacrylate). This thesis describes the experimental and theoretical studies on the copolymerization of NAI and MMA using RDRP methodology.

Chapter I of thesis describes the literature about, copolymerization of NAI and MMA monomers using conventional free radical polymerization methods, drawbacks of conventional free radical polymerization methods, importance and need of RDRP methods, mechanism of atom transfer radical polymerization (ATRP), synthesis of NAI monomers, copolymerization of NAI and MMA monomers using RDRP methods, computational studies on free radical polymerization and importance of *ab initio* methods in the free radical polymerization process.

Chapter II of thesis describe the synthesis of four NAI monomers with electron releasing and electron withdrawing substituents on the aromatic ring viz. *N*-phenylitaconimide, *N*-(4-methylphenyl)itaconimide, *N*-(4-methoxyphenyl)itaconimide and *N*-(4-chlorophenyl)itaconimide. It also describe the synthesis of three different functionalized alkyl bromides viz. *N*-phenyl(3-bromo-3-methyl)succinimide, *N*-phenyl(3-bromo-4-methyl)succinimide and *N*-phenyl(3-bromomethyl)succinimide. The obtained compounds are characterized by DSC, IR, ¹H-NMR, ¹³C-NMR and elemental analysis. The vibrational frequency and ¹H-NMR (δ) values of the synthesized compounds are also calculated using density functional theory (DFT) methods. A good

correlation was obtained between the experimentally found and theoretically calculated vibrational frequency as well as $^1\text{H-NMR}$ (δ) values of the synthesized compounds.

Chapter III presents the synthesis of copolymers of NAI and MMA with different architectures viz. random [poly(NAI-*ran*-MMA)] and block [poly(NAI-*ran*-MMA)-*b*-poly(MMA) and poly(NAI-*ran*-MMA)-*b*-poly(NAI)] via ATRP process. To study the effect of pendant groups on copolymerization and properties of copolymers, various copolymers were synthesized by varying the substituent on aromatic ring of NAI. The obtained copolymers were characterized using IR, $^1\text{H-NMR}$, $^{13}\text{C-NMR}$, elemental analysis, GPC, DSC and TG/ DTG. The ATRP kinetics of the copolymerization of NAI with MMA was confirmed by investigating the linearity in plots of number average molecular weight with monomer conversion and monomer concentrations with time. Thermal characterization of poly(NAI-*ran*-MMA) copolymers shows 60-117% enhancements in T_g as compared to poly(methyl methacrylate). The molecular weight and T_g of poly(NAI-*ran*-MMA) copolymers increased with the increase in electron releasing capacity of the substituent on the aromatic ring. The poly(NAI-*ran*-MMA) copolymers are stable up to 300 °C and degraded in single step. The block copolymers poly(NAI-*ran*-MMA)-*b*-poly(MMA) and poly(NAI-*ran*-MMA)-*b*-poly(NAI) were synthesized using poly(NAI-*ran*-MMA) macroinitiators via activators generated by electron transfer (AGET)-ATRP method. An increase in the molecular weights of block copolymers as compared to the macroinitiator was observed which agreed well with theoretical calculated value. The molecular weight of poly(NAI-*ran*-MMA)-*b*-poly(MMA) copolymers was found to be 50-80% higher as compared to the poly(NAI-*ran*-MMA)-*b*-poly(NAI) copolymers. The poly(NAI-*ran*-MMA)-*b*-poly(NAI) block copolymers were having higher T_g as compared to the poly(NAI-*ran*-MMA)-*b*-poly(MMA) block copolymers. The poly(NAI-*ran*-MMA)-*b*-poly(MMA) block copolymers were stable up to 280 °C and degraded in three steps. Whereas, the poly(NAI-*ran*-MMA)-*b*-poly(NAI) block copolymers were stable up to 330 °C and degraded in two steps.

Chapter IV of thesis investigates the capability of *N*-phenyl(3-bromo-3-methyl)succinimide, *N*-phenyl(3-bromo-4-methyl)succinimide and *N*-phenyl(3-bromomethyl)succinimide as initiators for the ATRP of NAI and MMA monomer. The equilibrium constants of the ATRP (K_{ATRP}) for these alkyl bromides along with a commercial ATRP initiator (ethyl- α -bromoisobutyrate) were determined using UV-Vis-NIR and DOSY-NMR spectroscopy. Alternatively, these compounds along with some

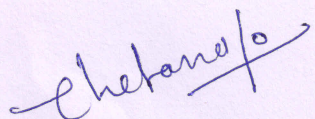
similar alkyl halides (R–X) were investigated using DFT methods for their possible chain initiation activity of ATRP process. The B3LYP functional and 6-31+G(d)/LanL2DZ basis set was used for the prediction of geometries and energetics associated with the homolytic C–X bond dissociation. The relative values of K_{ATRP} and its variation with system parameters (such as, substituent, temperature and solvent) was investigated. A good agreement was obtained between the experimentally determined and theoretically calculated K_{ATRP} values of the mentioned compounds. The predicted initiator *N*-phenyl(3-bromo-3-methyl)succinimide was successfully tested for the copolymerization of PI and MMA using AGET-ATRP process. The obtained results showed that the newly synthesized initiator *N*-phenyl(3-bromo-3-methyl)succinimide performs better in terms of control on rate of polymerization, % conversion of monomer, molecular weights and PDI as compared to the commercially available ATRP initiator viz. ethyl- α -bromoisobutyrate.

Chapter V of thesis deals with the mechanistic aspect for the atom transfer radical copolymerization of PI and MMA system. The mechanism of copolymerization of PI and MMA system was studied via microstructure analysis. The triad fractions of PI-MMA copolymer were determined using ^1H decoupled ^{13}C -NMR spectroscopy. The triad fractions for PI-MMA copolymer were also calculated using both terminal and penultimate model. For this the resulting copolymers were treated as a dimer (based on terminal model) and trimer (based on both terminal and penultimate model). A good agreement was obtained for the penultimate model calculations with experimentally determined triad fractions and no correlation with the triad fractions calculated using terminal model. This shows that the copolymerization PI and MMA monomer via ATRP proceeds with the “penultimate group effect”. The penultimate group effects was also studied for the structural and thermodynamic properties (viz. bond length, bond dissociation enthalpy, free energy and K_{ATRP} values) of the chosen dimers and trimers.

Chapter VI of thesis gives the summary, conclusions and future scope of the research.

Declaration

I declare that the thesis entitled “**Experimental and Theoretical Studies on Reversible Deactivation Radical Polymerization of *N*-arylitaconimides with Methyl Methacrylate**” has been prepared by me under the supervision of Dr. Rashmi Chauhan and co-supervision of Prof. Raghu Nath Behera, Department of Chemistry, BITS Pilani KK Birla Goa campus. No part of this thesis has formed the basis for the award of any degree or fellowship previously.



Chetana Anand Deoghare

BITS Pilani KK Birla Goa campus

Zuarinagar

Goa

Date: 14/03/2018

ACKNOWLEDGEMENT

The journey to the completion of my Ph. D. thesis was no “walk in the park”. It was filled with challenges which I feel were helpful in making me the person I am today. I now have a greater understanding and appreciation for the polymer synthesis and computational chemistry. Although, I was tested beyond what I thought were my limits, I succeeded, and consequently evolved into a stronger, more patient and determined individual. This however was possible due to the overwhelming support and encouragement I received from many people.

Firstly, I express my gratitude to my supervisors, Dr. Rashmi Chauhan and Prof. Raghu Nath Behera. You have been a great inspiration over the course of my Ph. D. thesis. Your enthusiasm, patience and dedication went a long way in making my research enjoyable. I greatly appreciate your encouragement and involvement through the provision of ideas and feedback while I was writing my thesis.

Additionally, I am grateful to Prof. Souvik Bhattacharya (Vice Chancellor, BITS, Pilani), Prof. G. Raghurama (Director, BITS, Pilani - K. K. Birla Goa Campus), Prof. P. K. Das (Associate Dean, Academic Research, BITS, Pilani - K. K. Birla Goa Campus) and Prof. Anjan Chattopadhyay (Head of the Department, Chemistry) for providing me with the facilities to conduct my research work at BITS, Pilani - K. K. Birla Goa Campus.

I express my gratitude to the members of the Doctoral Advisory Committee, Prof. N. N. Ghosh and Prof. R. N. Panda, Department of Chemistry, for their valuable guidance and co-operation. I also express my sincere thanks to members of (Departmental Research Committee, Department of Chemistry), Prof. Bhavana P., Prof. Amrita Chatterjee, Prof. R. N. Behera, Prof. Mainak Banerjee, and Prof. Anjan Chattopadhyay for their support.

I am thankful to Prof. Vishnu S. Nadkarni (Department of Chemistry, Goa University) for continuously helping in GPC analysis, without his help my thesis would have not end up. I am thankful to Prof. C. Baby (Sophisticated Analytical Instrumental Facility, IIT Madras) for helping in $^1\text{H-NMR}$ and $^{13}\text{C-NMR}$ analysis. I also thankful to, Sophisticated Analytical Instrumental Facility-IIT Bombay and IISc. Bangalore for sample analysis

throughout my Ph. D. My special thanks to Dr. S. Vengatesan (Central Electro Chemical Research Institute) who has done the thermal analysis my all samples.

“The financial support”, without this it would have been not possible for me to carry out my Ph. D. Therefore, I am truthfully thankful to, Department of Science and Technology (Junior Research Fellowship from January 2011 – June 2012 and Senior Research Fellowship from July 2012 – November 2012); BITS, Pilani-K.K. Birla Goa Campus (Institute fellowship from December 2012 – September 2015); and Council of Scientific and Industrial Research (Senior Research Fellowship from October 2015 – July 2016) for their financial support.

The persistence and silent sacrifices of my husband ‘Anand’ and son ‘Aarush’, which were help me to complete this long journey. My achievements are the results of their devotions towards ensuring that I rise with self-confidence. I also express my sincere thanks to all my family members (specially my parents) for their moral support to finish this voyage. Thanks to Lord for his grace and blessings.

I cannot end without thanking my friend, lab mates and many office people helping me directly and indirectly in my thesis.

Chetana Anand Deoghare

TABLE OF CONTENTS

	Page No.
Acknowledgement	iii
Abstract	v
Table of content for chapters	viii
List of figures	xiii
List of tables	xvii
List of schemes	xix
List of symbols and abbreviations	xx
 Chapters	
Chapter I: Introduction	
1.1 Overview	1
1.2 Conventional Free Radical Polymerization	2
1.3 Conventional Free Radical Copolymerization of Itaconimides	3
1.4 Reversible-Deactivation Radical Polymerization	4
1.5 Atom Transfer Radical Polymerization	5
1.6 Kinetics of Atom Transfer Radical Polymerization	7
1.7 Components Atom Transfer Radical Polymerization and Their Effects on K_{ATRP} and k_p	9
1.7.1 Monomers	9
1.7.2 Initiators	9
1.7.3 Catalysts	10
1.7.4 Temperature and Solvents	11
1.8 Modifications on Atom Transfer Radical Polymerization	12
1.9 Synthesis of Itaconimides	13
1.10 Mechanism of Copolymerization	15
1.10.1 Terminal Model	15
1.10.2 Penultimate Model	16
1.10.3 Complex Participation Model	17
1.10.4 Discrimination Between the Terminal and Penultimate Model	18
1.10.5 Microstructure Analysis of Copolymers of NAI and MMA	19
1.11 Mechanism and Kinetics of Copolymerizations of Itaconimides	20
1.12 Maleimides and Their Copolymerization via Reversible-Deactivation Radical Polymerization	23
1.12.1 Atom Transfer Radical Polymerization of Maleimides	24
1.13 Living Polymerizations of Itaconimides	25
1.13.1 Anionic Polymerization	25
1.13.2 Reversible-Deactivation Radical Polymerization	26
1.14 Computational Study on Free Radical Polymerization	27

1.14.1 Methods of Molecular Modeling	28
1.14.2 The Density Functional Theory Methods	29
1.14.3 Basis Sets	32
1.15 Gaps in the Existing Research	33
1.16 Objectives of the Proposed Research	34
1.17 Plan of Thesis	34

Chapter II: Synthesis and Characterization of *N*-arylitaconimides and Bromo Derivatives of Succinimide

2.1 Overview	37
2.2 Experimental Section	37
2.2.1 Materials and Methods	37
2.2.2 Synthesis of Itaconic Anhydride	38
2.2.3 Synthesis of <i>N</i> -arylitaconamic Acid	39
2.2.4 Synthesis of NAI Monomers	39
2.2.5 Synthesis of Bromo Derivatives of Succinimide	40
2.2.5.1 BSI-3	40
2.2.5.2 BSI-34	41
2.2.5.3 BSI-33	41
2.3 Results and Discussion	42
2.3.1 Characterization of Itaconic Anhydride	42
2.3.2 Characterization of NAI Monomers	43
2.3.2.1 PI	43
2.3.2.2 MPI	44
2.3.2.3 MOPI	45
2.3.2.4 CPI	46
2.3.3 Characterization of <i>N</i> -phenylcitraconimide	47
2.3.4 Characterization of Bromo Derivatives of Succinimide	48
2.3.4.1 BSI-3	48
2.3.4.2 BSI-34	50
2.3.4.3 BSI-33	51
2.3.5 Vibrational Frequencies of NAI Monomers	54
2.3.6 Vibrational Frequencies of Bromo Derivatives of Succinimide	55
2.3.7 ¹ H-NMR (δ) Values of NAI Monomers	56
2.3.8 ¹ H-NMR (δ) Values of Bromo Derivatives of Succinimide	57
2.4 Conclusions	59

Chapter III: Synthesis and Characterization of Copolymers of *N*-arylitaconimides and Methyl Methacrylate

3.1 Overview	60
3.2 Experimental Section	60

3.2.1 Materials and Methods	60
3.2.2 Synthesis of Random Copolymers of NAI and MMA via n-ATRP	61
3.2.3 Synthesis of Random Copolymers of NAI and MMA via AGET-ATRP	62
3.2.4 Synthesis of Block Copolymers of NAI and MMA via AGET-ATRP	63
3.3 Results and Discussion	64
3.3.1 Structural Characterization of Poly(NAI- <i>ran</i> -MMA)* Copolymers	64
3.3.1.1 IR Analysis	64
3.3.1.2 ¹ H-NMR Analysis	64
3.3.1.3 ¹³ C-NMR Analysis	64
3.3.2 Kinetic Studies of Poly(NAI- <i>ran</i> -MMA)* Copolymers	68
3.3.3 Random Copolymers of NAI and MMA via AGET-ATRP	72
3.3.4 Effects of Pendant Group and Methodology on Copolymer Composition	75
3.3.5 Effects of Pendant Group and Methodology on Molecular Weights of Copolymers	77
3.3.6 Effects of Pendant Group and Methodology on Thermal Properties of Copolymers	78
3.3.6.1 DSC	78
3.3.6.2 TG/ DTG	80
3.3.7 Block Copolymers of NAI and MMA Monomers	82
3.3.8 Structural Characterization of Block Copolymers	84
3.3.8.1 IR Analysis	84
3.3.8.2 ¹ H-NMR Analysis	84
3.3.8.3 Elemental Analysis	91
3.3.9 Effect of Architecture on Molecular Weights	91
3.3.10 Effect of Architecture on Thermal Properties	94
3.3.10.1 DSC	94
3.3.10.2 TG/ DTG	97
3.4 Conclusions	99

Chapter IV: Investigation of Bromo Succinimides as Potential ATRP Initiators

4.1 Overview	101
4.2 Experimental Section	102
4.2.1 Materials and Methods	102
4.2.2 Synthesis of <i>N</i> -phenylsuccinimide	102
4.2.3 Synthesis of Copolymers of NAI and MMA using BSI-33 as Initiator	105
4.2.4 Experimental Determination of ATRP Equilibrium Constant (K_{ATRP})	106
4.2.4.1 Determination of [BrCu ^{II} Bpy]	107

4.2.4.2 Determination of Termination Rate Constant (k_t)	112
4.2.5 Computational Details	115
4.2.6 Theoretical Calculation of ATRP Equilibrium Constant (K_{ATRP})	115
4.3 Results and Discussion	116
4.3.1 Experimental K_{ATRP} Values of Alkyl Bromides	116
4.3.2 Theoretical K_{ATRP} Values of Alkyl Halides	118
4.3.2.1 Structural Features of Alkyl Halides and Alkyl Radicals	119
4.3.2.2 Homolytic Bond Dissociation Enthalpies and Free Energies	121
4.3.2.3 Relative Equilibrium Constants (K_{ATRP})	124
4.3.3 Comparison of Experimentally Determined and DFT Calculated K_{ATRP} Values	127
4.3.4 AGET-ATRP of PI and MMA using BSI-33 as Initiator	127
4.3.5 Characterization of Poly(NAI- <i>ran</i> -MMA) [§] Copolymers	131
4.3.5.1 IR Analysis	131
4.3.5.2 ¹ H-NMR Analysis	131
4.3.5.3 Effect of Initiator Structure on Copolymer Composition	132
4.3.5.4 Effect of Initiator Structure on Molecular Weights of Copolymers	134
4.3.5.5 Effect of Initiator Structure on Thermal Properties of Copolymers	135
4.4 Conclusions	137

Chapter V: Mechanistic Studies of the Copolymerization of *N*-phenylitaconimide and Methyl Methacrylate via ATRP

5.1 Overview	139
5.2 Experimental Section	139
5.2.1 Synthesis of Copolymers of PI and MMA	139
5.2.2 Structural Characterization of Copolymers	140
5.2.3 Determination of Triad Fractions Using ¹³ C{ ¹ H}-NMR Spectroscopy	143
5.3 Computational Details	147
5.4 Results and Discussion	151
5.4.1 Reactivity Ratios of PI and MMA Monomers via Terminal Model	151
5.4.1.1 Structure of Transition State for Dimer Formation	151
5.4.1.2 Free Energy of Activation (ΔG^\ddagger)	153
5.4.1.3 Rate Constant of Propagation (k_p)	154
5.4.1.4 Activation Energy and Frequency Factor for Dimers	155
5.4.1.5 Reactivity Ratios of Monomers	156
5.4.2 Reactivity Ratios of PI and MMA Monomers via Penultimate Model	157
5.4.2.1 Structure of Transition State for Trimer Formation	158
5.4.2.2 Free Energy of Activation, Rate Constant of Propagation and Reactivity Ratios	160
5.4.2.3 Triad Fractions of PI-MMA Copolymerization	162

5.4.3 Effect of Neighboring and Penultimate Unit on Structural and Thermodynamic Parameters	164
5.4.3.1 Structural Features of Dimers and Trimers	164
5.4.3.2 Homolytic Bond Dissociation Enthalpies and Free Energies of Dimers and Trimers	172
5.4.3.3 Relative Equilibrium Constants (K_{ATRP}) of Dimers and Trimers	178
5.5 Conclusions	182

Chapter VI: Summary, Conclusions and Future Scope

6.1 Summary	184
6.2 Conclusions	186
6.3 Future Scope	188
References	190
List of publications	Appendix i
Brief biography of candidate	Appendix ii
Brief biography of supervisor	Appendix iii
Brief biography of co-supervisor	Appendix iv
Optimized geometries of dimers and trimer as well as K_{ATRP} data of dimers (for, X = Cl and I)	Appendix v

LIST OF FIGURES

S. No.	Figure	Page No.
2.1	IR spectrum of itaconic anhydride	42
2.2	¹ H-NMR spectrum of itaconic anhydride	42
2.3	(a) DSC scan, (b) IR and (c) ¹ H-NMR spectra of PI	43
2.4	(a) DSC scan, (b) IR and (c) ¹ H-NMR spectra of MPI	44
2.5	(a) DSC scan, (b) IR and (c) ¹ H-NMR spectra of MOPI	45
2.6	(a) DSC scan, (b) IR and (c) ¹ H-NMR spectra of CPI	46
2.7	(a) IR and (b) ¹ H-NMR spectra of <i>N</i> -phenylcitraconimide	47
2.8	(a) DSC scan, (b) IR, (c) ¹ H-NMR and (d) ¹³ C-NMR spectra of BSI-3	49
2.9	(a) DSC scan, (b) IR, (c) ¹ H-NMR and (d) ¹³ C-NMR spectra of BSI-34	50
2.10	(a) DSC scan, (b) IR, (c) ¹ H-NMR and (d) ¹³ C-NMR spectra of BSI-33	52
2.11	Correlation plot of experimentally found and theoretical calculated IR frequencies of NAI monomers	55
2.12	Correlation plot of experimentally found and theoretical calculated IR frequencies of bromo derivatives of succinimide	56
2.13	Correlation plot of experimentally found and theoretical calculated ¹ H-NMR (δ) values of NAI monomers	57
2.14	Correlation plot of experimentally found and theoretical calculated ¹ H-NMR (δ) values of bromo derivatives of succinimide	58
3.1	IR spectra of poly(NAI- <i>ran</i> -MMA)* copolymers	65
3.2	¹ H-NMR spectra of poly(NAI- <i>ran</i> -MMA)* copolymers	66
3.3	¹³ C-NMR spectra of poly(NAI- <i>ran</i> -MMA)* copolymers	67
3.4	Plots of \bar{M}_n of copolymers vs total conversion (in percent) of monomers	68
3.5	¹ H-NMR spectra of the reaction mixture of poly(NAI- <i>ran</i> -MMA)* copolymers at various time interval	70
3.6	Plots of $\ln \{[M]_t[I]_0/[M]_0[I]_t\}$ vs time (h) for poly(NAI- <i>ran</i> -MMA)* copolymers	71
3.7	Plots of total conversion (in percent) of monomers vs time (h) for poly(NAI- <i>ran</i> -MMA)* copolymers	72
3.8	IR spectra for poly(NAI- <i>ran</i> -MMA) [#] copolymers	73
3.9	¹ H-NMR spectra for poly(NAI- <i>ran</i> -MMA) [#] copolymers	74
3.10	Comparison of stabilization of NAI intermediate free radical by various substituent on aromatic ring	76
3.11	DSC scans for (a) poly(NAI- <i>ran</i> -MMA)* and (b) poly(NAI- <i>ran</i> -MMA) [#] copolymers	79
3.12	TG/ DTG scans for poly(NAI- <i>ran</i> -MMA)* copolymers	81
3.13	TG/ DTG scans for poly(NAI- <i>ran</i> -MMA) [#] copolymers	82

3.14	Comparative IR spectra of macroinitiators and block copolymers	86
3.15	Comparative ¹ H-NMR spectra of poly(PI- <i>ran</i> -MMA)*, poly(PI- <i>ran</i> -MMA)- <i>b</i> -poly(MMA) and poly(PI- <i>ran</i> -MMA)- <i>b</i> -poly(PI)	87
3.16	Comparative ¹ H-NMR spectra of poly(MPI- <i>ran</i> -MMA)*, poly(MPI- <i>ran</i> -MMA)- <i>b</i> -poly(MMA) and poly(MPI- <i>ran</i> -MMA)- <i>b</i> -poly(MPI)	88
3.17	Comparative ¹ H-NMR spectra of poly(MOPI- <i>ran</i> -MMA)*, poly(MOPI- <i>ran</i> -MMA)- <i>b</i> -poly(MMA) and poly(MOPI- <i>ran</i> -MMA)- <i>b</i> -poly(MOPI)	89
3.18	Comparative ¹ H-NMR spectra of poly(CPI- <i>ran</i> -MMA)*, poly(CPI- <i>ran</i> -MMA)- <i>b</i> -poly(MMA) and poly(CPI- <i>ran</i> -MMA)- <i>b</i> -poly(CPI)	90
3.19	GPC of macroinitiators, poly(NAI- <i>ran</i> -MMA)* and block copolymers, poly(NAI- <i>ran</i> -MMA)- <i>b</i> -poly(MMA)	93
3.20	GPC of macroinitiators, poly(NAI- <i>ran</i> -MMA)* and block copolymers, poly(NAI- <i>ran</i> -MMA)- <i>b</i> -poly(NAI)	94
3.21	DSC for (a) Poly(CPI- <i>ran</i> -MMA)- <i>b</i> -poly(MMA), (b) Poly(PI- <i>ran</i> -MMA)- <i>b</i> -poly(MMA), (c) Poly(MPI- <i>ran</i> -MMA)- <i>b</i> -poly(MMA) and (d) Poly(MOPI- <i>ran</i> -MMA)- <i>b</i> -poly(MMA)	95
3.22	DSC for (a) poly(CPI- <i>ran</i> -MMA)- <i>b</i> -poly(CPI), (b) poly(PI- <i>ran</i> -MMA)- <i>b</i> -poly(PI), (c) poly(MPI- <i>ran</i> -MMA)- <i>b</i> -poly(MPI) and (d) poly(MOPI- <i>ran</i> -MMA)- <i>b</i> -poly(MOPI)	96
3.23	TG/ DTG scans for poly(NAI- <i>ran</i> -MMA)- <i>b</i> -poly(MMA) copolymers	97
3.24	TG/ DTG scans for poly(NAI- <i>ran</i> -MMA)- <i>b</i> -poly(NAI) copolymers	99
4.1	IR spectra of <i>N</i> -phenylsuccinimide	103
4.2	(a) ¹ H-NMR and (b) ¹³ C-NMR spectra of <i>N</i> -phenylsuccinimide	104
4.3	Plot of absorbance with time at 745 nm for EBiB initiator (a) 70 mM and (b) 50 mM	108
4.4	Plot of absorbance with time at 745 nm for BSI-3 (a) 70 mM and (b) 50 mM	109
4.5	Plot of absorbance with time at 745 nm for BSI-34 (a) 70 mM and (b) 50 mM	110
4.6	Plot of absorbance with time at 745 nm for BSI-33 (a) 70 mM and (b) 50 mM	111
4.7	Plot of absorbance vs concentration of BrCu ^{II} Bpy at λ _{max} = 745 nm in acetonitrile	112
4.8	DOSY NMR spectrum of <i>N</i> -phenylsuccinimide in CD ₃ CN at 25 °C	114
4.9	Plots of diffusion time vs gradient strength for <i>N</i> -phenylsuccinimide in CD ₃ CN at 25 °C at (a) δ = 7.556 ppm and (b) δ = 2.816 ppm	114
4.10	Plots of $F(Y) = F[\text{BrCu}^{\text{II}}\text{Bpy}]$ vs time (s) for [R-Br] = 70 mM	117
4.11	Plots of $F(Y) = F[\text{BrCu}^{\text{II}}\text{Bpy}]$ vs time (s) for [R-Br] = 50 mM	118
4.12	The alkyl halides, 1 (1a-X to 1d-X), 2 (2a-X to 2d-X), 3 (3a-X to 3d-X) and 4-X (X = Cl, Br, I) investigated in this study	119
4.13	Correlation plot of bond dissociation enthalpies with R–X bond distances of the studied alkyl halides	121

4.14	Variation of enthalpies with the free energies for the R–X bond dissociation process for the studied alkyl halides	123
4.15	Correlation plot of relative K_{ATRP} values with R–X bond lengths for the studied alkyl halides.	126
4.16	Correlation plot of relative K_{ATRP} values with R–X bond enthalpies of studied alkyl halides	126
4.17	Plot of total conversion (in percent) of monomer with time for AGET-ATRP of PI and MMA	129
4.18	Plot of \bar{M}_n of copolymer with % conversion of monomer for AGET-ATRP of PI and MMA	129
4.19	Plot of $\ln \{[M]_0/[M]_t\}$ with time for AGET-ATRP of PI and MMA	130
4.20	^1H -NMR spectra of the reaction mixture for copolymerization of PI and MMA in CDCl_3 at various time intervals	130
4.21	IR spectra of poly(NAI- <i>ran</i> -MMA) ^s copolymers	132
4.22	^1H -NMR spectrum of poly(NAI- <i>ran</i> -MMA) ^s copolymer	133
4.23	DSC of poly(NAI- <i>ran</i> -MMA) ^s copolymers	136
4.24	TG/ DTG scans of poly(NAI- <i>ran</i> -MMA) ^s copolymers	137
5.1	(a) IR, (b) ^1H -NMR and (c) ^{13}C -NMR spectra of poly(PI- <i>ran</i> -MMA) copolymer	142
5.2	Carbonyl regions in $^{13}\text{C}\{^1\text{H}\}$ -NMR spectra for poly(PI- <i>ran</i> -MMA) with varied feed ratios	145
5.3	The splitting of MMA carbonyl regions in $^{13}\text{C}\{^1\text{H}\}$ -NMR spectra for poly(PI- <i>ran</i> -MMA) with varied feed ratios	146
5.4	The splitting of PI carbonyl regions in $^{13}\text{C}\{^1\text{H}\}$ -NMR spectra for poly(PI- <i>ran</i> -MMA) with varied feed ratios	147
5.5	Structure of monomers MMA, NHI, and PI used for dimer and trimer radical formation	150
5.6	B3LYP/ 6-31+G(d) optimized gas-phase geometries of the minimum energy conformations of the transition structures for dimer radicals	152
5.7	Plot of $\ln k_p$ vs $1/T$ for various dimer radical in gas phase	155
5.8	B3LYP/ 6-31+G(d) optimized gas-phase geometries of the minimum energy conformations of the transition structures of trimer radicals	160
5.9	B3LYP/ 6-31+G(d) optimized geometry of H-PI-MMA-Br and H-PI-MMA \cdot	164
5.10	B3LYP/ 6-31+G(d) optimized geometry of H-PI-PI-MMA-Br and H-PI-PI-MMA \cdot	165
5.11	Effect of the neighboring group (M_2) on the C-X bond length (\AA) of dimers (H- M_2 - M_1 -X) in gas phase at 25 °C (a) X = Cl, (b) X = Br and (c) X = I	168
5.12	Effect of the neighboring group (M_2) on the C-X bond length (\AA) of dimers (H- M_2 - M_1 -X) in gas phase at 80 °C (a) X = Cl, (b) X = Br and (c) X = I	169
5.13	Effect of the neighboring group (M_2) on the C-X bond length (\AA) of	170

	dimers (H-M ₂ -M ₁ -X) in anisole at 25 °C (a) X = Cl, (b) X = Br and (c) X = I	
5.14	Effect of the penultimate group (M ₃) on the C-Br bond length (Å) of trimers (H-M ₃ -M ₂ -M ₁ -Br) in gas phase at 25 °C	171
5.15	Effect of the neighboring group (M ₂) on the homolytic C-X bond dissociation enthalpy (ΔH) of dimers (H-M ₂ -M ₁ -X) in gas phase at 25 °C (a) X = Cl, (b) X = Br and (c) X = I	173
5.16	Effect of the neighboring group (M ₂) on the homolytic C-X bond dissociation enthalpy (ΔH) of dimers (H-M ₂ -M ₁ -X) in gas phase at 80 °C (a) X = Cl, (b) X = Br and (c) X = I	174
5.17	Effect of the neighboring group (M ₂) on the homolytic C-X bond dissociation enthalpy (ΔH) of dimers (H-M ₂ -M ₁ -X) in anisole at 25 °C (a) X = Cl, (b) X = Br and (c) X = I	175
5.18	Effect of the penultimate group (M ₃) on the homolytic C-Br bond dissociation enthalpy (ΔH) of trimers (H-M ₃ -M ₂ -M ₁ -Br) in gas phase at 25 °C	177
5.19	Effect of the neighboring group (M ₂) on the <i>K</i> / <i>K</i> ₀ ratio of dimers (H-M ₂ -M ₁ -X) in gas phase at 25 °C (a) X = Cl, (b) X = Br and (c) X = I	179
5.20	Effect of the neighboring group (M ₂) on the <i>K</i> / <i>K</i> ₀ ratio of dimers (H-M ₂ -M ₁ -X) in anisole at 25 °C (a) X = Cl, (b) X = Br and (c) X = I	180
5.21	Effect of the neighboring group (M ₂) on the <i>K</i> / <i>K</i> ₀ ratio of dimers (H-M ₂ -M ₁ -X) in gas phase at 80 °C (a) X = Cl, (b) X = Br and (c) X = I	181
5.22	Effect of the penultimate unit on the <i>K</i> / <i>K</i> ₀ ratio of trimer (H-M ₃ -M ₂ -M ₁ -Br) in gas phase at 25 °C	182

LIST OF TABLES

S. No.	Table	Page No.
1.1	Glass transition temperature and thermal stability of random copolymers of NAI and MMA synthesized via conventional FRP	4
1.2	Structures of various <i>N</i> -alkyl/ arylitaconimides with their physical properties and yield	14
1.3	Monomer reactivity ratios for copolymerization of <i>N</i> -alkyl/ arylitaconimide with MMA/ styrene calculated using terminal model	21
1.4	The values of R_p , k_p , E_a , and A for the radical polymerization of <i>N</i> -substituted phenylitaconimide monomers, at 60 °C in THF	22
1.5	Different DFT methods	31
2.1	B3LYP/ 6-31+G(d) optimized geometries of the NAI monomers and bromo derivatives of succinimide	53
2.2	Experimentally found and theoretically calculated vibrational frequency values (cm^{-1}) of NAI monomers	54
2.3	Experimentally found and theoretically calculated vibrational frequency values (cm^{-1}) of bromo derivatives of succinimide	55
2.4	Experimentally found and theoretically calculated $^1\text{H-NMR}$ (δ) values (ppm) of NAI monomers	57
2.5	Experimentally found and theoretically calculated $^1\text{H-NMR}$ (δ) values (ppm) of bromo derivatives of succinimide	58
3.1	Percent conversion of monomers with time, \bar{M}_n and PDI values of poly(NAI- <i>ran</i> -MMA)* copolymers	69
3.2	Elemental analysis and copolymer composition for poly(NAI- <i>ran</i> -MMA) synthesized via n-ATRP and AGET-ATRP.	77
3.3	\bar{M}_n and PDI for poly(NAI- <i>ran</i> -MMA) copolymers synthesized via n-ATRP and AGET-ATRP	78
3.4	T_g s observed in the DSC of poly(NAI- <i>ran</i> -MMA) copolymers synthesized via n-ATRP and AGET-ATRP	79
3.5	Results of the elemental analysis of block copolymers	91
3.6	\bar{M}_n of macroinitiator, percent conversion of monomer (MMA* and NAI [#]), \bar{M}_n and PDI of block copolymers	92
3.7	T_g s observed in the DSC scans of the block copolymers	96
4.1	K_{ATRP} values of alkyl bromides in acetonitrile at 25 °C	116
4.2	The R–X bond lengths of studied alkyl halides in gas phase and in the solution phase at 25 °C	120
4.3	Enthalpy and free energy for R–X homolytic cleavage of studied alkyl halides in gas phase and solution phase at 25 °C	122
4.4	Relative values of K_{ATRP} for R–X homolytic bond cleavage of studied alkyl halides in gas phase and in solution phase	125

4.5	The K_{ATRP} values for R–X homolytic bond cleavage of studied alkyl bromides	127
4.6	The variation of total conversion (in percent) of monomers with time, \bar{M}_n and PDI of Poly(PI- <i>ran</i> -MMA) [§] copolymers	128
4.7	Elemental analysis and copolymer composition for Poly(NAI- <i>ran</i> -MMA) [§] copolymers	134
4.8	T_g s observed in the DSC of poly(NAI- <i>ran</i> -MMA) [§] copolymers	136
5.1	Elemental analysis and copolymer compositions of poly(PI- <i>ran</i> -MMA) for various feed ratios	143
5.2	Free energy of activation for dimer radicals at various temperature in gas phase	153
5.3	Rate constant of propagation for dimer radicals at different temperatures in gas phase and in anisole	154
5.4	Activation energy and frequency factor for studied dimers in gas phase and in anisole	156
5.5	Reactivity ratios of various monomers (r_1 and r_M) calculated from the k_p values using the terminal model. The k_p values are calculated at the B3LYP/ 6-31+G(d) level	157
5.6	Free energy of activation and rate constant of propagation of trimer radicals in gas phase at 25 °C	161
5.7	The experimentally determined and theoretically calculated triad fractions based on terminal and penultimate model for PI-MMA copolymer system	163
5.8	Thermodynamic parameters for the homolysis of the M_1 -X bond in H- M_2 - M_1 -X ($M_1, M_2 = \text{MMA, NHI, and PI}$; and H- M_1 -X, (X = Cl, Br, I) in gas phase at 25 °C	166
5.9	Thermodynamic parameters for the homolysis of the M_1 -Br bond in H- M_3 - M_2 - M_1 -Br ($M_1, M_2, M_3 = \text{MMA, NHI, and PI}$) in gas phase at 25 °C	167
A1	B3LYP/ 6-31+G(d)/ LanL2DZ optimized geometries (gas phase) of studied alkyl halides (R-X) and its radicals (R \cdot) in gas phase at 25 °C	
A2	Free energy of activation for dimer radicals at various temperature in anisole	
A3	View of the lowest energy optimized geometries for all and H- M_2 - M_1 -Br dimers H- M_2 - M_1 \cdot dimer radical in gas phase at 25 °C	
A4	View of the lowest energy optimized geometries for all and H- M_3 - M_2 - M_1 -Br trimer H- M_3 - M_2 - M_1 \cdot trimer radical in gas phase at 25 °C	
A5	Thermodynamic parameters for the homolysis of the M_1 -X bond in H- M_2 - M_1 -X ($M_1, M_2 = \text{MMA, NHI, and PI}$; and H- M_1 -X, (X = Cl, Br, I) in anisole at 25 °C	
A6	Thermodynamic parameters for the homolysis of the M_1 -X bond in H- M_2 - M_1 -X ($M_1, M_2 = \text{MMA, NHI, and PI}$; and H- M_1 -X, (X = Cl,	

Br, I) in gas phase at 80 °C

LIST OF SCHEMES

S. No.	Scheme	Page No.
1.1	Mechanism of conventional FRP	3
1.2	Mechanism of transition-metal-catalyzed ATRP	6
1.3	Sub-equilibria in K_{ATRP}	6
1.4	Mechanism of AGET-ATRP	12
1.5	Synthesis of <i>N</i> -substituted itaconimide	13
2.1	Reaction scheme for the synthesis of NAI monomers	39
2.2	Reaction scheme for synthesis of bromo derivatives of succinimide	40
3.1	Reaction scheme for the synthesis of random copolymers of NAI and MMA	63
3.2	Reaction scheme for synthesis of block copolymers	83
4.1	Reaction scheme for synthesis of copolymers of NAI and MMA using BSI-33 as initiator	106
5.1	Reaction scheme for synthesis of copolymers of PI and MMA	140

List of Symbols and Abbreviations

Symbols	Description
Å	Angstrom
°C	Degree centigrade
cm	Centimetre
cm ³ min ⁻¹	Centimetre cube per minute
D	Diffusion coefficient
G	Guass
gmol ⁻¹	Gram per mole
gcm ⁻¹	Grams per centimetre
h	Hours
Hz	Hertz
h	Plank Constant
K_B	Boltzmann constant
kg	Kilogram
Kcal mol ⁻¹	Kilocalorie per mole
kJ mol ⁻¹	Kilojoules per mole
L	Litter
l	Length
µg	Microgram
µL	Microliter
µmol	Micromole
m	Meter
mg	Milligram
min	Minutes
mL	Mililiter
mM	Millimolar
mm	Millimetre
mol	Mole
\bar{M}_n	Number average molecular weight
nm	Nanometer
pH	Acidity measurement unit
ppm	Parts per million
s	Second
t	Time
η	Coefficient of viscosity
λ	Wavelength
%	Percentage
δ	Chemical shift values in ¹ H-NMR spectroscopy
Δ	Diffusion time

γ	gyromagnetic ratio
g	strength of the diffusion gradients

Abbreviation	Description
AGET	Activators generated electron transfer
- <i>alt</i> -	Alternate copolymer
ATRP	Atom transfer radical polymerization
AIBN	Azobisisobutyronitrile
BPO	Benzoyl peroxide
Bpy	Bipyridine
- <i>b</i> -	Block copolymer
b. p.	Boiling point
BDE	Bond dissociation enthalpy
BSI-33	<i>N</i> -phenyl(3-bromo-3-methyl)succinimide
BSI-34	<i>N</i> -phenyl(3-bromo-4-methyl)succinimide
BSI-3	<i>N</i> -phenyl(3-bromomethyl)succinimide (BSI-3)
<i>n</i> -BuLi	<i>n</i> -Butyllithium
[C] ₀	Initial concentration of BrCu ^I Bpy
CDCl ₃	Deuterated chloroform
ChPII	<i>N</i> -[4-(cholesteroxycarbonyl)-phenyl]itaconimide
Conc.	Concentrated
CPI	<i>N</i> -(4-chlorophenyl)itaconimide
CRP	Controlled radical polymerization
DP _n	Degree of polymerization
DFT	Density functional theory
DCM	Dichloromethane
DSC	Differential calorimetry
DTG	Differential thermogravimetry
DOSY	Diffusion ordered spectroscopy
E _a	Activation energy
EBiB	Ethyl- α -bromoisobutyrate
FR	Finemann Ross
FRP	Free radical polymerization
GPC	Gel permeation chromatography
- <i>g</i> -	Graft copolymer
HBr	Hydrobromic acid
HCl	Hydrochloric acid
HRMS	High resolution mass spectroscopy
[I] _t	Concentration of NAI at time t
[I] ₀	Initial concentration of NAI
KBr	Potassium bromide
K _{ET}	Equilibrium constant for electron transfer
K _{BH}	Equilibrium constant for R–X bond homolysis
K _{EA}	Equilibrium constant for electron affinity

k_{act}	Rate constant of activation
k_{deact}	Rate constant of deactivation
$K_{\text{ATRP}} (k_{\text{act}}/ k_{\text{deact}})$	ATRP equilibrium constant
k_i	Rate constant of initiation
k_p	Rate constant of propagation
k_t	Rate constant of termination
KT	Kelen Tudos
$[M]_0$	Initial concentration of MMA
MMA	Methyl Methacrylate
m.p.	Melting point
$[M]_t$	Concentration of MMA at time t
MPI	<i>N</i> -(4-methylphenyl)itaconimide
MOPI	<i>N</i> -(4-methoxyphenyl)itaconimide
$M_t^n Y/ L$	Transition metal halide complex in lower oxidation state
NAI	<i>N</i> -arylitaconimide
n-ATRP	Normal ATRP
NMP	Nitroxide mediated radical polymerization
PI	<i>N</i> -phenylitaconimide
PM	Penultimate Model
PRE	Persisting radical effect
PDI	Polydispersity index
PMMA	Poly(methyl methacrylate)
Poly(NAI- <i>ran</i> -MMA)*	Random copolymers of NAI and MMA synthesized <i>via</i> n-ATRP using EBiB as initiator
Poly(NAI- <i>ran</i> -MMA) [#]	Random copolymers of NAI and MMA synthesized <i>via</i> AGET-ATRP using EBiB as initiator
Poly(NAI- <i>ran</i> -MMA) [§]	Random copolymers of NAI and MMA synthesized <i>via</i> AGET-ATRP using BSI-33 as initiator
R^\bullet	Propagating Radical
- <i>ran</i> - or - <i>co</i> -	Random copolymer
RAFT	Reversible addition fragmentation chain transfer
ROMP	Ring opening metathesis polymerization
R_p	Rate of polymerization
R-X	Alkyl halide
r_1	Reactivity ratio of NAI
r_M	Reactivity ratio of MMA
r_S	Reactivity ratio of styrene
RT	Room Temperature
SFRP	Stable free-radical polymerization
Sn(EH) ₂	Tin(II)-2-ethylhexanoate
T_f	Final temperature

T_g	Glass transition temperature
T_i	Initial temperature
T_{max}	Maximum temperature
TMS	Tetramethylsilane
TM	Terminal Model
THF	Tetrahydrofuran
TG	Thermogravimetry
TS	Transition state
$X-M_t^{n+1}Y/L$	Transition metal halide complex in higher oxidation state
[Y]	Concentration of $BrCu^{II}Bpy$

CHAPTER I

INTRODUCTION AND LITERATURE SURVEY

1.1 Overview

The incorporation of monomers with imide functionality (-CO-NH-CO-) such as nadimides, maleimides, citraconimides and itaconimides in polymers backbone, results in copolymers with interesting properties such as high thermal stability and glass transition temperature (T_g). These monomers can be copolymerized via condensation polymerization methods or free radical polymerization (FRP) methods. Using the condensation polymerization methods such as ring opening metathesis polymerization, the imide functionality is incorporated in the polymer backbone and give “thermosets”. These imide monomers polymerized under FRP conditions give “thermoplastics”, in which the imide functionality appears as a pendant group in the polymer backbone [1-5].

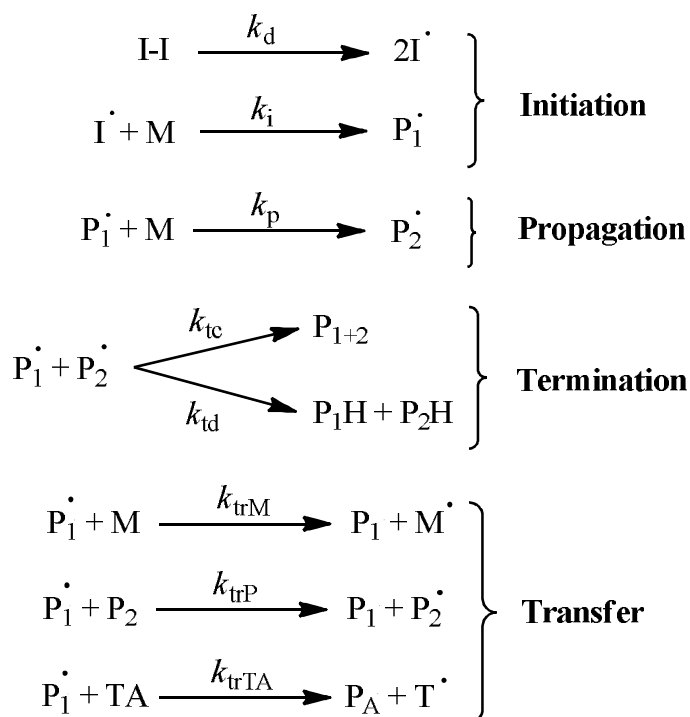
The *N*-alkyl/ arylmaleimides have been copolymerized with methyl methacrylate (MMA) using conventional FRP methods, thus giving copolymers with high T_g and thermal stability [6-13]. The itaconimides with an exocyclic double bond are more reactive than corresponding maleimides and citraconimides with endocyclic double bond and can be incorporated to a greater extent in polymer backbone as compared to the corresponding maleimides and citraconimides [14-15]. Also, the maleimides are obtained from petrochemicals via maleic acid, whereas itaconimides are obtained from renewable resource viz. D-Glucose. Most of the acrylic monomers viz. itaconic acids and its derivatives are synthesized from renewable resource (i.e. plants) via fermentation of starch [16-18]. The copolymerizations of *N*-alkyl/ arylitaconimides have also been obtained with monomers such as styrene and MMA, giving *N*-alkyl/ arylimide as the pendant groups. Most of the existing literature deals with conventional FRP of *N*-arylitaconimide (NAI) and MMA monomers and on “random” architecture [5, 14-15, 19-20]. The conventional methods of polymerization offer a poor control on architecture and molecular weight of copolymers. These limitations can be overcome by using reversible-deactivation radical polymerization (RDRP) techniques [21-22]. There are handful reports available on MMA-NAI copolymer systems reporting architecture other than “random”. The block copolymers of *N*-phenylitaconimide and its chloro derivatives with

MMA were synthesized via RDRP technique [23]. The limited work has been done on the copolymerization of NAI and MMA monomers using RDRP. Hence, it is of interest to study the copolymerization of NAI and MMA monomers via RDRP methodology.

This chapter summarizes the literature related to the different RDRP methods, copolymerization of itaconimides via conventional FRP, synthesis of itaconimides, computational study on FRP and basic principles of density functional theory methods.

1.2 Conventional Free Radical Polymerization

FRP is one of the most commercially significant polymerization process utilized in the industries for the production of approximately 60% of all synthetic polymers. It is a chain polymerization happening via sequence of initiation, propagation, termination, and chain transfer reactions (**Scheme 1.1**). In contrast to other chain polymerization methods, such as ionic and coordination polymerization, it has the advantage of being tolerant of mild conditions, reagent, solvent impurities and availability of broad range of monomer functionalities, thus making it an attractive option for industry. In FRP, low stationary steady-state concentration of propagating radicals was established by balancing the rate of termination ($k_t \approx 10^8 \text{ M}^{-1}\text{s}^{-1}$) with a very slow continuous initiation ($k_i \approx 10^4 \text{ M}^{-1}\text{s}^{-1}$). In order to propagate the chains with a high degree of polymerization (> 1000) the rate of propagation must be thousands times faster than that of termination. Hence, the synthesis of polymers with well-defined and complex architectures under FRP conditions are difficult, as the polymers chains are slowly initiated and continuously terminate after 1s life span. The copolymers synthesized using conventional FRP methods are having poor control over the molecular weight. However, it is difficult to synthesize the copolymers with different molecular architecture in terms of chain topology, composition, and diverse functionality [21, 24-25].

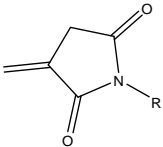


Scheme 1.1: Mechanism of conventional FRP.

1.3 Conventional Free Radical Copolymerization of Itaconimides

The *N*-alkyl/ arylitaconimide monomers have been homopolymerized and copolymerized with monomers such as styrene and acrylic monomers. The copolymerization of *N*-alkyl/ arylitaconimide with acrylic monomers were carried out in THF or toluene solvent and AIBN as initiator in nitrogen atmosphere at 60-65 °C. The copolymers were mostly white in color and soluble in THF, dioxane, DMF and DMSO. The thermal properties of the copolymers (feed composition of monomers = 2:8::NAI:MMA) were measured using differential scanning calorimetry (DSC) and thermogravimetry (TG) techniques and summarized in the **Table 1.1**. The molecular weights of the copolymers of *N*-alkyl/ arylitaconimide with acrylic monomers were reported in the range of 1×10^3 to 1×10^4 g mol^{-1} with broad polydispersity index (PDI) = 2.5-4.5 [5-7, 14-15, 19-20, 26-28].

Table 1.1: Glass transition temperature and thermal stability of random copolymers of NAI and MMA synthesized via conventional FRP (feed composition of monomers = 2:8::NAI:MMA).

 where, R =	T_g (°C)	T_i (°C)	T_{max} (°C)	T_f (°C)	Char yield (%) at 600 °C	Ref.
4-chlorophenyl	149	226	323	353	21	[14]
3-chlorophenyl	142	232	442	374	19	
2-chlorophenyl	180	259	372	391	28	
phenyl	165	203	223	252	19	[15]
4-methylphenyl	167	214	259	310	19	[19]
4-carboxyphenyl	134	231	313	360	32	
4-methoxy-3-chlorophenyl	163	-	-	-	27	
2-methoxy-5-chlorophenyl	185	-	-	-	25	[20]
3-methoxyphenyl	133	-	-	-	22	
4-methoxyphenyl	149	-	-	-	10	

here, T_i = initial degradation temperature, T_{max} = maximum degradation temperature, T_f = final degradation temperature.

1.4 Reversible-Deactivation Radical Polymerization

RDRP (also known as 'controlled'/ 'living' radical polymerization) has opened new paths to synthesize the polymers with complex architectures and site specific functionality [29-34]. In RDRP, a stationary steady-state concentration of propagating radicals is obtained by matching the rates of activation and deactivation process. Termination process must be thousands times slower than propagation and initiation should be very fast, preferably faster than propagation, resulting in the simultaneous growth of all propagating chains and enabling the polymers with controlled architectures. The RDRP systems that have most often been used are stable free-radical polymerization (SFRP) or nitroxide mediated radical polymerization (NMP), atom transfer radical polymerization (ATRP), and reversible addition fragmentation chain transfer (RAFT) process [35]. The SFRP and ATRP systems obey the persisting radical effect (PRE) [36-37] and a steady-state of propagating radicals was obtained via the activation-deactivation process rather than

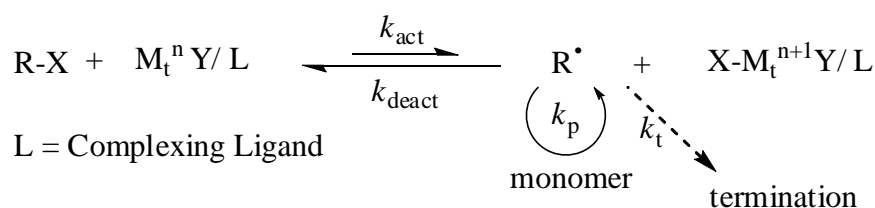
initiation-termination as in the conventional FRP. In SFRP or NMP, alkoxyamines are used as persisting radicals. The thermally unstable C-O bond in alkoxyamines decomposes upon heating to provide the initiating species for polymerization. The utilization of alkoxyamines in SFRP or NMP is originally limited due to lack of suitable synthetic procedures for their preparation. Most of the literature known methods result in low yield and a large range of by-products [38]. The RAFT process is based on degenerative transfer and does not show PRE [39-40]. In RAFT process the dithioesters are the initiating species which may impart the color and odor to the polymer and can make their purification and storage difficult. In most of the ATRP reactions, alkyl halides are used as persisting radicals. The C-X bond of alkyl halides in presence of transition metal complex undergoes homolysis to give the initiating alkyl radical [33, 41-42]. Out of all RDRP process, ATRP is an eye-catching and vastly used technique in the laboratories, due to its simple experimental setups, easy accessibility of wide range of monomers and solvents for the polymerization, as well as due to commercial availability of initiators (viz. alkyl halides) and catalytic systems (transition metal complexes) [43-44].

1.5 Atom Transfer Radical Polymerization

ATRP was discovered in the mid-1990s by Krzysztof Matyjaszewski group in Carnegie Mellon University. ATRP is having its main origin from atom transfer radical addition, which forms the 1:1 adduct of alkyl halides and alkenes and catalyzed by transition metal complexes [45-46]. It is one of the most successful RDRP techniques to tailor the copolymers with a wide range of complex architectures with controlled molecular weight and narrow PDI [47]. ATRP has been productively used to design the polymers with linear, stars, cyclic, comb, brushes, networks, dendritic, and hyperbranched topology, composition (such as statistical, blocks, stereoblocks, multi block copolymers, multisegmented block copolymers, graft, periodic, alternating, and gradient copolymers) and functionalities (that can be incorporated into the side chains, end groups as well in many arms of star shaped polymers and hyperbranched polymeric materials) [48-50].

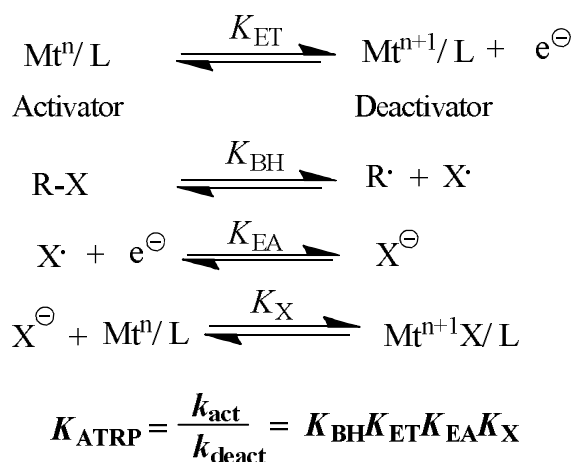
The basic mechanism of ATRP process (**Scheme 1.2**) involves homolytic cleavage of alkyl halide (R-X) bond (activation step) by a transition metal complex in its lower oxidation state (the activator, $M_t^n Y/L$) generating (with rate constant of activation, k_{act}) reversibly the propagating radical (R^\bullet) and the transition metal halide complex in its

higher oxidation state (the deactivator, $X-M_t^{n+1}Y/L$). In the deactivation step (with rate constant of deactivation, k_{deact}), the halide atom (X) is transferred back from the activator to the propagating radical, also through homolytic bond dissociation. The activation and deactivation process occurs throughout the polymerization. The deactivation of the generated radicals should be suitably fast to make sure that only a few number of monomers are going to add into the propagating radicals during each and every step of the reaction [24-25, 31, 36, 44, 51].



Scheme 1.2: Mechanism of transition-metal-catalyzed ATRP.

ATRP is controlled by the equilibrium between propagating radicals and dormant species mostly in the form of initiating alkyl halides or macromolecular species [24-25, 52]. The ATRP equilibrium constant (K_{ATRP}) can be expressed as the combination of the following four equilibrium constants (**Scheme 1.3**), oxidation of the metal complex or electron transfer (K_{ET}), alkyl halide bond homolysis (K_{BH}), reduction of a halogen to a halide ion or electron affinity (K_{EA}) and association of the halide ion to the metal complex or it is also called “halogenophilicity”.



Scheme 1.3: Sub-equilibria in K_{ATRP} .

Experimentally, K_{ATRP} can be determined from the polymerization kinetics. For example, in a $Cu^I Y/L$ ($Y = Cl/ Br$) catalyzed polymerization reaction when excess of the deactivating species ($X-Cu^{II}Y/L$) is used and the concentration of other species such as activator, initiator and monomer do not change significantly and the rate of propagation (R_p) is known. Alternatively, K_{ATRP} can also be determined from the rate of formation of a dormant species/ persistent radical using Fischer-Fukuda equation for the persistent radical effect [53-56]. Theoretically, the relative values of K_{ATRP} can be estimated from the homolytic bond dissociation energy of the initiating R-X under certain conditions [57-60].

1.6 Kinetics of Atom Transfer Radical Polymerization

ATRP is controlled by maintaining the rapid dynamic equilibrium between activators and deactivators. Several experimental [61-66] as well as theoretical [53, 67-70] studies have been reported on kinetic and thermodynamic parameters of ATRP for various systems. In the copper catalyzed ATRP, the rate of ATRP process (R_p) depends on the concentration of monomer $[M]$ and propagating radical $[P^*]$ as shown in the equation 1.1. The radical concentration depends on the position of the equilibrium (shown in **Scheme 1.2**) and equilibrium constant of ATRP (K_{ATRP}) [71].

$$R_p = k_p[M][P^*] = k_p K_{ATRP} [M] [[I]_0] \times [Cu^I Y/L] / [X - Cu^{II} Y/L] \dots\dots\dots 1.1$$

where k_p = rate constant of propagation, $[I]_0$ = initial concentration of initiator R-X and $[Cu^I Y/L]$ = concentration of activator, $[M]$ = concentration of monomer, $[X-Cu^{II}Y/L]$ = concentration of deactivator. The rate of polymerization is first order with respect to concentrations of each of the monomer, initiator, and Cu^I complex, under homogeneous circumstances [53]. In ATRP, conversion of monomers with time follows first order kinetics. This specifies that there is steady concentration of active species in the polymerization. The accurate kinetic law for the deactivator ($X-Cu^{II}L/ Y$) was more complex due to the impulsive generation of Cu^{II} via PRE [36, 51, 72]. In ATRP, the synthesis of polymers with predetermined molecular weights and low PDI requires a sufficient concentration of deactivator (equation 1.2). For the same monomer, the transition metal complex (lower oxidation state) that deactivates the growing polymers

chains more rapidly will result in polymers with narrow PDI with smaller k_p/k_{deact} ratio. On the other hand, the PDI must narrow with an increasing concentration of deactivating species, resulting in slower polymerization rates [73].

$$\frac{M_w}{M_n} = 1 + \frac{1}{DP_n} + \left[\frac{(k_p[R-X]_0)}{(k_{deact}[X-Cu^{II}L])} \right] \left(\frac{1}{p} - 1 \right) \dots\dots\dots 1.2$$

where, DP_n = degree of polymerization, p = monomer conversion and $[R-X]$ = concentration of alkyl halides.

In typical ATRP, a very tiny fraction (about 5%) from the all growing polymer chains will be terminated at some point in the initial stage of the polymerization, but more than 90% of the polymeric chains will continue to grow till the end of polymerization. Other characteristics of ATRP process involve linear increase in average molecular weight with conversion of monomer and PDI normally less than 1.5. [22, 74]. Experimentally, the absolute values of the rate constants k_p and k_t can be determined by with the help of pulsed laser polymerization in combination with the size exclusion chromatography (PLP-SEC). In the copolymerization reactions to minimize the secondary reactions such as depropagation, PLP-SEC needs to be used in combination with polymerization models [75]. It is thus valuable to have alternative methods for specifying k_p values of the copolymerization process. In particular, the use of quantum chemistry to calculate k_p values in free radical polymerization system is particularly attractive. Quantum chemistry can be applied to any reaction type and extracting quantitative values of the k_p does not rely on assuming a polymerization model used in the copolymerization reaction. On the other hand, the rate constant of polymerization reactions can be explained with the use of Arrhenius equation. Two parameters are then required to determine the rate constant of polymerization reactions, viz. the frequency factor (A) and an activation energy (E_a). These parameters are calculated through the classical transition state theory as:

$$k(T) = A e^{\left(\frac{-E_a}{k_b T}\right)} = \frac{k_b T}{h} \frac{Q^\ddagger}{Q^R} e^{\left(\frac{-E_a}{k_b T}\right)} \dots\dots\dots 1.3$$

where, k_B = Boltzmann constant, h = Planck's constant, T = absolute temperature, E_a =

activation energy of the polymerization process calculated from the difference between the free energy of activation of the transition state and the free energy of the reactants and $Q =$ product of the partition functions ($q^{\text{translational}}$, $q^{\text{vibrational}}$, $q^{\text{rotational}}$ and $q^{\text{electronic}}$) for the transition state (‡) and reactants ($^{\text{R}}$) [76].

1.7 Components Atom Transfer Radical Polymerization and Their Effects on K_{ATRP} and k_p

1.7.1 Monomers

ATRP is liberal to many functional groups present on the monomers, such as hydroxy, amino, amido, ether, ester, epoxy and siloxy. The list of monomers productively polymerized by ATRP is quite wide-ranging and take accounts of styrene and its derivatives [77], acrylates, methacrylates, [78-79], methacrylamides [80], vinyl pyridine [81], acrylonitrile [82], vinyl acetate [83] and vinyl chloride [84] etc. The polymerizations of acrylates performed in bulk with alkyl-2-bromopropionate initiator and well defined Polyacrylates with molecular weights up to $1 \times 10^5 \text{ gmol}^{-1}$ with PDI < 1.1 were reported. A wide range of acrylates such as 2-hydroxyethyl acrylate with various side chains have been polymerized using ATRP [85-86] and glycidyl acrylate [87]. Poly(*tert*-butylacrylate) was also prepared in a well-controlled fashion [88]. The simplistic polymerization of MMA using ATRP is due to the large range of available catalysts for the ATRP reaction, leads to easy activation of the dormant species and the high values of the ATRP equilibrium constants [89]. Most of the polymerizations of MMA were carried out in solution at temperatures ranging from 70-90 °C and a well defined PMMA can be synthesized within the molecular weight range from $1 \times 10^3 \text{ gmol}^{-1}$ to $1.8 \times 10^5 \text{ gmol}^{-1}$ with low PDI = 1.1-1.2 [90-91].

1.7.2 Initiators

The role of initiators in ATRP is very important to establish the number of growing polymeric chains. In the polymerization, the initiation is fast with transfer and termination negligible, leads to the number of growing chains constant and equal to the initial initiator concentration [92-94]. Various types of initiators, usually alkyl halides, have been used productively in ATRP. The halogenated alkanes viz. CHCl_3 , CCl_4 and

CCl_3Br are the first used ATRP initiators for polymerization of MMA [95-97]. Benzylic halides are used as initiators for the ATRP of styrene and its derivatives, due to its structural resemblance. However, this kind of initiator is not useful for the polymerization of MMA [78, 98]. Many α -haloesters have been successfully used as initiators for well controlled ATRP reactions of acrylates. Most commercially available ATRP initiators such as ethyl-2-bromoisobutyrate, ethyl-2-chloroisobutyrate, 2-bromoisobutyrate, methyl-2-bromopropionate are good for the ATRP of many acrylates due to their structural resemblance [61, 99-103]. Polyhalogenated α -haloketones e.g., $\text{CCl}_3\text{COCH}_3$ and CHCl_2COPh are used as initiators for polymerization of MMA [99, 104-105]. Initiator 2-bromopropionitrile has been used for the polymerization of acrylonitrile monomer and it is one of the fast radical generators in ATRP, due to the presence of the strong electron-withdrawing cyano group [103, 106-107]. Many end-functional polymers of styrene have been prepared using sulfonyl chlorides as initiator, where functionalities were introduced onto the aromatic ring [108-109].

For an efficient ATRP initiator, the rate of initiation should be faster than the rate of propagation with minimum side reactions. The choice of initiators can be made from following considerations, (i) tertiary alkyl halides are superior initiators than secondary ones, which are superior than primary alkyl halides, (ii) presence of different functional groups can enhance the activity of the initiators, e. g. $\text{CN} > \text{C(O)R} > \text{C(O)OR} > \text{Ph} > \text{Cl} > \text{Me}$, (iii) the R-X bond strength of alkyl chlorides are found to be higher than the corresponding alkyl bromides, which are in turn higher than their iodide counterparts ($\text{R-Cl} > \text{R-Br} > \text{R-I}$) [33, 43-44, 78, 110-111]. The alkyl iodides are light sensitive and use of it in the laboratory requires special precautions. The C-I bond may be cleaved heterolytically and there are probable difficulties of the ATRP process by degenerative transfer [112]. To avoid halogen exchange the similar halogen and metal salt must be used to obtain better polymerization control. Iniferters are successfully used as initiators for the ATRP of MMA [113-115]. Several studies have been done on ATRP of MMA using ethyl- α -bromoisobutyrate as initiator due to its structural resemblance with monomer [53, 116-122].

1.7.3 Catalysts

The perfect catalysts for ATRP reaction should be very much discerning for atom transfer step and it should deactivate very fast with diffusion controlled rate constants.

Also, it should have simple tunable activation rate constants to meet particular conditions for specific monomers. ATRP has been successfully governed by a variety of transition metals, such as, Copper [35, 123], Titanium [124], Molybdenum [125-126], Rhenium [127], Iron [107, 128-130], Ruthenium [131], Osmenium [132-133], Rhodium [134], Cobalt [135], Nickel [136-137] and Palladium [138]. Out of all, the ‘copper’ catalysts are mostly used in ATRP, in terms of its versatility and cost, suitable to broad range of monomers in various solvent systems. ATRP of monomers such as styrene, acrylates, amides, and acrylonitrile has been successfully carried out using copper complexes. In reaction Cu^{I} forms tetrahedral or square planer complexes and Cu^{II} forms trigonal bipyramidal complex with tetradentate or with two bidentate ligands [45-46, 139-140]. Ligands help to fine-tune the atom transfer equilibrium and to make available suitable catalyst solubility. Ligands such as multidentate alkyl amines [141-142], bipyridine [143-144], pyridineimines [145], phosphines [107, 146] or ethers [147] have been used in ATRP.

In ATRP there is an admirable linear correlation of the K_{ATRP} and electrochemical redox potentials of the catalyst. The redox properties of the catalyst can be attuned over a very broad range viz. > 500 mV, corresponding to a range of K_{ATRP} values (on both sides of) eight orders of magnitude. More reducing catalysts are characterized by higher K_{ATRP} . However, the K_{ATRP} also depends on the affinity of the transition complex to halogens viz. halogenophilicity (**Scheme 1.3**). Therefore, the late transition-metal complexes are more reducing but have poorer attraction to halogens. This may allow one to decide the suitable complexes for different monomers polymerization and to evade side reactions coupled with the oxidation and reduction of growing free radicals [25, 33-35, 43].

1.7.4 Temperature and Solvents

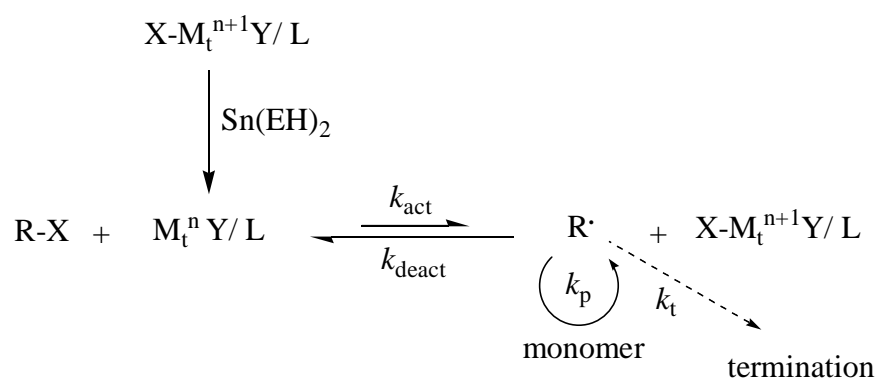
ATRP can be performed over a very wide range of temperatures viz. from subzero to even up to 150 °C [35]. Similarly, with increase of reaction temperature the activation rate constants and the values of K_{ATRP} increases. Temperature has pronounced effect on ATRP kinetics, with the slight increase of reaction temperature (50 °C to 70 °C) the k_p values were increase with the 10^3 order of magnitude [75].

ATRP reactions can be successfully carried out in bulk, many organic solvents, CO_2 , water (homogeneous as well as in heterogeneous medium such as emulsion, inverse emulsion, miniemulsion, microemulsion, suspension, precipitation) and even in the gas

phase and from the solid surfaces [24-25, 33-35, 43-44]. The activation rate constants, deactivation rate constants and equilibrium constants for the activation-deactivation sequence in copper-catalyzed ATRP are dependent on the nature of the solvent. Increase in polarity of the medium the rate of activation increases and slows down the rate of deactivation, eventually resulting in a higher value of K_{ATRP} . In ATRP, it has been found that the k_p values were smaller in more polar solvents as compared to the less polar solvent. For example the k_p values (determined using PLP-SEC) for MMA polymerization in THF and DMSO solvent were reported as $2.67 \times 10^3 \text{ Lmol}^{-1}\text{s}^{-1}$ and $4.62 \times 10^2 \text{ Lmol}^{-1}\text{s}^{-1}$, respectively [53-60].

1.8 Modifications on Atom Transfer Radical Polymerization

The Cu^{I} complexes are sensitive to air and other oxidant [148]. To overcome this drawback as well as to reduce the amount of the catalyst in reaction, several modifications have been reported such as, reverse ATRP, simultaneous reverse and normal initiation ATRP, activators generated electron transfer (AGET) ATRP, activators regenerated by electron transfer ATRP, initiators for continuous activator regeneration ATRP, supplemental activators and reducing agents ATRP and electrochemically mediated ATRP [24-25, 33, 43-44]. The general mechanism for the AGET-ATRP is shown in **Scheme 1.4**.



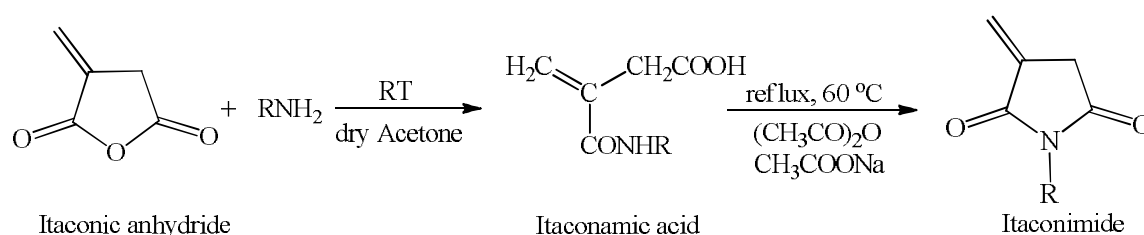
Scheme 1.4: Mechanism of AGET-ATRP.

In a typical AGET-ATRP process, alkyl halide (R-X) is used as initiator, a transition-metal complex in its higher oxidation state (such as, $\text{X-M}_t^{\text{n+1}}\text{Y/L}$) is used as

catalyst in contrast to normal ATRP (n-ATRP) (where a transition-metal complex in its lower oxidation states ($M_t^n Y/L$) is used as catalyst). The activator is generated *in situ* by the reduction of $X-M_t^{n+1}Y/L$ complex with a reducing agent, such as tin(II) 2-ethylhexanoate [$Sn(EH)_2$] [121, 149], D-glucose [150], ascorbic acid [151-152], phenol [153], thiophenol [154] or triethylamine [155]. After the formation of activator, the subsequent steps of AGET-ATRP follow the same mechanism as n-ATRP (**Section 1.5**). In AGET-ATRP, the small amount of catalyst is continuously regenerated by the reducing agent to account for unavoidable levels of radical termination. Thus, AGET-ATRP has all the advantages of normal ATRP and includes additional benefits of simplistic preparation, storage and handling of ATRP catalysts.

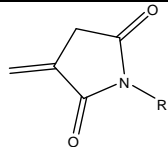
1.9 Synthesis of Itaconimides

The synthesis of itaconimides was generally carried out in two steps. The synthesis of itaconamic acid by the reaction of itaconic anhydride with amine followed by its cyclization using a dehydrating agent as shown in the reaction **Scheme 1.5** [5, 14-15, 19-20]. The *N*-phenylitaconimide can also be obtained from dehydration of their respective itaconamic acid using conc. H_2SO_4 as catalyst in methanol [156]. The *N*-alkylitaconimides such as *N*-*n*-butyl itaconimide and *N*-*tert*-butyl itaconimide can be synthesized from their respective itaconamic acid using *p*-toluene sulphonic acid as catalyst [8]. The *N*-substituted itaconic acid easily undergo isomerization in presence of amine to give its corresponding citraconimide [157-160]. The presence of various substituents on -*N*- can alter the polarity of imides groups thus affecting the properties of the itaconimide monomers. The effect of substituent 'R' on melting point (m.p.) or boiling point (b.p.) and the percentage yield for various itaconimide monomers synthesized in the literature is summarized in **Table 1.2**.



Scheme 1.5: Synthesis of *N*-substituted itaconimide.

Table 1.2: Structures of various *N*-alkyl/ arylitaconimides with their physical properties and yield.

 where R =	m.p. (°C)	b.p. (°C) [mmHg]	Yield (%)	Ref.
phenyl	110-117	-	30-58	[6, 8, 15, 23, 156, 161-163]
4-carboxyphenyl	184-244	-	80-85	[19, 162, 164-165]
3-carboxyphenyl	122-124	-	-	[166]
2-carboxyphenyl	160-162	-	-	[166]
4-chloresteroxycarbonyl)phenyl	160	-	24.2	[165]
4-(chlorocarbonyl)phenyl	193-197	-	68.5	[164-165]
4-methoxyphenyl	105-113	-	38-65	[6, 161-162, 167]
3-methoxyphenyl	48-50	-	-	[166-167]
2-methoxyphenyl	119-120	-	-	[166]
4-ethoxyphenyl	129-130	-	-	[6]
4-methylphenyl	118-126	-	30-77	[6,15,23, 161-162]
2-ethylphenyl	75-119	-	45-47	[8, 161]
4-ethoxycarbonylphenyl	129-130	-	58	[6]
4-acetoxyphenyl	150-152	-	45	[6]
<i>iso</i> -butyl	-	115 [5.0]	38	[7]
methyl	38-45	-	22	[7]
	-	98-100 [12]	-	[168]
ethyl	-	62-63 [0.5]	-	[8]
	-	98-100 [12]	-	[168]
	-	66 [0.3]	41	[7]
<i>n</i> -propyl	-	66 [0.3]	18	[7]
	-	108-112 [12]	-	[168]
<i>iso</i> -propyl	-	79-80 [0.5]	-	[8]
	-	101 [1.0]	28	[7]
<i>n</i> -butyl	-	55-85 [0.5]	38	[7, 169]
	-	117-112 [12]	-	[168]
<i>tert</i> -butyl	-	55-56 [0.5]	-	[8]
β -chloroethyl	-	93 [0.1]	26	[7]
benzyl	146-147	-	-	[161]
	-	110 [20]	38	[7]
<i>n</i> -octyl	-	106-108 [0.5]	-	[8]

cyclohexyl	80-81	-	-	[8]
2-nitrophenyl	84-86	-	-	[162]
3-nitrophenyl	150-152	-	-	[162]
4-nitrophenyl	145-150	-	-	[162]
2-hydroxyphenyl	80-82	-	-	[170]
3-hydroxyphenyl	111-112	-	-	[170]
4-hydroxyphenyl	148-150	-	65	[169-170]
4-chlorophenyl	119, 125-132	-	40-45	[6, 14, 23, 161, 163, 170-171]
2-chlorophenyl	82-124	-	40-45	[14, 23, 163, 166, 40]
3-chlorophenyl	115, 123-125	-	40-45	[14, 23, 31, 34, 171]
4-bromophenyl	127-135	-	-	[163, 166]
2-bromophenyl	124-125	-	-	[170]
3-bromophenyl	144-145	-	-	[170]
2-methylphenyl	67-68	-	-	[8, 170]
3-methylphenyl	93-97	-	-	[8, 170]
2-isopropylphenyl	96-97	-	-	[8]
4-ethylphenyl	115-116	-	-	[8]
1-anthryl	89	-	42.5	[172]
2-anthryl	194	-	51.4	[172]
2,6-dimethylphenyl	128-130	-	-	[8, 173]
2,6-diethylphenyl	85-86	-	-	[8]
2,6-diisopropylphenyl	121-122	-	40-45	[8]
4-methoxy-3-chlorophenyl	186.4	-	70	[174]
2-methoxy-5-chlorophenyl	135.4	-	70	[174]
cyclohexyl	80-81	-	45-52	[8]
allyl	104-105	-	-	[161]
octadecyl	60-61	-	-	[8]

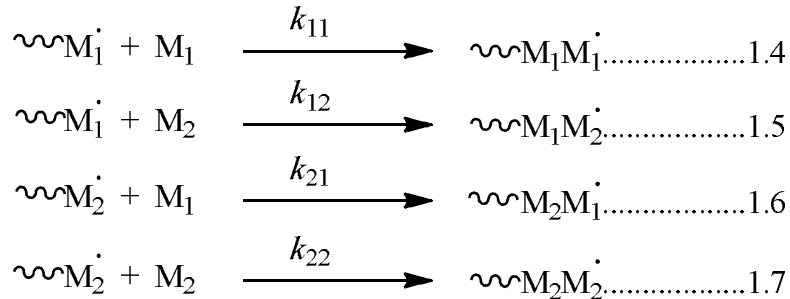
1.10 Mechanism of Copolymerization

In literature three main mechanisms proposed for free radical copolymerizations are as follows:

1.10.1 Terminal Model

According to the terminal model the chemical reactivity of the propagating radical in copolymerization is reliant only on the characteristics of the monomer unit at the growing end. Copolymerization of the two monomers generates the possibility of two types of propagating radicals, one with M_1 at the propagating end (M_1^{\cdot}) and the other

with M_2 at the propagating end (M_2^\cdot). Monomers M_1 and M_2 can each add either to a propagating chain ending in M_1 or to one which is ending in M_2 , giving four possible propagating reactions as:

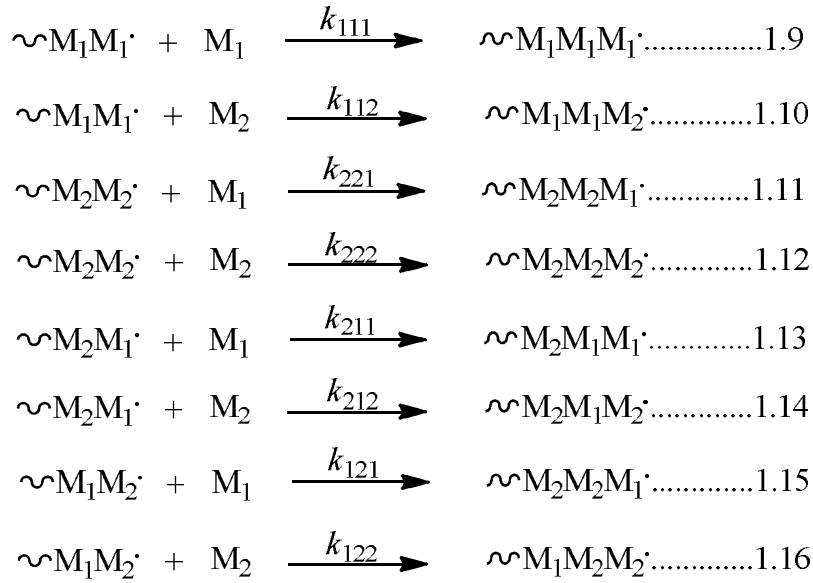


where, k_{11} is the rate constant for a propagating chain ending in M_1^\cdot adding to monomer M_1 , k_{12} that for a propagating chain ending in M_2^\cdot adding to monomer M_2 , and so on. The reactivity ratio is the ratio of the rate constant of reactive propagating monomer adding to its own type of monomer to the rate constant of its addition to the different monomer. The final equation for calculating reactivity ratios r_1 and r_2 values for monomers M_1 and M_2 using terminal model is [21, 175],

$$r_1 = \frac{k_{11}}{k_{12}} \text{ and } r_2 = \frac{k_{22}}{k_{21}} \dots \dots \dots 1.8$$

1.10.2 Penultimate Model

The failure of the terminal model is observed for some comonomers indicating that the reactivity of the propagating radicals is affected by the next-to-last (penultimate) monomer. This behavior is referred as second-order Markov or penultimate behavior. The failure of the terminal model is relatively observed where the monomers contain highly bulky or polar substituent and where the reactivity of one of monomers is significantly greater than second monomer. Penultimate model involves eight propagation rate constants and has six reactivity ratios (with four monomer reactivity ratios viz. r_1, r_1', r_2, r_2' and two radical reactivity ratios viz. s_1 and s_2) which are given as below:

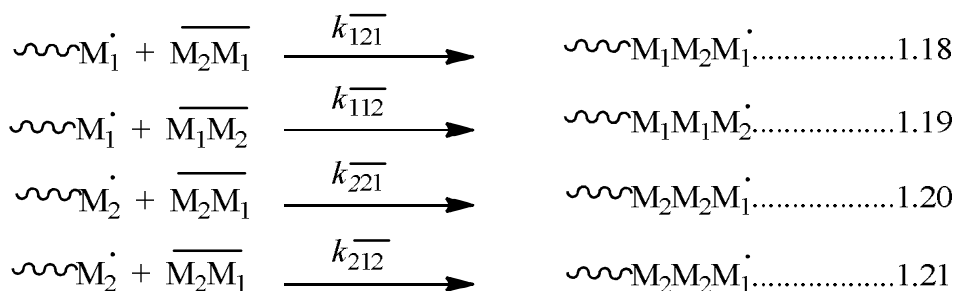


$$r_1 = \frac{k_{111}}{k_{112}} \quad r'_1 = \frac{k_{211}}{k_{212}} \quad r_2 = \frac{k_{222}}{k_{221}} \quad r'_2 = \frac{k_{122}}{k_{121}} \quad s_1 = \frac{k_{211}}{k_{111}} \quad s_2 = \frac{k_{122}}{k_{222}} \dots \dots 1.17$$

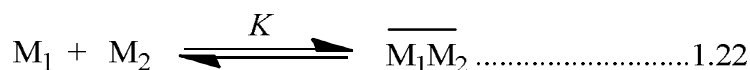
The radical reactivity ratio is the ratio of the propagation rate constant for reaction in which the penultimate monomer differs from the terminal monomer compared to the rate constant where the penultimate and terminal monomers are the identical [21, 175].

1.10.3 Complex Participation Model

The complex participation model is also known as “copolymerization with simultaneous depropagation”. The deviation from the terminal model is also observed when the comonomer complex contends with each of the entity monomers in propagation step. The complex participation model depends on the copolymer composition, temperature and monomer concentration. It involves eight propagation rate constants, the initial four propagation steps of the individual monomers (equation 1.4-1.7) as explained for the terminal model and the next four propagation steps of the comonomer complex as given follows:



where, $\overline{M_1M_2}$ and $\overline{M_1M_2}$ are complex adding to a propagating centre at the $M_1\dot{}$ and $M_2\dot{}$ ends respectively. The equilibrium between uncomplexed and complexed monomers is given in equation 1.22.



There are total six reactivity ratios including two radical reactivity ratios.

$$r_1 = \frac{k_{11}}{k_{12}} \quad r_{1c} = \frac{k_{112}}{k_{121}} \quad r_2 = \frac{k_{222}}{k_{221}} \quad r_{2c} = \frac{k_{221}}{k_{212}} \quad s_{1c} = \frac{k_{112}}{k_{11}} \quad s_{2c} = \frac{k_{221}}{k_{22}} \dots\dots\dots 1.23$$

This model is useful mostly for studying the mechanism of copolymerization in “bulk” [21].

1.10.4 Discrimination Between the Terminal and Penultimate Model

In an effort to find the “best” copolymerization model for definite copolymerization system, researchers have tried to fit these selected models to a variety of copolymer characteristics properties such as composition, average sequence length and rate of propagation. There are two common approaches to find the “best” mechanistic model for a free radical copolymerization process. The very first approach is ‘to perform an experiment which is intended to validate a meticulous step (or steps) in the reaction mechanism’. This approach is well explained by Hill et al. [176] to show that the penultimate unit effect could exist in free radical copolymerization of certain monomers. The second approach is ‘to investigate the fit of suggested models for the obtained data’. Though, the analysis is only valuable as the various experimental results have been

collected. The statistical model discrimination methods were used to select experimental conditions so that each experiment will enclose the highest probable amount of information as well as the potency and failure of the challenging models. Statistical model discrimination methods also illustrate how to analyze the data consistently to conclude which model provides the “best” description of the obtained experimental data. Discovering the model that provides the best picture of resulting copolymerization is important for designing and controlling the rate of copolymerization processes. Additionally, if the modeling postulations are correct, finding the model which affords the best explanation of experimental data will help to identify the most probable mechanism of copolymerization system [177].

In 1994, Burke et al. [178] have put forward the systematic application of statistical model discrimination methods to reduce the required number of experiments to discriminate between “terminal and penultimate models” for copolymerization of styrene and acrylonitrile to spread over the entire range of feed compositions. The authors have used triad fraction data to explain the penultimate unit effects in the copolymerization of styrene and acrylonitrile monomer system. In 1997, Andrzej Kaim [179] used statistical model discrimination methods to find the correct mechanism of copolymerization of styrene and MMA system. The obtained results show that the copolymerization system is having limited penultimate unit effect than terminal. Later, in 2003, he used multiresponse maximum likelihood method and statistical tests, to discriminate between terminal and the penultimate model, for the same system in bulk [180]. He explained that the investigated statistical methods are suitable for kinetic-model discrimination when they are applied to a *posteriori* data of copolymer composition. In 2005, Pramil Deb [181] used the non-linear curve-fitting regression method to determine the reactivity ratios suggesting the effects of terminal and penultimate groups in copolymerization of styrene and MMA monomers.

1.10.5 Microstructure Analysis of Copolymers of NAI and MMA

The physical and chemical properties of polymers are affected by their microstructure, which involves the monomer allotment and the stereochemical arrangement of the various groups in the polymer chain [182-183]. Microstructural studies of polymers are having enormous help in developing the structure–property relationship [184]. The microstructure of the polymers can be investigated by NMR spectroscopy. ¹³C-NMR

spectroscopy has been extensively used to study the microstructure of many vinyl copolymers [185-190]. Anand et al. [171] reported the microstructure analysis of *N*-(*o*-/*m*-/*p*-chlorophenyl)itaconimide-MMA copolymers using ¹H decoupled ¹³C-NMR experiments and theoretically via Harwood program and Monte Carlo simulation method. The carbonyl carbon signals of MMA and NAI of copolymers were used for the determination of the sequence distribution triads. Chauhan et al. [191] reported the microstructure analysis of the *N*-(5-chloro-2-methoxyphenyl)itaconimide-MMA and *N*-(5-chloro-3-methoxyphenyl)itaconimide-MMA copolymers by ¹H decoupled ¹³C-NMR spectra showed that the mechanism of copolymerization follows the first-order Markov model.

1.11 Mechanism and Kinetics of Copolymerizations of Itaconimides

For the free radical copolymerization of itaconimides and MMA, the higher reactivity ratio has been reported in the literature for itaconimide monomers as compared to MMA. The reactivity ratios of the monomers can be determined using its feed ratios and the copolymer composition. The copolymer composition can be determined using different analytical tools such as IR, ¹H-NMR, UV-Vis absorption spectroscopy and elemental analysis. The monomer reactivity ratios for the copolymerization *N*-alkyl/ arylitaconimide with MMA/ styrene based on terminal model were reported. The monomer feed composition and polymers composition were used to calculate the reactivity ratios with the help of Finemann Ross (FR) method (equation 1.24) or Kelen Tudos (KT) method (equation 1.25) [21].

$$\frac{F_M (f_M - f_I)}{F_M f_M} = \frac{f_M F_M^2 r_M}{F_M F_I^2} - r_I \dots\dots\dots 1.24$$

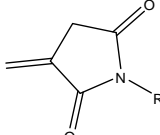
where, f and F are the mole fractions of monomer in the copolymer and the feed, respectively. The subscript M and I denotes MMA and *N*-alkyl/ arylitaconimide, respectively.

$$\eta = \left(r_M + \frac{r_I}{\alpha} \right) \xi - \frac{r_I}{\alpha} \dots\dots\dots 1.25$$

where, η and α are the parameters depending on f and F.

In literature mostly terminal model was used to find the reactivity ratios of NAI monomers and penultimate model has not been investigated [5, 14-15, 19-21]. Although, the possibility for a penultimate group effect especially for the radical terminated with MMA was considered. This is because, the selected copolymerization systems contains NAI as one of its component, which is bulky with electron withdrawing substituent on the double bond. The reactivity ratios of monomers of *N*-alkyl/ arylitaconimides with MMA/ styrene calculated using terminal model are given in **Table 1.3**.

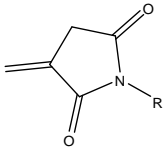
Table 1.3: Monomer reactivity ratios for copolymerization of *N*-alkyl/ arylitaconimide with MMA/ styrene calculated using terminal model.

 where, R =	Copolymerization with MMA		Copolymerization with styrene		Ref.
	r_1	r_M	r_1	r_s	
phenyl	1.26	0.23	0.12	0.14	[6]
	-	-	0.88	0.06	[156]
	1.47	0.39	-	-	[15]
2-chlorophenyl	0.81	0.35	-	-	[14]
3-chlorophenyl	1.15	0.32	-	-	[14]
4-chlorophenyl	1.31	0.36	-	-	[14]
	-	-	0.32	0.19	[6]
4-methylphenyl	1.33	0.24	0.23	0.15	[6, 15]
4-ethoxycarbonylphenyl	-	-	0.12	0.24	[6]
4-acetoxypheyl	-	-	0.15	0.25	[6]
4-methoxy-3-chlorophenyl	1.54	0.32	-	-	[174]
2-methoxy-5chlorophenyl	1.23	0.15	-	-	[174]
3-methoxyphenyl	0.99	1.0	-	-	[167]
4-methoxyphenyl	1.11	0.93	-	-	[167]
4-carboxyphenyl	0.46	0.68	-	-	[19]
methyl	1.00	0.45	0.14	0.23	[6]
ethyl	0.42	0.51	-	-	[7]
<i>n</i> -Propyl	-	-	0.04	0.29	[7]
<i>i</i> -Propyl	-	-	0.07	0.27	[7]
<i>n</i> -Propyl	-	-	0.03	0.23	[7]
<i>i</i> -Butyl	-	-	0.10	0.36	[7]
β -chloroethyl	-	-	0.20	0.11	[7]
benzyl	-	-	0.36	0.20	[7]

here, r_1 = reactivity ratio of *N*-alkyl/ arylitaconimide, r_M = reactivity ratio of MMA, r_s = reactivity ratio of styrene

Yamazaki et al. [11] determined the values k_p and k_t for polymerization of *N*-butylitaconimide, *N*-cyclohexylitaconimide, and *N*-*tert*-butylitaconimide using electron spin resonance spectroscopy. The k_p for poly(*N*-*n*-butylitaconimide), poly(*N*-cyclohexylitaconimide) and poly(*N*-*tert*-butylitaconimide) in ($\text{Lmol}^{-1}\text{s}^{-1}$) were found to be 550, 1370 and 750, respectively. Similarly, the k_t for poly(*N*-*n*-butylitaconimide), poly(*N*-cyclohexylitaconimide) and poly(*N*-*tert*-butylitaconimide) in ($\text{Lmol}^{-1}\text{s}^{-1}$) were reported 1.2×10^6 , 1.0×10^6 and 1.2×10^6 , respectively. The values of k_p and k_t are varying according to the structure of primary, secondary and tertiary alkyl groups. Sato et al. [156] reported activation energy (E_a) for free radical polymerization of *N*-phenylitaconimide to be 51.2 kJ mol^{-1} . Oishi [6] reported the values of rate of polymerization (R_p), k_p , E_a and frequency factor (A) of radical polymerizations of various itaconimides monomers from the time-conversion relationship and it is given in the **Table 1.4**. Hence, it was found that the rate of polymerization will be higher for *N*-(substituted phenyl)itaconimides than *N*-alkylitaconimides and the polymerization reactivity of *N*-(substituted phenyl)itaconimides depend on the number, position, and bulkiness of the alkyl substituent on the *N*-phenyl ring. When an alkyl group was introduced into the aromatic ring of NAI, especially into the *meta* or *para* position, the rate of polymerization increased compared to unsubstituted aromatic ring of NAI. However, in the polymerization of *N*-(2,6-di-substituted phenyl)itaconimides, the rates of polymerization decreased as the bulkiness of the alkyl substituent increased. It could be due to the steric effect of two alkyl substituent on the *ortho* positions of the aromatic ring of NAI which plays a vital role for the polymerization of these monomers [6].

Table 1.4: The values of R_p , k_p , E_a , and A for the radical polymerization of *N*-substituted phenylitaconimide monomers, at $60 \text{ }^\circ\text{C}$ in THF [6].

 where R =	$R_p = k_p[\text{AIBN}]^m[\text{M}]^n$		k_p ($\text{Lmol}^{-1}\text{s}^{-1}$)	E_a (kcal mol^{-1})	A (s^{-1})
	m	n			
phenyl	0.6	1.2	1.58×10^{-3}	19.5	9.9×10^9
4-chlorophenyl	0.5	1.1	8.83×10^{-4}	16.1	3.1×10^7
4-methylphenyl	0.5	1.0	1.28×10^{-3}	20.1	1.7×10^{10}
(4-ethoxycarbonylphenyl)	0.5	1.2	1.08×10^{-3}	20.9	5.6×10^{10}
(4-methoxyphenyl)	0.5	1.3	2.58×10^{-3}	18.6	4.2×10^{10}

1.12 Maleimides and Their Copolymerization via Reversible-Deactivation Radical Polymerization

The copolymers of maleimides with suitable monomers have been prepared with varied architecture and topology via NMP, RAFT, and mostly by ATRP. The copolymerization of styrene (St) and the maleimides such as *N*-phenylmaleimide, *N*-benzylmaleimide, and *N*-cyclohexylmaleimide has been reported via NMP. The obtained poly(St-*co*-maleimide) terpolymers are having well controlled molecular weights and narrow PDI (1.55) [192]. The NMP of styrene as a donor and the maleimides such as *N*-phenylmaleimide, *N*-benzylmaleimide, and *N*-cyclohexylmaleimide as acceptor monomers is reported by Butz et al. [193]. These copolymerizations are characterized by high polymerization rates and very short induction periods with moderate PDI (1.5-1.6).

The one pot copolymerization of 1,6-bismaleimide hexane (BMIH) and excessive styrene has been done via RAFT, resulting into the star shaped polystyrene. The polystyrene arms were grafted from the preformed core, which was formed *in situ* during the copolymerization of BMIH and St. [194]. An alternating copolymers of 4-vinylbenzyl methoxytetra(oxyethylene) ether and a series of *N*-alkyl/ aryl substituted maleimides were synthesized by RAFT [195]. Wei et al. [196] reported an alternate copolymers of *N*-phenylmaleimide with ethyl α -ethylacrylate using RAFT. A double thermo responsive block copolymers of styrene derivatives and *N*-alkylmaleimides can be conveniently produced in a one-step procedure using RAFT [197]. The controlled radical copolymerizations of *N*-phenylmaleimide and *N*-cyclohexylmaleimide with naturally occurring (+)-*d*-limonene has been done via RAFT. The obtained copolymers were chiral and highly sequence-regulated in nature with high T_g (220-250 °C) [198]. The RAFT dispersion copolymerization of styrene with *N*-phenylmaleimide using a poly(methacrylic acid) macro chain transfer agent were reported by Pengcheng et al. [199]. The obtained PMA-*b*-poly(styrene-*alt*-*N*-phenylmaleimide) diblock copolymer are having 2D lamellae morphologies and were stable up to 347 °C with T_g 219 °C. Poly(triethylene glycol acrylate)-*b*-poly(*tert*-butyl acrylate) block copolymer micelles have been synthesized with a fluorescent dithiomaleimide group incorporated into the micelle core was synthesized by RAFT. The synthesized block copolymers and its self-assembly is having the applicability to tissue imaging [200].

1.12.1 Atom Transfer Radical Polymerization of Maleimides

The functional periodic copolymers of *N*-benzylmaleimide and *N*-(2-(amino-*t*BOC)-ethylene)-maleimide with styrene via ATRP have been reported by Marie-Alix et al. [201]. Jean-Francois et al. [202] reported the ATRP of styrene and various *N*-alkylmaleimides such as *N*-propylmaleimide, *N*-benzylmaleimide, *N*-methylmaleimide. The obtained alternative copolymers are useful in the preparation of functional periodic microstructures due its acceptor-donor nature. The double thermoresponsive diblock copolymers of 4-vinylbenzylmethoxytetrakis (oxyethylene) ether with *N*-(3-trimethylsilyl) propargylmaleimide and *N*-(3-triethylsilyl) propargylmaleimide have been synthesized via ATRP [197]. ATRP of *N*-(2-acetoxy-ethyl)maleimide and *N*-phenylmaleimide with styrene has been successfully carried out using 1-phenylethylbromide/ Cu^IBr / bipyridine catalytic system. The obtained copolymers were having predominantly alternating structure with designed molecular weight viz. 7.4×10^2 gmol⁻¹ and narrow PDI = 1.1 [203]. ATRP was employed to prepare graft copolymers of MMA using *N*-methylolmaleimide-styrene copolymers backbone. The thermal stability and T_g of the obtained copolymer was enhanced due to the rigidity of maleimides units and their ability to form hydrogen bonds [204]. The self-condensing ATRP of *N*-[4-(α -bromoisobutyryloxy)phenyl]maleimide and a large excess of styrene typically leads to hyperbranched copolymers. The physical properties such as T_g and melt properties of the obtained copolymers have been enhanced due to highly crossed branched architecture [205]. Hyperbranched copolymers were synthesized by the atom transfer radical copolymerization of *N*-(4- α -bromobutyryloxy phenyl)maleimide monomer with styrene. The T_g of the resulting hyperbranched copolymer increased with increasing mole fraction of maleimides in polymer backbone [206]. The copolymers of MMA and *N*-cyclohexylmaleimide have been synthesized via ATRP using CuBr/ bipyridine catalyst system in anisole, shows the improved thermal stability of copolymers as compared to PMMA [207]. Haddleton et al. [208] have synthesized poly(PEG-methacrylate)-*alt*-maleimide and poly(glycerol-methacrylate)-*alt*-maleimide copolymers by ATRP. The obtained α -functional methacrylate copolymers have been successfully used in coupling reactions with glutathione and protein for the synthesis of a series of conjugates. The one-pot synthesis of star shaped Polystyrene via ATRP of *N*-[2-(2-bromoisobutyryloxy)ethyl]maleimide with a large excess of styrene were reported by Qingchun et al. [194]. The block copolymers of *N*-phenylmaleimide and 2-hydroxyethyl

methacrylate could be suitable for various applications in the field of polymer science due to their morphological and thermal properties [209].

1.13 Living Polymerizations of Itaconimides

1.13.1 Anionic Polymerization

Apart from the free radical copolymerization of itaconimide monomers via conventional methods as mentioned in the **Section 1.3**. The itaconimides have also been polymerized via other methods such as anionic polymerization and RDRP. Itaconimides have two electron-withdrawing carbonyl groups and therefore may give high molecular weight materials by anionic polymerization. Itaconimides can be readily polymerized with basic initiators that involve carbide, nitride, alkali metal and oxide anions such as *sec*-butyllithium, lithium diethylamide and *tert*-butoxide [210]. The polymerization of *N*-(4-methoxyphenyl)itaconimide, *N*-phenylitaconimide, *N*-(4-chlorophenyl)itaconimide, *N*-(4-tolyl)itaconimide and *N*-(2-ethylphenyl)itaconimide has been done using *sec*-butyllithium and *n*-butyllithium (*n*-BuLi) as initiators in THF, toluene or DMF solvents at -50 °C. The softening temperature of the obtained polymers was found to be in the range of 250-300 °C. The rate of polymerization was dependent on the nature of solvent. When toluene was used as a solvent for the polymerization of *N*-(*p*-methoxyphenyl)itaconimide at 25 °C, the polymer was obtained in less amount, while at -50°C, the conversion was only 20%. However, in THF the conversion increased to 80% at -70 °C. The polymerization was faster in THF solvent than in toluene [8]. The polymerization of an optically active [4-*N'*-(α -methylbenzyl)aminocarbonylphenyl]itaconimide is reported by Oishi et al. [26] in DMF at 0 °C using *n*-butyllithium as a catalyst. The obtained polymer was a white powder and had negative optical activity. The specific rotations $[\alpha]_D$ of polymer was about -46.6 to -52.1° at concentration 1.0 gmol⁻¹, $l = 10$ cm in THF. The *N*-alkylitaconimides and *N*-phenylitaconimides are polymerized using *sec*-butyllithium as initiator in toluene or THF as solvent at -78 °C. The *N*-*n*-butylitaconimide monomer gave a high molecular weight polymer ($\bar{M}_n = 4.1 \times 10^4$ gmol⁻¹) in toluene [8]. The polymerization of an optically active *N*-[4-(cholesteroxycarbonyl)-phenyl]itaconimide (ChPII) was achieved in toluene or THF at 0°C with *n*-BuLi as catalyst. The molecular weight and PDI for poly(ChPII) were obtained 6.3×10^3 gmol⁻¹ to 4.0×10^3 gmol⁻¹ and 4.0-2.3, respectively. The results were

similar to those for polymers obtained using FRP conditions. The specific rotation for poly(ChPII) was found to be $+1.7-3.9^\circ$ [27]. Matsumoto et al. [211] reported the polymerization of *N-n*-butylitaconimide using *n*-BuLi as catalyst in toluene at -78°C . The molecular weight of obtained poly(*N-n*-butylitaconimide) was found to be $12.3 \times 10^4 \text{ g mol}^{-1}$ with $\text{PDI} = 3.0$. Asymmetric homopolymerization of achiral *N*-diphenylmethylitaconimide were reported by Oishi et al. [212]. An optically active polymers were obtained with specific rotation in the range of $+7.5^\circ$ to -18.4° than other systems used for the polymerization. The molecular weight of poly(*N*-diphenylmethylitaconimide) was found to be $1.5 \times 10^3 \text{ g mol}^{-1}$ to $3 \times 10^3 \text{ g mol}^{-1}$ and attributed to configurational chirality rather than conformational.

For the anionic polymerization, the reactions must be conducted under inert conditions, viz. in the absence of moisture or other electrophiles due to the high nucleophilicity of the carbanionic chain ends [24]. To the best of our knowledge the cationic polymerization of itaconimides is not reported and it could be due to the presence of two electrons withdrawing carbonyl group.

1.13.2 Reversible-Deactivation Radical Polymerization

Many reports are available on the RDRP of maleimides but very few reports are available on RDRP of itaconimide monomers. The very first study on RDRP of itaconimide monomers was reported by Anand et al. [23]. They have synthesized and characterized the block architecture of MMA and NAI monomers (*N*-phenylitaconimide and *N*-(4-methylphenyl)itaconimide and its chloro derivatives) using reverse ATRP. The macroinitiator with a chlorine chain-end (PMMA-Cl) was prepared using AIBN/ $\text{FeCl}_3 \cdot 6\text{H}_2\text{O}$ / PPh_3 as the initiating system and used to polymerize the selected NAI monomers. However, only oligomeric blocks of NAI monomer have been incorporated with long reaction duration (7 days) having low molecular weight (viz. $1.0 \times 10^3 \text{ g mol}^{-1}$ to $1.8 \times 10^3 \text{ g mol}^{-1}$) of the copolymers. Satoh et al. [213] called the itaconimide monomers as bio-based polymer materials and reported the block copolymers of itaconimides [such as *N*-phenylitaconimide and *N*-(*p*-tolyl)itaconimide] and itaconic acid esters [such as di-*n*-butyl itaconate and bis(2-ethylhexyl) itaconate] via RAFT. The obtained triblock copolymers are having soft poly(itaconate) and hard poly(itaconimide) segments. The different triblock copolymers of *N*-phenylitaconimide/ *N*-(*p*-tolyl)itaconimide and itaconic acid esters having molecular weight in the range of $8.7 \times 10^3 \text{ g mol}^{-1}$ to 6.7×10^4

gmol^{-1} with PDI = 1.5-1.1. The polymers obtained from the NAI exhibited relatively high T_g (240-260 °C) and it is degraded at ~ 300 °C. The block copolymer are obtained with microphase-separated morphology might act as a thermoplastic elastomers between the two blocks' T_g s while exhibiting the high service temperature.

1.14 Computational Study on Free Radical Polymerization

Apart from experimental methods, the computational chemistry based on quantum mechanics has been applied to the investigation of reaction kinetics in FRP. The *ab initio* and *semi-empirical* methods are widely used to predict various rates and equilibrium constants of importance to radical polymerizations including propagation, chain transfer and reactions involving the control agents. At the microscopic level, computational chemistry can be used to model the interactions between substituents and control agents or catalyst under varying conditions, and to explain reaction mechanisms. This facilitates a balanced selection or design of these agents or catalyst through structure-reactivity studies. Over the last decade, increase in computing power and the development of highly cost-effective composite *ab initio* procedures have allowed to investigate the thermodynamic and kinetic properties of a wide variety of radical reactions within 'chemical accuracy'[68, 175, 214]. The quantum mechanics can be considered as a influential and cost-effective tool for the kinetic characterization of many individual reactions in FRP. Especially the polymerization that cannot be fully analyzed through experiments it can be analyzed by using quantum mechanics. The recent focus on copolymerization reactions where secondary reactions such as termination and transfer plays a major role has emphasized this feature due to the increased complexity of these kinetic schemes. The quantum mechanics calculations are well-matched to stand and direct the experimental analysis of FRP kinetics as well as to expand the understanding of polymerization mechanisms.

Cuccato et al. [215] explained the importance and applications of molecular mechanics in FRP. Percec et al. [216-217] have explored the DFT methods to study the activation and deactivation rate constants of ATRP process using alkyl halides as model compounds. These authors have also reported the ATRP equilibrium constant (K_{ATRP}) values for many alkyl halides (methyl vinyl ketone, vinyl fluoride, vinylidenedifluoride, vinyl chloride, vinyl bromide, butadiene, acrylonitrile, *N,N*-dimethylacrylamide) and their dimers, which act as the dormant species for the polymerization process. Many

theoretical reports are available on the kinetic studies of MMA polymerization and its tacticity control in polymerization [218-219]. The (propagation rate coefficient) k_p of some important monomers such as styrene[220], MMA [221], methyl acrylate [222], vinyl acetate [223], acetonitrile [224], vinyl chloride [225] has been well reported. Coote et al. [175] have explored the modeling of kinetic parameters for free radical polymerizations of vinylic monomers such as methyl acrylates, MMA, styrene, vinyl acetate. They have presented a detail description of failure of terminal model (to describe simultaneously the composition and propagation rate in free-radical copolymerization) and the importance of penultimate models in FRP. A high-level “*ab initio*” molecular orbital calculation was used to study the degree and beginning of the penultimate unit effect in ATRP involving the comonomers methyl acrylate, MMA and propylene [226]. The penultimate unit effects have important implications for initiator design; which need to be taken into account in the synthesis of block, gradient, and random copolymers. In a study by Heuts et al.[227], the effects of the penultimate unit on the activation energies for the addition of a series of propyl radicals to various alkenes have been calculated. Coote et al. [228] have extended the work of Heuts et al. by examining γ -substituent effects in small-radical addition reactions, providing direct evidences for “explicit penultimate unit effect” in the reaction activation energies, and suggesting that polar as well as direct interactions are likely to be important in determining this behavior.

1.14.1 Methods of Molecular Modeling

The methods for molecular modeling may be categorized into four main groups: one of them uses classical physics (viz. mechanics) and the rest use quantum mechanics to model the behavior and interactions of molecules.

1. *Molecular mechanics*: This method is based on conventional classical mechanics. The atoms are considered as spheres that are connected to other atoms by a spring (representing the bond). The energy of the molecule is expressed as a function of bond stretching, bond bending and atom crowding etc. which uses the expression of force field to find the possible minima in the energy surface [229-231].

2. *Ab initio methods*: Here, the Schrödinger equation is used to calculate the wide variety of quantum chemical properties. The main calculation is the wave function determination. From the results of the wave function, other chemical properties and

behaviors can be determined. In this method, the inputs are usually the fundamental constants, 100% of the final determination is done mathematically [232].

3. *Semi-empirical methods*: In semi-empirical methods, a fraction of the calculation comes from experimental data or from other sources, and the rest comes from mathematics. The major advantages of the semi-empirical method are; it is faster and able to perform calculations on larger molecules (with some compromise on accuracy) [233].

4. *Density functional theory methods (DFT)*: DFT methods are the latest computational methods increasing in reputation among computational chemists. The DFT method determines properties of the molecules from calculating the electron density rather than calculating molecular properties based on the determination of the wave function [234-235]. It uses "*functional*" to determine the electron density and the properties of a molecule. A *functional* is defined as a function of a function, for example, the energy of the molecule is a functional of the electron density.

1.14.2 The Density Functional Theory Methods

DFT is an all-purpose computational method and it can be applied to the most of the reaction systems. The most important improvement to DFT methods is a significant increase in computational accuracy without the additional increase in computing time. DFT methods are now standard in virtually all of the most popular software packages, including Gaussian, GAMESS, Hyper Chem, and Spartan [234-236].

DFT try to find (to calculate) all the properties of atom and molecules from the electron density. The idea of calculating atomic and molecular properties using the electron density originated from the calculations made independently by Fermi and Dirac in 1920. The Thomas-Fermi model [237] is the result of independent work of Fermi and Thomas where atom were modelled as system with positive potential viz. nucleus located in the uniform electron gas. At present, DFT calculations on molecules are based on the Kohn-Sham approach [238] which is based on two theorems reported by Hohenberg and Kohn in 1964 [237-239]. The first Kohn-Sham theorem says that any ground state property can be calculated from the electron density $\rho(x, y, z)$ alone, and so it is important to search for methods to calculate molecular properties from the electron density. The second theorem states that the variation approach might generate a way to calculate the energy and electron density of the molecule. The ground-state electronic

energy, E_0 , a functional of electron density ρ , is written as a sum of the kinetic energy, E_T , the electronuclear interaction energy, E_V , the Coulomb energy, E_J , and the exchange/correlation energy, E_{xc} .

$$E_0 = E_V[\rho] = E_T[\rho] + E_V[\rho] + E_J[\rho] + E_{xc}[\rho] \dots\dots\dots 1.26$$

The first three terms on the right side of the above expression (equation 1.26) are easy to evaluate from ρ and include the main contributions to the ground-state. The fourth term (E_{xc}), although not easy to evaluate accurately, will be a relatively small term. Thus, the idea of expressing the molecular energy as a sum of terms out of it which a relatively small term involves the unknown functional (and even large error in this term will not introduce much error into the total energy of the molecule) is fulfilled. Thus, the key to accurate calculation of molecular properties in the Kohn-Sham formalism of DFT is to get a good approximation to E_{xc} . Various approximate functional $E_{xc}[\rho]$ are used in molecular DFT calculations. Three types of exchange/ correlation functionals are presently in use:

- (i) functionals based on the local spin density approximation (LSDA),
- (ii) functionals based on the generalized gradient approximation (GGA), and
- (iii) functionals which employ the “exact” Hartree-Fock exchange as component.

When the DFT calculations use exchange-correlations energy functionals (E_{xc}) that involves not only LSDA but both electron density and its gradient, the functionals are known as gradient-corrected or the generalized-gradient approximation (also known as non-local). The exchange-correlation energy functional can be written as the sum of an exchange-energy functional and corrected-energy functional as $E_{XC} = E_x + E_c$. Some examples are the Gill 1996 (G96), the Lee-Yang-Par (LYP), the Perdew 1986 (P86), etc. The so called “hybrid methods” combine Hartree-Fock approximation to the exchange energy and a DFT approximation to the exchange energy, to include electron correlation. A well-liked hybrid DFT functional is based on exchange energy functional developed by Becke in 1993, further modified by Stevens et al. in 1994 with the introduction of additional term called LYP 1988 correlation-energy functional. This combined exchange-correlation functional known as the Becke3LYP or B3LYP functional as given below;

$$E_{xc}^{B3LYP} = (1 - a_0 - a_x)E_x^{LSDA} + a_0E_x^{HF} + a_xE_x^{B88} + (1 - a_c)E_c^{VWN} + a_cE_c^{LYP} \dots 1.27$$

where, E_x^{LSDA} = accurate LSDA non-gradient-corrected exchange functional (pure DFT), E_x^{HF} = KS-orbital-based HF exchange energy functional, E_x^{B88} = Becke 88 exchange functional, E_c^{VWN} = the Vosko, Wilk, Nusair function (which is part of accurate function for the homogeneous electron gas of the LDA and LSDA), E_c^{LYP} = LYP correlation functional, E_x and E_c are gradient corrected. The parameter a_0 , a_x , and a_c give the best fit of the calculated energy to molecular atomization energy. **Table 1.5** provides a good summary of sample methods by name, acronym and type. The B3LYP functional is considered to be the most useful in terms of “industry standard” and of practical applications [238-241].

Table 1.5: Different DFT methods.

Name of the method	Type	Acronym
Hartree-Fock Slater functional	Hartree-Fock with local density approximation exchange	HFS
Vosko, Wilks, and Nusair	Local Density Approximation (emphasis oneelectron correlation approximation)	VWN
Becke correlation functional; Lee, Yang, Parrelectron exchange functional	Gradient-corrected LDA functional	BLYP
Becke 3-term correlation functional; Lee, Yang, and Parr exchange functional	Hybrid DFT	B3LYP
Perdew 1986 functional	Gradient-corrected LDA functional	P86
Becke 3-term correlation functional; Perdew correlation term	Hybrid DFT	P3P86
Modified Perdew-Wang one parameter hybrid for kinetics	Hybrid DFT	MPW1K

1.14.3 Basis Sets

Most of the molecular quantum mechanics methods begin the calculations with the choice of a set of basis functions χ_r , which are used to express the molecular orbitals ϕ_i as;

$$\phi_i = \sum_r c_{ri} \chi_r \dots\dots\dots 1.28$$

The use of sufficient basis set is necessary for success of the calculations. Basis sets are typically built into modern computational chemistry software or a chemist can use resources such as the “Gaussian Basis Set Order Form” to find a desired basis set for incorporation in a calculation [242].

At present, there are many of basis sets composed of Gaussian-type orbitals. The smallest of these are called 'minimal basis set'. As the name suggests, minimal basis sets are designed to increase the speed of calculation, and are hardly ever used for research purposes. These are primarily used to obtain a “first look” at one or more molecular properties. Examples of minimal of basis sets are STO-3G and STO-6G. Minimal basis sets observe all electrons as being of equal importance.

Split-valence basis sets are the next step up in terms of effectiveness and importance. Split-valence basis sets are considering the valence electrons (those on the outermost orbitals) involved in bonding and chemical reactions, as opposed to the core electrons (which are typically not involved in reactions). Split-valence basis sets carry out a fast and filthy approximation of the behavior of the core electrons, and then do a more thorough and careful calculation of the valence electrons. Examples of split-valence basis sets are 3-21G and 6-31G.

Typically, the location of electrons is described in terms of their electron configuration. For example, for carbon we describe the configuration as, $1s^2 2s^2 2p^2$. This accounts for all six of the carbon electrons. However, some of those electrons might occasionally “wander away” into a “d” orbital and polarization takes that into account. As such, polarization gives a more accurate description of where the electron is and where the electron can go. A 'polarized basis set' is indicated by an asterisk “*” in some places, or by the orbital name in others. For example, we can have 3-21G* basis set or 3-21G(d) basis set. Both refer to the same basis set.

Electrons are characteristically found near to the nucleus of the atom. We are interested in determining the possibility of where electrons are and that probability is highest close to the nucleus. It then holds that as the distance from the nucleus gets larger (bigger atomic radius), so there is less probability of finding the electron. At larger distances from the nucleus, we can stop our calculations, because we typically will not find the electrons there. For some systems, especially anions, radicals and atoms in the excited states, we use 'diffuse basis sets' to extend the distance away from the nucleus that we are looking for electrons. These basis sets are indicated by a "+" symbol, such as 3-21+G. A basis set like 6-31+G(d) would be a polarized diffuse split-valence basis set [242-243].

1.15 Gaps in the Existing Research

1. The copolymers of NAI with MMA have been synthesized mostly via conventional FRP, which have poor control over the molecular weight. Also, the copolymers so obtained have broad PDI. To synthesize the polymers with desirable molecular weight and architectures (in terms of their chain topology, composition and diverse functionality), the polymerization needs to be carried out under controlled conditions.
2. The block copolymer offers the ability to combine the properties of two different polymers into one block copolymer. The block copolymers of NAI and MMA are important due to the combination of glassy PMMA and thermally stable poly(NAI), which offers its applications for higher temperature service. The reported copolymers of NAI with MMA are mostly "random" and other architectures such as "block" are not well reported.
3. In copolymerization, the measurement of individual k_p using experimental techniques (i.e. PLP-SEC and NMR spectroscopy) requires the use of definite polymers model. Hence, the experimental results has to be interpreted via copolymerization model. Also, the direct access to the kinetics of cross propagation reaction via experimental techniques is very difficult. Thus, an alternative (computational) methods based on quantum chemistry for studying copolymerization process are becoming attractive. In principle, computational methods can be applied to any type of reaction without the limitations of an experimental investigation and the rate constants are obtained without using any

polymerization model. Thus, an alternative methods such as the *ab initio* methods have been explored to study the mechanism of ATRP of NAI-MMA monomer system.

1.16 Objectives of the Proposed Research

1. To synthesize the *N*-arylitacconimides viz. *N*-phenylitacconimide, *N*-(4-methylphenyl)itacconimide, *N*-(4-methoxyphenyl)itacconimide, *N*-(4-chlorophenyl)itacconimide, and bromo derivatives of succinimide viz. *N*-phenyl(3-bromo-3-methyl)succinimide, *N*-phenyl(3-bromo-4-methyl)succinimide, *N*-phenyl(3-bromomethyl)succinimide and to study them experimentally as well as theoretically using *ab initio* methods.
2. To investigate the conditions for reversible deactivation radical polymerization of *N*-arylitacconimides with methyl methacrylate using commercially available ethyl- α -bromoisobutyrate initiator.
3. To synthesize and characterize the copolymers of *N*-arylitacconimides and methyl methacrylate using EBiB initiator with varied architectures.
4. To investigate the potential of bromo derivatives of succinimide as initiators for reversible deactivation radical polymerization of *N*-arylitacconimides with methyl methacrylate.
5. To study the mechanistic aspect of ATRP and to investigate the penultimate unit effect in ATRP of NAI-MMA monomer system using *ab initio* methods.

1.17 Plan of Thesis

The thesis comprises six chapters and each of these chapters has been described below:

1.17.1 Chapter I: Introduction

This chapter gives a literature survey about mechanism of FRP, copolymerization of NAI and MMA monomers using conventional FRP methods, drawbacks of conventional FRP

methods, different RDRP methods, synthesis of NAI monomers, copolymerization of NAI and MMA monomers using RDRP methods, computational studies on FRP, DFT and its importance in FRP. In this chapter, the gaps in existing research and objectives of the proposed work have also been discussed.

1.17.2 Chapter II: Synthesis and Characterization of *N*-arylitaconimides and Bromo Derivatives of Succinimide

It describes the synthesis and characterization of various NAI monomers viz. *N*-phenylitaconimide, *N*-(4-methylphenyl)itaconimide, *N*-(4-methoxyphenyl)itaconimide and *N*-(4-chlorophenyl)itaconimide as well as bromo derivatives of succinimide [such as *N*-phenyl(3-bromo-3-methyl)succinimide, *N*-phenyl(3-bromo-4-methyl)succinimide, *N*-phenyl(3-bromomethyl)succinimide]. The characterization of NAI monomers and bromo derivatives of succinimide was carried out using DSC, IR, ¹H-NMR spectroscopy and elemental analysis. Similarly, these compounds are also studied using DFT methods.

1.17.3 Chapter III: Synthesis and Characterization of Copolymers of *N*-arylitaconimides and Methyl Methacrylate

It describes the synthesis of copolymers of NAI and MMA monomers with two different architectures viz. random [poly(NAI-*ran*-MMA)] and block [poly(NAI-*ran*-MMA)-*b*-poly(MMA), poly(NAI-*ran*-MMA)-*b*-poly(NAI)] using ATRP process. The structural characterization of copolymers was carried out using DSC, IR, ¹H-NMR, ¹³C-NMR spectroscopy and elemental analysis. GPC was used for the molecular characterization of the obtained copolymers. Thermal characterization of the copolymers was carried out using DSC and TG/DTG techniques. Effects of pendant group on the copolymerization kinetics and properties of the copolymers have been investigated systematically.

1.17.4 Chapter IV: Investigation of Bromo Succinimides as Potential ATRP Initiators

It deals with finding of the characteristic ability of newly synthesized bromo derivatives succinimide as an ATRP initiators. Experimentally, the ATRP equilibrium constant (K_{ATRP}) values of the said compounds were determined using UV-Vis-NIR spectroscopy

with support of DOSY-NMR spectroscopy. Theoretically, the K_{ATRP} values of the said compounds along with similar alkyl halides were calculated using DFT methods. The predicted potential initiator, *N*-phenyl(3-bromo-3-methyl)succinimide, has been successfully tested for the copolymerization of NAI and MMA via AGET-ATRP process.

1.17.5 Chapter V: Mechanistic Studies of the Copolymerization of *N*-phenylitaconimide and Methyl Methacrylate via ATRP

It describes the experimental and theoretical studies of the mechanistic aspect for the atom transfer radical copolymerization of PI and MMA system. The mechanism of copolymerization of PI and MMA system was studied via microstructure analysis. The triad fractions of PI-MMA copolymer were determined using ^1H decoupled ^{13}C -NMR spectroscopy. The triad fractions for PI-MMA copolymer were also calculated for the terminal and penultimate model using DFT methods. The kinetic (k_p , E_a and A) and thermodynamic (ΔH , ΔG and K_{ATRP}) parameters were calculated for the copolymerization of PI and MMA system using DFT methods.

1.17.6 Chapter VI: Summary, Conclusions and Future Scope

This chapter contains the summary, conclusions and future scope of thesis

CHAPTER II

SYNTHESIS AND CHARACTERIZATION OF *N*-ARYLITACONIMIDES AND BROMO DERIVATIVES OF SUCCINIMIDE

2.1 Overview

This chapter describes the synthesis and characterization of *N*-arylitaconimide (NAI) monomers viz. *N*-phenylitaconimide (PI), *N*-(4-methylphenyl)itaconimide (MPI), *N*-(4-methoxyphenyl)itaconimide (MOPI), *N*-(4-chlorophenyl)itaconimide (CPI) and the bromo derivatives of succinimide viz. *N*-phenyl(3-bromo-3-methyl)succinimide (BSI-33), *N*-phenyl(3-bromo-4-methyl)succinimide (BSI-34), *N*-phenyl(3-bromomethyl)succinimide (BSI-3). The characterization of the obtained compounds was carried out using DSC, IR, ¹H-NMR, ¹³C-NMR spectroscopy and elemental analysis. The selected vibrational frequencies and ¹H-NMR (δ) values of these compounds were calculated using DFT methods and compared with the experimental results.

2.2 Experimental Section

2.2.1 Materials and Methods

Itaconic acid (99.0%), phosphorus pentoxide (95.0%), *p*-toluidine (98.0%), *p*-anisidine (98.0%), *p*-chloroaniline (95.0%), bromine (95.0%) and silica gel (60-120 mesh) for column chromatography were used as supplied. Chloroform (99.7%), acetic anhydride (98.0%) and aniline (99.5%) were distilled before use. Acetone (99.0%) was dried overnight over potassium carbonate followed by distillation. Anhydrous sodium acetate (99.5%) was obtained by fusion. Dichloromethane (DCM, 99.0%) and toluene (99.0%) were dried using fused calcium chloride and were purified by distillation. Benzoyl peroxide (95.0%) was purified from chloroform. All the above chemicals were obtained from S. D. Fine Chem Limited, Mumbai, India. HBr gas was prepared by the bromination of 1,2,3,4-tetrahydro-naphthalene (99.0%, Sigma-Aldrich, Bangalore, India) using literature procedure [244-245].

IR spectra of the NAI monomers and bromo derivatives of succinimide were recorded on a Shimadzu IR-Affinity-1, spectrophotometer in the region 4000 to 400 cm^{-1} using KBr pellet. The melting point of the compounds was determined using TGA/ DTA analyzer from TA instruments, model: SDT Q600. For this the samples were heated at the rate of 10 $^{\circ}\text{C}$ per minute in nitrogen atmosphere (flow rate = 50 $\text{cm}^3\text{min}^{-1}$). The ^1H -NMR and ^{13}C -NMR spectra of the compounds were obtained by dissolving the samples in deuterated chloroform (CDCl_3) using Bruker AV III 500 MHz FT-NMR and a Bruker DRX500 spectrometer, respectively. Chemical shifts (δ) are given relative to tetramethylsilane (TMS). Elemental analysis of the compounds was carried out using Vario Micro Cube elemental analyzer. The Oxygen analysis of compounds was carried out using Thermo Finnigan, Italy, FLASH EA 1112 series. The HRMS of the compounds were recorded using 1290 Infinity UHPLC System, 1260 infinity Nano HPLC with Chipcube, 6550 iFunnel Q-TOF.

The DFT methods were used for the calculation of selected vibrational frequencies and ^1H -NMR (δ) values of the synthesized compounds. All the geometries were fully optimized using the hybrid B3LYP exchange correlation functional with 6-31+G(d) basis set. Frequency calculations were performed for all the compounds to check (no imaginary frequencies) the stationary points as minima on the potential energy surface. A scaling factor of 0.9613 was used for frequency calculation. The Gauge-Independent Atomic Orbital method inbuilt in Gaussian09 software [246] was used for computing NMR properties of the said compounds. All the ^1H -NMR calculations were carried out with HF/ 6-311+G(2d,p) method from the B3LYP/ 6-31+G(d) optimized geometry.

2.2.2 Synthesis of Itaconic Anhydride

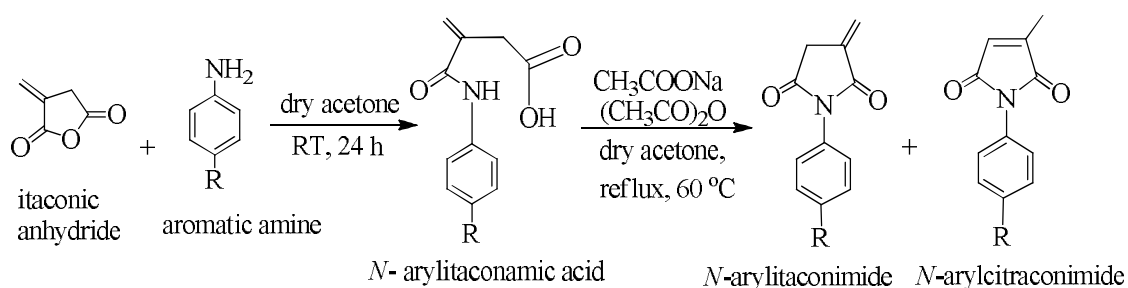
In a two-litre reaction kettle equipped with mechanical stirrer and reflux condenser, itaconic acid (0.75 mol) was dissolved in one litre of chloroform. To this solution, P_2O_5 (1.0 mol) was added and the reaction mixture was refluxed for 24 h with stirring. The reaction mixture was then decanted leaving a residue at the bottom of the kettle and the solution was concentrated using rotary vacuum evaporator. On cooling the obtained solution to 0 $^{\circ}\text{C}$, itaconic anhydride crystallizes out which was then separated by filtration followed by drying in hot air oven at 40 $^{\circ}\text{C}$. The two crops of white crystals were obtained (Yield 90%, m.p. 65 $^{\circ}\text{C}$).

2.2.3 Synthesis of *N*-arylitaconamic Acid

In a one-litre reaction kettle equipped with a mechanical stirrer, itaconic anhydride (0.25 mol) was dissolved in 100 mL of dry acetone. To this solution, aromatic amine (0.25 mol) dissolved in 100 mL of dry acetone was added slowly with vigorous stirring. The corresponding *N*-arylitaconamic acid starts precipitating out. The stirring was continued for another 12 h. The obtained precipitate was filtered, dissolved in saturated solution of sodium bicarbonate and reprecipitated with 5M HCl. The precipitate was filtered, washed with distilled water and dried in oven at 80 °C giving pure *N*-arylitaconamic acid in 55-95% yield.

2.2.4 Synthesis of NAI Monomers

To the solution of *N*-arylitaconamic acid (0.15 mol) in 100 mL of dry acetone, acetic anhydride (0.25 mol) and anhydrous sodium acetate (0.25 mol) were added. The reaction mixture was refluxed until *N*-arylitaconamic acid gets converted into the NAI monomer. The progress of reaction was monitored by thin layer chromatography. The reaction mixture was then cooled to room temperature and poured in an excess of ice cold water to precipitate the NAI monomer. The precipitate obtained was filtered and washed with saturated solution of sodium bicarbonate followed by distilled water. The product was then dried in oven at 50 °C. The crude product was purified by column chromatography using 10% ethyl acetate and 90% hexane as an eluent giving pure NAI monomer in 45-60% yield. The reaction sequence used for the synthesis of *N*-arylitaconimide monomers is shown in reaction **Scheme 2.1**.

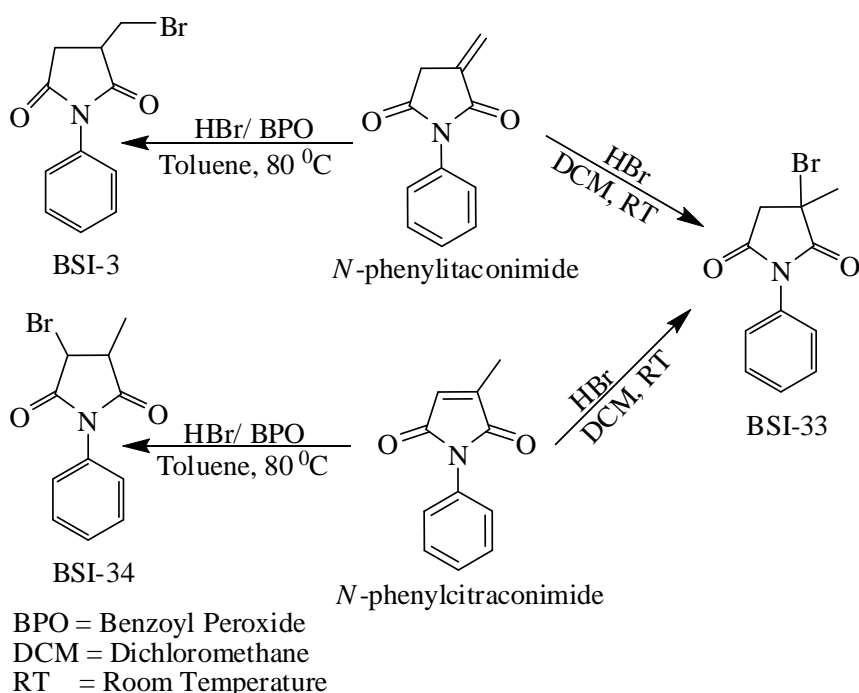


where R = -H (PI), -CH₃ (MPI), -OCH₃ (MOPI) and -Cl (CPI)

Scheme 2.1: Reaction scheme for the synthesis of NAI monomers.

2.2.5 Synthesis of Bromo Derivatives of Succinimide

The bromo derivatives of succinimide have been synthesized by the hydrobromination of PI or *N*-phenylcitraconimide with HBr gas. The hydrobromination reaction follows Markovnikov's addition (electrophilic addition) of HBr across the double bond in absence of peroxide and anti-Markovnikov's addition (free radical addition) of HBr in presence of peroxide. The reaction scheme employed for the synthesis of bromo derivatives of succinimide is shown in **Scheme 2.2**.



Scheme 2.2: Reaction scheme for synthesis of bromo derivatives of succinimide.

2.2.5.1 BSI-3

To the solution of PI (0.01 mol) in 50 mL of toluene, the HBr gas was purged for 24 h at 80 °C in presence of benzoyl peroxide. The resultant reaction mixture was stirred for another 12h. The obtained reaction mixture was concentrated by using rotary evaporator. The crude product was purified by column chromatography using petroleum ether and diethyl ether as solvent system followed by crystallization from DCM and hexane. The compound dissolved in minimum amount of DCM, and hexane was added drop wise till

the solution becomes turbid. The obtained turbid solution was then kept in ice to get the yellowish crystals of BSI-3.

2.2.5.2 BSI-34

Step I- Synthesis of *N*-phenylcitraconimide

While preparing the *N*-arylitaconimide monomers in **Section 2.2.4**, the obtained crude compound was purified by column chromatography gave *N*-phenylitaconimide (75 %) and *N*-phenylcitraconimide (25%, m.p. 100 °C).

Step II- Synthesis of BSI-34

To the solution of *N*-phenylcitraconimide (0.01 mol) in 50 mL of toluene, HBr gas was purged for 24 h at 80 °C in presence of benzoyl peroxide. The resultant reaction mixture was stirred for another 12 h. The obtained reaction mixture was concentrated by using rotary evaporator. The crude product was purified by column chromatography using petroleum ether and diethyl ether as solvent system followed by crystallization from DCM and hexane. The compound dissolved in minimum amount of DCM, and hexane was added drop wise till the solution becomes turbid. The obtained turbid solution was then kept in ice to get the yellowish crystals of BSI-34.

2.2.5.3 BSI-33

To the solution of PI or *N*-phenylcitraconimide (0.01 mol) in 50 mL of DCM, HBr gas was purged for 24 h at room temperature in absence of benzoyl peroxide. The resultant reaction mixture was stirred for another 12 h. The obtained reaction mixture was concentrated by using rotary evaporator. The crude product was purified by column chromatography using petroleum ether and diethyl ether as solvent system followed by crystallization from DCM and hexane. The compound dissolved in minimum amount of DCM, and hexane was added drop wise till the solution becomes turbid. The obtained turbid solution was then kept in ice to get the yellowish crystals of BSI-33.

2.3 Results and Discussion

2.3.1 Characterization of Itaconic Anhydride

The purified itaconic anhydride was characterized by using IR and $^1\text{H-NMR}$ spectroscopy and it is displayed in the **Figure 2.1** and **Figure 2.2**, respectively.

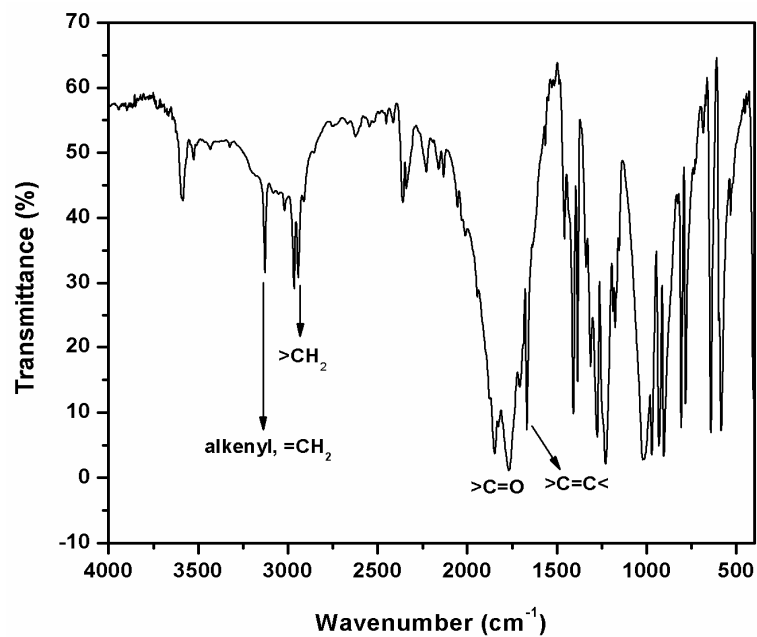


Figure 2.1: IR spectrum of itaconic anhydride.

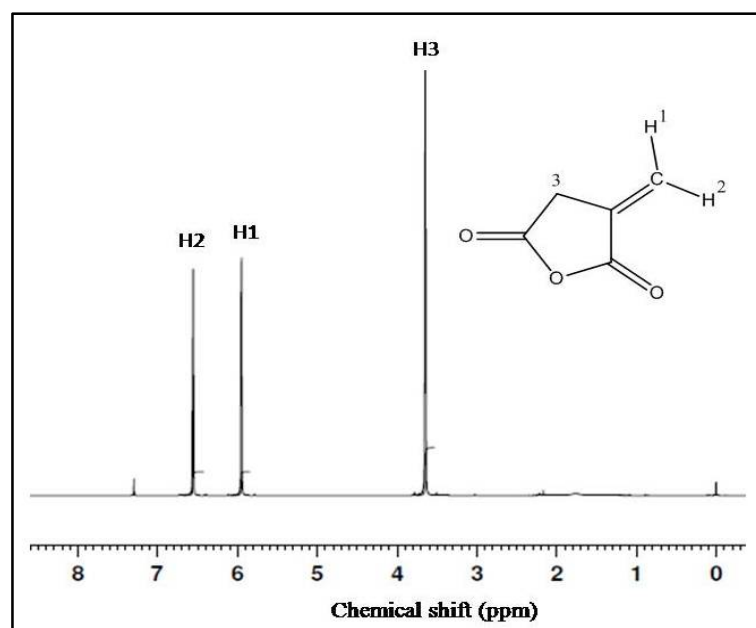


Figure 2.2: $^1\text{H-NMR}$ spectrum of itaconic anhydride.

2.3.2 Characterization of NAI Monomers

The purified NAI monomers were characterized by using DSC, IR, $^1\text{H-NMR}$ spectroscopy and elemental analysis (**Figure 2.3** to **Figure 2.6**).

2.3.2.1 PI, (Yield 50%, m.p. 118 °C)

IR (KBr, cm^{-1}): 3098 (aromatic C-H stretch), 3050 (alkenyl C-H stretch), 2994, 2955 (C-H stretch), 1789 and 1714 ($>\text{C}=\text{O}$ of imide), 1663 ($>\text{C}=\text{C}<$ stretch of double bond in ring), 1593, 1501, 1453 (aromatic $>\text{C}=\text{C}<$ stretch), 761 (oop C-H bending) [5, 14-15].

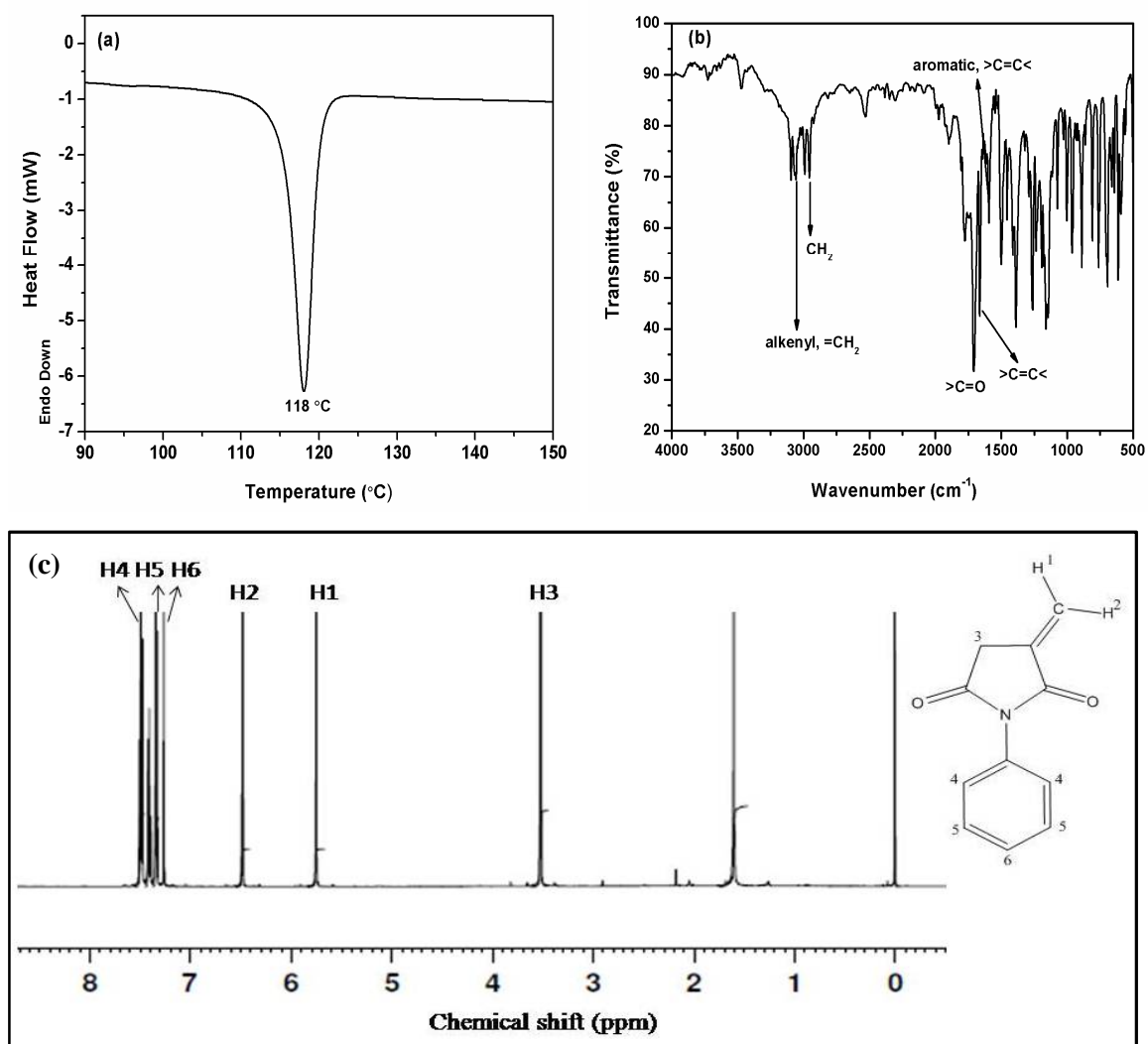


Figure 2.3: (a) DSC scan, (b) IR and (c) $^1\text{H-NMR}$ spectra of PI.

$^1\text{H-NMR}$ (CDCl_3 , ppm) δ : 7.4 (m, H4, C_6H_5), 7.3 (m, H5, C_6H_5), 7.2 (m, H6, C_6H_5), 6.4 (m, H2, of vinylic CH_2), 5.6 (m, H1, of vinylic CH_2), 3.4 (m, H3, CH_2 of ring) [5, 14-15].

Elemental analysis (CHNO): Found - %C, 71.97; %H, 4.98; %N, 7.58; %O, 16.47. Calculated - %C, 70.58; %H, 4.85; %N, 7.48; %O, 17.09.

2.3.2.2 MPI, (Yield 58%, m.p. 129 °C)

IR (KBr, cm^{-1}): 3107 (aromatic C-H stretch), 3038 (alkenyl C-H stretch), 2960, 2918 (C-H stretch), 1779 and 1706 ($>\text{C}=\text{O}$ of imide), 1666 ($>\text{C}=\text{C}<$ stretch of double bond in ring), 1588, 1511, 1458 (aromatic $>\text{C}=\text{C}<$ stretch), 798 (oop C-H bending) [5, 14-15].

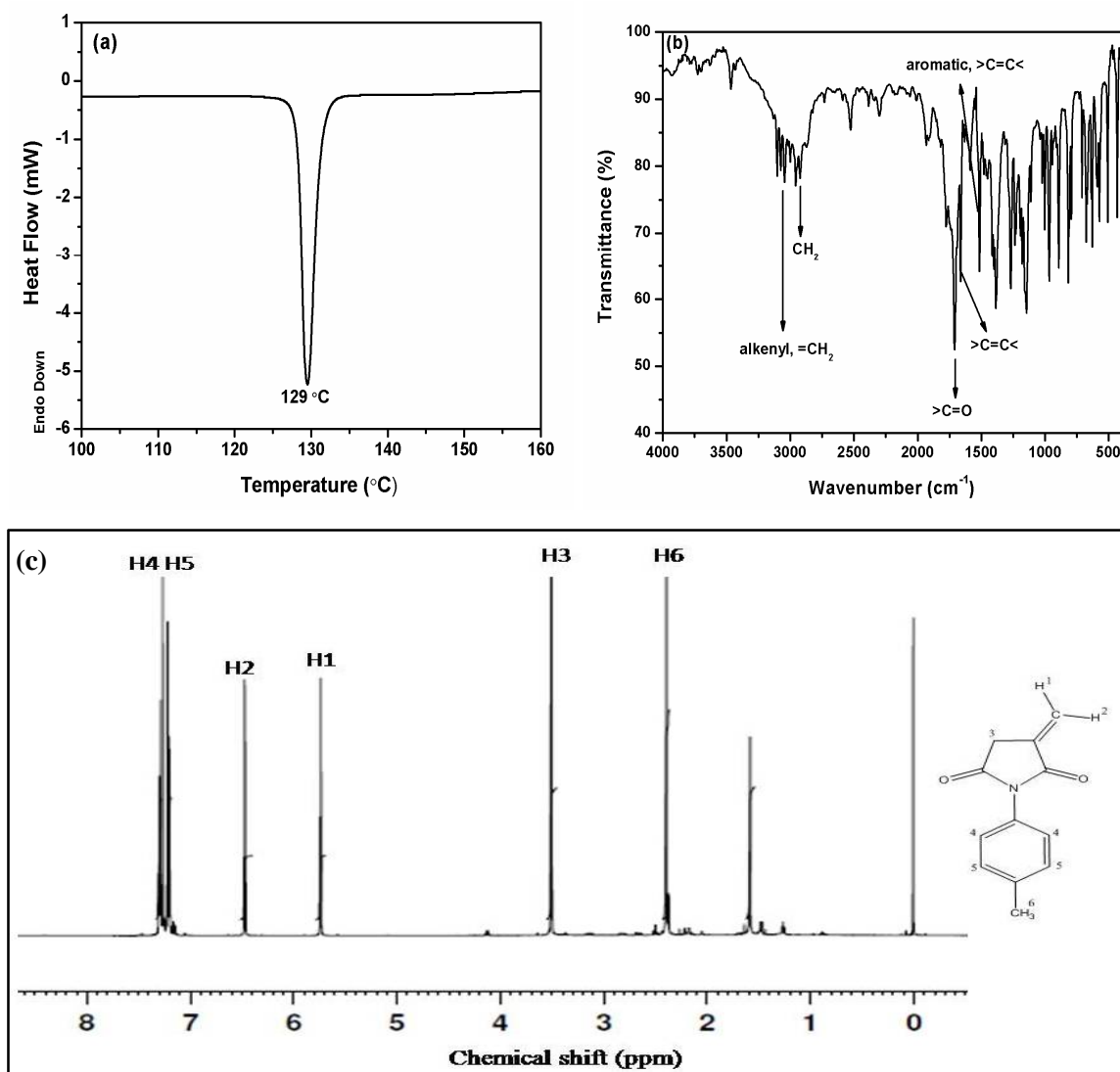


Figure 2.4: (a) DSC scan, (b) IR and (c) $^1\text{H-NMR}$ spectra of MPI.

$^1\text{H-NMR}$ (CDCl_3 , ppm) δ : 7.3 (m, H4, C_6H_5), 7.2 (m, H5, C_6H_5), 6.5 (m, H2, of vinylic CH_2), 5.7 (m, H1, of vinylic CH_2), 3.5 (m, H3, CH_2 of ring), 2.4 (m, H6, CH_3) [5, 14-15].

Elemental analysis (CHNO): Found - %C, 72.89; %H, 5.62; %N, 7.05; %O, 14.44. Calculated - %C, 71.63; %H, 5.51; %N, 6.96; %O, 15.90.

2.3.2.3 MOPI, (Yield 54%, m.p. 115 °C)

IR (KBr, cm^{-1}): 3099 (aromatic C-H stretch), 3066 (alkenyl C-H stretch), 2990, 2971 (C-H stretch), 1778 and 1708 ($>\text{C}=\text{O}$ of imide), 1658 ($>\text{C}=\text{C}<$ stretch of double bond in ring), 1609, 1519, 1468 (aromatic $>\text{C}=\text{C}<$ stretch), 791 (oop C-H bending) [19-20].

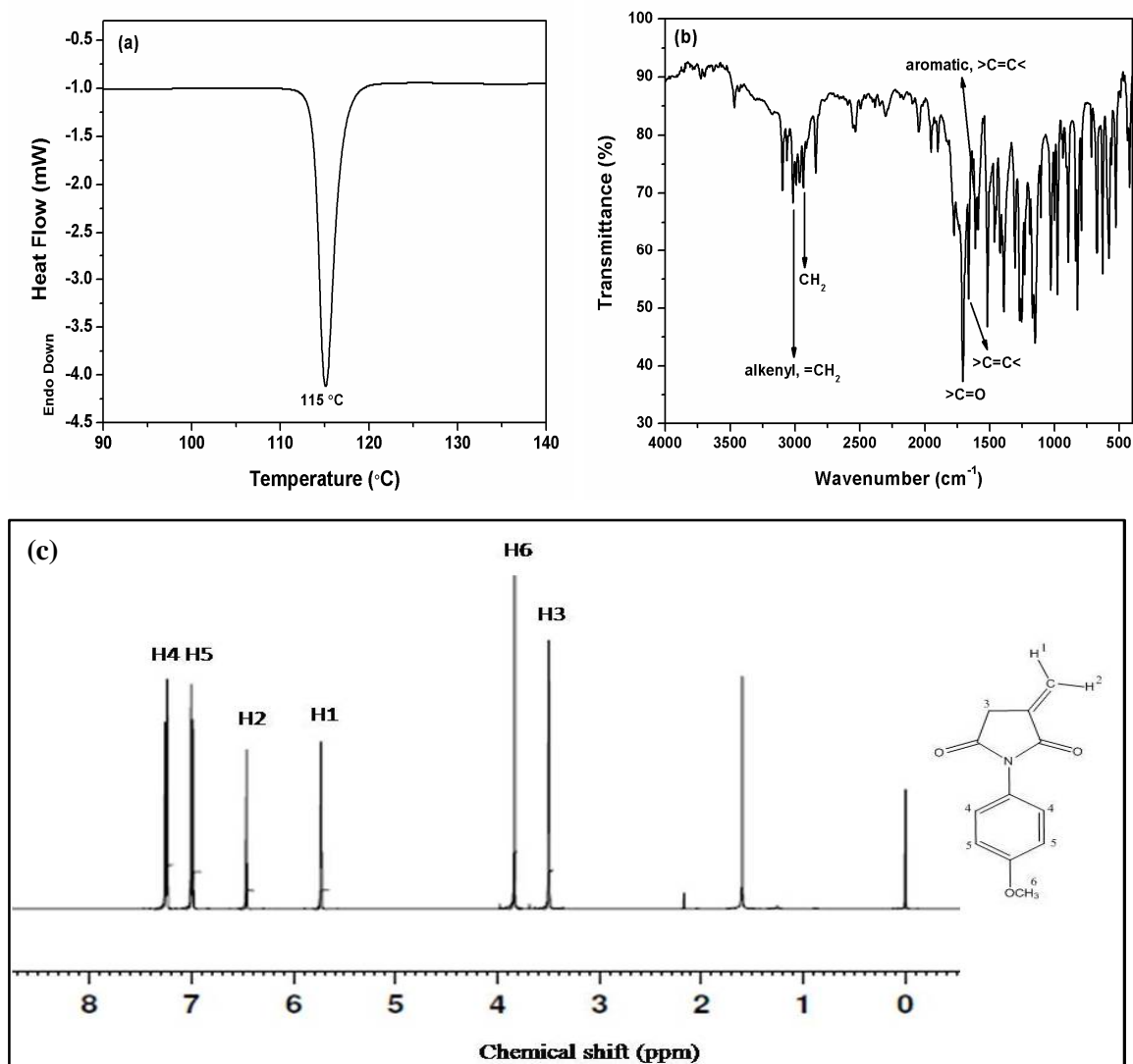


Figure 2.5: (a) DSC scan, (b) IR and (c) $^1\text{H-NMR}$ spectra of MOPI.

$^1\text{H-NMR}$ (CDCl_3 , ppm) δ : 7.2 (m, H4, C_6H_5), 7.0 (m, H5, C_6H_5), 6.5 (m, H2, of vinylic CH_2), 5.7 (m, H1, of vinylic CH_2), 3.8 (m, H6, OCH_3) 3.5 (m, H3, CH_2 of ring) [19-20].

Elemental analysis (CHNO): Found - %C, 67.99; %H, 5.26; %N, 6.58; %O, 21.17. Calculated - %C, 66.35; %H, 5.10; %N, 6.45; %O, 22.10.

2.3.2.4 CPI, (Yield 34%, m.p. 132 °C)

IR (KBr, cm^{-1}): 3099 (aromatic C-H stretch), 3064 (alkenyl C-H stretch), 2998, 2962 (C-H stretch), 1782 and 1717 ($>\text{C}=\text{O}$ of imide), 1665 ($>\text{C}=\text{C}<$ stretch of double bond in ring), 1578, 1505, 1409 (aromatic $>\text{C}=\text{C}<$ stretch), 740 (C-Cl stretch) [5, 14-15].

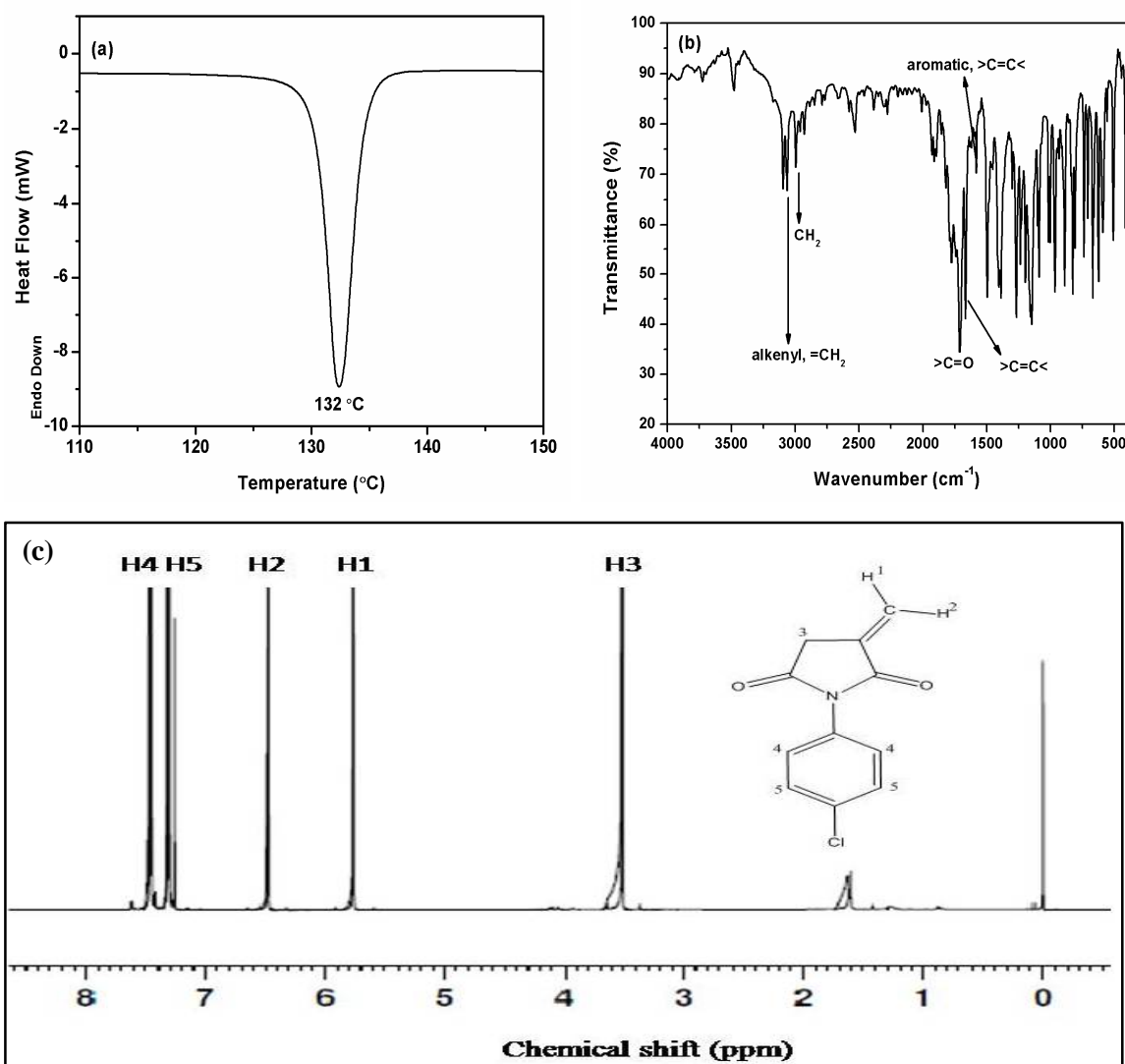


Figure 2.6: (a) DSC scan, (b) IR and (c) $^1\text{H-NMR}$ spectra of CPI.

$^1\text{H-NMR}$ (CDCl_3 , ppm) δ : 7.5 (m, H4, C_6H_5), 7.3 (m, H5, C_6H_5), 6.5 (m, H2, of vinylic CH_2), 5.8 (m, H1, of vinylic CH_2), 3.5 (m, H3, CH_2 of ring) [5, 14-15].

Elemental analysis (CHNO): Found - %C, 60.81; %H, 3.73; %N, 6.40; %O, 20.21.
Calculated - %C, 59.61; %H, 3.64; %N, 6.32; %O, 20.22.

2.3.3 Characterization of *N*-phenylcitraconimide

The IR and $^1\text{H-NMR}$ spectra of *N*-phenylcitraconimide is given in **Figure 2.7**.

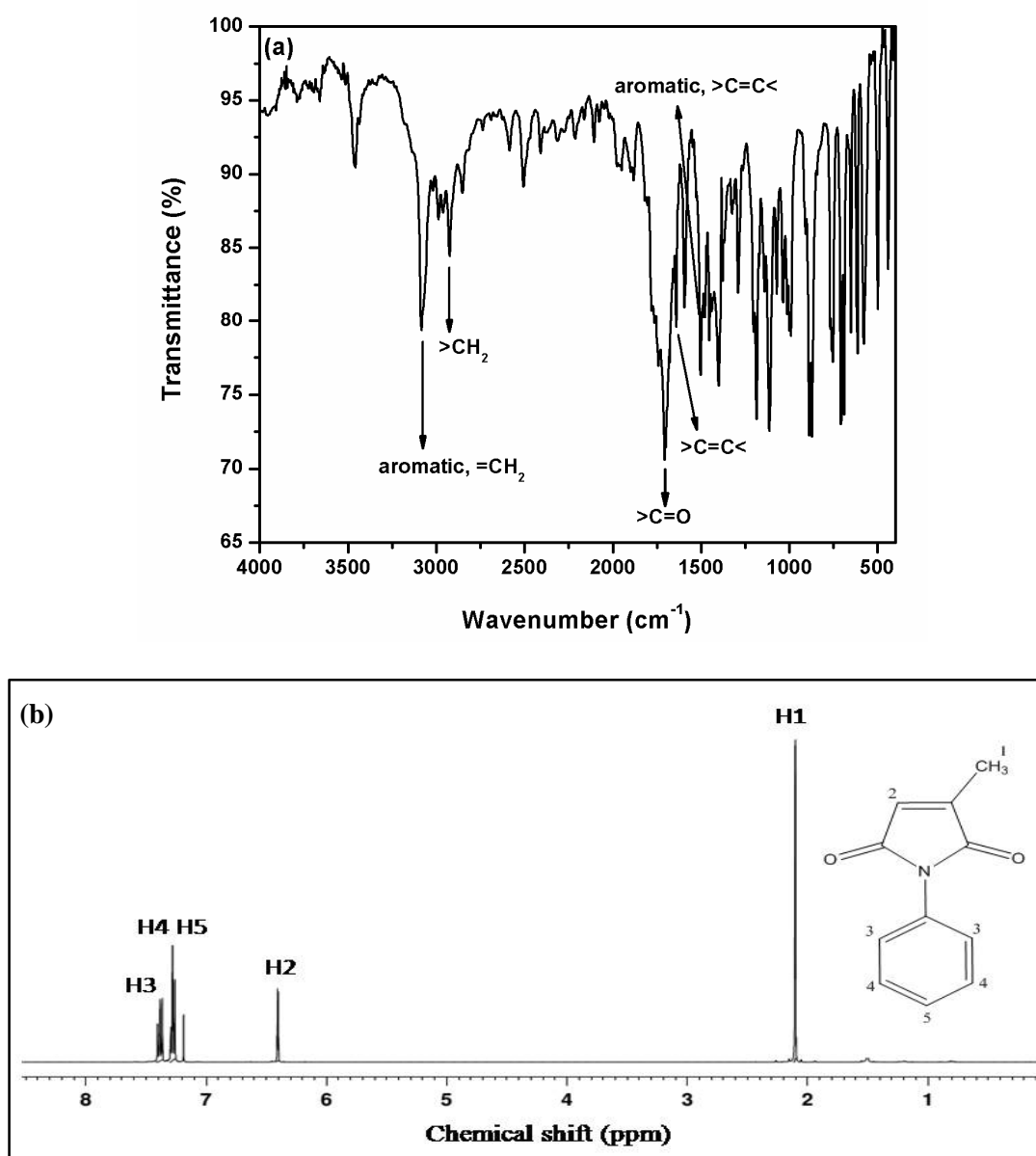


Figure 2.7: (a) IR and (b) $^1\text{H-NMR}$ spectra of *N*-phenylcitraconimide.

IR (KBr, cm^{-1}): 3082 (aromatic C-H stretch), 3069 (alkenyl C-H stretch), 2923 (C-H stretch), 1717 and 1701 ($>\text{C}=\text{O}$ of imide), 1641 ($>\text{C}=\text{C}<$ stretch of double bond in ring), 1593, 1505, 1409 (aromatic $>\text{C}=\text{C}<$ stretch), 876 (oop C-H bending).

$^1\text{H-NMR}$ (CDCl_3) δ : 7.4 (m, H3, C_6H_5), 7.3 (m, H4, C_6H_5), 7.2 (m, H5, C_6H_5), 6.4 (q, H2, of CH), 2.1 (d, H1, of CH_3).

Elemental analysis (CHNO): Found - %C, 71.69; %H, 4.88; %N, 7.52; %O, 16.67. Calculated - %C, 70.58; %H, 4.85; %N, 7.48; %O, 17.09.

2.3.4 Characterization of Bromo Derivatives of Succinimide

The purified BSI-3, BSI-34 and BSI-33 were characterized using DSC, IR, $^1\text{H-NMR}$, $^{13}\text{C-NMR}$ spectroscopy, HRMS and elemental analysis (**Figure 2.8** to **Figure 2.10**).

2.3.4.1 BSI-3 (Yield 50%, *m.p.* 179 °C)

IR (KBr, cm^{-1}): 3069 (aromatic C-H stretch), 1784, and 1703 ($>\text{C}=\text{O}$ of imide), 1590, 1491, and 1447 (aromatic $>\text{C}=\text{C}<$ stretch), 758 (oop C-H bending), 595 (C-Br stretch).

$^1\text{H-NMR}$ (CDCl_3) δ : 7.3 (m, H4, C_6H_5), 7.4 (m, H5, C_6H_5), 7.5 (m, H6, C_6H_5), 4.0 (dd, H1', $^1\text{J} = 8.4$ Hz, $^2\text{J} = 4.5$ Hz, CH_2), 3.7 (dd, H1, $^1\text{J} = 8.4$ Hz, $^2\text{J} = 3.5$ Hz, CH_2), 3.5 (m, H2, CH), 2.9 (dd, H3', $^1\text{J} = 14.8$ Hz, $^2\text{J} = 5.0$ Hz, CH_2), 3.1 (dd, H3, $^1\text{J} = 14.8$ Hz, $^2\text{J} = 9.5$ Hz, CH_2).

$^{13}\text{C-NMR}$ (125 MHz, CDCl_3) δ : 175.81 and 174.52 ($>\text{C}=\text{O}$), 129.33, 128.97, 128.52, and 131.74 (C_6H_5), 41.20 (CH_2Br), 33.38 (CH), 32.32 (CH_2).

Elemental analysis (CHNOBr): Found - %C, 49.02; %H, 3.71; %N, 5.13; %O, 11.88; %Br, 30.26. Calculated - %C, 49.28; %H, 3.76; %N, 5.22; %O, 11.94; %Br, 29.80.

HRMS (EI): (m/z) 267.7751 ($[\text{M}]^+$; 95%), 269.4687 ($[\text{M}+2]^+$; 90%); Calculated mass for $\text{C}_{11}\text{H}_{10}\text{O}_2\text{Br}$; 268.1066, Observed mass for $\text{C}_{11}\text{H}_{10}\text{NO}_2\text{Br}$; 268.6219.

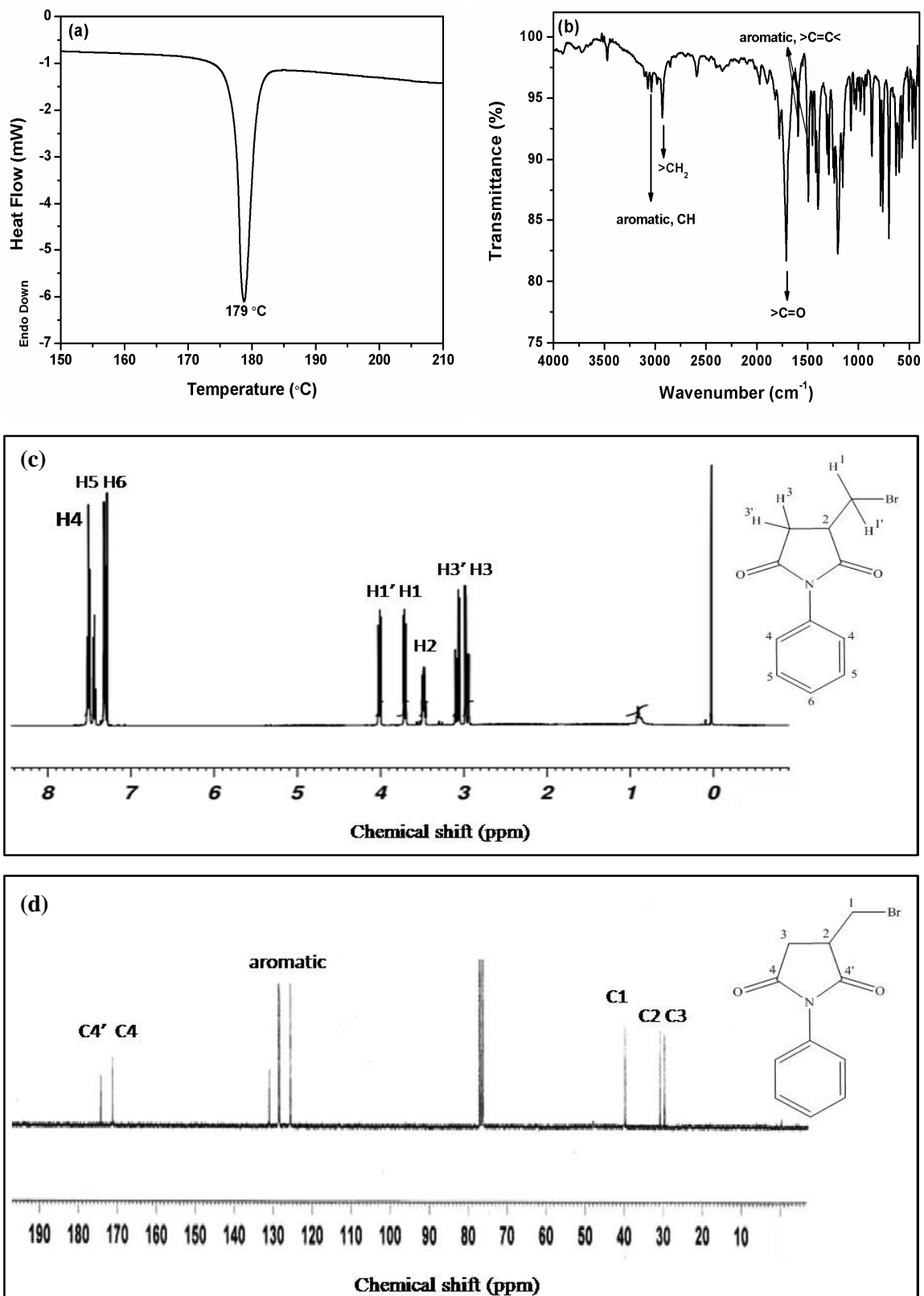


Figure 2.8: (a) DSC scan, (b) IR, (c) ¹H-NMR and (d) ¹³C-NMR of BSI-3.

2.3.4.2 BSI-34 (Yield 65%, m.p. 119 °C)

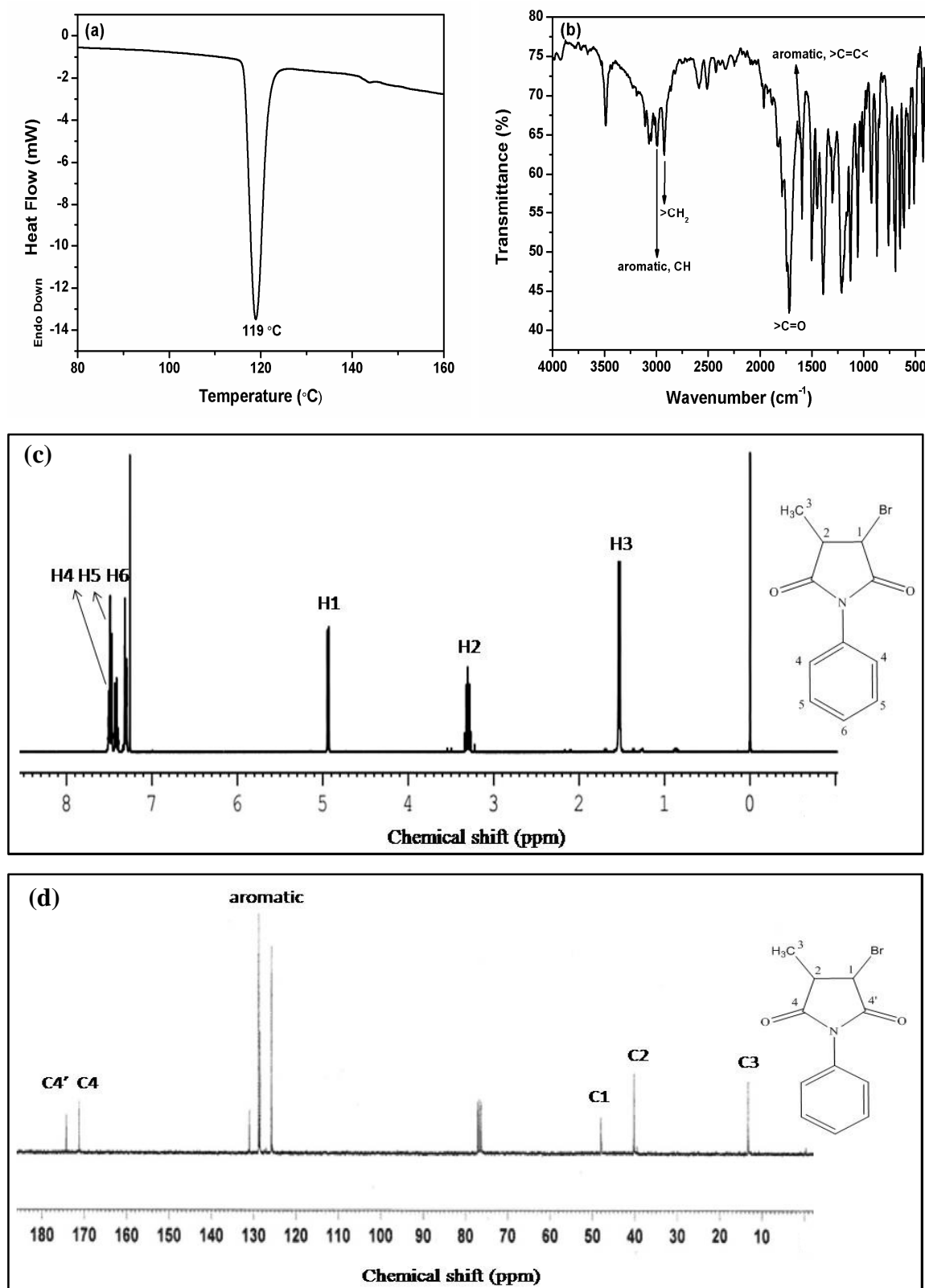


Figure 2.9: (a) DSC scan, (b) IR, (c) ¹H-NMR and (d) ¹³C-NMR of BSI-34.

IR (KBr, cm^{-1}): 3077 (aromatic C-H stretch), 1791 and 1716 ($>\text{C}=\text{O}$ of imide), 1591, 1501 and 1444 (aromatic $>\text{C}=\text{C}<$ stretch), 763 (oop C-H bending), 520 (C-Br stretch).

$^1\text{H-NMR}$ (CDCl_3) δ : 7.3 (m, H4, C_6H_5), 7.4 (m, H5, C_6H_5), 7.5 (m, H6, C_6H_5), 4.9 (d, H1, $^2\text{J} = 7.6$ Hz, CH), 3.3 (m, H2, CH), 1.5 (d, H3, $^2\text{J} = 7.2$ Hz, CH_3).

$^{13}\text{C-NMR}$ (125 MHz, CDCl_3) δ : 174.74 and 171.65 ($>\text{C}=\text{O}$), 131.45, 129.37, 129.07 and 126.28 (C_6H_5), 48.29 (C-Br), 40.68 (CH), 14.47 (CH_3).

Elemental analysis (CHNOBr): Found - %C, 49.27; %H, 3.76; %N, 5.04; %O, 11.92; %Br, 30.01. Calculated - %C, 49.28; %H, 3.76; %N, 5.22; %O, 11.94; %Br, 29.80.

HRMS (EI): (m/z) 267.9651 ($[\text{M}]^+$; 60%), 269.4657 ($[\text{M}+2]^+$; 60%); Calculated mass for $\text{C}_{11}\text{H}_{10}\text{NO}_2\text{Br}$; 268.1066, Observed mass for $\text{C}_{11}\text{H}_{10}\text{NO}_2\text{Br}$; 268.7154.

2.3.4.3 BSI-33 (Yield 65%, *m.p.* 114 °C)

IR (KBr, cm^{-1}): 3048 (aromatic C-H stretch), 1751 and 1714 ($>\text{C}=\text{O}$ of imide), 1591, 1501 and 1452 (aromatic $>\text{C}=\text{C}<$ stretch), 760 (oop C-H bending), 512 (C-Br stretch).

$^1\text{H-NMR}$ (CDCl_3) δ : 7.5 (m, 2 H, C_6H_5), 7.4 (m, 2 H, C_6H_5), 7.3 (m, 1 H, C_6H_5), 3.5 (d, 1 H, $^1\text{J} = 18.8$ Hz, CH_2), 3.2 (d, 1 H, $^1\text{J} = 18.8$ Hz, CH_2), 2.1 (s, 3 H, CH_3).

$^{13}\text{C-NMR}$ (125 MHz, CDCl_3) δ : 174.74 and 171.65 ($>\text{C}=\text{O}$), 131.47, 129.34, 129.04 and 126.26 (C_6H_5), 51.29 (C-Br), 47.68 (CH_2), 27.47 (CH_3).

Elemental Analysis (CHNOBr): Found - %C, 50; %H, 3.82; %N, 5.36; %O, 12.05 %Br, 28.77. Calculated - %C, 49.28; %H, 3.76; %N, 5.22; %O, 11.94; %Br, 29.80.

HRMS (EI): (m/z) 267.8351 ($[\text{M}]^+$; 25%), 269.4401 ($[\text{M}+2]^+$; 25%); Calculated mass for $\text{C}_{11}\text{H}_{10}\text{NO}_2\text{Br}$; 268.1066, Observed mass for $\text{C}_{11}\text{H}_{10}\text{NO}_2\text{Br}$; 268.5376.

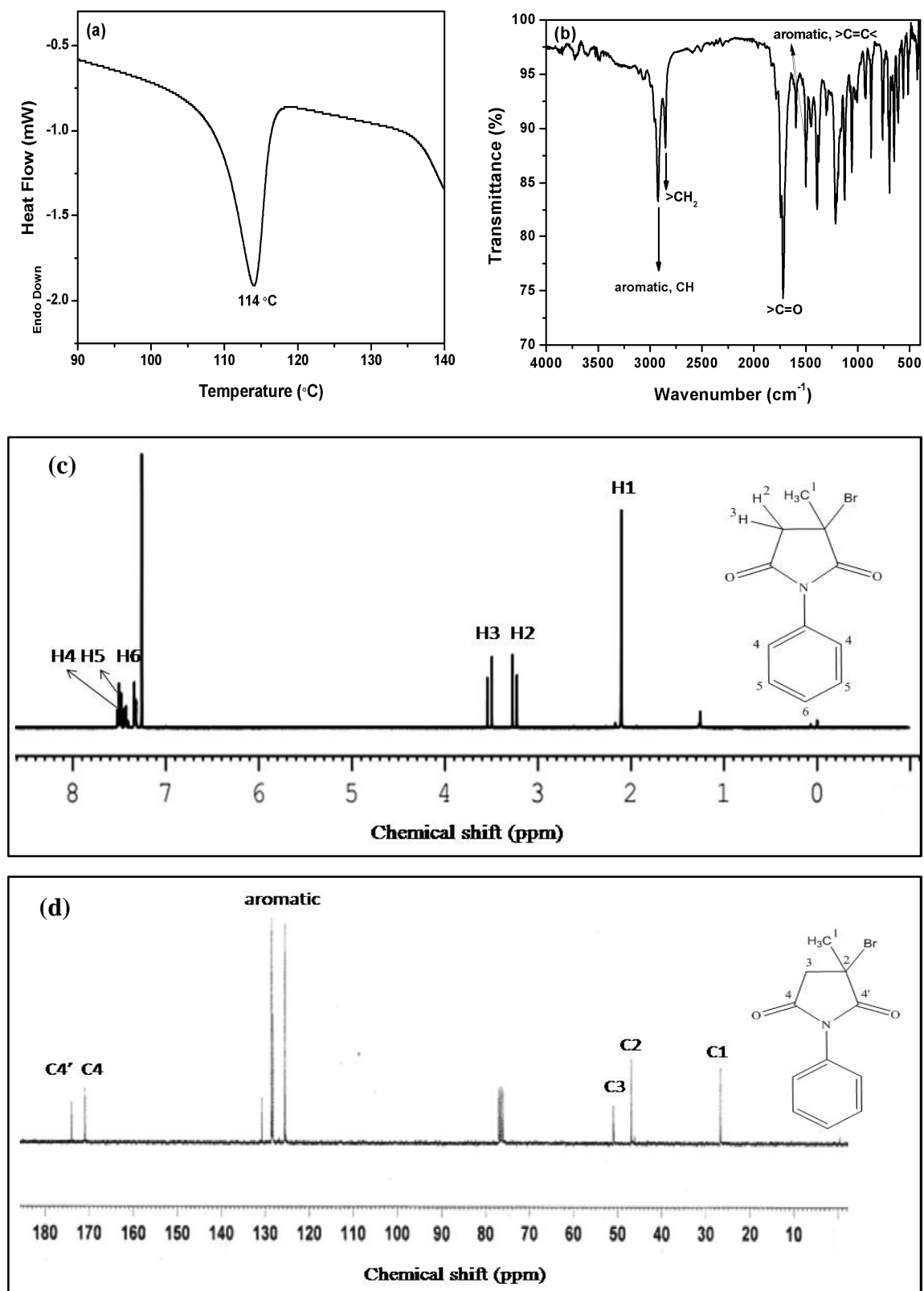
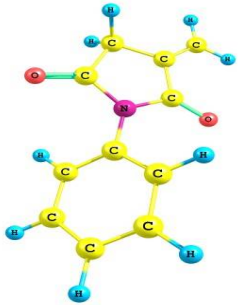
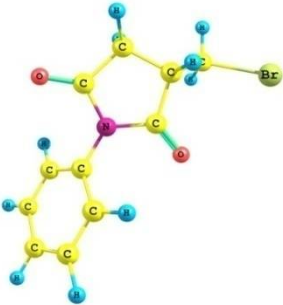
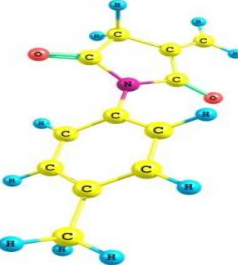
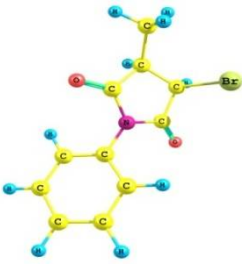
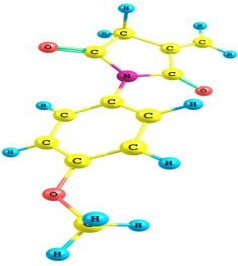
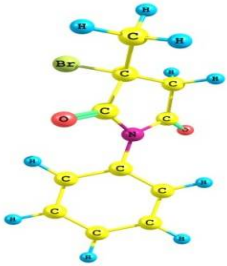
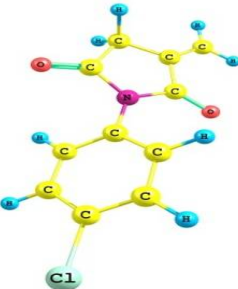


Figure 2.10: (a) DSC scan, (b) IR, (c) ¹H-NMR and (d) ¹³C-NMR of BSI-33.

The selected vibrational frequencies and $^1\text{H-NMR}$ (δ) values of the synthesized compounds have been studied using DFT methods. For this the geometry of the NAI monomers and bromo derivatives of succinimide was fully optimized using B3LYP/ 6-31+G(d) level. The optimized geometries of the compounds are given in the **Table 2.1**.

Table 2.1: B3LYP/ 6-31+G(d) optimized geometries of the NAI monomers and bromo derivatives of succinimide.

Optimized geometry of NAI monomers		Optimized geometry of bromo derivatives of succinimide	
PI		BSI-3	
MPI		BSI-34	
MOPI		BSI-33	
CPI			

To check (no imaginary frequencies) the stationary points as minima on the potential energy surface, the frequency calculations were performed for all NAI monomers and bromo derivatives of succinimide. The $^1\text{H-NMR}$ (δ) values of the synthesized compounds were calculated using TMS as an internal standard in gas phase at 25 °C. The calculated vibrational frequencies and $^1\text{H-NMR}$ (δ) values of the compounds were compared with the experimentally obtained values as given below:

2.3.5 Vibrational Frequencies of NAI Monomers

The experimentally found and theoretically calculated vibrational frequencies (selected bond) for all the NAI monomers are given in **Table 2.2** and correlation plot between the experimentally (Ex.) found and theoretically (Th.) calculated values of selected vibrational frequencies is given in **Figure 2.11**.

Table 2.2: Experimentally found and theoretically calculated vibrational frequency values (cm^{-1}) of NAI monomers.

Nature of bond	PI		MPI		MOPI		CPI	
	Ex.	Th.	Ex.	Th.	Ex.	Th.	Ex.	Th.
Aromatic C-H stretch	3098	3107	3107	3119	3099	3111	3199	3220
Alkenyl C-H stretch	3050	3046	3038	3040	3066	3068	3164	3219
Alkyl C-H stretch	2994 2955	2982 2948	2960 2918	2982 2947	2990 2971	3089 3028	2998 2962	3102 3067
>C=O of imide	1789 1714	1766 1713	1775 1706	1835 1780	1775 1708	1834 1779	1775 1717	1837 1782
>C=C< stretch	1663	1661	1666	1727	1658	1727	1665	1727
Aromatic >C=C< stretch	1593 1501 1453	1614 1504 1496	1588 1511 1458	1663 1629 1557	1609 1519 1468	1663 1630 1556	1578 1505 1409	1645 1627 1536
oop C-H bending	761	768	798	806	791	816	807	812

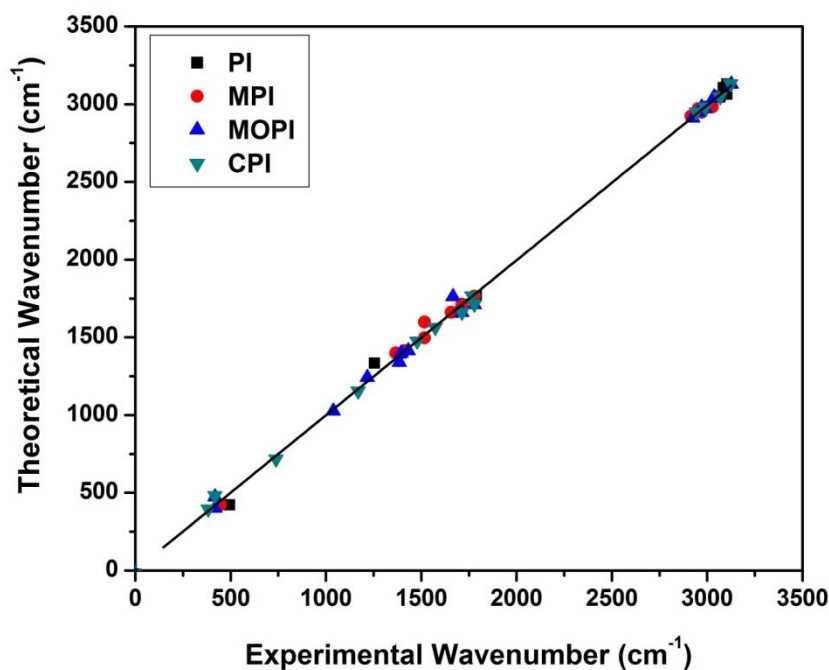


Figure 2.11: Correlation plot of experimentally found and theoretically calculated IR frequencies of NAI monomers.

2.3.6 Vibrational Frequencies of Bromo Derivatives of Succinimide

The experimentally found and theoretically calculated vibrational frequencies (selected bond) for the bromo derivatives of succinimide are given in **Table 2.3** and correlation plot between the experimentally found and theoretically calculated values of selected vibrational frequencies of bromo derivatives of succinimide is given in **Figure 2.12**.

Table 2.3: Experimentally found and theoretically calculated vibrational frequency values (cm^{-1}) of bromo derivatives of succinimide.

Nature of bond	BSI-3		BSI-34		BSI-33	
	Ex.	Th.	Ex.	Th.	Ex.	Th.
Aromatic C-H stretch	3069	3064	3077	3070	3048	3040
Aromatic C=C stretch	1590	1588	1591	1588	1591	1579
	1494	1512	1501	1509	1501	1588
	1447	1437	1444	1481	1452	1481
Alkyl C-H stretch	-	-	3004	3034	3010	3004
	-	-	2953	2953	2934	2935
Methylene	3013	3009	-	-	3072	3037

C-H stretch	2985	2937			2925	2929
Methyne C-H stretch	2985 2931	2942 2937	3051 2886	3061 2852	-	-
>C=O of imide	1784 1703	1718 1777	1791 1716	1779 1721	1751 1714	1779 1720
C-H bending	758	765	763	770	760	765
C-Br stretch	595	601	520	519	512	496

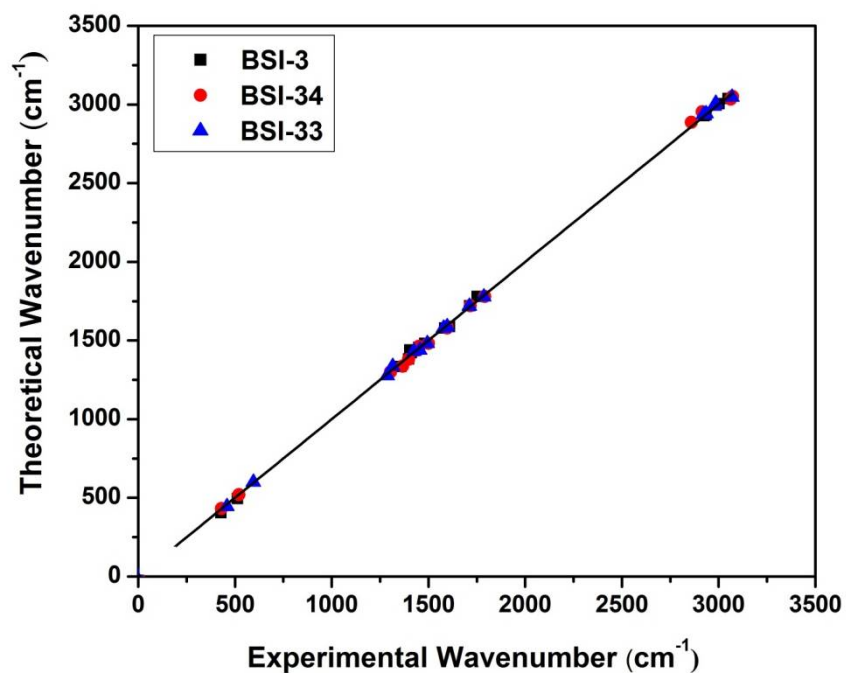


Figure 2.12: Correlation plot of experimentally found and theoretically calculated IR frequencies of bromo derivatives of succinimide.

2.3.7 $^1\text{H-NMR}$ (δ) Values of NAI Monomers

The experimentally found and theoretically calculated $^1\text{H-NMR}$ (δ) values for all the NAI monomers are given in **Table 2.4**. The correlation plot between the experimentally found and theoretically calculated $^1\text{H-NMR}$ (δ) values for monomers are shown in **Figure 2.13**.

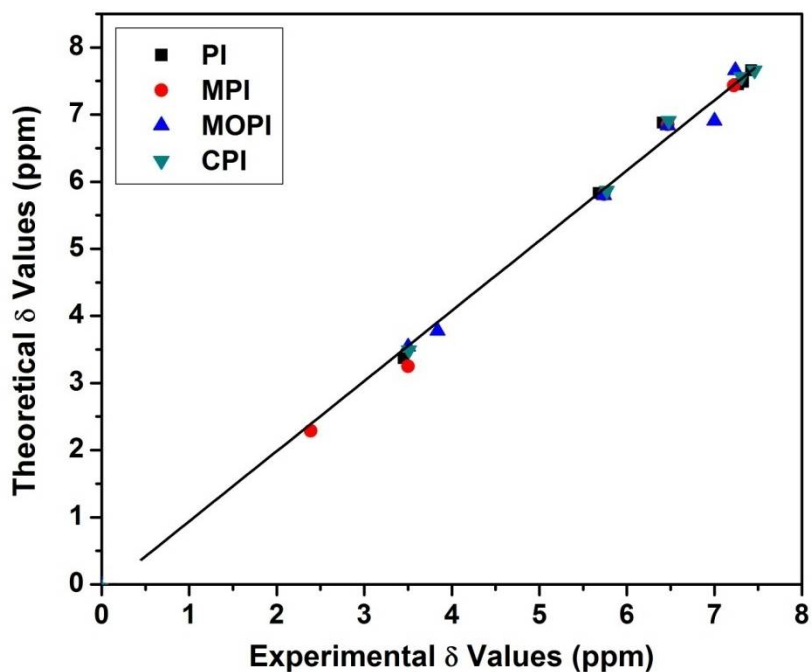


Figure 2.13: Correlation plot of experimentally found and theoretically calculated ^1H -NMR (δ) values of NAI monomers.

Table 2.4: Experimentally found and theoretically calculated ^1H -NMR (δ) values (ppm) of NAI monomers.

NAI monomer	Methylene Protons		Vinyl Protons		Methyl Protons		Methoxy Protons		Phenyl Protons	
	Ex.	Th.	Ex.	Th.	Ex.	Th.	Ex.	Th.	Ex.	Th.
PI	3.45	3.41	6.41 5.68	6.88 5.83	-	-	-	-	7.42 7.33 7.27	7.65 7.64 7.49
MPI	3.50	3.47	6.47 5.74	6.85 5.81	2.39	2.37	-	-	7.32 7.22	7.37 7.27
MOPI	3.50	3.52 3.02	6.47 5.74	6.84 5.80	-	-	3.84	3.58	7.24 7.00	7.64 7.10
CPI	3.09	3.11	6.40 5.70	6.91 5.87	-	-	-	-	7.46 7.31	7.65 7.55

2.3.8 ^1H -NMR (δ) Values of Bromo Derivatives of Succinimide

The experimentally found and theoretically calculated ^1H -NMR (δ) values for bromo derivatives of succinimide are given in **Table 2.5** and correlation plot between the

experimentally found and theoretically calculated $^1\text{H-NMR}$ (δ) values is shown in **Figure 2.14**.

Table 2.5: Experimentally found and theoretically calculated $^1\text{H-NMR}$ (δ) values (ppm) of bromo derivatives of succinimide.

Bromo derivatives of succinimide	Methyl protons		Methylene protons		Methyne protons		Phenyl protons	
	Ex.	Th.	Ex.	Th.	Ex.	Th.	Ex.	Th.
BSI-3	-	-	4.02	3.94	3.49	3.40	7.52	7.54
	-	-	3.71	3.80	-	-	7.44	7.48
	-	-	3.09	3.05	-	-	7.31	7.46
	-	-	2.95	2.94	-	-	-	-
BSI-34	1.53	1.23	-	-	4.93	4.78	7.50	7.53
	-	-	-	-	3.31	3.15	7.43	7.47
	-	-	-	-	-	-	7.30	7.42
BSI-33	2.11	2.05	3.53	3.45	-	-	7.51	7.58
	-	-	3.25	3.18	-	-	7.48	7.47
	-	-	-	-	-	-	7.33	7.52

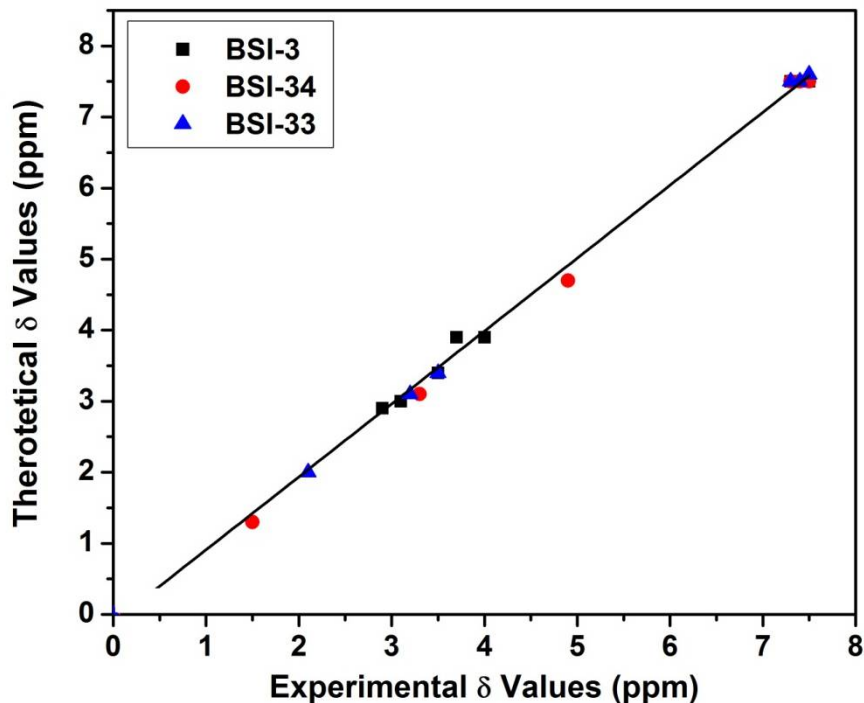


Figure 2.14: Correlation plot of experimentally found and theoretically calculated $^1\text{H-NMR}$ (δ) values of bromo derivatives of succinimide.

2.4 Conclusions

The synthesis and characterization of different NAI monomers and bromo derivatives of succinimide have been carried out successfully. A good correlation was obtained between the experimentally found and theoretically calculated vibrational frequencies and $^1\text{H-NMR}$ (δ) values of the synthesized compounds. This supports that the chosen DFT method of calculation is quite appropriate for further studies.

CHAPTER III

SYNTHESIS AND CHARACTERIZATION OF COPOLYMERS OF *N*-ARYLITACONIMIDES AND METHYL METHACRYLATE

3.1 Overview

This chapter describes the synthesis of copolymers of NAI monomers (such as PI, MPI, MOPI, CPI) and MMA with two different architectures viz. random [poly(NAI-*ran*-MMA)] and block [poly(NAI-*ran*-MMA)-*b*-poly(MMA), poly(NAI-*ran*-MMA)-*b*-poly(NAI)] using ATRP methodology. The effects of the pendant groups were also investigated by using the NAI monomers with various substituent on the aromatic ring. The substituent on the aromatic ring of NAI varied from strongly activating groups such as $-\text{OCH}_3$ to weakly deactivating group $-\text{Cl}$. Various properties of the poly(NAI-*ran*-MMA) copolymers synthesized via normal-ATRP (n-ATRP) and AGET-ATRP were compared. The structural characterization of copolymers was carried out using IR, ^1H -NMR, ^{13}C -NMR spectroscopy and elemental analysis. The molecular and thermal characterization of copolymers was carried out by using GPC and DSC/ TGA, respectively.

3.2 Experimental Section

3.2.1 Materials and Methods

2,2'-bipyridine (Bpy) (99.5%) was used as supplied. MMA (99.0%) was purified by washing with 5% NaOH solution to remove the inhibitor, followed by repeated washing with distilled water until it became neutral. It was then kept on anhydrous magnesium sulfate to remove the traces of water, followed by vacuum distillation with calcium hydride. Acetone (99.0%) was purified by distillation. The above chemicals were obtained from S. D. Fine Chem Limited, Mumbai, India. Ethyl- α -bromoisobutyrate (EBiB) (98.0%), CuBr_2 (99.9%) and $\text{Sn}(\text{EH})_2$ (95.0%) were used as supplied. CuBr (99.9%) was purified by stirring overnight in glacial acetic acid and washing with absolute ethanol and diethyl ether, followed by drying under vacuum. These chemical

were purchased from Sigma-Aldrich Chemicals Private Limited, Bangalore, India). Anisole (99.0%, SRL Private limited, Mumbai, India) was purified by washing with 5% NaOH solution and then with distilled water. It was then kept on anhydrous potassium carbonate to remove the traces of water followed by vacuum distillation over sodium benzophenone.

IR spectra of the copolymers were recorded on a Shimadzu IR-Affinity-1, FT-IR spectrophotometer in the region 4000 to 400 cm^{-1} using KBr pellet. The ^1H and ^{13}C -NMR spectra of the copolymers were recorded on a Bruker AV III 500 MHz with an operating frequency of 500.13 MHz for ^1H and 125.75 MHz for ^{13}C , which is equipped with a 5mm broadband gradient probe. Chemical shifts are reported in ppm relative to TMS in CDCl_3 . Elemental analysis of the copolymers was performed using Vario Micro Cube elemental analyzer. The instrument provides an elemental detection limit of < 50 ppm with error limit for standard compounds is in the range of $\pm 0.01\%$ to $\pm 0.10\%$. The analysis has been done using 2 ± 0.05 mg of powdered samples. The Oxygen analysis of copolymers was carried out using Thermo Finnigan, Italy, FLASH EA 1112 series. The elemental analysis for copolymer has been repeated twice. Molecular-mass characteristics of the copolymers were determined by GPC in THF as an eluent at flow rate of 0.75 mL per minute and column temperature of 25 $^\circ\text{C}$ with an Agilent 1260 HPLC-GPC system equipped with column: PL gel 5 micron Mixed D: 300 mm \times 7.5 mm with a differential refractometer. Polystyrene standards with molecular weight in the range of 10^3 to 10^5 gmol^{-1} were used for calibration. Thermal characterization of copolymers was carried out using TGA/ DTA analyzer from TA Instruments, model: SDT Q600. DSC scans were recorded in nitrogen atmosphere (flow rate = 60 $\text{cm}^3\text{min}^{-1}$) at heating rate of 10 $^\circ\text{C}$ per minute using 3 ± 1 mg of powdered samples. For the uniform thermal history, all the samples were first heated to 150 $^\circ\text{C}$, cooled to room temperature and then again heated to 600 $^\circ\text{C}$. The second heating scan was used for the determination of glass transition of copolymer. Thermal stability was determined by recording TG/ DTG curves in nitrogen atmosphere (flow rate = 60 $\text{cm}^3\text{min}^{-1}$) at heating rate of 10 $^\circ\text{C}$ per minute using 3 ± 1 mg of powdered samples. The DTG plots (dy/dx) of the copolymers were obtained by taking the ratios of difference of weight loss (in percentage) (dy) with respect to the difference of temperature (dx).

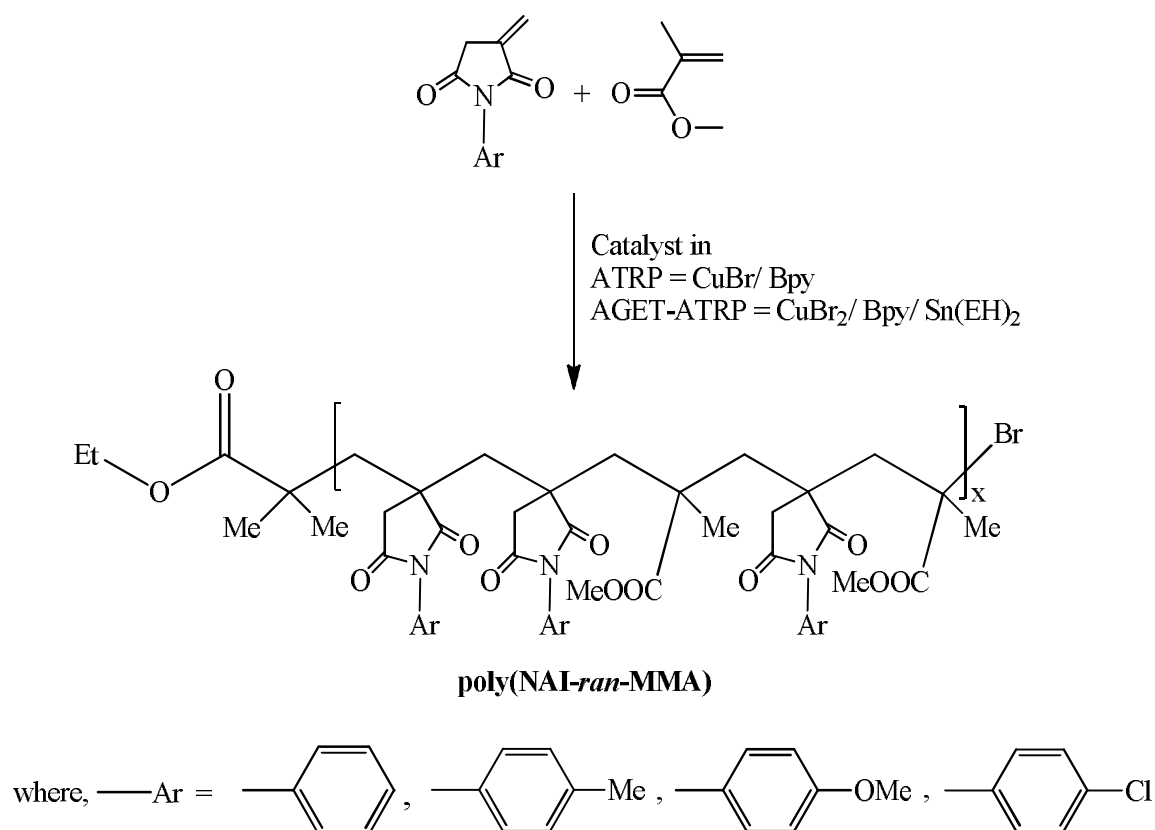
3.2.2 Synthesis of Random Copolymers of NAI and MMA via n-ATRP

The solution of NAI (0.01 mol) and MMA (0.04 mol) in dry anisole (10 mL) were taken in reaction flask equipped with reflux condenser and a magnetic bead. In this reaction mixture, CuBr (0.25 mmol) and Bpy (0.75 mmol) were added. The reaction mixture was subjected to freeze-vacuum-thaw cycle twice. Initiator EBiB (0.25 mmol) dissolved in 4 mL of dry anisole (which was separately degassed using freeze-vacuum-thaw cycle twice) was then charged to the reaction flask through a nitrogen purged syringe. The whole reaction mixture was again repeatedly subjected to freeze-vacuum-thaw cycle. The reaction flask was maintained at 80 °C. The termination of polymerization reaction was done by the addition of methanol in excess to the reaction mixture. The precipitated out copolymer was filtered and washed with hot methanol to remove the unreacted monomers. For removal of the copper catalyst, the copolymer was dissolved in acetone and the resultant solution was passed through the alumina bed. The filtrate was concentrated using rotary evaporator, reprecipitated with hot methanol, filtered and dried under the vacuum. The percentage yield of the copolymers determined using gravimetric method was found in the range of 40-50%. For all the NAI monomers, the copolymerization with MMA under similar conditions were carried out in nine different reactions flasks and quenched at different time intervals viz. 5 h, 15 h, 30 h, 45 h, 60 h, 75 h, 90 h, 105 h and 120 h. The obtained copolymers are designated as poly(PI-*ran*-MMA)*, poly(MPI-*ran*-MMA)*, poly(MOPI-*ran*-MMA)* and poly(CPI-*ran*-MMA)*.

3.2.3 Synthesis of Random Copolymers of NAI and MMA via AGET-ATRP

In AGET-ATRP of NAI and MMA monomers, CuBr₂/ Bpy/ Sn(EH)₂ were used as catalyst. The NAI, MMA, EBiB, CuBr₂, Bpy, Sn(EH)₂ were taken in the ratio of 1: 4: 0.025: 0.025: 0.075: 0.0125. The termination of polymerization reaction was done by the addition of methanol in excess to the reaction mixture. The precipitated copolymer was purified using the similar procedure as reported for the purification of random copolymers synthesized via n-ATRP (**Section 3.2.2**). The percentage yield of the copolymers was obtained using gravimetric method and was found in the range of 80-90%. The copolymers are designated as poly(PI-*ran*-MMA)[#], poly(MPI-*ran*-MMA)[#], poly(MOPI-*ran*-MMA)[#] and poly(CPI-*ran*-MMA)[#].

The reaction scheme for the synthesis of random copolymers of NAI and MMA monomers using n-ATRP and AGET-ATRP is given in the **Scheme 3.1**.



Scheme 3.1: Reaction scheme for the synthesis of random copolymers of NAI and MMA.

3.2.4 Synthesis of Block Copolymers of NAI and MMA via AGET-ATRP

The block copolymers poly(NAI-*ran*-MMA)-*b*-poly(MMA) and poly(NAI-*ran*-MMA)-*b*-poly(NAI) were synthesized using the similar procedure as given for random copolymers synthesized via AGET-ATRP (**Section 3.2.3**). Here, poly(NAI-*ran*-MMA)* (0.125 mmol) was used as the macroinitiator for the homopolymerization of MMA monomer (0.025 mol) in 14 mL of dry anisole using CuBr₂ (0.125 mmol), Bpy (0.375 mmol), Sn(EH)₂ (0.063 μmol) as catalyst. Similarly, for the synthesis of [poly(NAI-*ran*-MMA)-*b*-poly(NAI)] copolymers, the NAI monomer (0.025 mol) in 20 mL of dry anisole was used for the polymerization. The reactions were quenched after 24 h and the obtained block copolymers were purified as mentioned in the procedure of n-ATRP (**Section 3.2.2**). The percentage yield of the block copolymers was obtained using

gravimetric method and was found in the range of 65-75% and 50-60% for poly(NAI-*ran*-MMA)-*b*-poly(MMA) and poly(NAI-*ran*-MMA)-*b*-poly(NAI), respectively.

3.3 Results and Discussion

3.3.1 Structural Characterization of Poly(NAI-*ran*-MMA)* Copolymers

The peak assignments for IR and ¹H-NMR spectra of the poly(NAI-*ran*-MMA)* copolymers were compared with the respective IR and ¹H-NMR spectra of NAI monomers discussed in chapter II, Section 2.3.2.

3.3.1.1 IR Analysis

In the IR spectra of poly(NAI-*ran*-MMA)* copolymers (**Figure 3.1**), the asymmetric and symmetric stretch for –CH₃ of MMA were observed in the regions 2940-2922 cm⁻¹ and 2853-2845 cm⁻¹, respectively. The >C=O of NAI showed two characteristics bands in the regions 1794-1784 cm⁻¹ and 1744-1724 cm⁻¹, respectively. The >C=O of MMA merged with the carbonyl peak of NAI in the region 1744-1724 cm⁻¹. The characteristic three bands of >C=C< stretch for aromatic ring were observed in the regions 1612-1598 cm⁻¹, 1525-1502 cm⁻¹ and 1494-1542 cm⁻¹, respectively. The peaks observed in the region 540-525 cm⁻¹ were assigned to C-Br stretches.

3.3.1.2 ¹H-NMR Analysis

In the ¹H-NMR spectra of poly(NAI-*ran*-MMA)* copolymers (**Figure 3.2**), the characteristic peaks of phenyl of NAI were observed in the region $\delta = 7.6-6.9$ ppm. The peaks of –OCH₃ and –CH₂ (adjacent to the carbonyl group) of the side chain were observed, at $\delta = 3.6 \pm 0.10$ ppm and $\delta = 3.5 \pm 0.12$ ppm, respectively. The peaks of –CH₂ and –CH₃ of the copolymer backbone were observed in the region $\delta = 2.8-1.7$ ppm and $\delta = 1.4-0.8$ ppm, respectively. For poly(MPI-*ran*-MMA)* and poly(MOPI-*ran*-MMA)* peaks for –CH₃ and –OCH₃ attached to the aromatic ring were observed at $\delta = 2.4$ ppm and $\delta = 3.8$ ppm, respectively.

3.3.1.3 ^{13}C -NMR Analysis

In the ^{13}C -NMR spectra of poly(NAI-*ran*-MMA)* copolymers (**Figure 3.3**), the carbonyl carbons of NAI monomers were observed in the regions $\delta = 182\text{-}178$ ppm ($>^2\text{C}=\text{O}$) and $\delta = 175\text{-}174$ ppm ($>^1\text{C}=\text{O}$), respectively. The carbonyl carbon of MMA was observed in the region $\delta = 178\text{-}175$ ppm. The aromatic carbons of NAI were observed in the region $\delta = 130\text{-}113$ ppm. The peak corresponding to $-\text{OCH}_3$ of MMA was observed at $\delta = 55 \pm 0.40$ ppm. The peaks for other carbons in the backbone and the side chain were observed in the region $\delta = 54\text{-}18$ ppm. The signals corresponding to $-\text{CH}_3$ of poly(MPI-*ran*-MMA)* and $-\text{OCH}_3$ of poly(MOPI-*ran*-MMA)* attached to aromatic ring were observed at $\delta = 21$ ppm and $\delta = 160$ ppm, respectively.

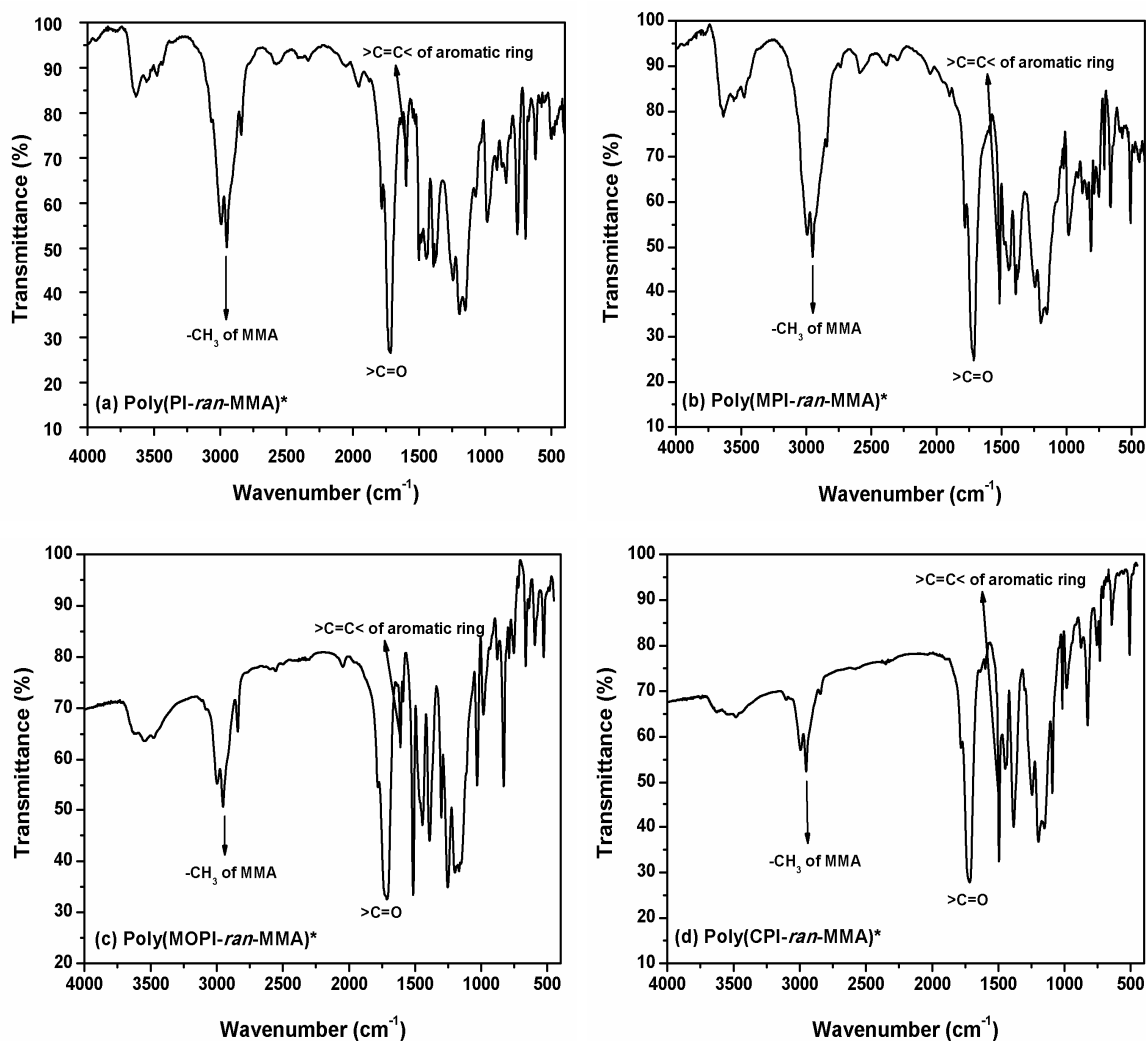


Figure 3.1: IR spectra of poly(NAI-*ran*-MMA)* copolymers.

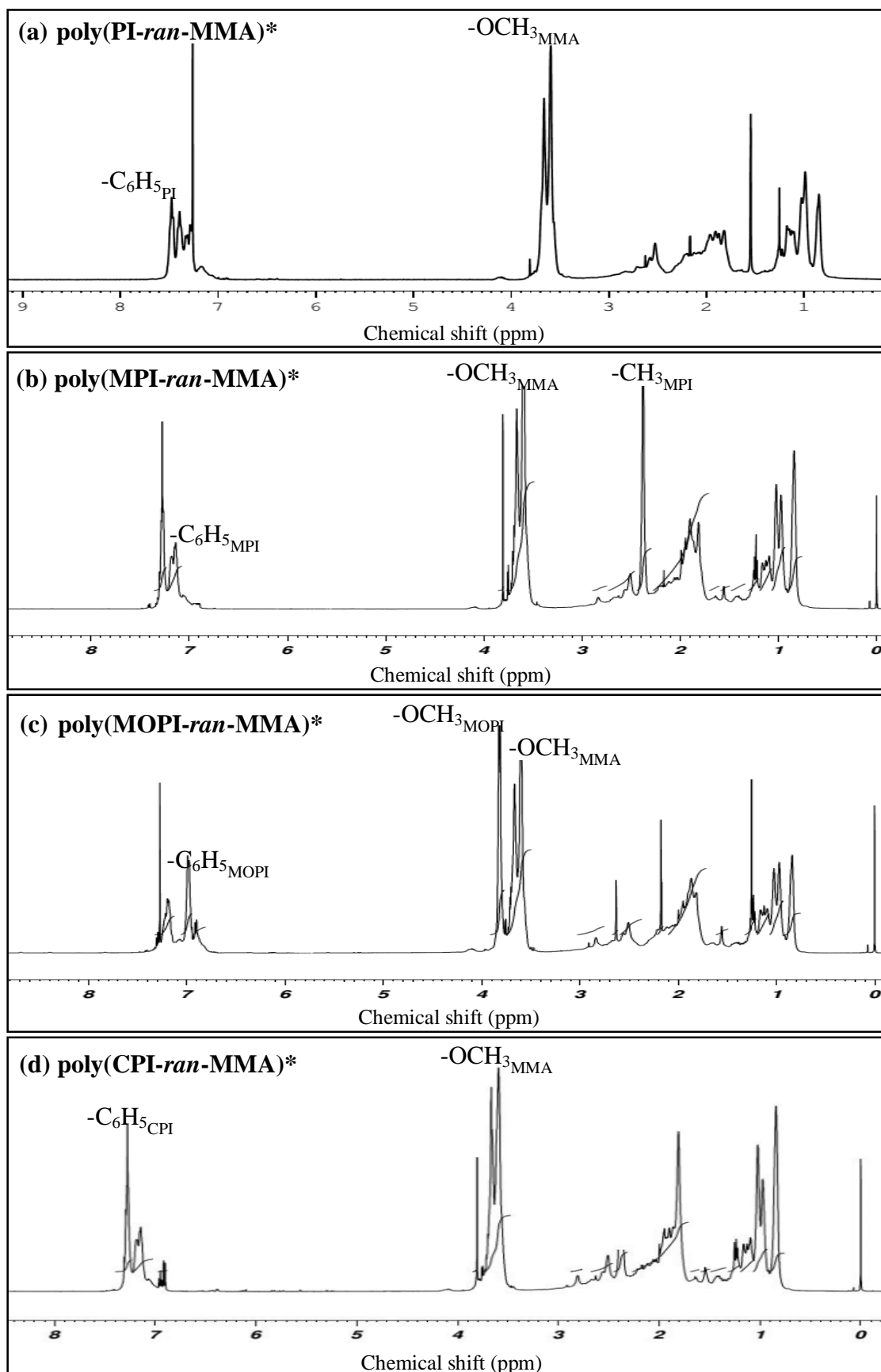


Figure 3.2: $^1\text{H-NMR}$ spectra of poly(NAI-ran-MMA)* copolymers.

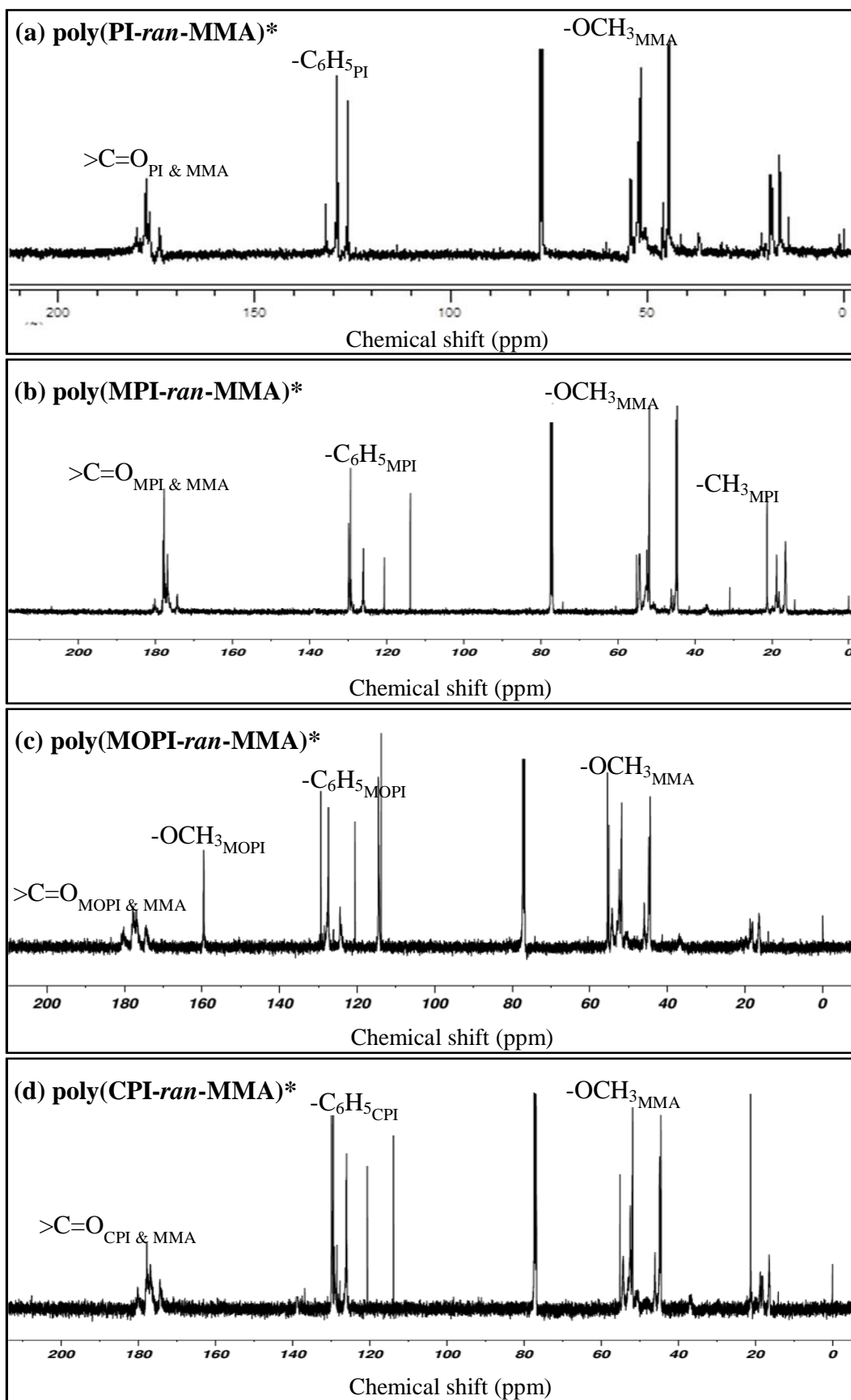


Figure 3.3: ^{13}C -NMR spectra of poly(NAI-ran-MMA)* copolymers.

3.3.2 Kinetic Studies of Poly(NAI-*ran*-MMA)* Copolymers

The characteristic experimental features of effective and well controlled n-ATRP reaction of poly(NAI-*ran*-MMA)* copolymers were established for each of the NAI monomers viz. PI, MPI, MOPI and CPI. For this, NAI and MMA were copolymerized in the feed ratio of 2:8 and the copolymerizations were quenched at different time intervals (**Scheme 3.1**). The copolymers were purified and the molecular weights were determined using GPC (**Table 3.1**). For all the copolymer systems the molecular weight (\bar{M}_n) varied linearly with total percentage conversion of monomers (**Figure 3.4**), which is the characteristic for controlled radical polymerization.

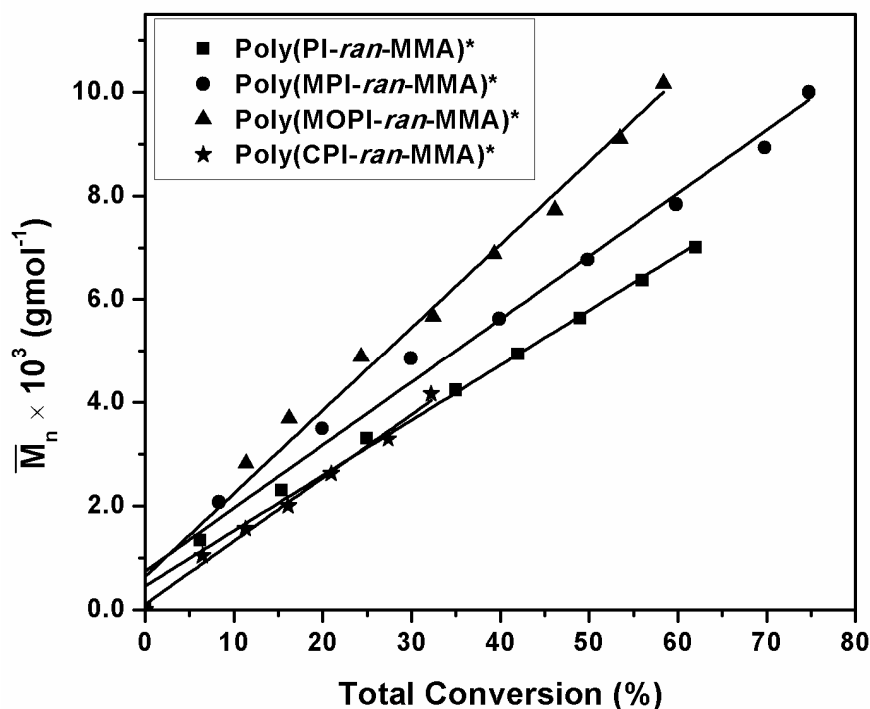


Figure 3.4: Plots of \bar{M}_n of copolymers vs total conversion (in percent) of monomers.

For the copolymerization of NAI and MMA monomers, the rate of propagation depends on the concentration of both monomers and follows second order kinetics as given below [247];

$$\ln \frac{[M]_t [I]_0}{[I]_t [M]_0} = k_p ([M]_0 - [I]_0) t \dots\dots\dots 3.1$$

where, $[M]_0$ and $[I]_0$ are the initial concentrations of MMA and NAI, $[M]_0 \neq [I]_0$. $[M]_t$ and $[I]_t$ are the concentrations of MMA and NAI at time t, and k_p is the rate constant of propagation.

Table 3.1: Percent conversion of monomers with time, \bar{M}_n and PDI values of poly(NAI-*ran*-MMA)* copolymers.

Copolymer designation	Duration (h)	Conversion of NAI (%)	Conversion of MMA (%)	Total conversion of monomers (%)	\bar{M}_n (1×10^3 g mol ⁻¹)	PDI
poly(PI- <i>ran</i> -MMA)*	5	18	08	07	1.3	1.5
	15	24	12	15	2.3	1.5
	30	32	20	25	3.3	1.5
	45	45	25	35	4.2	1.6
	60	56	32	42	4.9	1.4
	75	65	45	49	5.6	1.5
	90	78	57	56	6.4	1.5
	105	87	68	62	6.9	1.5
	120	98	80	65	7.0	1.5
poly(MPI- <i>ran</i> -MMA)*	5	22	08	10	2.0	1.5
	15	30	18	20	3.8	1.4
	30	42	25	30	4.9	1.4
	45	48	32	40	5.8	1.4
	60	57	45	50	6.8	1.3
	75	68	57	60	7.5	1.3
	90	76	68	70	8.9	1.3
	105	86	75	75	10.2	1.3
	120	97	85	78	10.3	1.3
poly(MOPI- <i>ran</i> -MMA)*	5	20	10	11	2.8	1.4
	15	32	19	16	3.7	1.4
	30	44	27	24	4.9	1.4
	45	50	34	32	5.7	1.4
	60	58	47	39	6.9	1.5
	75	69	58	46	7.7	1.5
	90	77	69	53	9.1	1.3
	105	88	77	58	10.5	1.3
	120	98	86	60	10.6	1.3
poly(CPI- <i>ran</i> -MMA)*	24	07	09	6	1.0	1.5
	48	15	17	11	1.6	1.5
	72	23	26	16	2.0	1.4
	96	32	37	21	2.6	1.4
	120	43	48	27	3.3	1.4
	144	54	59	32	4.2	1.4

To determine $[M]_t$ and $[I]_t$, the known amount of the standard, viz. 1,1,2,2-tetrachloroethane was added in the reaction mixture and $^1\text{H-NMR}$ was recorded at various time intervals (**Figure 3.5**).

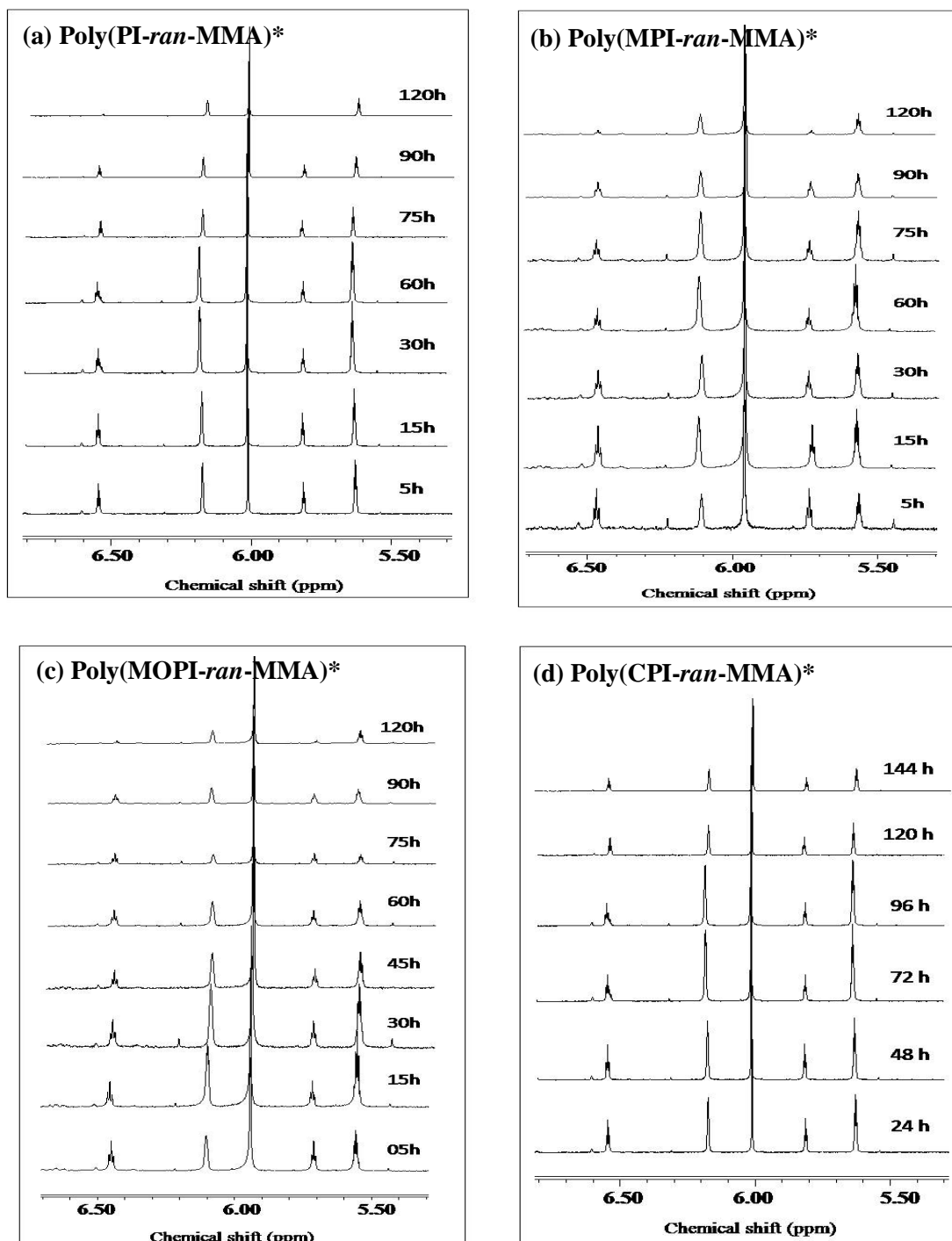


Figure 3.5: $^1\text{H-NMR}$ spectra of the reaction mixture of poly(NAI-ran-MMA)* copolymers at various time interval.

The intensity of the peak corresponding to the vinylic proton of monomers, NAI at $\delta = 6.5 \pm 0.2$ ppm and MMA at $\delta = 6.2 \pm 0.2$ ppm were compared with the peak of the standard at $\delta = 6.0 \pm 0.2$ ppm. The linear variation of $\ln \{[M]_t[I]_0 / [I]_t[M]_0\}$ vs time (**Figure 3.6**) for all poly(NAI-*ran*-MMA)* copolymers shows that copolymerization of NAI and MMA follows second order kinetics. The k_p values (in $\text{Lmol}^{-1}\text{s}^{-1}$) determined from the slope of graphs for poly(PI-*ran*-MMA)*, poly(MPI-*ran*-MMA)*, poly(MOPI-*ran*-MMA)* and poly(CPI-*ran*-MMA)* were found to be, 1.97×10^2 , 8.21×10^2 , 9.25×10^2 and 8.25×10^1 , respectively, and were observed to increase in the order, poly(CPI-*ran*-MMA)* < poly(PI-*ran*-MMA)* < poly(MPI-*ran*-MMA)* < poly(MOPI-*ran*-MMA)*.

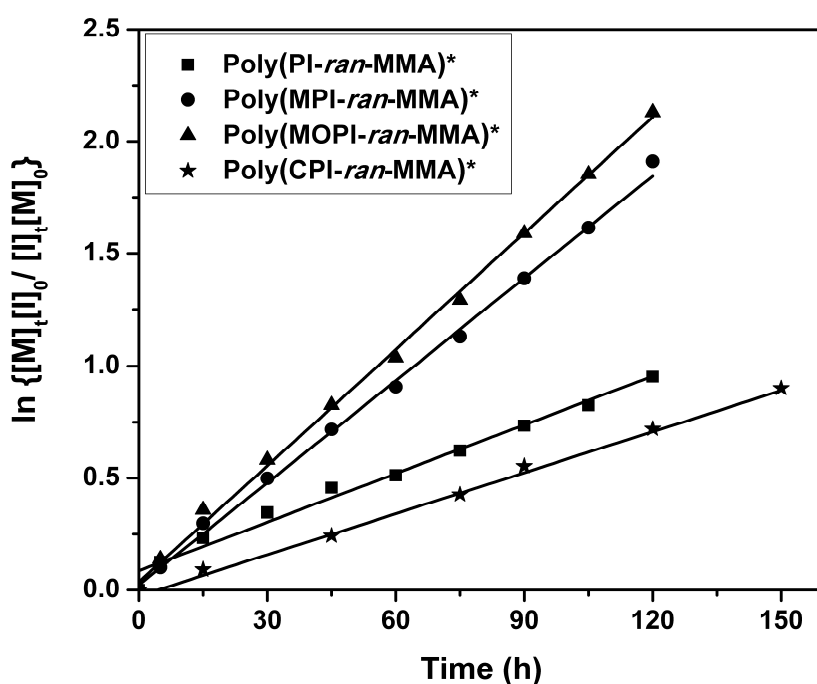


Figure 3.6: Plots of $\ln \{[M]_t[I]_0 / [M]_0[I]_t\}$ vs time (h) for poly(NAI-*ran*-MMA)* copolymers.

A typical linear variation of percent conversion of monomers with time is observed in the beginning which start deviating from linearity [except for poly(CPI-*ran*-MMA)] when the conversion is $>40\%$ (**Figure 3.7**). The heterogeneity of the system due to the limited solubility of the Cu^{II} complex may lead to this deviation from linearity [35]. Also, Cu^{I} complexes are sensitive to air and other oxidant, this may limit the formation of high molecular weights. Therefore, the random copolymers have also been synthesized via AGET-ATRP as shown in **Scheme 3.1** and their properties are compared

with the copolymers synthesized via n-ATRP. These copolymers are designated as poly(PI-*ran*-MMA)[#], poly(MPI-*ran*-MMA)[#], poly(MOPI-*ran*-MMA)[#] and poly(CPI-*ran*-MMA)[#].

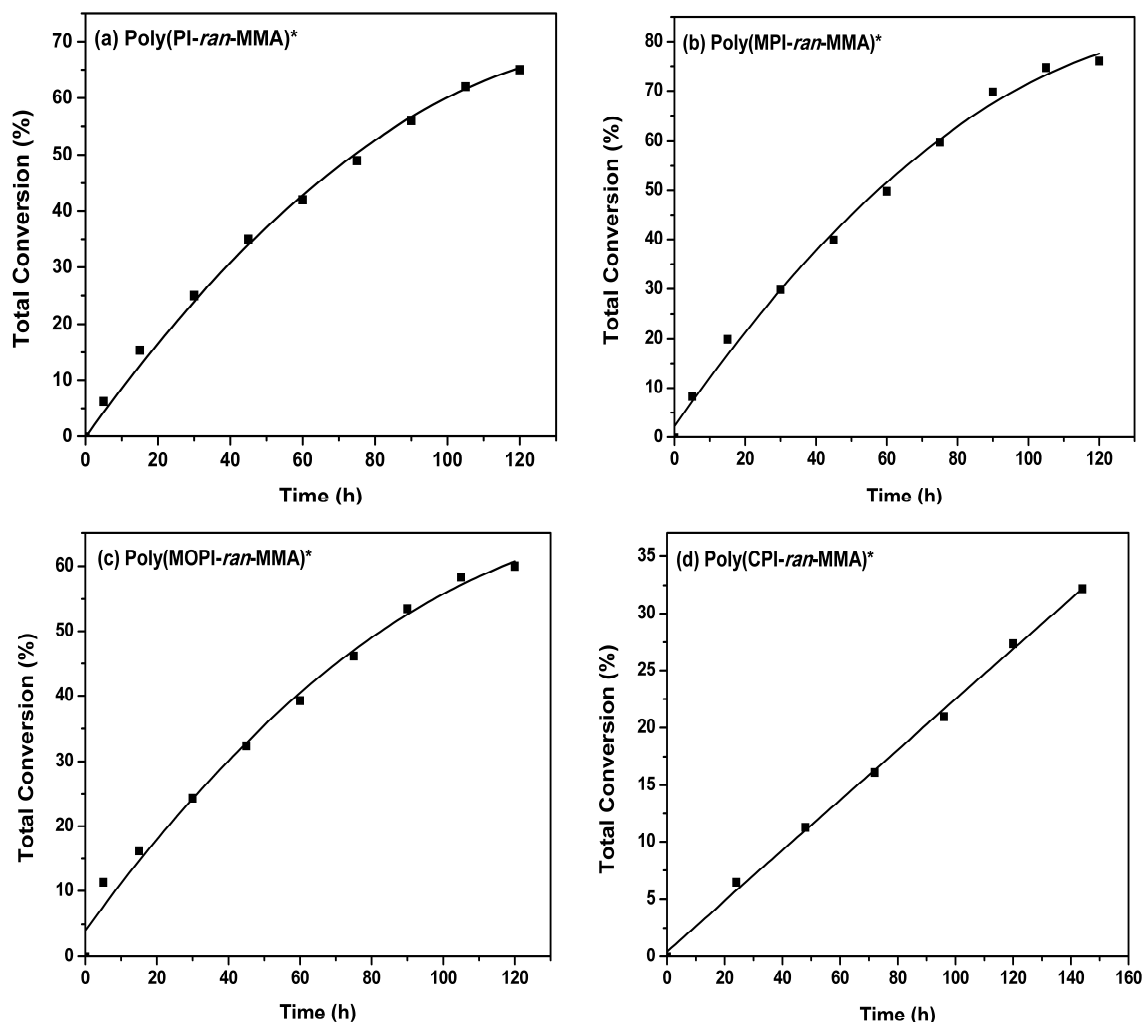


Figure 3.7: Plots of total conversion (in percent) of monomers vs time (h) for poly(NAI-*ran*-MMA)* copolymers.

3.3.3 Random Copolymers of NAI and MMA via AGET-ATRP

A significant enhancement in the yield was obtained when the copolymerization was carried out via AGET-ATRP. The yield of 80-90% was obtained in 45h as compared to 40-50% yield for poly(NAI-*ran*-MMA)* synthesized via n-ATRP in the same duration. This shows that, (i) the rate of copolymerization of NAI and MMA monomers via AGET-ATRP were greater than copolymerization via n-ATRP method, and (ii) the side

reactions such as termination of the propagating radical are minimized using AGET-ATRP method.

The IR and $^1\text{H-NMR}$ spectra of the poly(NAI-*ran*-MMA) $^\#$ copolymers are given in **Figure 3.8** and **Figure 3.9**, respectively.

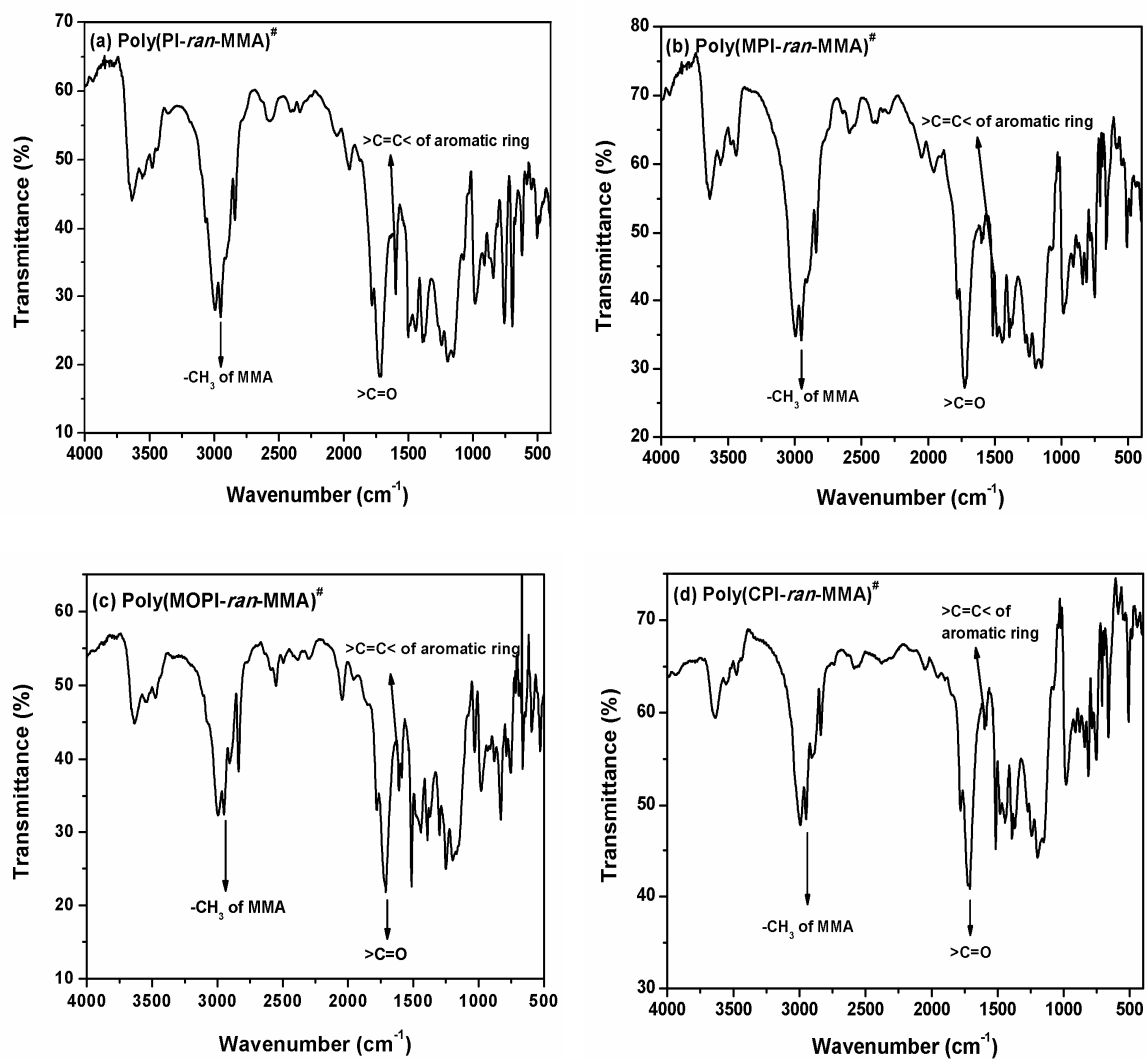


Figure 3.8: IR spectra for poly(NAI-*ran*-MMA) $^\#$ copolymers.

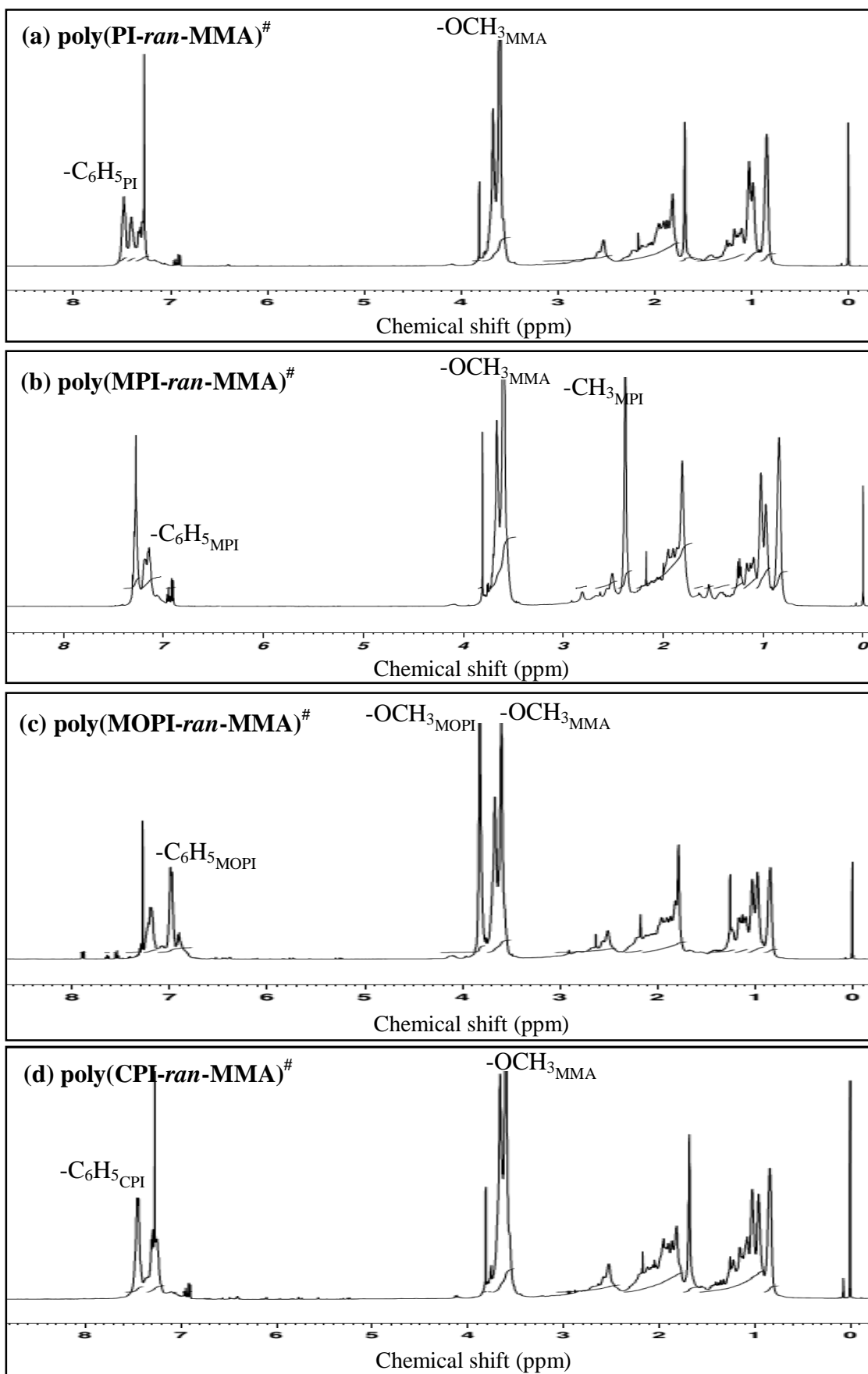


Figure 3.9: ¹H-NMR spectra for poly(NAI-ran-MMA)[#] copolymers.

3.3.4 Effects of Pendant Group and Methodology on Copolymer Composition

The elemental analysis of the copolymers shows the presence of carbon, hydrogen, oxygen, nitrogen and bromine. The mole fraction of monomers (MMA and NAI) in copolymers synthesized via n-ATRP and AGET-ATRP were calculated (from CHNO analysis) using following equations 3.2 and 3.3:

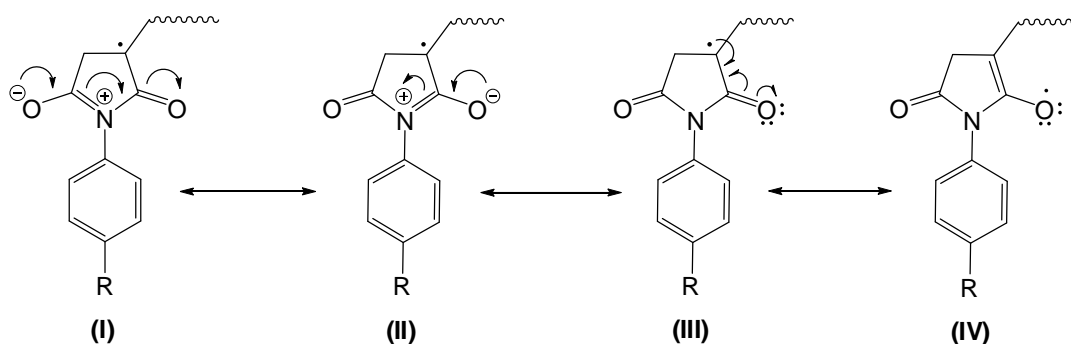
$$\%N = \frac{14n_I}{100n_M+W_I n_I+195} \times 100 \dots\dots\dots 3.2$$

$$\%Br = \frac{80}{100n_M+W_I n_I+195} \times 100 \dots\dots\dots 3.3$$

where, %N is the percentage of the nitrogen and %Br is the percentage of the bromine in the copolymer. W_I is the molecular weight of NAI monomer, n_M and n_I are the number of moles of MMA and NAI in copolymers, 195 is the molecular weight of EBiB and 80 is the molecular weight of bromine. Also, the mole fraction of monomers (MMA and NAI) in copolymers synthesized via n-ATRP and AGET-ATRP were calculated from the $^1\text{H-NMR}$ spectra of the copolymers (**Figure 3.2** and **Figure 3.9**). The mole fraction of monomers was determined by taking the ratio of the intensity of signals attributed to methoxy protons ($-\text{OCH}_3$) of MMA and aromatic protons of NAI. The results of copolymer composition are given in **Table 3.2**. A good correlation was obtained between the mole fractions calculated from %N and calculated from the $^1\text{H-NMR}$ spectra of the copolymers.

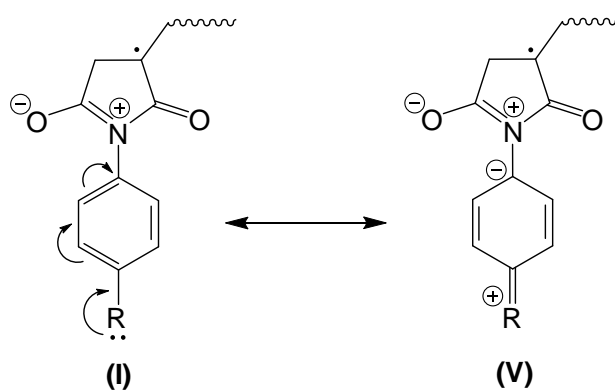
When we compared the feed composition of monomers (which was maintained 2:8::NAI:MMA for all the copolymerization reactions), an enhanced incorporation of NAI in the copolymer backbone was observed (**Table 3.2**). A higher mole fraction of the NAI with electron releasing substituent was observed as compared to NAI with electron withdrawing substituent on the aromatic ring of the pendant group. The mole fraction of NAI in the copolymer backbone increased in the order, $\text{poly}(\text{CPI-}i\text{ran-MMA}) < \text{poly}(\text{PI-}i\text{ran-MMA}) < \text{poly}(\text{MPI-}i\text{ran-MMA}) < \text{poly}(\text{MOPI-}i\text{ran-MMA})$, for the same feed compositions. The trend is similar as that for experimentally determined k_p values. This can be understood from the structure of the intermediate with terminal NAI free radical which exists in resonating forms as shown in **Figure 3.10**. The electron releasing groups viz. $-\text{OCH}_3$ and $-\text{CH}_3$ on aromatic ring stabilizes **I** and **II** via mesomeric effect, thus

(a) Proposed resonating structures (I to IV) for copolymer with NAI terminal free radical:



where, R = -H, -CH₃, -OCH₃ and -Cl.

(b) Mesomeric resonating effect:



where, R = -OCH₃ and -Cl

(c) Inductive effect:

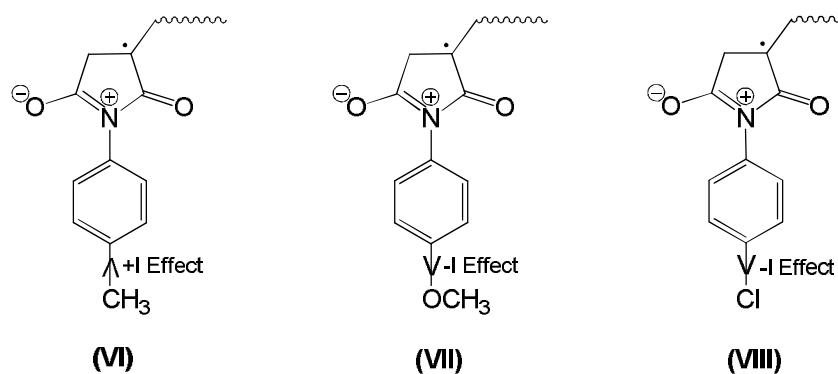


Figure 3.10: Comparison of stabilization of NAI intermediate free radical by various substituents on aromatic ring.

making the free radical at ‘carbon’ centre to be more available for free radical polymerization increasing k_p . This also increases the stability of the incipient free radical for the corresponding NAI monomer thus increasing its reactivity towards the growing copolymer resulting in higher incorporation in copolymer backbone. The increase in the mole fractions of monomers on copolymer backbone has been observed for the copolymers synthesized via AGET-ATRP as compared to n-ATRP.

Table 3.2: Elemental analysis and copolymer composition for poly(NAI-*ran*-MMA) synthesized via n-ATRP and AGET-ATRP. Experimental conditions: n-ATRP: [NAI]/ [MMA]/ [EBiB]/ [CuBr]/ [Bpy] = 20/ 80/ 1/ 1/ 3. AGET-ATRP: [NAI]/ [MMA]/ [EBiB]/ [CuBr₂]/ [Sn(EH)₂]/ [Bpy] = 20/ 80/ 1/ 1/ 0.25/ 3, in anisole at 80 °C.

Copolymer designation	C (%)	H (%)	N (%)	O (%)	Br (%)	Mole fraction (from % N)		Mole fraction (from ¹ H-NMR)	
						NAI	MMA	NAI	MMA
poly(PI- <i>ran</i> -MMA)*	63.84	7.17	2.39	19.71	6.89	0.36	0.64	0.35	0.66
poly(MPI- <i>ran</i> -MMA)*	63.61	6.92	2.98	19.30	7.19	0.47	0.53	0.45	0.54
poly(MOPI- <i>ran</i> -MMA)*	59.92	5.77	3.12	21.24	9.95	0.50	0.50	0.51	0.49
poly(CPI- <i>ran</i> -MMA)*	65.54	6.91	2.31	17.84	7.40	0.33	0.67	0.31	0.66
poly(PI- <i>ran</i> -MMA) [#]	61.94	6.50	3.33	20.25	7.98	0.42	0.58	0.40	0.59
poly(MPI- <i>ran</i> -MMA) [#]	59.31	5.85	3.42	21.30	10.12	0.49	0.51	0.48	0.50
poly(MOPI- <i>ran</i> -MMA) [#]	57.75	5.40	4.09	22.09	10.67	0.55	0.45	0.56	0.44
poly(CPI- <i>ran</i> -MMA) [#]	63.35	7.57	2.93	19.71	7.40	0.39	0.61	0.40	0.60

3.3.5 Effects of Pendant Group and Methodology on Molecular Weights of Copolymers

The nature of the pendant group significantly affected the molecular weights of the copolymers synthesized via n-ATRP as well as via AGET-ATRP (**Table 3.3**). The molecular weights of poly(NAI-*ran*-MMA) copolymers and the rate of copolymerizations were observed to increase in the order, poly(CPI-*ran*-MMA) < poly(PI-*ran*-MMA) < poly(MPI-*ran*-MMA) < poly(MOPI-*ran*-MMA), which is in

accordance with the reactivity of the NAI comonomers. For the same copolymerization duration (45h) the molecular weight of the copolymers synthesized via AGET-ATRP was observed to be almost 2-3 times greater as compared to copolymers synthesized via n-ATRP. The PDI values were obtained in the range of 1.3-1.6 for the copolymers synthesized via n-ATRP. However, the PDI values were obtained in the range of 1.2-1.3 for the copolymers synthesized via AGET-ATRP.

Table 3.3: \bar{M}_n and PDI for poly(NAI-*ran*-MMA) copolymers synthesized via n-ATRP and AGET-ATRP.

Copolymer designation	\bar{M}_n ($1 \times 10^3 \text{ g mol}^{-1}$)	PDI
poly(PI- <i>ran</i> -MMA)*	4.0	1.6
poly(MPI- <i>ran</i> -MMA)*	5.0	1.4
poly(MOPI- <i>ran</i> -MMA)*	6.0	1.4
poly(CPI- <i>ran</i> -MMA)*	4.0	1.3
poly(PI- <i>ran</i> -MMA)#	10.0	1.3
poly(MPI- <i>ran</i> -MMA)#	12.0	1.2
poly(MOPI- <i>ran</i> -MMA)#	19.0	1.2
poly(CPI- <i>ran</i> -MMA)#	0.9	1.3

3.3.6 Effects of Pendant Group and Methodology on Thermal Properties of Copolymers

3.3.6.1 DSC

The DSC scans of all the poly(NAI-*ran*-MMA) copolymers synthesized via n-ATRP and AGET-ATRP are shown in **Figure 3.11a** and **Figure 3.11b**, respectively. The shift in the base line corresponding to the T_g of the copolymer, was observed in all the samples. The T_g of the copolymers was determined by extrapolation of the two linear regions, before (onset temperature) and after (offset temperature) the T_g and the middle of the incline was considered as exact T_g of the copolymer [21]. The T_g of the poly(NAI-*ran*-MMA)* and poly(NAI-*ran*-MMA)# copolymers was observed in the ranges of 160-180 °C and 198-217 °C, respectively. The details of T_g s for the copolymers are given in the **Table 3.4**. A significantly increased T_g (60-80% via n-ATRP and 98-117% via AGET-ATRP) was observed for all the poly(NAI-*ran*-MMA) copolymers as compared to PMMA ($T_g = \sim 105$ °C [249]).

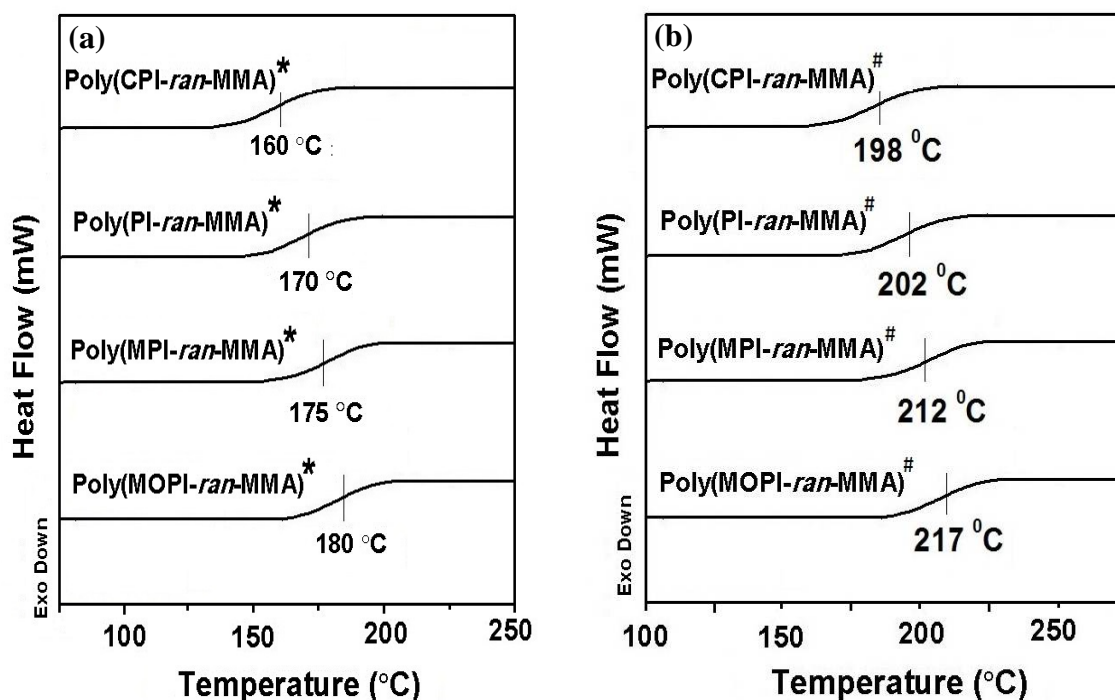


Figure 3.11: DSC scans for (a) poly(NAI-*ran*-MMA)* and (b) poly(NAI-*ran*-MMA)[#] copolymers.

Table 3.4: T_g s observed in the DSC of poly(NAI-*ran*-MMA) copolymers synthesized via n-ATRP and AGET-ATRP.

Copolymer designation	T_o (°C)	T_g (°C)	T_e (°C)
poly(CPI- <i>ran</i> -MMA)*	141	160	182
poly(PI- <i>ran</i> -MMA)*	152	170	192
poly(MPI- <i>ran</i> -MMA)*	156	175	194
poly(MOPI- <i>ran</i> -MMA)*	160	180	199
poly(CPI- <i>ran</i> -MMA) [#]	178	198	220
poly(PI- <i>ran</i> -MMA) [#]	182	202	224
poly(MPI- <i>ran</i> -MMA) [#]	192	212	234
poly(MOPI- <i>ran</i> -MMA) [#]	197	217	239

T_o = onset temperature and T_e = endset temperature

This can be explained on the basis of polarity and rigidity of the imide functionality in the pendant group. Hence, the T_g of the copolymers increased in the order, poly(CPI-*ran*-MMA) < poly(PI-*ran*-MMA) < poly(MPI-*ran*-MMA) < poly(MOPI-*ran*-MMA) and this trend was similar in n-ATRP as well as AGET-ATRP. The T_g of poly(PI-*ran*-MMA), poly(MPI-*ran*-MMA), poly(MOPI-*ran*-MMA) and poly(CPI-*ran*-MMA) synthesized via conventional FRP with feed composition of 2: 8: NAI: MMA, have been reported as, 165

°C [15], 167 °C [15], 166 °C [20] and 149 °C [14], respectively. On comparing the T_g of various poly(NAI-*ran*-MMA) copolymers with the same composition, 5-10% enhancement was observed in T_g of copolymers when synthesized via n-ATRP. However, as compared to conventional free radical polymerization, 22-35% enhancement was observed in the T_g of copolymers synthesized via AGET-ATRP.

3.3.6.2 TG/DTG

The TG/DTG curves of the poly(NAI-*ran*-MMA) copolymers synthesized via n-ATRP and AGET-ATRP are given in **Figure 3.12** and **Figure 3.13**, respectively. The copolymers synthesized via n-ATRP were stable upto 300 °C, whereas those synthesized via AGET-ATRP were stable upto 330 °C. The % weight loss in the region 150-250 °C, observed in all copolymers could be due to the moisture or the solvent molecules trapped in the copolymers. The major weight loss (56-62 %) for poly(NAI-*ran*-MMA) copolymers was observed in the region of 300-450 °C and it is attributed to random scissions of main chains and the scissions of methoxycarbonyl side groups. A further 10-12 % weight loss was observed in the region 450-550 °C and it could be due to the simultaneous scissions of end groups [251-252]. The char yield was found to be 9-17% at 600 °C for copolymers synthesized via n-ATRP and 10-13% at 600 °C for copolymers synthesized via AGET-ATRP. As the electron releasing tendency of the substituent on aromatic ring of pendant group increased, marginal increase (5-10%) in thermal stability of the copolymers was observed. The order of thermal stability was observed to be similar in n-ATRP and AGET-ATRP such as, poly(CPI-*ran*-MMA) < poly(PI-*ran*-MMA) < poly(MPI-*ran*-MMA) < poly(MOPI-*ran*-MMA).

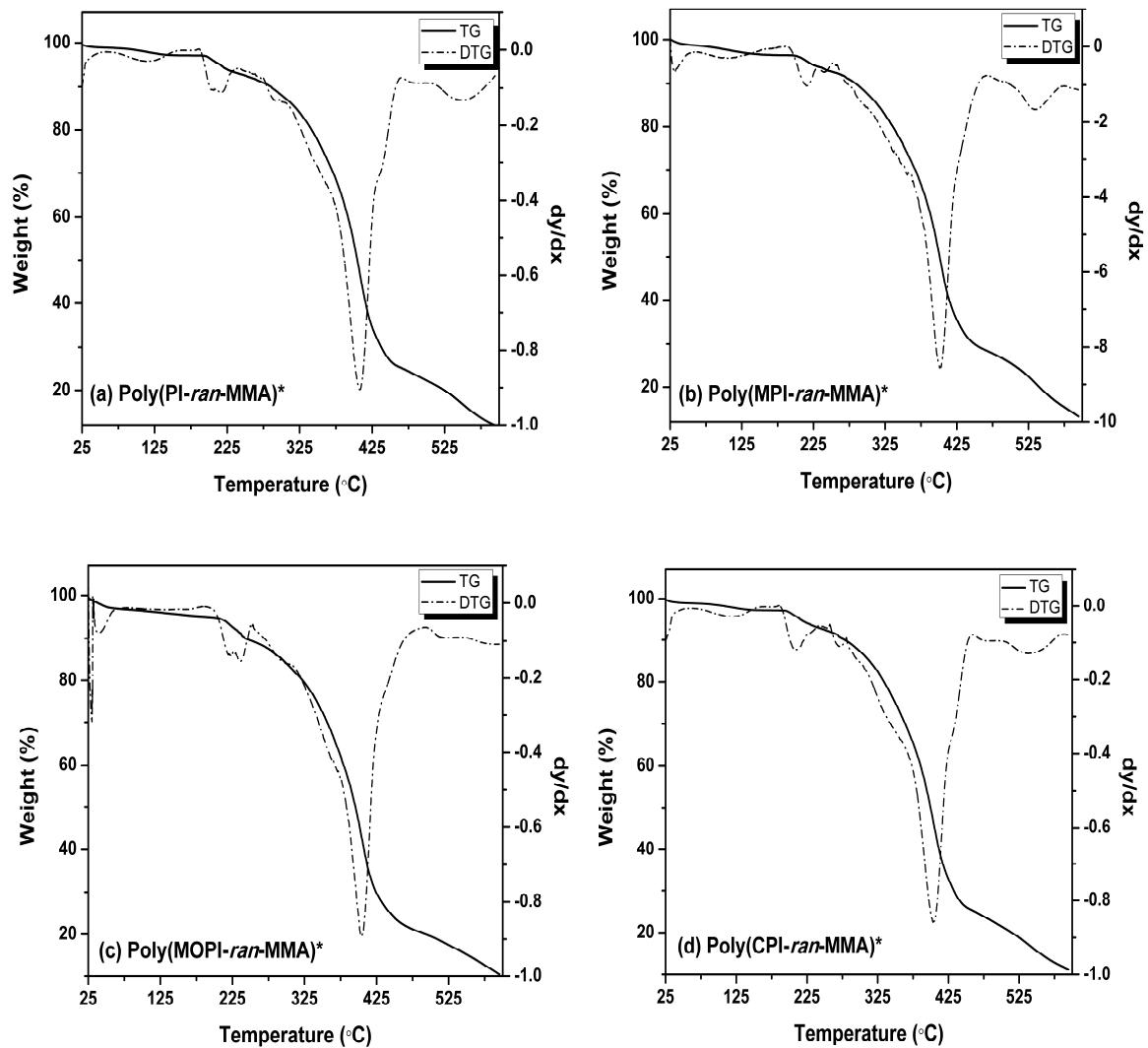


Figure 3.12: TG/ DTG scans for poly(NAI-ran-MMA)* copolymers.

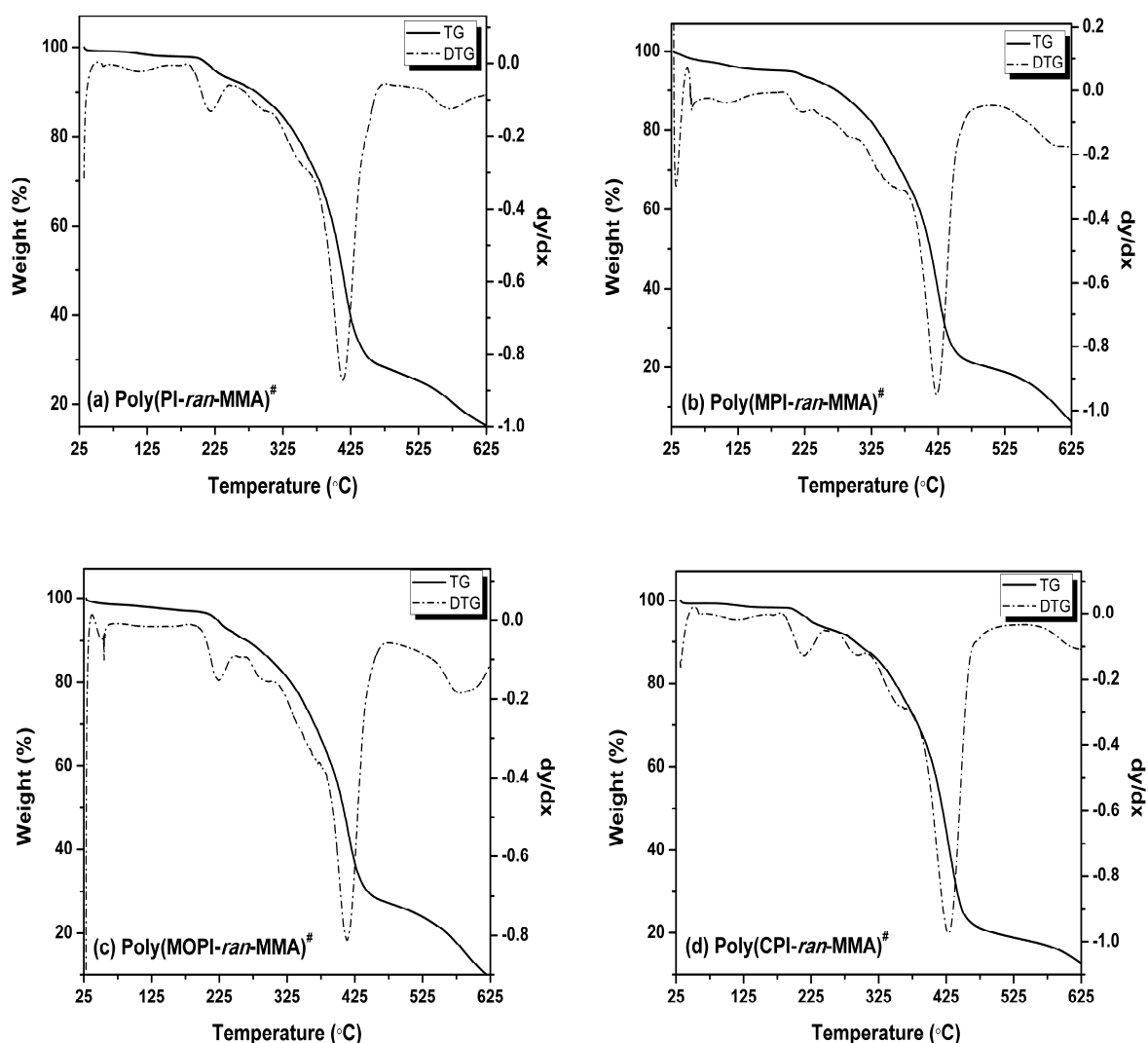
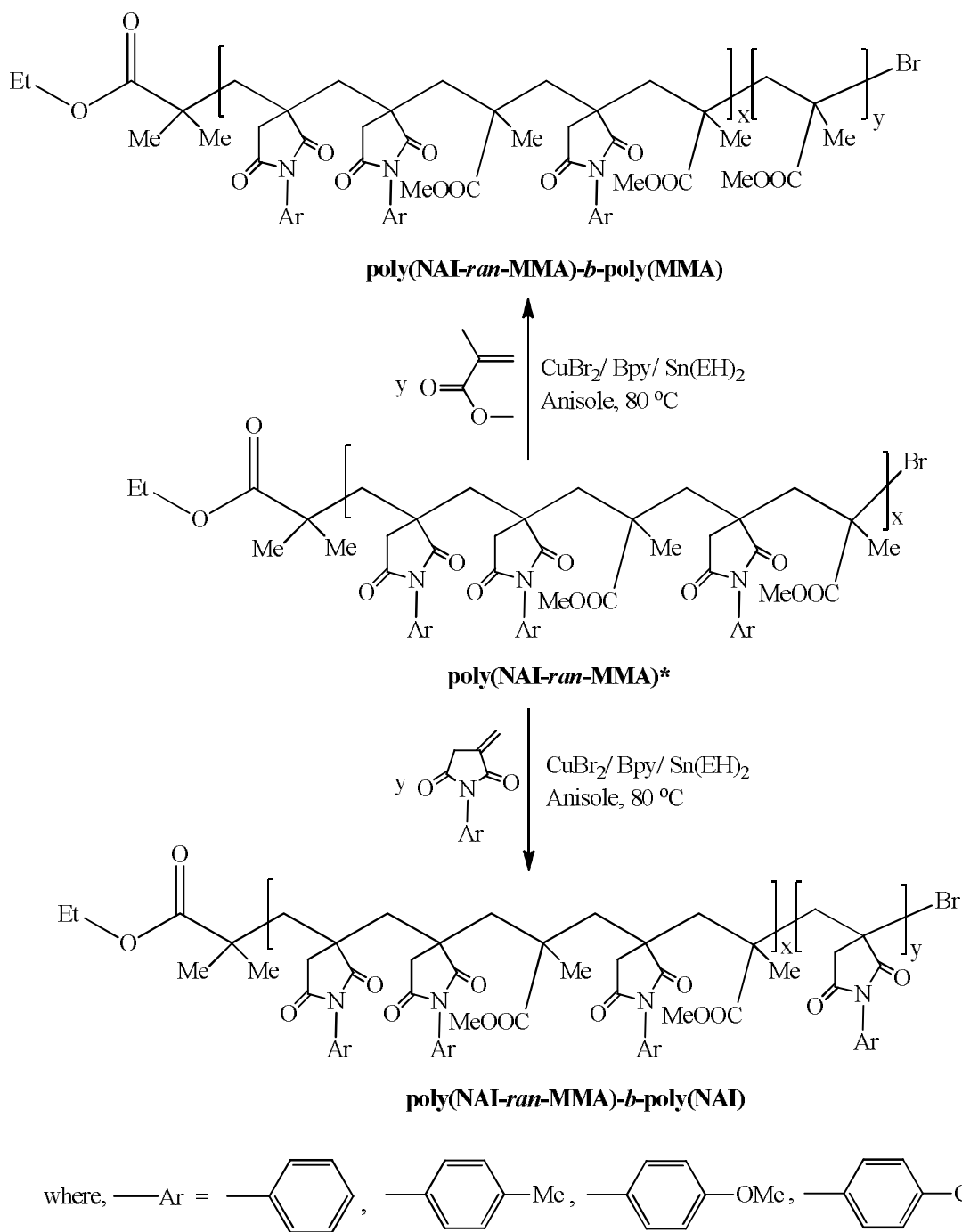


Figure 3.13: TG/ DTG scans for poly(NAI-*ran*-MMA)[#] copolymers.

3.3.7 Block Copolymers of NAI and MMA Monomers

To investigate the effect of architecture on the thermal properties and to further confirm the “living” nature of the poly(NAI-*ran*-MMA)^{*} copolymers, the block copolymers such as poly(NAI-*ran*-MMA)-*b*-poly(MMA) and poly(NAI-*ran*-MMA)-*b*-poly(NAI) were synthesized as shown in **Scheme 3.2**. The inactivation of the Cu^I complex due to air oxidation makes it difficult to prepare different architectures. Hence, AGET-ATRP is used for synthesis of block copolymers. Poly(NAI-*ran*-MMA)^{*} synthesized via n-ATRP are having lower in molecular weight as compared to poly(NAI-*ran*-MMA)[#] synthesized via AGET-ATRP. While achieving a higher length of the second block also to avoid any

probable limitation due to the solubility of the block copolymer the poly(NAI-*ran*-MMA)* were used as macroinitiators.



Scheme 3.2: Reaction scheme for synthesis of block copolymers.

3.3.8 Structural Characterization of Block Copolymers

3.3.8.1 IR Analysis

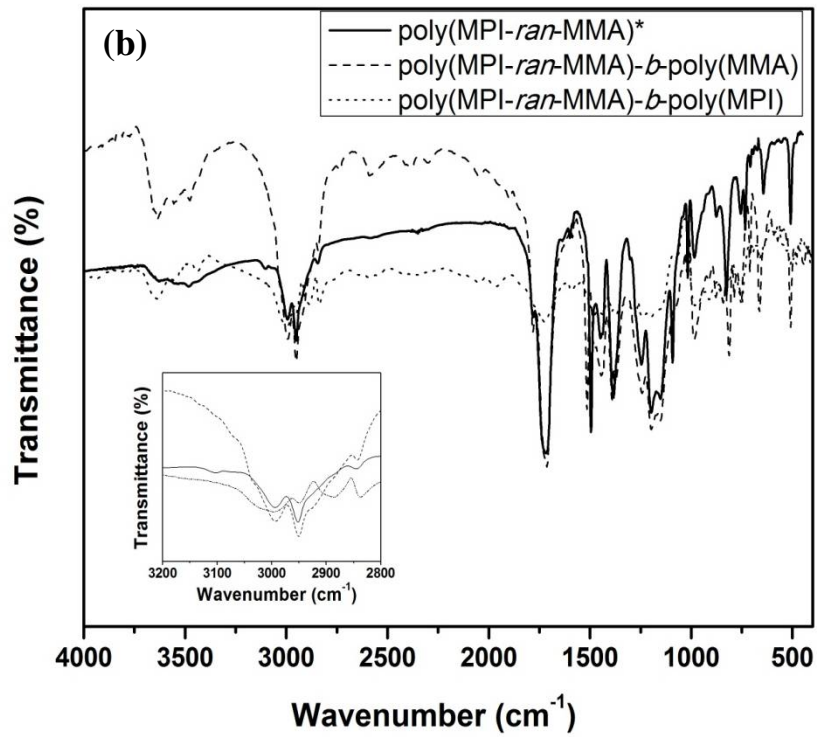
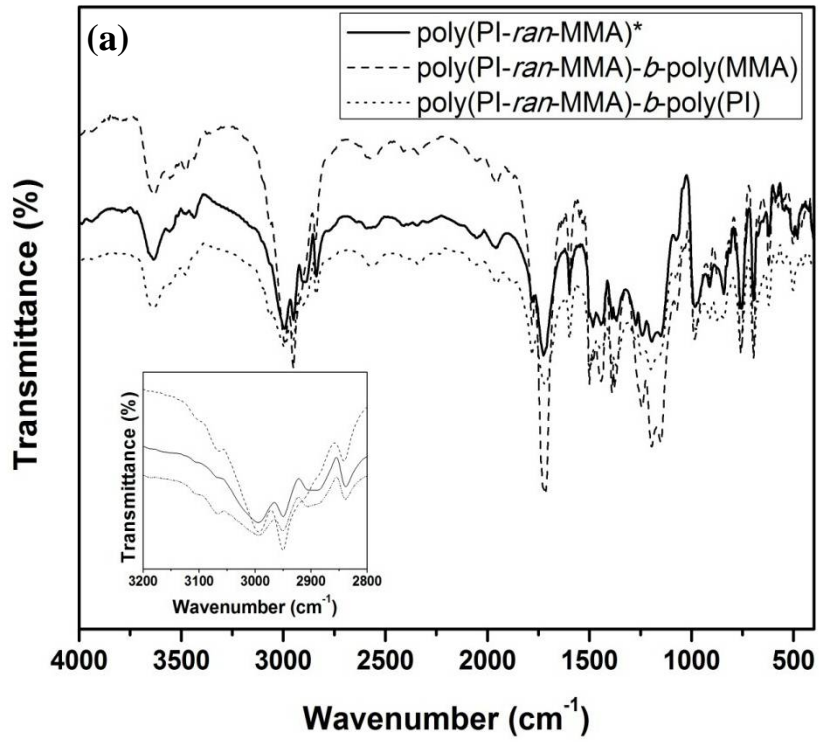
The comparative IR spectra of macroinitiators and block copolymers are shown in **Figure 3.14**. For poly(NAI-*ran*-MMA)-*b*-poly(MMA) block copolymer, the C-H stretch peaks corresponding to $-\text{CH}_3$ of MMA and the C-H stretch peaks corresponding to aromatic ring of NAI were observed in the regions $2853\text{-}2845\text{ cm}^{-1}$ and $3020\text{-}3000\text{ cm}^{-1}$, respectively. Due to the incorporation of PMMA block, the relative peak intensity of C-H stretch for $-\text{CH}_3$ of MMA in the region $2853\text{-}2845\text{ cm}^{-1}$ has been increased for block copolymers as compared to the macroinitiator.

Similarly, in the comparative IR spectra of macroinitiator and block copolymer, poly(NAI-*ran*-MMA)-*b*-poly(NAI) [due to the incorporation of poly(NAI) block] the relative peak intensity of C-H stretch for aromatic ring in the region $3020\text{-}3000\text{ cm}^{-1}$ has been increased for block copolymers as compared to the macroinitiator, as expected (**Figure 3.14**).

3.3.8.2 $^1\text{H-NMR}$ Analysis

The comparative $^1\text{H-NMR}$ spectra of macroinitiators and block copolymers are shown in **Figure 3.15** to **Figure 3.18**. For the poly(NAI-*ran*-MMA)-*b*-poly(MMA) block copolymers, the relative peak intensity of aromatic protons of NAI ($\delta = 7.6\text{-}7.2\text{ ppm}$) and the relative peak intensity of $-\text{OCH}_3$ protons of MMA ($\delta = 3.6 \pm 0.2\text{ ppm}$) were compared with corresponding macroinitiators. Due to the incorporation of PMMA block, the relative peak intensity of $-\text{OCH}_3$ protons of MMA ($\delta = 3.6 \pm 0.2\text{ ppm}$) increased and the peak intensity of aromatic protons of NAI ($\delta = 7.6\text{-}7.2\text{ ppm}$) decreased, as expected.

Similarly, in the comparative $^1\text{H-NMR}$ spectra of macroinitiators and block copolymers, poly(NAI-*ran*-MMA)-*b*-poly(NAI) [due to the incorporation of poly(NAI) block] an increase in the relative peak intensity of aromatic protons of NAI as compared to the peak intensity of $-\text{OCH}_3$ protons of MMA was observed (**Figure 3.15** to **Figure 3.18**).



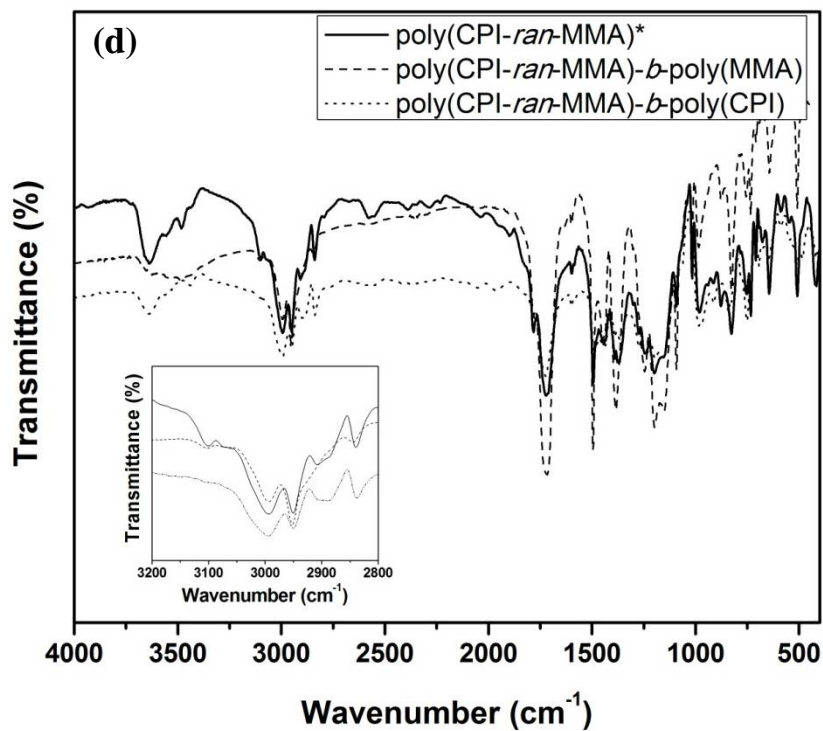
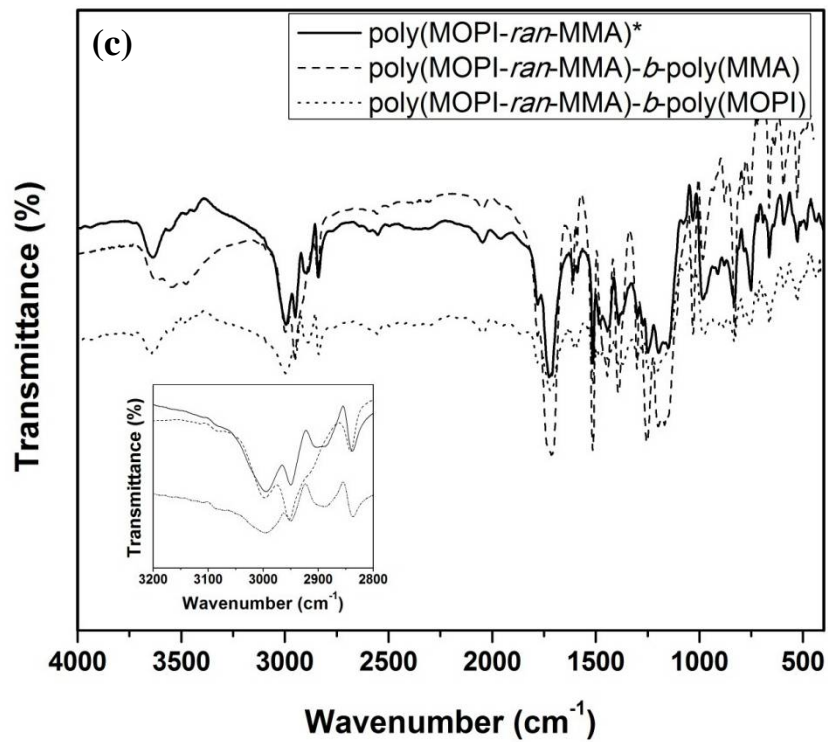


Figure 3.14: Comparative IR spectra of macroinitiators and block copolymers.

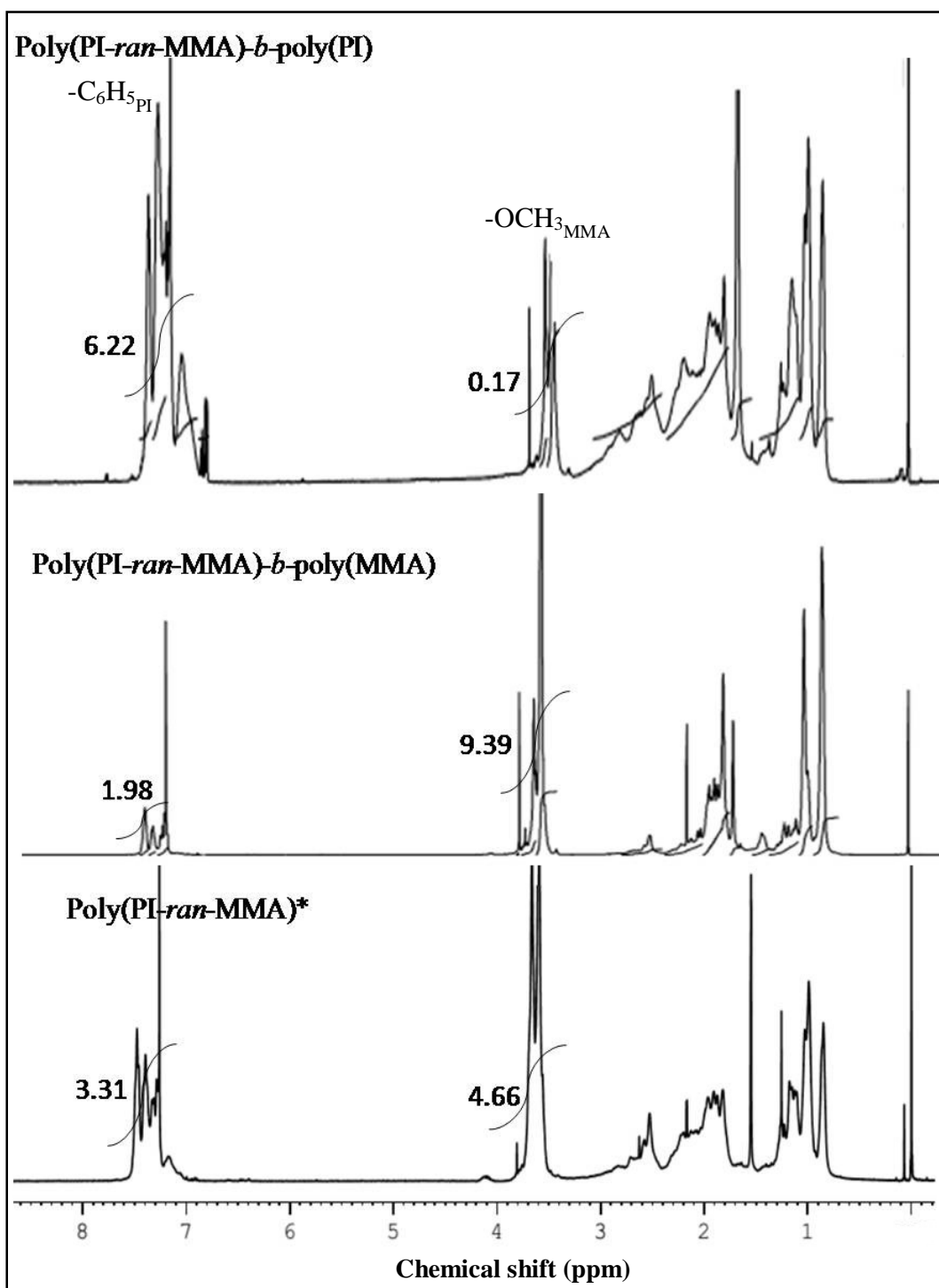


Figure 3.15: Comparative ^1H -NMR spectra of poly(PI-*ran*-MMA)*, poly(PI-*ran*-MMA)-*b*-poly(MMA) and poly(PI-*ran*-MMA)-*b*-poly(PI).

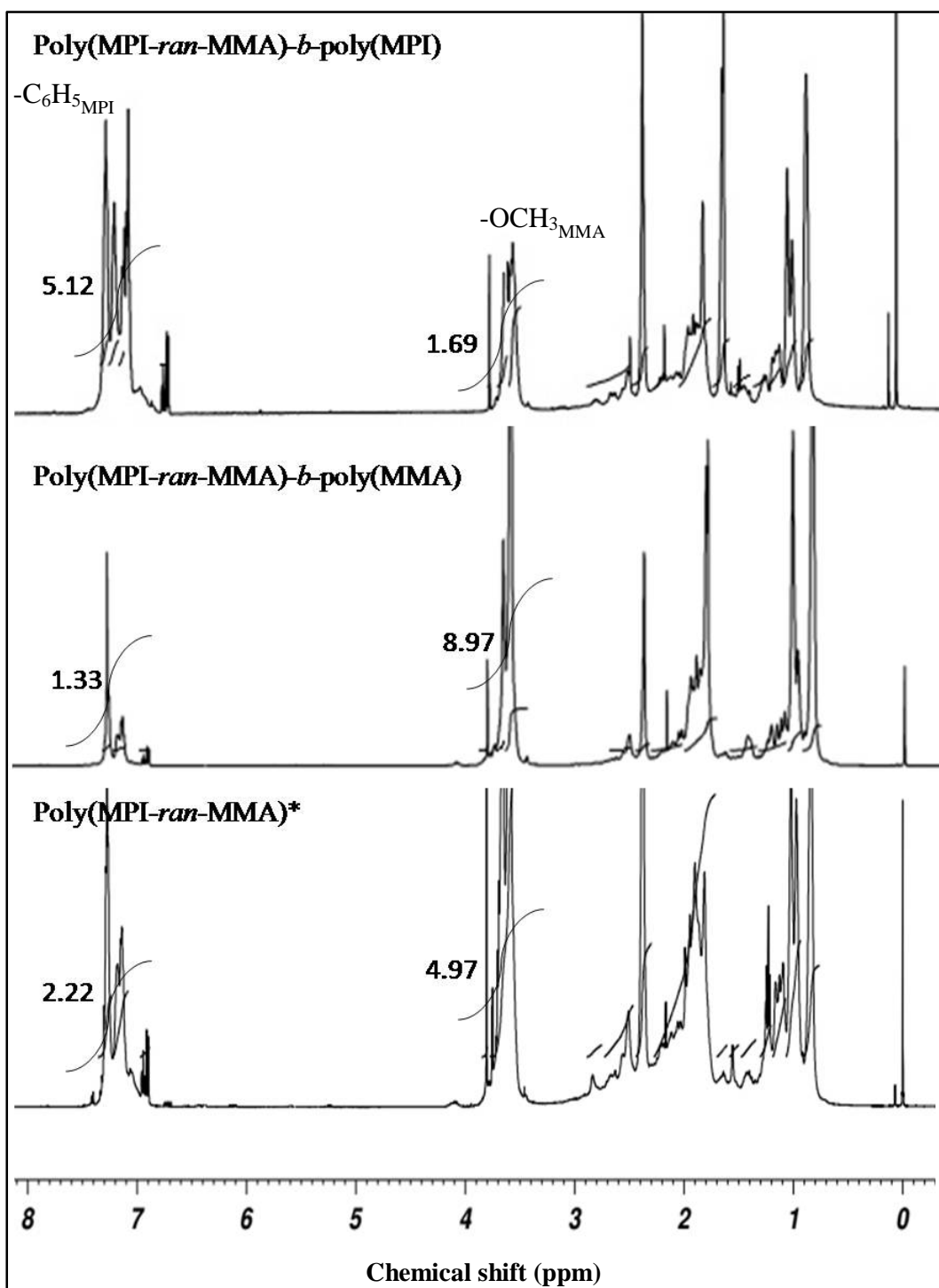


Figure 3.16: Comparative $^1\text{H-NMR}$ spectra of poly(MPI-ran-MMA)*, poly(MPI-ran-MMA)-b-poly(MMA) and poly(MPI-ran-MMA)-b-poly(MPI).

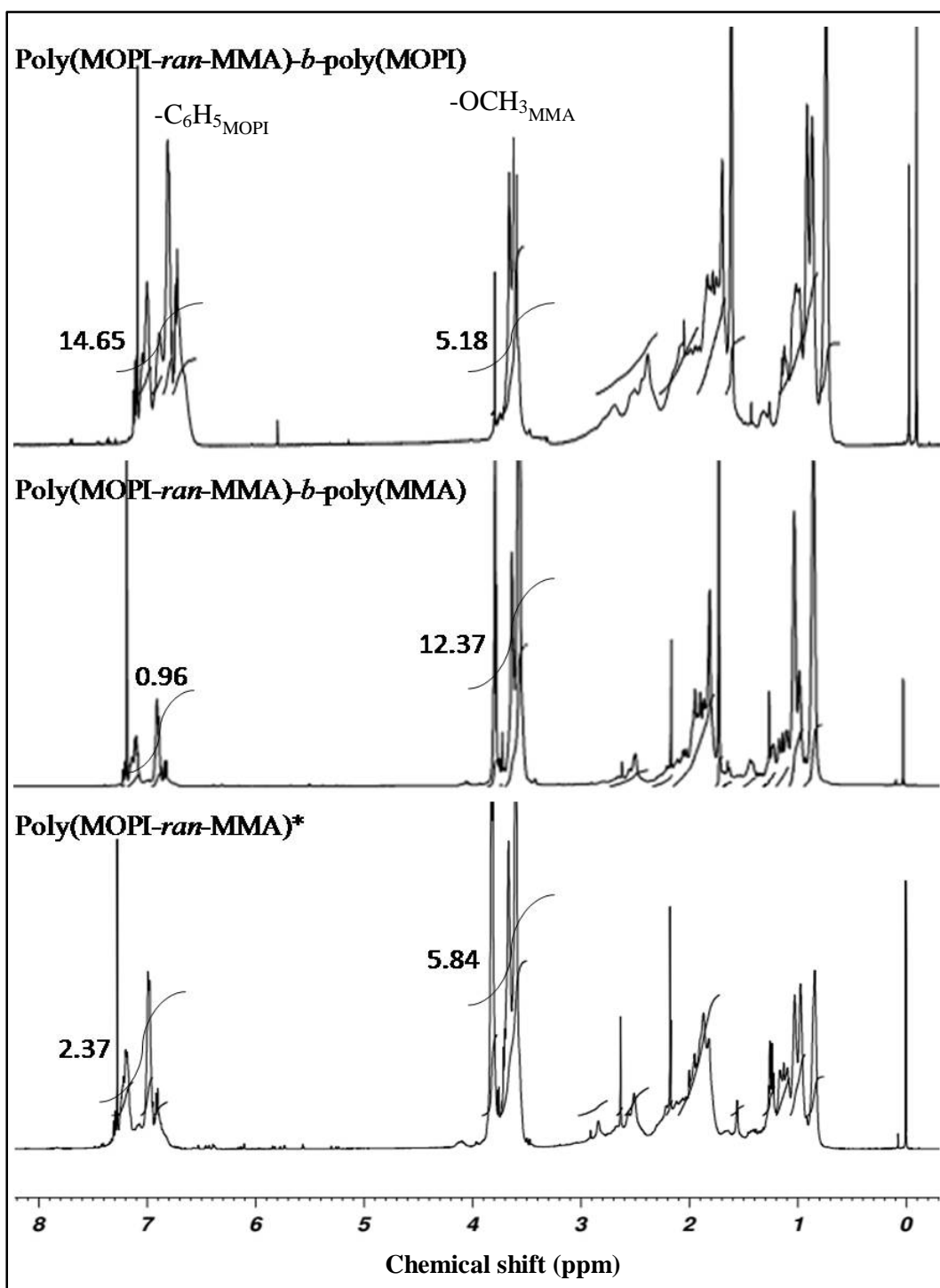


Figure 3.17: Comparative ^1H -NMR spectra of poly(MOPI-*ran*-MMA)*, poly(MOPI-*ran*-MMA)-*b*-poly(MMA) and poly(MOPI-*ran*-MMA)-*b*-poly(MOPI).

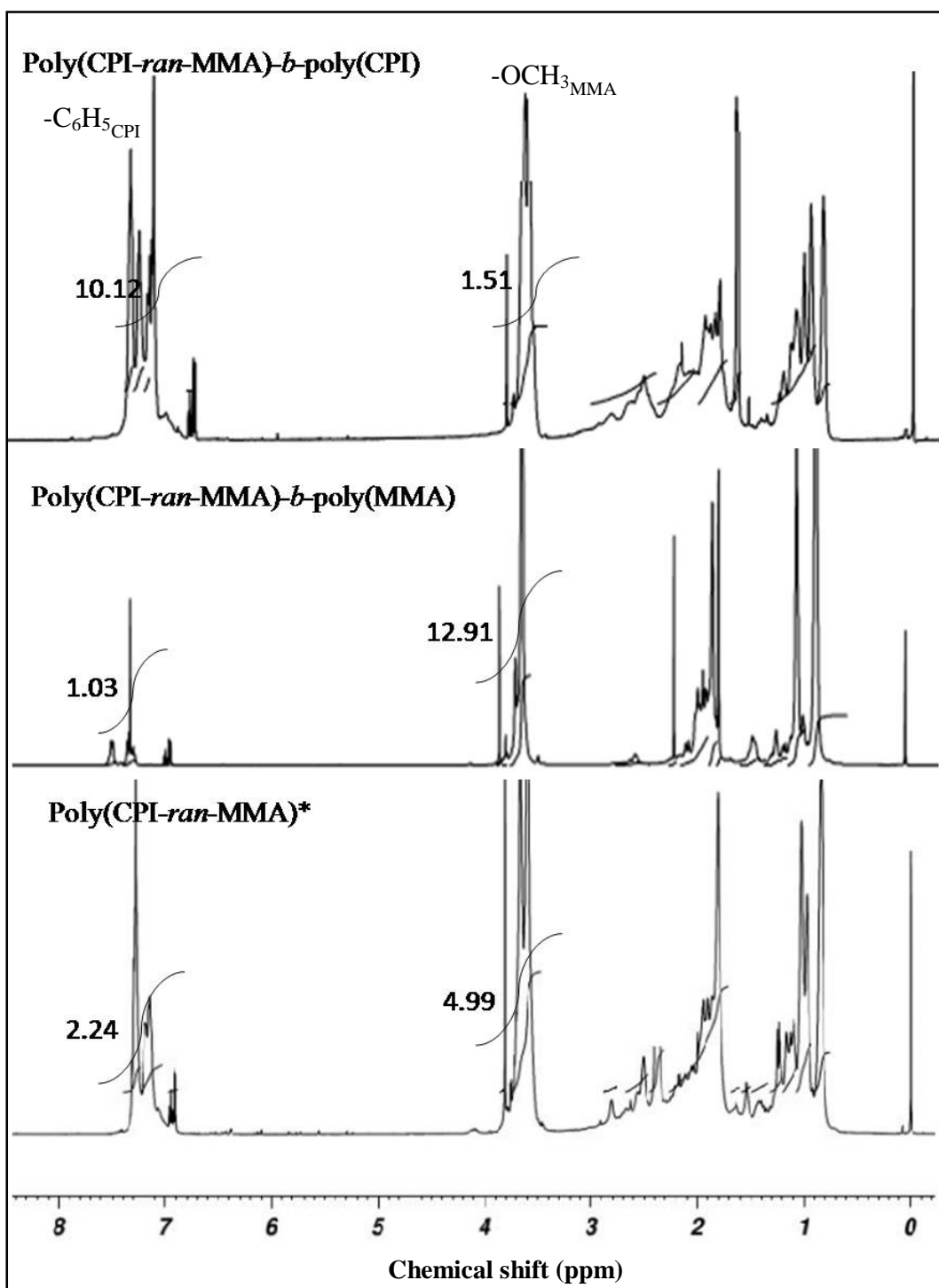


Figure 3.18: Comparative $^1\text{H-NMR}$ spectra of poly(CPI-ran-MMA)*, poly(CPI-ran-MMA)-*b*-poly(MMA) and poly(CPI-ran-MMA)-*b*-poly(CPI).

3.3.8.3 Elemental Analysis

The details of an elemental analysis of block copolymers poly(NAI-*ran*-MMA)-*b*-poly(MMA) and poly(NAI-*ran*-MMA)-*b*-poly(NAI) are given in **Table 3.5**. The good agreement was observed between the experimentally determined and theoretically calculated values of elemental analysis. Theoretically calculated values of elemental analysis have been obtained from the mole fractions data of monomers (of macroinitiators), molecular weight of macroinitiator and the molecular weight of block copolymers [248].

Table 3.5: Results of the elemental analysis of block copolymers.

Block copolymer designation	Experimental			Theoretical		
	C (%)	H (%)	N (%)	C (%)	H (%)	N (%)
poly(PI- <i>ran</i> -MMA)- <i>b</i> -poly(MMA)	59.84	7.69	0.57	60.31	6.40	0.38
poly(MPI- <i>ran</i> -MMA)- <i>b</i> -poly(MMA)	57.33	7.03	1.20	58.34	6.62	1.38
poly(MOPI- <i>ran</i> -MMA)- <i>b</i> -poly(MMA)	60.37	7.45	1.30	63.04	7.28	1.42
poly(CPI- <i>ran</i> -MMA)- <i>b</i> -poly(MMA)	59.16	7.90	0.23	62.05	7.05	0.33
poly(PI- <i>ran</i> -MMA)- <i>b</i> -poly(PI)	66.01	6.56	4.44	66.41	6.39	4.79
poly(MPI- <i>ran</i> -MMA)- <i>b</i> -poly(MPI)	58.75	6.40	4.09	54.47	6.61	3.83
poly(MOPI- <i>ran</i> -MMA)- <i>b</i> -poly(MOPI)	63.02	5.78	4.78	63.99	5.85	4.65
poly(CPI- <i>ran</i> -MMA)- <i>b</i> -poly(CPI)	59.31	5.85	3.42	60.42	6.05	3.30

3.3.9 Effect of Architecture on Molecular Weights

Experimentally, the molecular weights of the block copolymers (**Table 3.6**) were determined using GPC. Theoretical molecular weights of the block copolymers were calculated by using the following equation [249],

$$\bar{M}_n = \left[\left(\frac{[M]_0}{[IM]_0} \right) \times \alpha \times W_M \right] + W_{IM} \dots\dots\dots 3.4$$

where, $[M]_0$ = initial concentration of the MMA, $[IM]_0$ = initial concentration of the poly(NAI-*ran*-MMA) copolymers, W_M = molecular weight of the MMA, W_{IM} = molecular weight of the poly(NAI-*ran*-MMA)* copolymers (determined by GPC) and α = monomer conversion.

The increase in molecular weights of block copolymers as compared to the macroinitiator was observed. The experimentally found molecular weights of block copolymers are in good agreement with the molecular weights calculated theoretically. The GPC curves of the macroinitiator and the corresponding block copolymers poly(NAI-*ran*-MMA)-*b*-poly(MMA) and poly(NAI-*ran*-MMA)-*b*-poly(NAI) are given in **Figure 3.19** and **Figure 3.20**, respectively.

Table 3.6: \bar{M}_n of macroinitiator, percent conversion of monomer (MMA* and NAI[#]), \bar{M}_n and PDI of bock copolymers.

Block copolymer designation	\bar{M}_n of macroinitiator ($1 \times 10^3 \text{ gmol}^{-1}$)	Conversion of monomer (%)	\bar{M}_n of block copolymers ($1 \times 10^5 \text{ gmol}^{-1}$)		PDI
			Experimental	Theoretical	
poly(PI- <i>ran</i> -MMA)- <i>b</i> -poly(MMA)	4.2	42*	2.10	2.00	1.2
poly(MPI- <i>ran</i> -MMA)- <i>b</i> -poly(MMA)	4.9	26*	1.00	1.10	1.3
poly(MOPI- <i>ran</i> -MMA)- <i>b</i> -poly(MMA)	5.7	24*	1.10	1.20	1.2
poly(CPI- <i>ran</i> -MMA)- <i>b</i> -poly(MMA)	4.1	20*	0.80	0.81	1.4
poly(PI- <i>ran</i> -MMA)- <i>b</i> -poly(PI)	4.2	14 [#]	0.90	0.93	1.3
poly(MPI- <i>ran</i> -MMA)- <i>b</i> -poly(MPI)	4.9	12 [#]	0.95	0.96	1.3
poly(MOPI- <i>ran</i> -MMA)- <i>b</i> -poly(MOPI)	5.7	10 [#]	1.10	1.00	1.2
poly(CPI- <i>ran</i> -MMA)- <i>b</i> -poly(CPI)	4.1	09 [#]	0.80	0.80	1.3

The \bar{M}_n of the poly(NAI-*ran*-MMA)-*b*-poly(MMA) block copolymers were observed to increase in the order, poly(CPI-*ran*-MMA)-*b*-poly(MMA) < poly(MPI-*ran*-MMA)-*b*-poly(MMA) < poly(MOPI-*ran*-MMA)-*b*-poly(MMA) < poly(PI-*ran*-MMA)-*b*-poly(MMA). Similarly, the \bar{M}_n of the poly(NAI-*ran*-MMA)-*b*-poly(NAI) block copolymers increased in the order, poly(CPI-*ran*-MMA)-*b*-poly(CPI) < poly(PI-*ran*-MMA)-*b*-poly(PI) < poly(MPI-*ran*-MMA)-*b*-poly(MPI) < poly(MOPI-*ran*-MMA)-*b*-poly(MOPI). From **Scheme 3.2**, it can be inferred that the propagating polymer chain for

the poly(NAI-*ran*-MMA)-*b*-poly(NAI) block copolymer have a terminal '*N*-arylimide' substituted free radical. This free radical is stabilized by electron releasing group at *para* position of aromatic ring. For different *N*-arylimide substituted free radical, the stability increases in the order, $-\text{Cl}$ (-I, inductive effect) $<$ $-\text{H}$ $<$ $-\text{CH}_3$ (+I, inductive effect) $<$ $-\text{OCH}_3$ (+M, mesomeric effect) (**Figure 3.10**). The increase in stability of free radical increases the selectivity of growing polymer chain and reduces the loss of growing radical due to side reactions such as termination or chain transfer. The mesomeric effect of (electron releasing group) $-\text{OCH}_3$ on aromatic ring of MOPI stabilizes incipient free radical for MOPI monomer as compared to the others resulting in higher molecular weight of copolymer. The molecular weight of poly(NAI-*ran*-MMA)-*b*-poly(MMA)

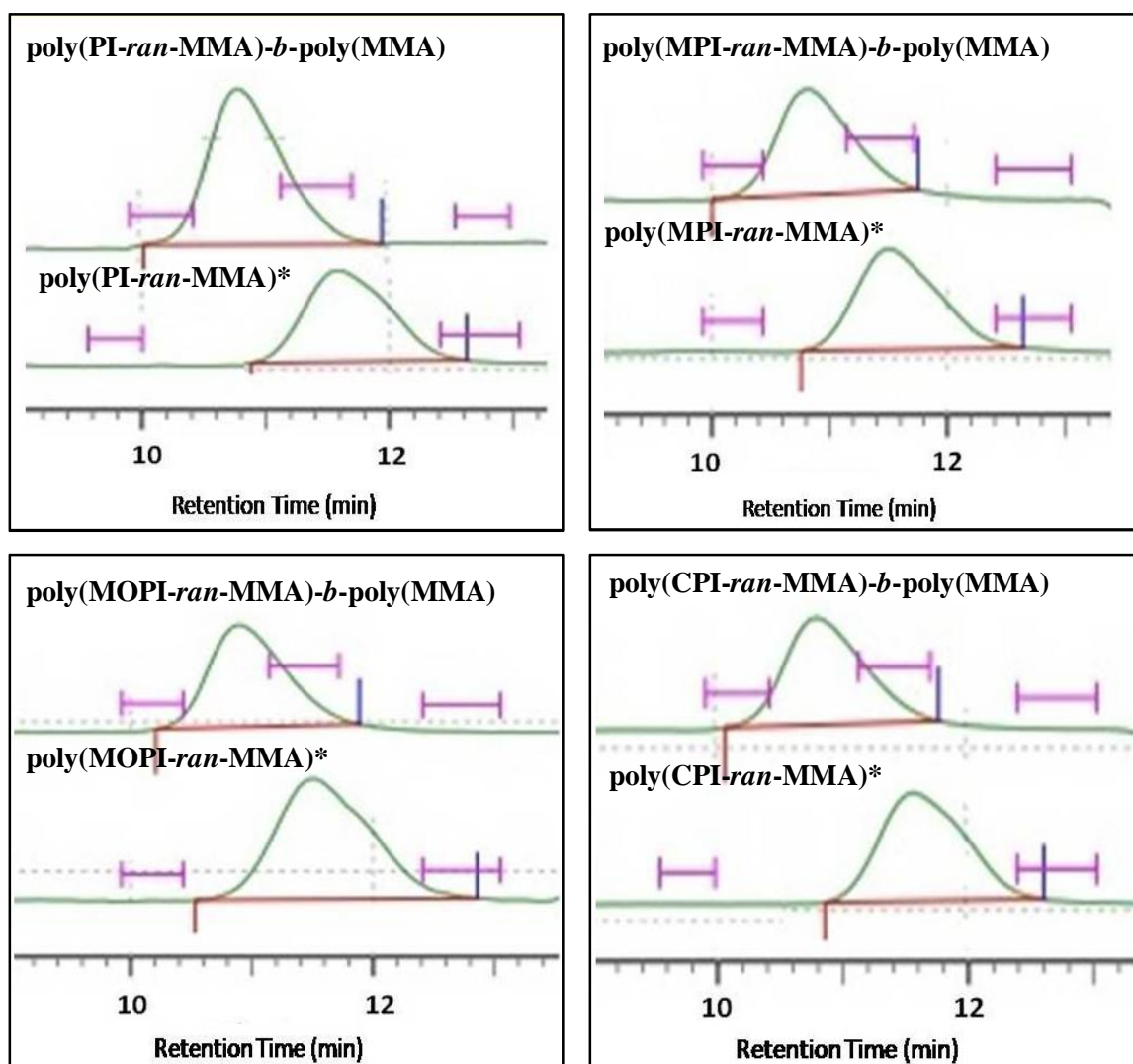


Figure 3.19: GPC of macroinitiators, poly(NAI-*ran*-MMA)* and block copolymers, poly(NAI-*ran*-MMA)-*b*-poly(MMA).

copolymers was found to be 50-80% more as compared to the poly(NAI-*ran*-MMA)-*b*-poly(NAI) copolymers, due to the low reactivity of NAI monomers toward homopolymerization.

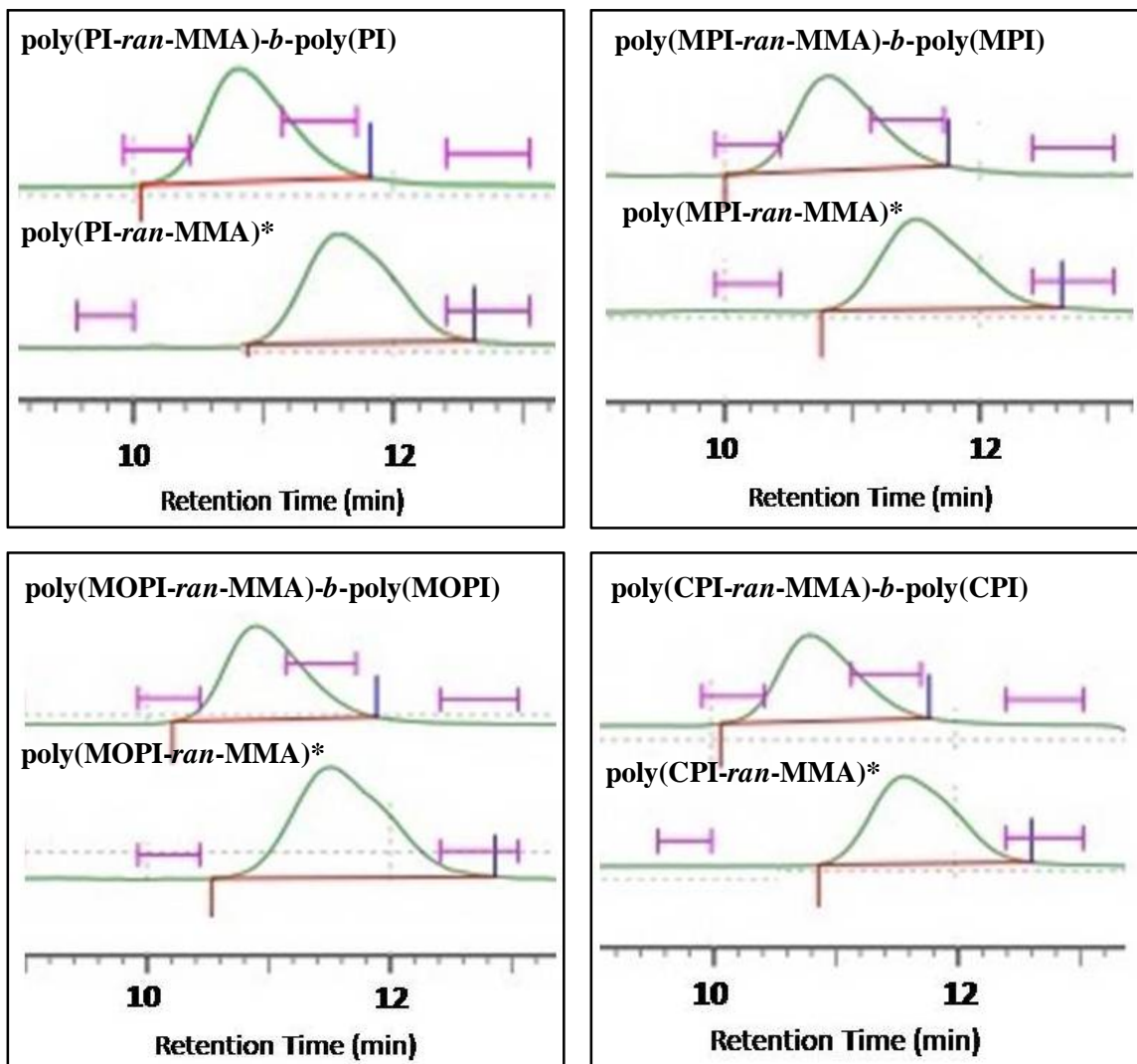


Figure 3.20: GPC of macroinitiators, poly(NAI-*ran*-MMA)* and block copolymers, poly(NAI-*ran*-MMA)-*b*-poly(NAI).

3.3.10 Effect of Architecture on Thermal Properties

3.3.10.1 DSC

The DSC of poly(NAI-*ran*-MMA)-*b*-poly(MMA) block copolymers given in **Figure 3.21**, show shift in the base line corresponding to the glass transition temperature. The T_g

of the copolymers was determined by extrapolation of the two linear regions, before (onset temperature) and after (offset temperature) the T_g and the middle of the incline was considered as exact T_g of the copolymer [21]. The T_g for the virgin PMMA was observed in the region of 100-105 °C [250-251]. The T_g corresponding to the two blocks of copolymer are observed in all the scans, first for the incorporated PMMA block in the temperature range of 104-114 °C and second for the macroinitiator [poly(NAI-*ran*-MMA)] used for its synthesis in the temperature range of 177-186 °C, indicating the phase separation between the two blocks. The details of T_g s for the copolymers are given in the **Table 3.3**.

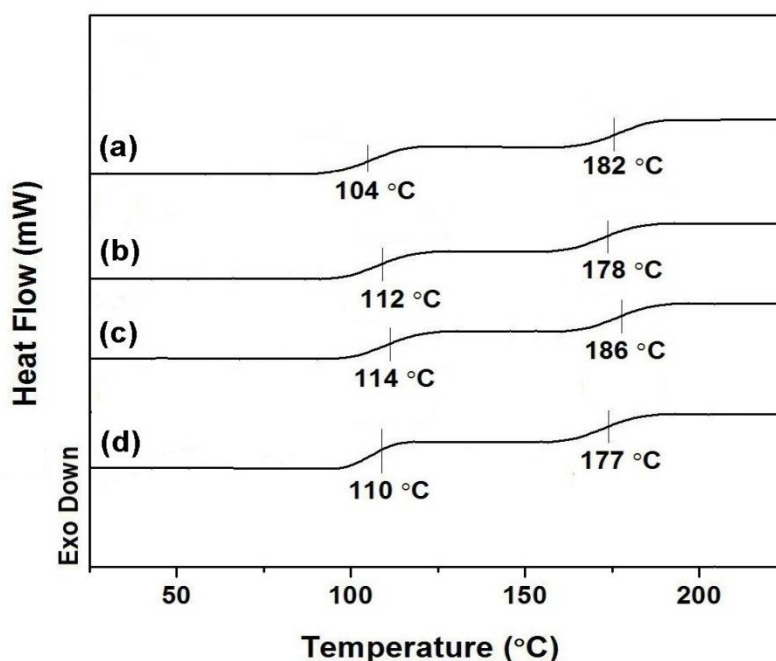


Figure 3.21: DSC of (a) poly(CPI-*ran*-MMA)-*b*-poly(MMA), (b) poly(PI-*ran*-MMA)-*b*-poly(MMA), (c) poly(MPI-*ran*-MMA)-*b*-poly(MMA) and (d) poly(MOPI-*ran*-MMA)-*b*-poly(MMA).

The DSC of poly(NAI-*ran*-MMA)-*b*-poly(NAI) block copolymers are given in **Figure 3.22**. The T_g in the temperature range of 179-182 °C was attributed to poly(NAI-*ran*-MMA) block [i.e. the macroinitiator used for the synthesis of poly(NAI) block]. Similarly, for poly(NAI) block the T_g was observed in the temperature range of 242-265 °C. The details of T_g s for the copolymers are given in the **Table 3.7**. In literature, the T_g reported for the homopolymers, poly(CPI), poly(PI), poly(MPI) and poly(MOPI) are 238

°C, 220 °C, 232 °C, and 220 °C, respectively [5]. The T_g of the poly(NAI) block was increased in the order, poly(CPI-*ran*-MMA)-*b*-poly(CPI) < poly(PI-*ran*-MMA)-*b*-poly(PI) < poly(MPI-*ran*-MMA)-*b*-poly(MPI) < poly(MOPI-*ran*-MMA)-*b*-poly(MOPI).

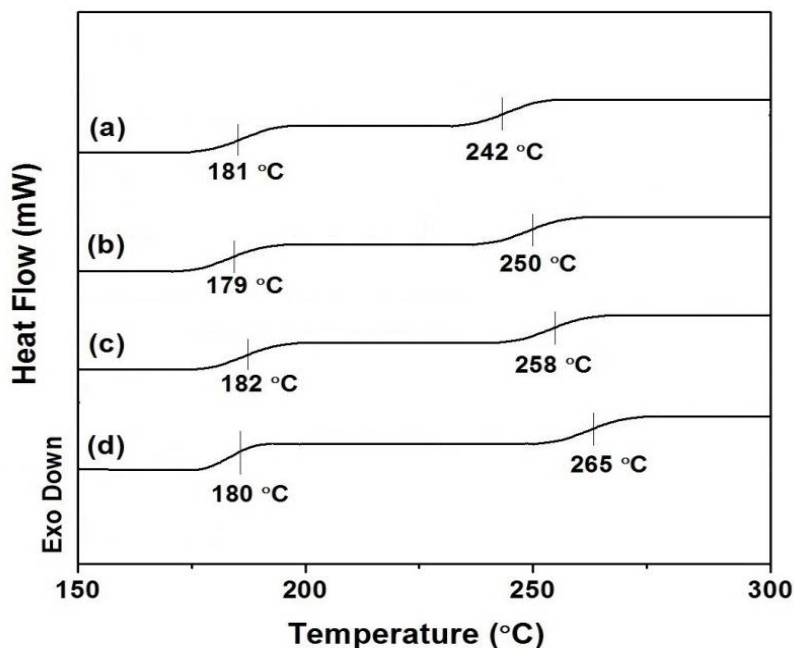


Figure 3.22: DSC of (a) poly(CPI-*ran*-MMA)-*b*-poly(CPI), (b) poly(PI-*ran*-MMA)-*b*-poly(PI), (c) poly(MPI-*ran*-MMA)-*b*-poly(MPI) and (d) poly(MOPI-*ran*-MMA)-*b*-poly(MOPI).

Table 3.7: T_g s observed in the DSC of the block copolymers.

Copolymer Designation	First block			Second block		
	T_o (°C)	T_g (°C)	T_e (°C)	T_o (°C)	T_g (°C)	T_e (°C)
poly(PI- <i>ran</i> -MMA)- <i>b</i> -poly(MMA)	91	112	133	160	178	190
poly(MPI- <i>ran</i> -MMA)- <i>b</i> -poly(MMA)	92	114	135	169	186	205
poly(MOPI- <i>ran</i> -MMA)- <i>b</i> -poly(MMA)	90	110	129	165	177	200
poly(CPI- <i>ran</i> -MMA)- <i>b</i> -poly(MMA)	85	104	125	162	182	198
poly(PI- <i>ran</i> -MMA)- <i>b</i> -poly(PI)	160	179	190	229	250	269
poly(MPI- <i>ran</i> -MMA)- <i>b</i> -poly(MPI)	163	182	195	240	258	271
poly(MOPI- <i>ran</i> -MMA)- <i>b</i> -poly(MOPI)	165	180	200	246	265	286
poly(CPI- <i>ran</i> -MMA)- <i>b</i> -poly(CPI)	162	181	198	221	242	265

T_o = onset temperature and T_e = endset temperature

This can be attributed to the increase in the polarity and rigidity of the pendant group with increase in electron releasing capacity of the substituent on the aromatic ring of NAI. The poly(NAI-*ran*-MMA)-*b*-poly(NAI) block copolymers are having higher T_g as compared to the poly(NAI-*ran*-MMA)-*b*-poly(MMA) block copolymers.

3.3.10.2 TG/DTG

The TG/DTG scans of the poly(NAI-*ran*-MMA)-*b*-poly(MMA) copolymers are shown in **Figure 3.23**.

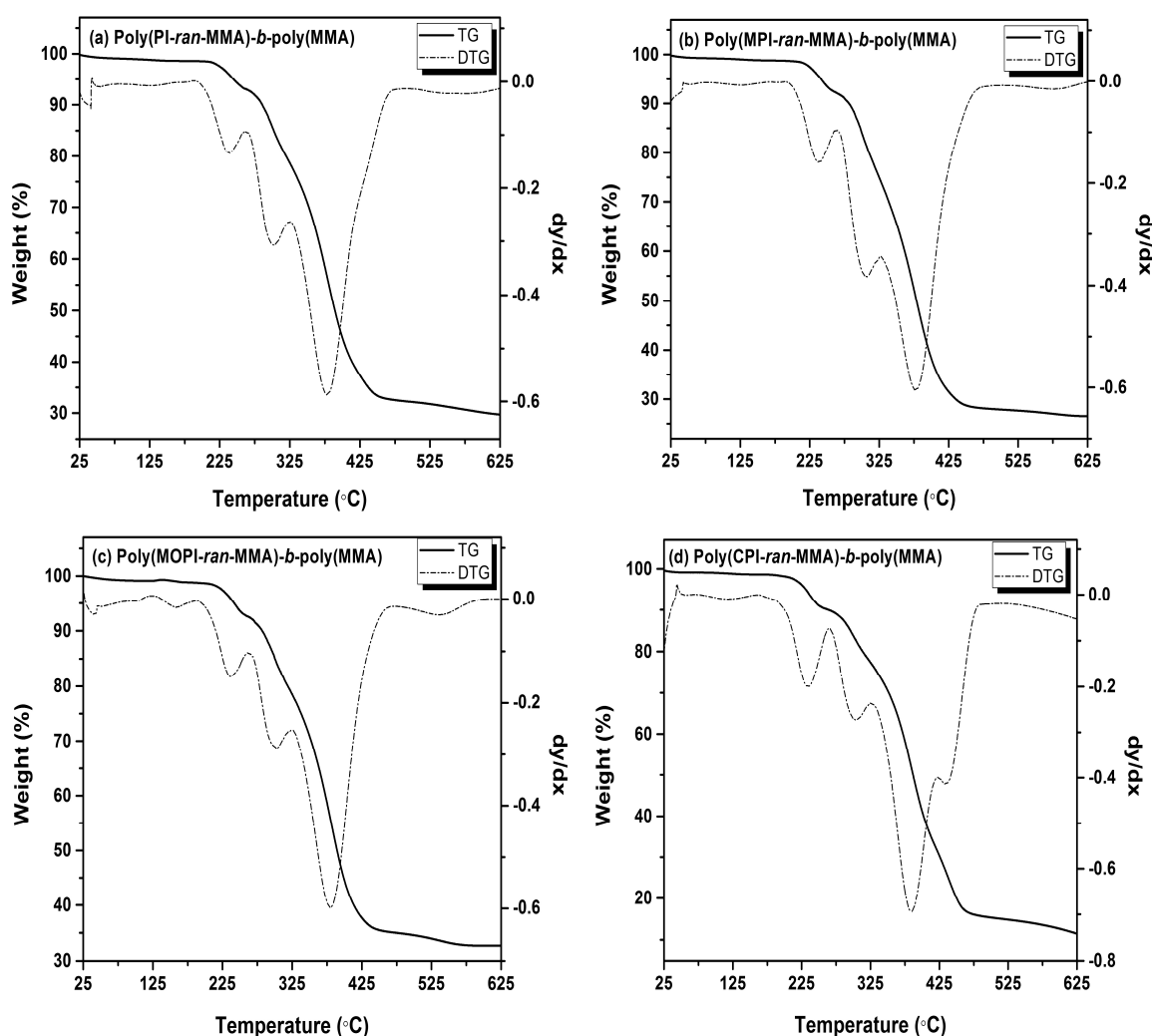


Figure 3.23: TG/DTG scans for poly(NAI-*ran*-MMA)-*b*-poly(MMA) copolymers.

In contrast to PMMA, which is stable up to 150 °C [250-251], poly(NAI-*ran*-MMA)-*b*-poly(MMA) copolymers are stable upto 280 °C. For poly(NAI-*ran*-MMA)-*b*-poly(MMA) copolymers, the degradation in the region 280-350 °C was attributed to

head-to-head linkages. The major weight loss (43-48%) in the region 350-450 °C may be due to the scissions of methoxycarbonyl side groups and random scissions of main chains [251]. However, only 2-5% weight loss is observed due to the simultaneous scissions of end groups in the region 450-550 °C. This may be due to high molecular weight of block copolymers resulting in lesser number of chains per gram of sample. The char yield was found to be higher for block copolymers as compared to the macroinitiators (9-17% at 600 °C) and it is in the range of 10-33% at 600 °C. The char yield of the block copolymers was observed to increase in the order, poly(CPI-*ran*-MMA)-*b*-poly(MMA) < poly(PI-*ran*-MMA)-*b*-poly(MMA) < poly(MOPI-*ran*-MMA)-*b*-poly(MMA).

The TG/ DTG scans of the poly(NAI-*ran*-MMA)-*b*-poly(NAI) block copolymers are shown in **Figure 3.24**. The block copolymers were stable up to 330 °C and showed two steps degradation in the temperature ranges 330-410 °C and 410-500 °C. The weight loss (22-28%) in the region 330-410 could be due to the scissions of small groups at the end of polymer chain such as methoxycarbonyl side groups. The major weight loss (48-55%) in the region 410-450 °C is attributed to the random scissions of main chains which leads to the formation of macroradicals which further undergo unzipping to give the monomers as reported by Katiyar et al. [253]. The random chain scission for the block copolymers (410 °C) starts at temperature 60 °C higher than virgin PMMA. This may be due to the formation of more stable imide substituted free radical (as an intermediate) in this step compared to the methyl carboxylato substituted free radical intermediate in the random chain scission of virgin PMMA. Due to the higher incorporation of aromatic ring, the char yield was found to be higher (~ 15-22% at 600 °C) for block copolymers as compared to the macroinitiators (~ 9-17% at 600 °C) used for its synthesis and follow the order, poly(CPI-*ran*-MMA)-*b*-poly(CPI) < poly(PI-*ran*-MMA)-*b*-poly(PI) < poly(MOPI-*ran*-MMA)-*b*-poly(MOPI) < poly(MPI-*ran*-MMA)-*b*-poly(MPI).

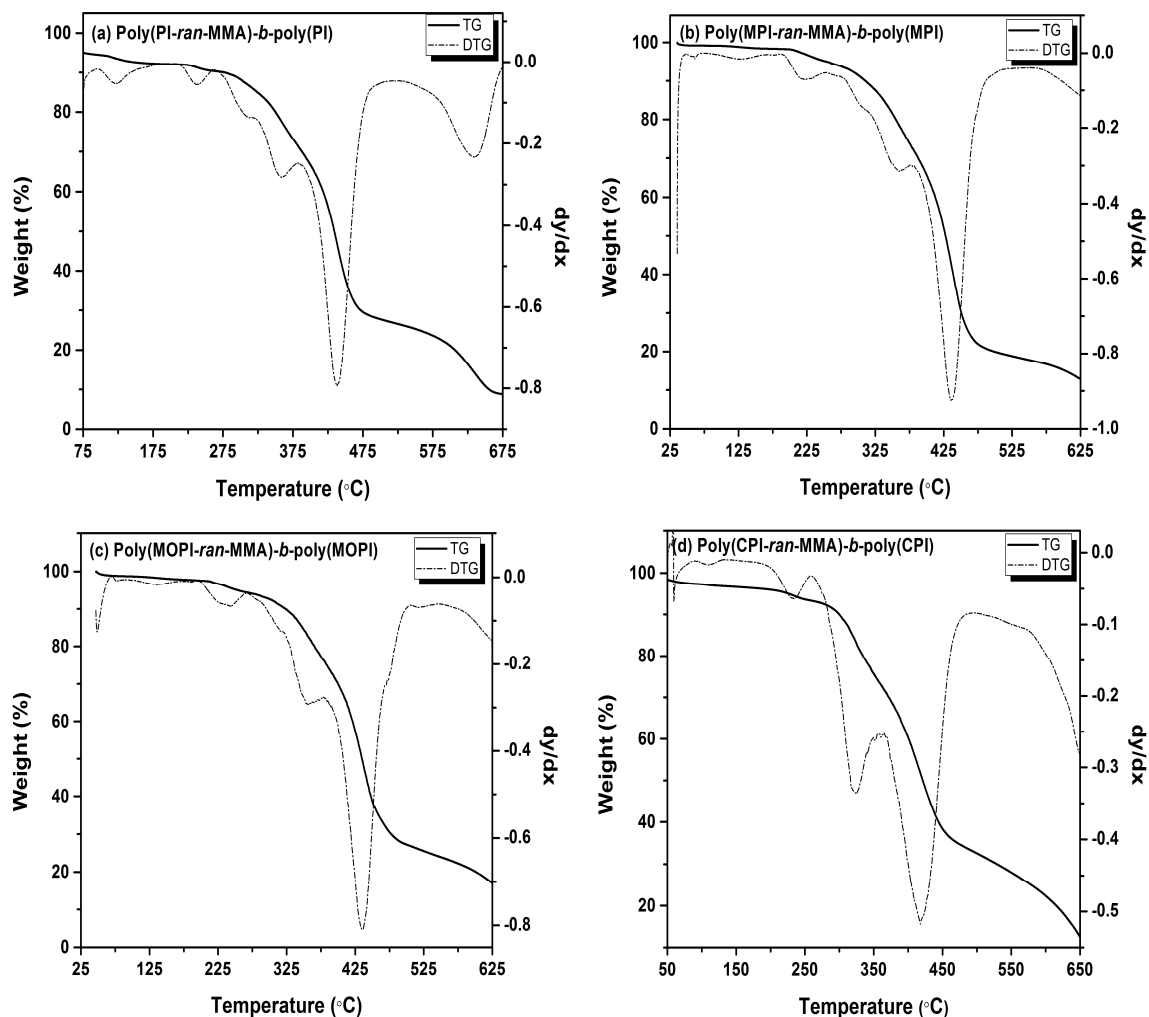


Figure 3.24: TG/ DTG scans for poly(NAI-ran-MMA)-b-poly(NAI) copolymers.

3.4 Conclusions

The copolymerization of NAI monomers (with various substituents on aromatic ring) were carried out with MMA via n-ATRP and AGET-ATRP, resulting in ‘N-arylimide’ as pendant group. The poly(NAI-ran-MMA)* synthesized via n-ATRP shows linear increase in the molecular weight with percent conversion of monomers indicating that the reaction is occurring under controlled conditions. The linear variation of $\ln \left\{ \frac{[M]_t[I]_0}{[I]_t[M]_0} \right\}$ vs time, indicates that the reaction follows second order kinetics. The rate of copolymerization, molecular weight and T_g of poly(NAI-ran-MMA) copolymers were found to be higher for the copolymers synthesized via AGET-ATRP as compared to the n-ATRP. With the increase in the electron releasing tendency of substituents on aromatic ring of the pendant group, an increase in the rate of copolymerization, molecular weights

and T_g of the poly(NAI-*ran*-MMA) copolymers was observed. The block copolymers [poly(NAI-*ran*-MMA)-*b*-poly(MMA) and poly(NAI-*ran*-MMA)-*b*-poly(NAI)] were synthesized using poly(NAI-*ran*-MMA)* macroinitiator via AGET-ATRP. An increased molecular weights of block copolymers was observed as compared to the macroinitiator, which agreed well with theoretical values. The T_g corresponding to the two blocks of the copolymers, observed in DSC further confirms the architecture of the copolymer as “block”. The T_g corresponding to the two blocks *i.e.* Poly(NAI-*ran*-MMA) and Poly(NAI) were observed in the temperature range of 179-182 °C and 242-265 °C, respectively. This results in an overall higher T_g of copolymers synthesized in this study as compared to PMMA which has a softening temperature of ~105 °C. Thus, the living copolymers of NAI and MMA with block architecture were successfully synthesized and characterized. These copolymers with 20-40% increase in softening temperature and 15-20% increase in molecular weight as compared to previously reported copolymers of NAI and MMA (using conventional methods of polymerization) may be useful as ‘thermoplastics’ in the higher temperature range.

CHAPTER IV

INVESTIGATION OF BROMO SUCCINIMIDES AS POTENTIAL ATRP INITIATORS

4.1 Overview

The copolymerizations of NAI monomers with MMA using EBiB initiator (which resembles to one of the chosen monomer i.e. MMA) have been discussed in chapter III. The molecular weights of the obtained poly(NAI-*ran*-MMA) copolymers (section 3.3.5) were found to be less than $1.9 \times 10^4 \text{ gmol}^{-1}$, which may have occurred due to the chosen initiator. In ATRP, the rate constants of activation and deactivation depend on the structure of initiators (i.e. alkyl halides) and its reactivity. Also, for an efficient ATRP process, the rate of initiation should be faster than the rate of propagation to minimize the side reaction. Previous studies on NAI and MMA copolymer systems have shown higher reactivity ratios for NAI monomers as compared to MMA [14-15,19-20]. Hence, it will be of interest to investigate the initiators (obtained from renewable resources) having structural similarities with the other monomer (i.e. NAI).

This chapter deals with the experimental and theoretical determination of K_{ATRP} values of synthesized bromo derivatives of succinimide [viz. *N*-phenyl(3-bromo-3-methyl)succinimide, *N*-phenyl(3-bromo-4-methyl)succinimide and *N*-phenyl(3-bromomethyl)succinimide] along with a commercial ATRP initiator (EBiB). Experimentally, the K_{ATRP} values are determined using UV-Vis-NIR, DOSY-NMR spectroscopy and Fischer-Fukuda equation for the persistent radical effect. Alternatively, these compounds along with some similar alkyl halides (R-X) are also investigated theoretically using DFT methods for their possible chain initiation activity for the ATRP process. The predicted initiator *N*-phenyl(3-bromo-3-methyl)succinimide has been successfully tested for the copolymerization of NAI and MMA via AGET-ATRP process.

4.2 Experimental Section

4.2.1 Materials and Methods

Succinic anhydride (99.0%) and acetonitrile dry (99.5%) were used as supplied from S. D. Fine Chem Limited, Mumbai, India.

Diffusion ordered spectroscopy (DOSY)-NMR measurements were performed on Bruker Avance (AV III) 500 MHz NMR spectrometer equipped with a 5-mm broadband observe z-axis gradient probe which delivers a maximum gradient strength of 50 Gcm^{-1} . Experiments were carried out with active temperature regulation, at $25 \text{ }^\circ\text{C}$. Self diffusion coefficients were measured using the stimulated echo, bipolar gradient (stebpgp1s) pulse sequence. The diffusion coefficient (D) is experimentally determined by monitoring the signal intensity decay in a 1D pulsed-field gradient spin-echo experiment spectrum as a function of the applied gradient strength [254]. In the two dimensional DOSY experiment [255-256], the decay of magnetization as a function of increasing gradient intensity (the gradient ramp) is observed. The gradient ramp in this experiment was adjusted between 2 and 95% strength of the gradient amplifier using 16 equidistant steps. Each experiment was acquired with a spectral width of 4500 Hz and 16k complex points. The diffusion time (Δ) of 100 ms is used and the duration of the gradient pulse (δ) 1ms is used. After Fourier transformation and baseline correction, the spectra were processed with DOSY processing tools from Bruker Topspin 2.1 package. Data were analyzed using the variable gradient fitting routines, and in all cases the proton resonances were fit with a single exponential decay function using peak intensities. The spectroscopic measurements were performed on Jasco V-570, UV-Vis-NIR spectrometer. Molecular-mass characteristics of the copolymers were determined by GPC in THF as an eluent at flow rate of 0.75 mL per minute and column temperature of $25 \text{ }^\circ\text{C}$ with an Agilent 1260 HPLC-GPC system equipped with column: PL gel 5 micron Mixed D: $300 \text{ mm} \times 7.5 \text{ mm}$ with a differential refractometer. Polystyrene standards with molecular weight in the range of 10^3 to 10^5 gmol^{-1} were used for calibration. Thermal characterization of copolymers was carried out using TGA/ DTA analyzer from TA Instruments, model: SDT Q600. DSC scans were recorded in nitrogen atmosphere (flow rate = $60 \text{ cm}^3 \text{ min}^{-1}$) at heating rate of $10 \text{ }^\circ\text{C}$ per minute using $3 \pm 1 \text{ mg}$ of powdered samples. For the uniform thermal history, all the samples were first heated to $150 \text{ }^\circ\text{C}$, cooled to room temperature

and then again heated to 600 °C. The second heating scan was used for the determination of glass transition of copolymer. Thermal stability was determined by recording TG/DTG curves in nitrogen atmosphere (flow rate = 60 cm³min⁻¹) at heating rate of 10 °C per minute using 3 ± 1 mg of powdered samples. The DTG plots (dy/ dx) of the copolymers were obtained by taking the ratios of difference of weight loss (in percentage) (dy) with respect to the difference of temperature (dx).

4.2.2 Synthesis of *N*-phenylsuccinimide

In a 500 mL reaction flask equipped with a magnetic bead, succinic anhydride (0.15 mol) was dissolved in 50 mL of acetone. To this solution, aniline (0.15 mol) dissolved in 50 mL of acetone was added slowly with vigorous stirring. The *N*-phenylsuccinamic acid starts precipitating out. The resulting precipitate was filtered, dissolved in saturated solution of sodium bicarbonate and reprecipitated with 5M HCl. The precipitate was filtered, washed with distilled water and dried in oven at 80 °C. To the solution of *N*-phenylsuccinamic acid (0.14 mol) in 40 mL of acetone, acetic anhydride (0.25 mol) and anhydrous sodium acetate (0.06 mol) were added. The reaction mixture was refluxed until a clear solution was obtained. The refluxing with stirring was continued for another 5 h. The reaction mixture was then cooled to room temperature and poured in excess of ice cold water. The precipitate obtained was filtered and washed with saturated solution of sodium bicarbonate followed by distilled water. The crude product was purified by column chromatography using 20% ethyl acetate and hexane as an eluent, giving pure *N*-phenylsuccinimide, (Yield 60%, m. p. 155 °C). The reaction scheme for the synthesis of *N*-phenylsuccinimide is given in (Chapter I, **Scheme 2.1**). The purified *N*-phenylsuccinimide was characterized using IR, ¹H-NMR ¹³C-NMR spectroscopy and elemental analysis. The IR spectra of *N*-phenylsuccinimide is given in the **Figure 4.1**. Similarly, the ¹H-NMR and ¹³C-NMR spectra of *N*-phenylsuccinimide is given in the **Figure 4.2**.

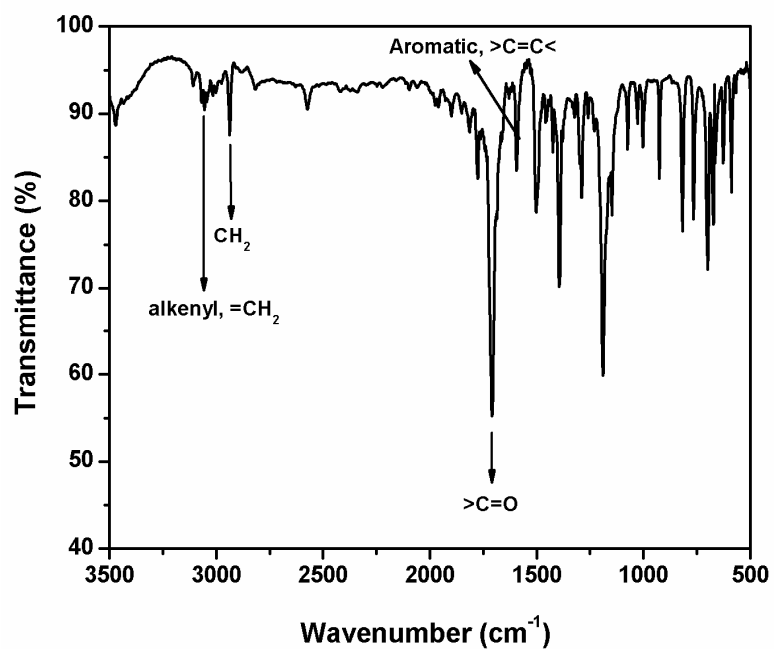


Figure 4.1: IR spectrum of *N*-phenylsuccinimide.

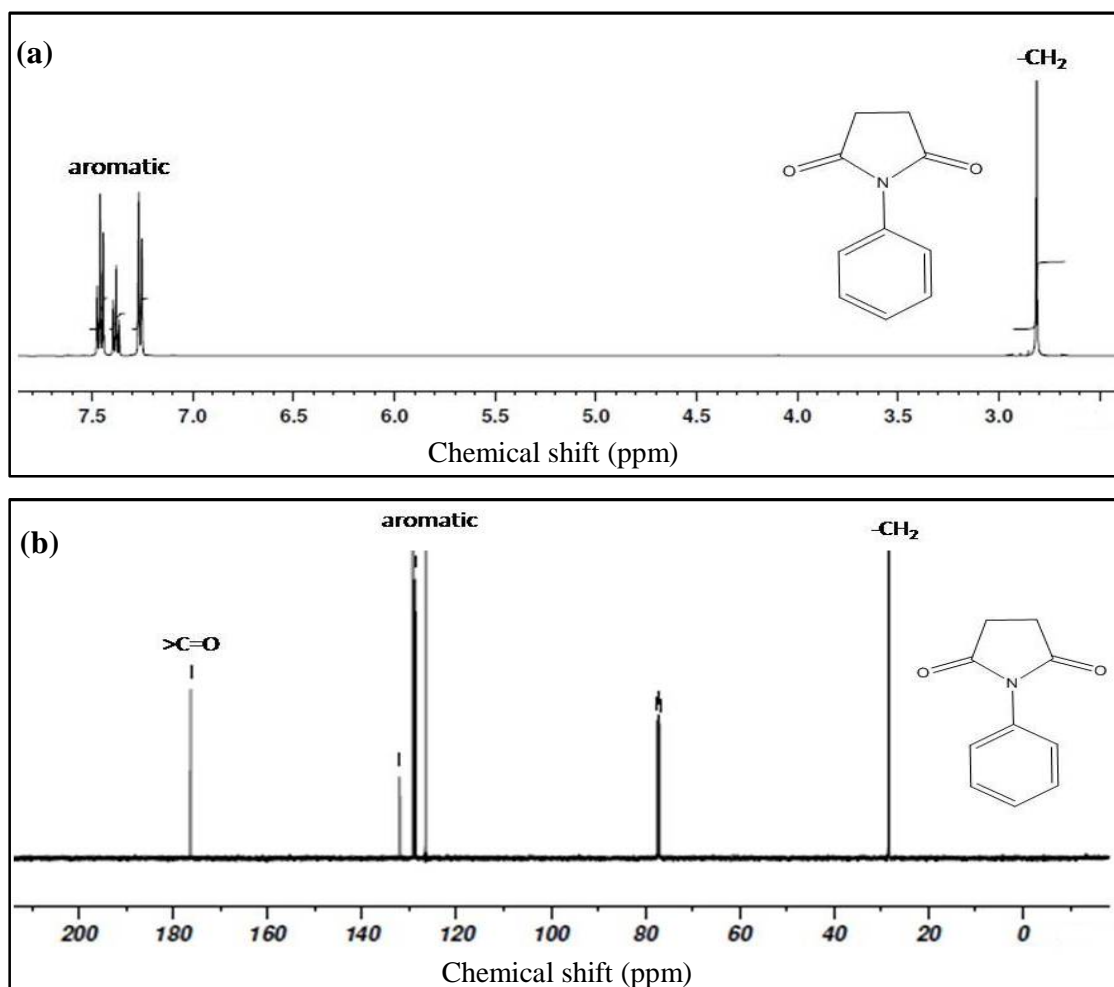


Figure 4.2: (a) ¹H-NMR and (b) ¹³C-NMR spectra of *N*-phenylsuccinimide.

IR (KBr, cm^{-1}): 3058 (aromatic C-H stretch), 2936 (C-H stretch), 1779 and 1711 ($>\text{C}=\text{O}$ of imide), 1592, 1500, 1450 (aromatic $>\text{C}=\text{C}<$ stretch), 758 (oop C-H bending).

$^1\text{H-NMR}$ (CDCl_3 , ppm) δ : 7.5 (m, 2 H, C_6H_5), 7.4 (m, 2 H, C_6H_5), 7.3 (m, 1 H, C_6H_5), 3.8 (s, 4 H, CH_2 of the ring).

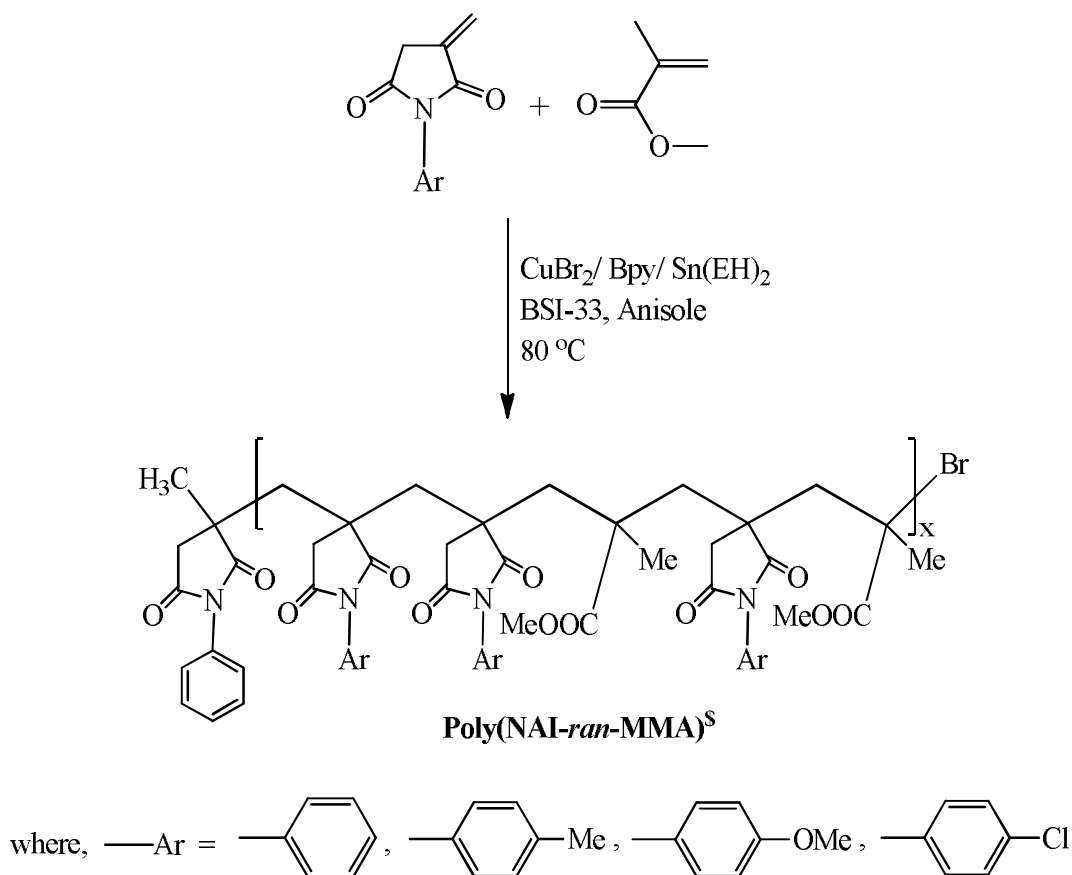
$^{13}\text{C-NMR}$ (CDCl_3 , ppm) δ : 176.29 ($>\text{C}=\text{O}$), [131.97; 129.20; 128.64; 126.51 (C_6H_5)], 28.41 (CH_2 of the ring).

Elemental Analysis (CHNO): Found - %C, 69.89; %H, 5.85; %N, 7.59; %O, 17.86; Calculated: %C, 68.56; %H, 5.18; %N, 8.00; %O, 18.27.

4.2.3 Synthesis of Copolymers of NAI and MMA using BSI-33 as Initiator

The reaction scheme for the synthesis of copolymers of PI and MMA using AGET-ATRP is shown in **Scheme 4.1**. The solution of NAI (0.01 mol) and MMA (0.04 mol) in 10 mL of dry anisole was taken in three-way 100 mL round bottom flask equipped with reflux condenser and a magnetic bead. To the reaction mixture, CuBr_2 (0.25 mmol), $\text{Sn}(\text{EH})_2$ (0.125 mmol) and Bpy (0.75 mmol) were added. The reaction mixture was subjected to freeze-vacuum-thaw cycle twice. BSI-33 (0.25 mmol) dissolved in 4 mL of dry anisole in a separate two way round bottom flask was degassed by subjecting to freeze-vacuum-thaw cycle twice and then charged to this reaction flask through a nitrogen purged syringe. The mixture was again subjected to freeze-vacuum-thaw cycle thrice. The reaction flask was now immersed in hot oil bath maintained at 80 °C. The polymerization was terminated by adding the reaction mixture in excess of methanol. The copolymer precipitated out was filtered and washed with hot methanol to remove any unreacted monomers. The obtained copolymer was dissolved in acetone and passed through the alumina bed to remove the catalyst. It was concentrated using rotary evaporator and reprecipitated with methanol. The obtained copolymer was filtered and dried under vacuum. The final yield of the copolymers was obtained using gravimetric method and was found in the range of 17-98%. The reactions under similar condition were carried out in ten different reactions flasks and quenched at different time intervals viz. 5 h, 10 h, 15 h, 20 h, 25 h, 30 h, 35 h, 45 h and 50 h.

The NAI monomers such as PI, MPI, MOPI and CPI were copolymerized with MMA using similar experimental procedure as given above and reactions were quenched after 45h. The obtained copolymers are designed as poly(PI-*ran*-MMA)[§], poly(MPI-*ran*-MMA)[§], poly(MOPI-*ran*-MMA)[§] and poly(CPI-*ran*-MMA)[§]. The properties of this copolymers were compared with poly(NAI-*ran*-MMA)[#] copolymers which have been synthesized in chapter III (**Section 3.2.3**).



Scheme 4.1: Reaction scheme for synthesis of copolymers of NAI and MMA using BSI-33 as initiator.

4.2.4 Experimental Determination of ATRP Equilibrium Constant (K_{ATRP})

The K_{ATRP} values of the studied bromo derivatives of succinimide were determined using Fischer-Fukuda equation for the persistent radical effect that takes into account the changes in catalyst and initiator concentration (equations 4.1-4.2) [37, 53].

$$F(Y) = 2k_t(K_{ATRP})^2t + c' \dots\dots\dots 4.1$$

$$\text{where, } F(Y) = \left(\frac{I_0C_0}{C_0-I_0}\right)^2 \left(\frac{1}{C_0^2(C_0-Y)} + \frac{2}{I_0C_0(C_0-I_0)} \ln\left(\frac{I_0-Y}{C_0-Y}\right) + \frac{1}{I_0^2(C_0-Y)}\right) \dots\dots\dots 4.2$$

In the above equations 4.1 and 4.2, Y = concentration of deactivating species $[\text{BrCu}^{\text{II}}\text{Bpy}]$, I_0 = initial concentration of bromo derivatives of succinimide (R-Br), C_0 = initial concentration of catalyst $[\text{BrCu}^{\text{I}}\text{Bpy}]$, k_t = termination rate constant, and t = time.

The K_{ATRP} is calculated from the (equation 4.1) slope of the plot of $F(Y)$ vs. t ($K_{ATRP} = \sqrt{\frac{\text{slope}}{2k_t}}$). The parameters I_0 and C_0 (from the above equation) are known. The other parameter $Y = [\text{BrCu}^{\text{II}}\text{Bpy}]$ and k_t were determined as follows;

4.2.4.1 Determination of $[\text{BrCu}^{\text{II}}\text{Bpy}]$

To a dry three way round bottom flask, dry acetonitrile (30 mL) was added and nitrogen was bubbled for five minutes. $\text{Cu}^{\text{I}}\text{Br}$ (3.7mM) and ligand Bpy (7.0 mM) were then added to the reaction flask and the contents were stirred for 30 minutes (to ensure the complete dissolution of $\text{Cu}^{\text{I}}\text{Br}$ and formation of $\text{BrCu}^{\text{II}}\text{Bpy}$ complex). The absorbance of the obtained solution at $\lambda_{\text{max}} = 745$ nm for $\text{BrCu}^{\text{II}}\text{Bpy}$ complex was set to zero. To this solution, EBiB (70 mM) (commercially available ATRP initiator) was added and the resulting mixture was stirred at room temperature (25 °C). Absorbance of the resulting solution was measured after every 15 minutes. A linear increase in the absorbance was observed showing the increase in the concentration of the $\text{BrCu}^{\text{II}}\text{Bpy}$ complex. To select the concentration range for the designed experiment, a similar experiment was repeated using 50 mM of EBiB.

Similarly, the experiments were performed using all other synthesized bromo derivatives of succinimide (viz. BSI-3, BSI-34 and BSI-33), at two different concentrations (viz. 70 mM and 50 mM). The plots of absorbance vs time at 745 nm are given in **Figure 4.3** to **Figure 4.6**. The concentration of the $\text{BrCu}^{\text{II}}\text{Bpy}$ complex was determined using values of the extinction coefficient for the complex $\text{BrCu}^{\text{II}}\text{Bpy}$, which was determined separately.

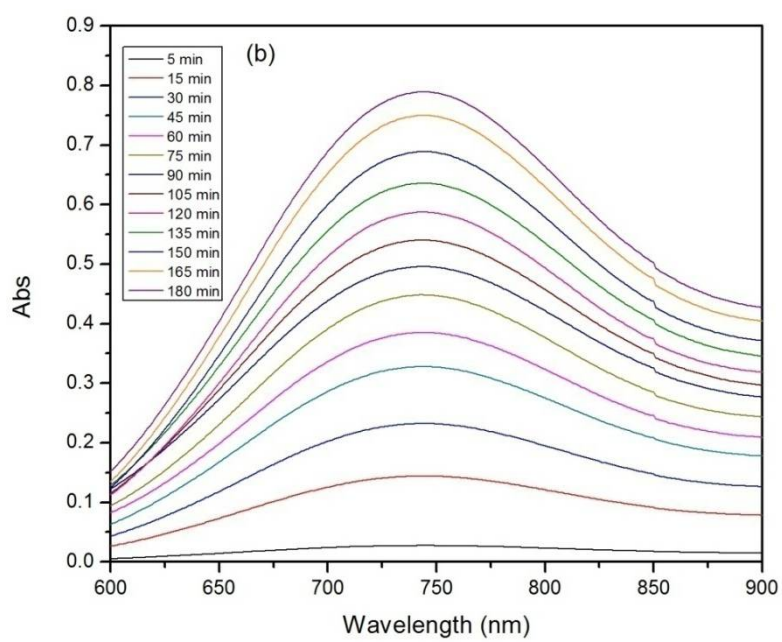
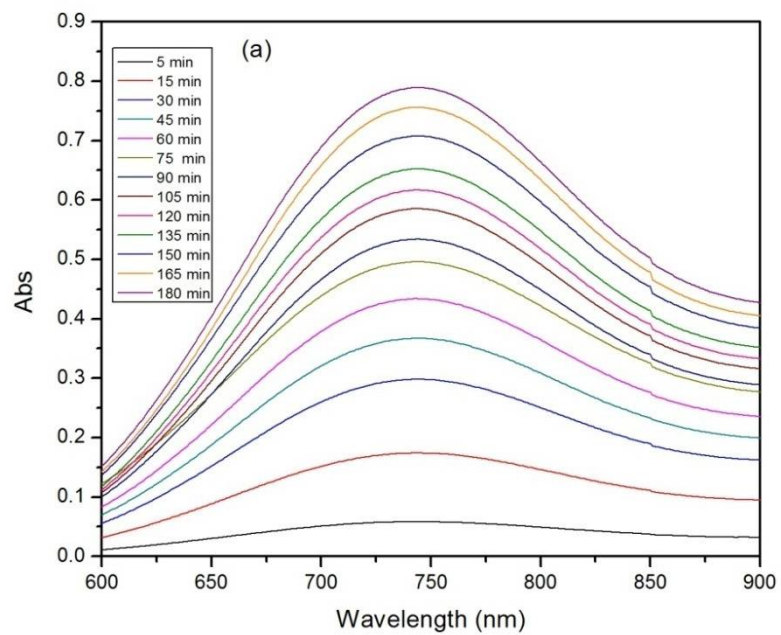


Figure 4.3: Plot of absorbance with time at 745 nm for EBiB initiator (a) 70 mM and (b) 50 mM.

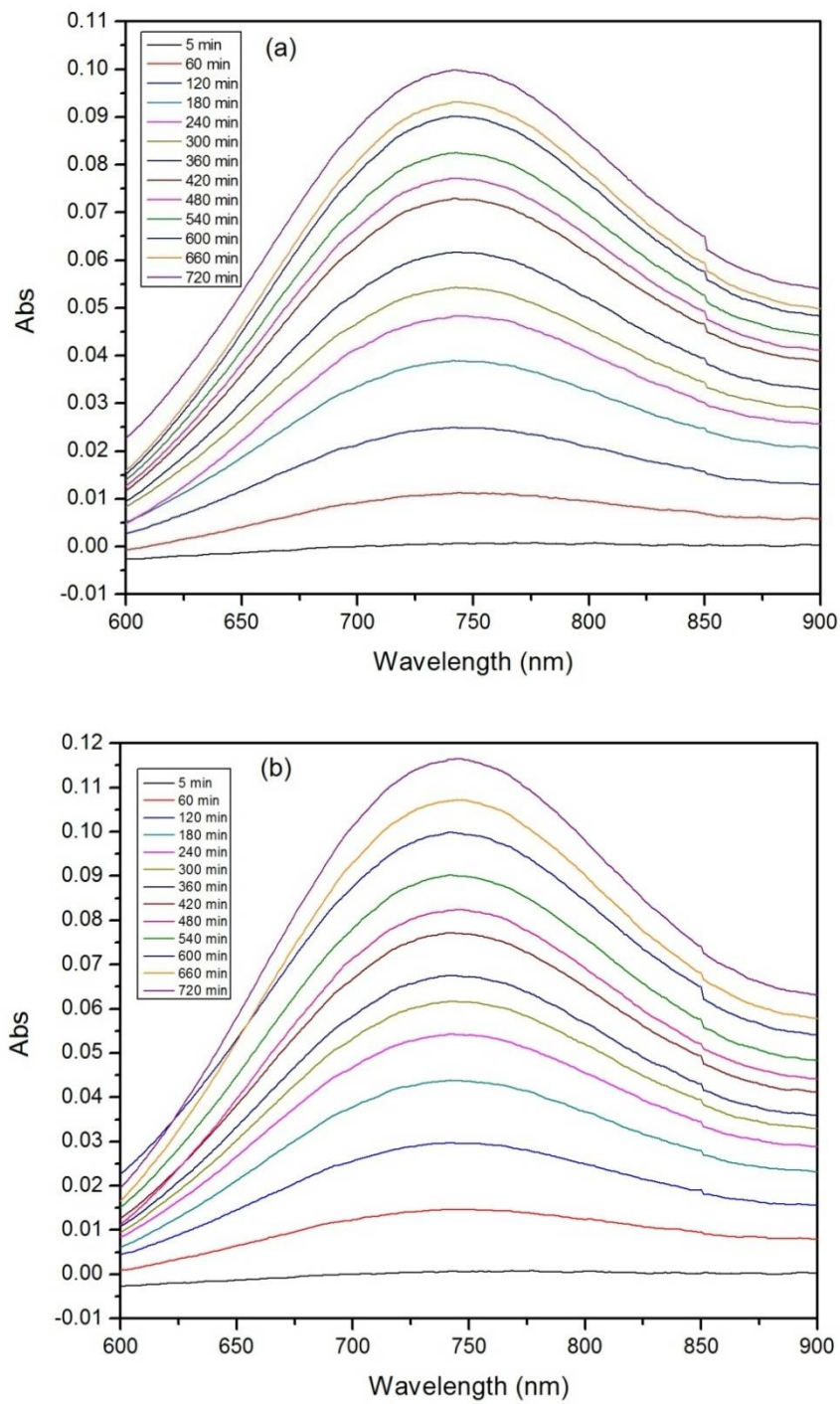


Figure 4.4: Plot of absorbance with time at 745 nm for BSI-3 (a) 70 mM and (b) 50 mM.

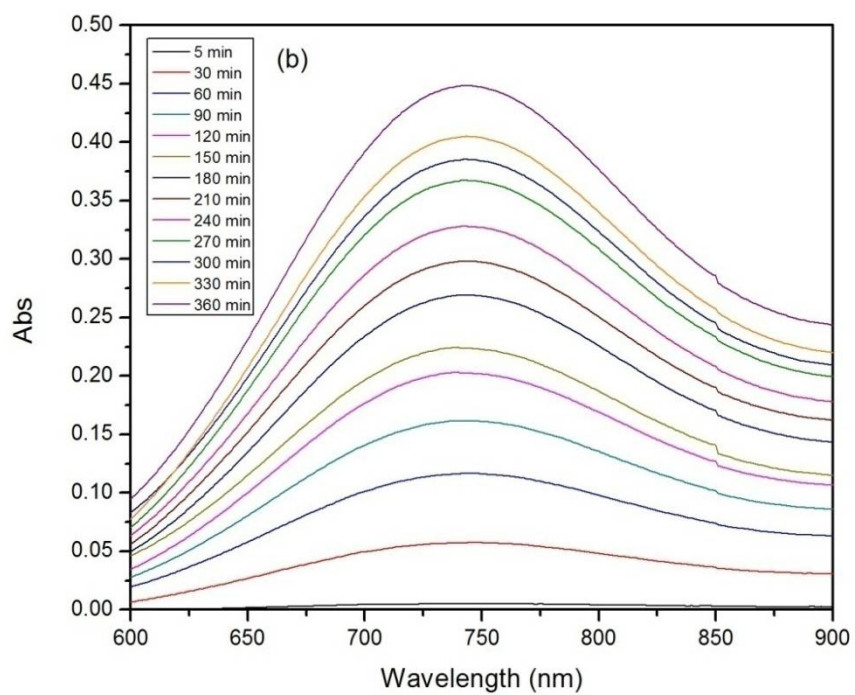
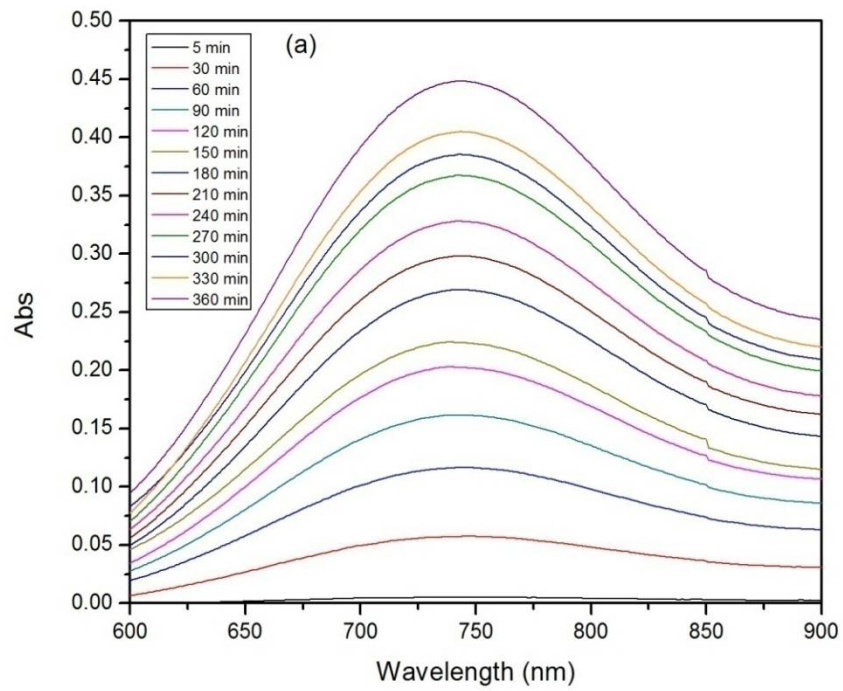


Figure 4.5: Plot of absorbance with time at 745 nm for BSI-34 (a) 70 mM and (b) 50 mM.

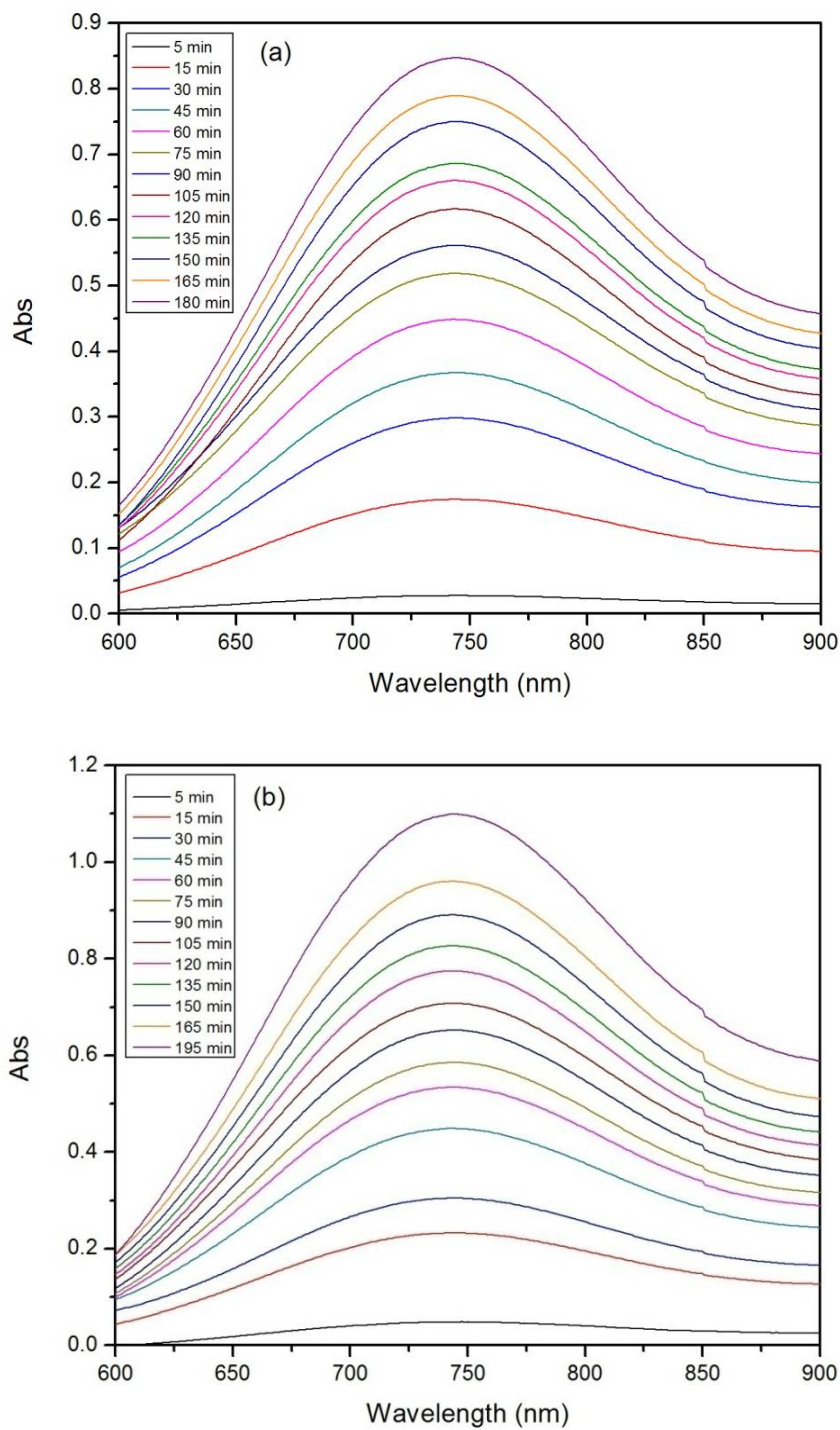


Figure 4.6: Plot of absorbance with time at 745 nm for BSI-33 (a) 70 mM and (b) 50 mM.

To determine the extinction coefficient, different solutions of known concentrations, ranging from 0.2 mM to 4.6 mM, of $\text{BrCu}^{\text{II}}\text{Bpy}$ complex in acetonitrile were prepared. The absorbance for each solution was measured using quartz cuvette (dimensions: $1.2 \times$

1.2 × 4.5 cm, 3.5 mL) at $\lambda_{\text{max}} = 745 \text{ nm}$. The extinction coefficient calculated (from the plot of concentration vs absorbance **Figure 4.7**) was found to be $327 \text{ M}^{-1}\text{cm}^{-1}$.

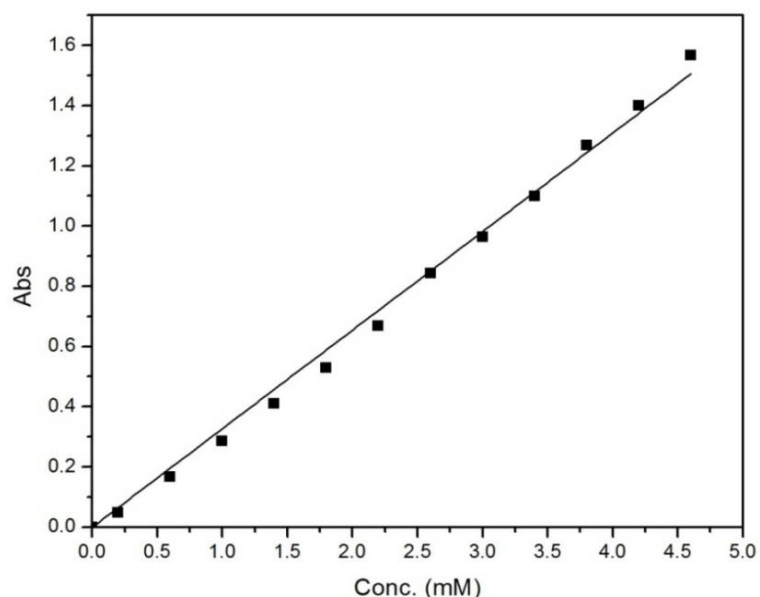


Figure 4.7: Plot of absorbance vs concentration of $\text{BrCu}^{\text{II}}\text{Bpy}$ complex at $\lambda_{\text{max}} 745 \text{ nm}$ in acetonitrile.

4.2.4.2 Determination of Termination Rate Constant (k_t)

In literature [215], a constant value ($2.5 \times 10^9 \text{ M}^{-1}\text{s}^{-1}$) of k_t has been assumed for small radicals in the calculation of K_{ATRP} . However, a more accurate value can be calculated theoretically using the following formula [257]

$$2k_t^D = 3.78 \times 10^{21} \times D \times d \dots\dots\dots 4.3$$

where, 'D' is the diffusion coefficient of the radical in a given medium and 'd' is the reaction distance. The later parameter can be approximated, using the approach of Gorrell and Dubois [258], according to the equation given below,

$$d = \left(\frac{V_m}{N_A} \right)^{1/3} \dots\dots\dots 4.4$$

where, V_m is the molar formula of a stable model compound structurally resembling the radical and N_A is Avogadro's number. *N*-phenylsuccinimide was used as model compound for the above synthesized bromo derivatives of succinimide. Taking its molecular weight ($M = 175.18 \text{ g mol}^{-1}$) and density ($\rho = 1.28 \text{ g cm}^{-3}$), the molar volume can be calculated as $V_m = M/d = 136.97 \text{ cm}^3 \text{ mol}^{-1}$, and using equation 4.4, a value of $d = 6.11 \times 10^{-8} \text{ cm}$ is obtained. With this estimation of the reaction distance (d) for the phenylsuccinimide radical the equation 4.3 can be rewritten as,

$$2k_t^D \approx 2.31 \times 10^{14} \times D \dots\dots\dots 4.5$$

The diffusion coefficient 'D' can be obtained from the classic Einstein-Stokes equation or some of its variations [259] or it can be calculated directly using pulsed field gradient NMR spectroscopic techniques [260]. The latter (more accurate) approach was employed in the present study. DOSY allows the measurement of translational diffusion of molecules in solution. The measurement of diffusion was carried out by observing the attenuation of the NMR signals during a pulsed field gradient experiment. The degree of attenuation is a function of the magnetic gradient pulse amplitude and occurs at a rate proportional to the diffusion coefficient of the molecule. In practice, a series of NMR diffusion spectra were acquired as a function of the gradient strength. It can be observed that the intensities of the resonances follow an exponential decay. The slope of this decay is proportional to the diffusion coefficient according to equation,

$$I = I_0 \exp (-D\gamma^2 g^2 \delta^2 \Delta - \delta/3 - \pi/2) \dots\dots\dots 4.6$$

where, I and I_0 are the signal intensities in the presence and absence of gradient, respectively, ' γ ' is the gyromagnetic ratio, g is the strength of the diffusion gradients, ' D ' is the diffusion coefficient of the observed spins, ' δ ' is the duration of the diffusion gradient and ' Δ ' is the diffusion time. All signals corresponding to the same molecular species were decayed at the same rate. The processing software evaluates this decay behavior and extracts the diffusion coefficient out of the signal decay curve. The two dimensional DOSY-NMR spectra were presented with chemical shift along the x-axis and the diffusion constant along the y axis. The DOSY-NMR spectrum of *N*-phenylsuccinimide (**Figure 4.8**) and its diffusion variable gradient is given in **Figure 4.9**.

From these data the diffusion coefficient of *N*-phenylsuccinimide in deuterated acetonitrile was found to be $1.65 \times 10^{-5} \text{ cm}^2 \text{ s}^{-1}$. Correspondingly, the value of the termination rate constant $2k_t$ for *N*-phenylsuccinimide in deuterated acetonitrile at 25 °C was obtained as $3.81 \times 10^9 \text{ M}^{-1} \text{ s}^{-1}$. This value of $2k_t$ (almost similar constant value i.e.

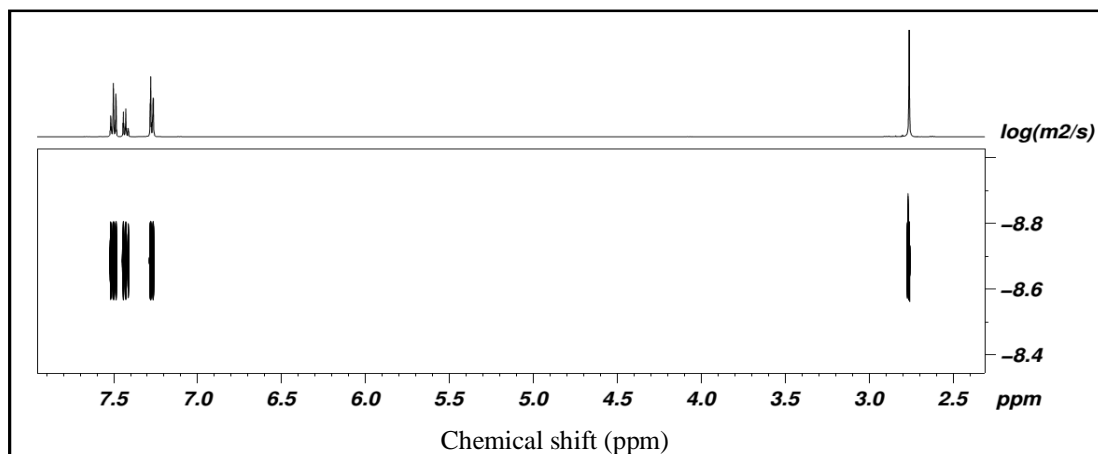


Figure 4.8: DOSY-NMR spectrum of *N*-phenylsuccinimide in CD_3CN at 25 °C.

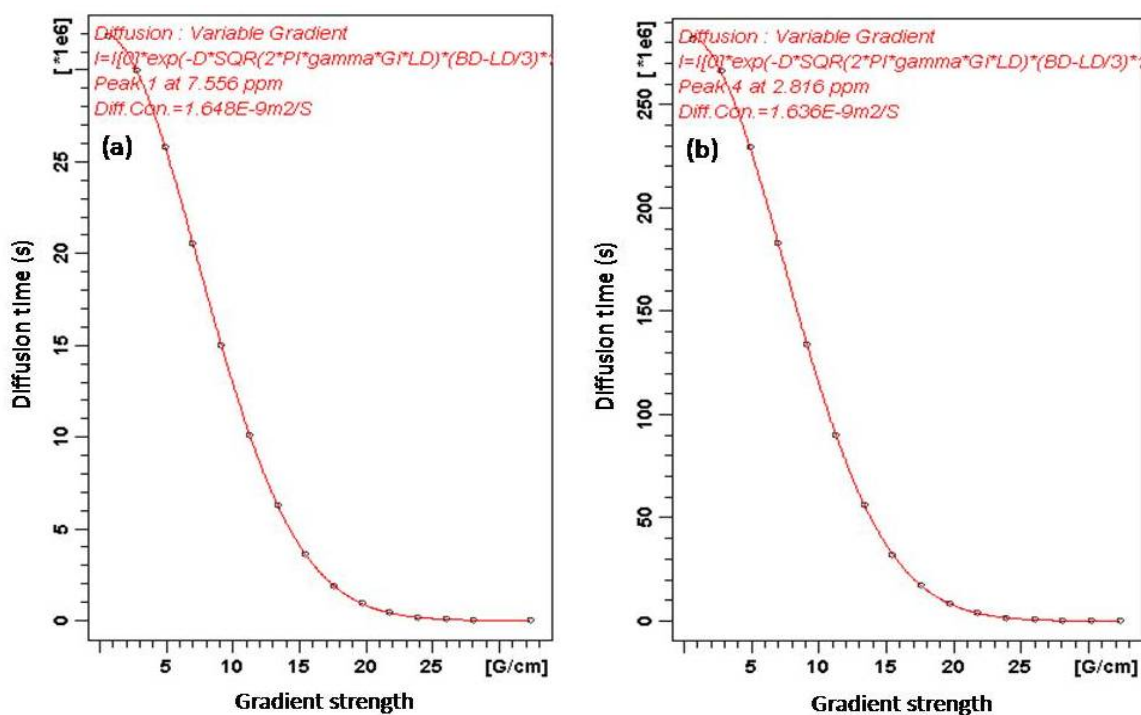


Figure 4.9: Plots of diffusion time vs gradient strength for *N*-phenylsuccinimide in CD_3CN at 25 °C at (a) $\delta = 7.556 \text{ ppm}$ and (b) $\delta = 2.816 \text{ ppm}$.

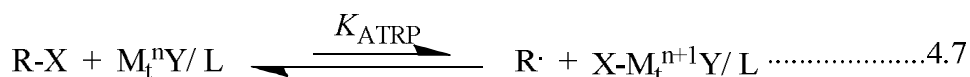
$3.52 \times 10^9 \text{ M}^{-1}\text{s}^{-1}$ used in the literature [53]) was used for the determination of K_{ATRP} values using acetonitrile as solvent for the above synthesized bromo derivatives of succinimide.

4.2.5 Computational Details

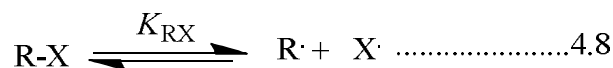
Gaussian09 [246] was used as source program for all theoretical calculations. All the geometries were fully optimized using the hybrid B3LYP exchange correlation functional with 6-31+G(d) basis set, except for Iodine, where LanL2DZ basis set was used. Frequency calculations were performed for all the compounds to check (no imaginary frequencies) the stationary points as minima on the potential energy surface. A scaling factor 0.9613 was used for the frequency calculation [261]. All the systems containing unpaired electron were optimized with spin unrestricted formalism. The spin contamination was found to be negligible (the mean value of the S^2 operator was close to the theoretical value of 0.75 for all radicals). A spin-orbit correction term was applied for $X = \text{Cl}, \text{Br}$ and I due to their atomic nature [262]. The DFT calculation includes only the average energy of the ground state ^2P term, the extra stability of the real ground-state $^2\text{P}_{3/2}$ term is taken from the literature values (0.8, 3.5 and 7.3 kcalmol $^{-1}$ for Cl, Br and I respectively) [263]. Solvent effects were studied using Tomasi's polarizable continuum model [263].

4.2.6 Theoretical Calculation of ATRP Equilibrium Constant (K_{ATRP})

Theoretically, the relative values of K_{ATRP} were estimated from the homolytic bond dissociation energy (BDE) of the initiating R–X under the following conditions.



The atom transfer equilibrium of ATRP process (equation 4.7), can be viewed as the sum of the following two equilibrium processes, viz. homolytic bond dissociation of alkyl halide (equation. 4.8) and $\text{X-M}_t^{n+1}\text{Y/L}$ bond formation (*halidophilicity*, equation. 4.9), so that $K_{\text{ATRP}} = K_{\text{RX}} \times K_{\text{X}}$.



The value of the equilibrium constant K_X depends on the type of catalyst/ ligand ($\text{M}_t^n\text{Y/L}$) and halogen, X. For similar conditions and using the same catalytic system (similar K_X), the overall equilibrium constant K_{ATRP} will depend on the energetics of alkyl halide R-X, and a knowledge of the equilibrium constant K_{RX} alone will enable to predict the relative value of K_{ATRP} [24-25].

4.3 Results and Discussion

4.3.1 Experimental K_{ATRP} Values of Alkyl Bromides

The K_{ATRP} values of above synthesized bromo derivatives of succinimide (viz. BSI-3, BSI-34 and BSI-3) and commercially available ATRP initiator (viz. EBiB) were determined using the modified Fischer-Fukuda equation for the persistent radical effect (equation 4.1). The values of $F(\text{BrCu}^{\text{II}}\text{Bpy})$ were obtained by putting the values of concentration of Y, C_0 and I_0 in equation 4.2. The plots of $F(\text{BrCu}^{\text{II}}\text{Bpy})$ vs time (t) were linear in nature for all the above mentioned alkyl bromides and these are given in the **Figure 4.10** and **Figure 4.11** for 70 mM and 50 mM concentration, respectively. The K_{ATRP} values were determined from the slope [plot of $F(\text{BrCu}^{\text{II}}\text{Bpy})$ vs t] and calculated value of $2k_t$. The results are summarized in **Table 4.1**.

Table 4.1: K_{ATRP} values of alkyl bromides in acetonitrile at 25 °C.

R-X	K_{ATRP}		
	70 mM	50 mM	Average
EBiB	1.40×10^{-09}	1.18×10^{-09}	1.29×10^{-09}
BSI-3	0.89×10^{-18}	1.39×10^{-18}	1.14×10^{-18}
BSI-34	1.07×10^{-11}	1.29×10^{-11}	1.18×10^{-11}
BSI-33	1.39×10^{-09}	1.40×10^{-09}	1.40×10^{-09}

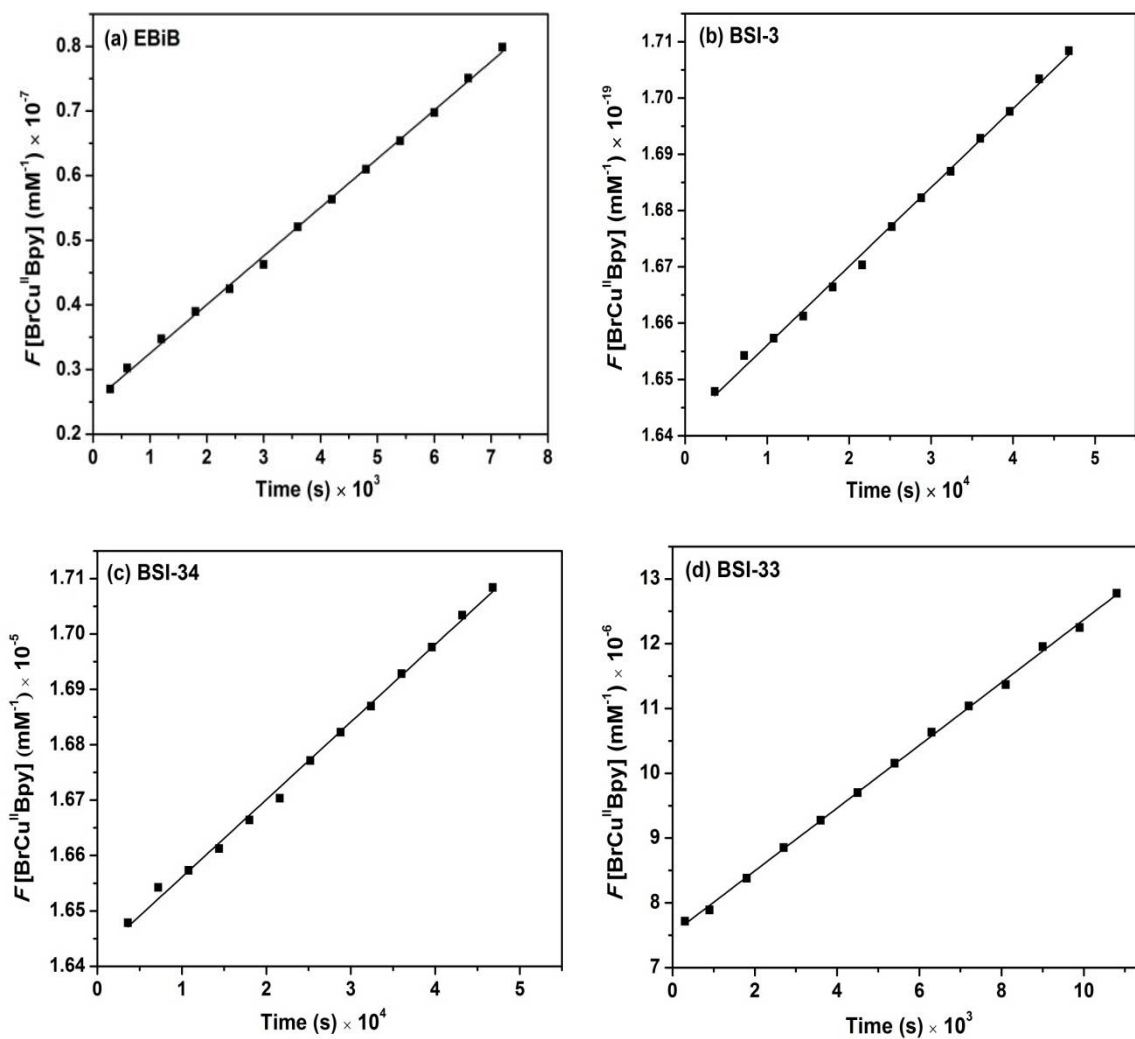


Figure 4.10: Plots of $F(Y) = F[\text{BrCu}^{\text{II}}\text{Bpy}]$ vs time (s) for $[\text{R-Br}] = 70 \text{ mM}$.

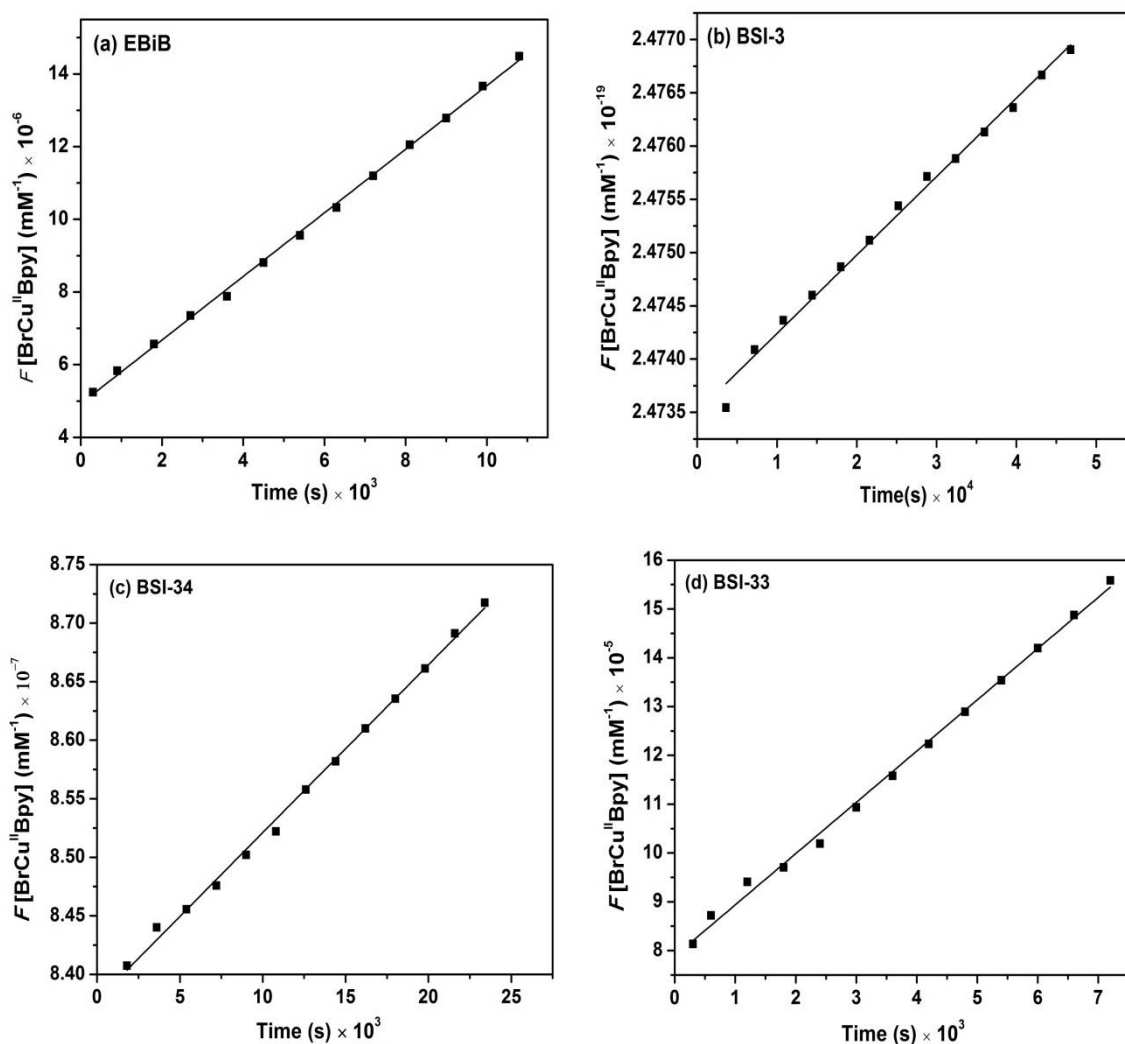


Figure 4.11: Plots of $F(Y) = F[\text{BrCu}^{\text{II}}\text{Bpy}]$ vs time (s) for $[\text{R-Br}] = 50 \text{ mM}$.

4.3.2 Theoretical K_{ATRP} Values of Alkyl Halides

As discussed in **Section 4.2.6**, knowledge of R-X bond dissociation of alkyl halides are crucial for determination of K_{ATRP} . In the following sections the different energetics of alkyl halides are discussed which was calculated using DFT methods. For the sake of simplicity the compounds BSI-3, BSI-34, BSI-33 and EBiB are designated as **1a-Br**, **2a-Br**, **3a-Br** and **4-Br**, respectively (**Figure 4.12**).

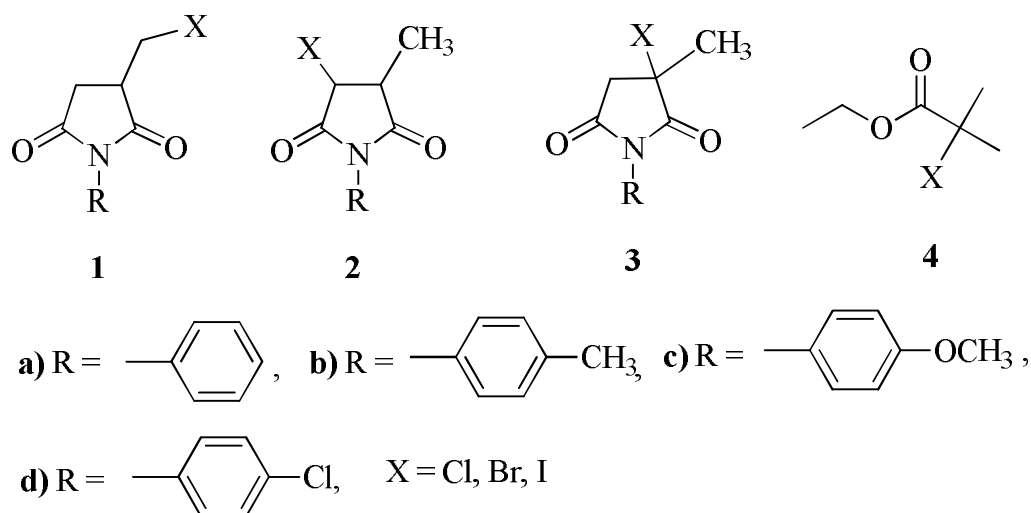


Figure 4.12: The alkyl halides, **1** (**1a-X** to **1d-X**), **2** (**2a-X** to **2d-X**), **3** (**3a-X** to **3d-X**) and **4-X** (X = Cl, Br, I) investigated in this study.

4.3.2.1 Structural Features of Alkyl Halides and Alkyl Radicals

The B3LYP/ 6-31+G(d)/ LanL2DZ optimized geometry of the studied alkyl halides and its radicals (in gas phase at 25 °C) is given in the (**Appendix v, Table A1**). The R–X bond distances (r_{R-X}) for the studied compounds (**Figure 4.12**) in gas phase as well as in two polar solvents (anisole and acetonitrile) are given in **Table 4.2**. They are between the ranges 1.809 Å to 2.202 Å for series **1**, 1.821 Å to 2.224 Å for series **2**, 1.844 Å to 2.261 Å for series **3**, and 1.855 Å to 2.278 Å for series **4** alkyl halides. The R–X bond distances follow the trends **1** < **2** < **3** < **4** for a given X and Cl < Br < I for a given series. The R–X bond lengths systematically increase for all the studied alkyl halides with increasing polarity of the medium and follow the trend gas phase < anisole < acetonitrile for a given R–X. The dihedral angles for the R–X bond with respect to the ring (or with respect to C(O)OC₂H₅ for **4**) are between 137°–177° for series **1** and **4**, and between 171°–172° for series **2** and **3**. The carbon atom bearing the unpaired electron for all the radicals are found to be planar in the sense that the sum of the three bond angles at this carbon are found to be 360° in all cases. The spin densities at this carbon varies from 0.87 to 1.17 in the order **1** > **2** > **3** ≈ **4**.

Table 4.2: The R–X bond lengths of studied alkyl halides in gas phase and in the solution phase at 25 °C.

R-X	r_{R-X} (Å)		
	Gas	Anisole	Acetonitrile
1a-Cl	1.809	1.817	1.822
1a-Br	1.966	1.973	1.977
1a-I	2.203	2.210	2.213
1b-Cl	1.810	1.818	1.822
1b-Br	1.966	1.973	1.977
1c-Cl	1.810	1.818	1.822
1c-Br	1.967	1.974	1.977
1c-I	2.203	2.267	2.270
1d-Cl	1.809	1.817	1.821
1d-Br	1.965	1.972	1.977
1d-I	2.202	2.202	2.213
2a-Cl	1.821	1.824	1.825
2a-Br	1.979	1.981	1.982
2a-I	2.225	2.227	2.228
2b-Cl	1.821	1.824	1.825
2b-Br	1.979	2.014	2.016
2c-Cl	1.822	1.825	1.826
2c-Br	1.979	1.982	1.982
2c-I	2.225	2.227	2.229
2d-Cl	1.821	1.824	1.825
2d-Br	1.978	1.980	1.981
2d-I	2.224	2.226	2.228
3a-Cl	1.844	1.848	1.850
3a-Br	2.008	2.014	2.016
3a-I	2.262	2.266	2.267
3b-Cl	1.844	1.848	1.849
3b-Br	2.009	2.014	2.016
3c-Cl	1.845	1.849	1.851
3c-Br	2.009	2.013	2.016
3c-I	2.263	2.267	2.270
3d-Cl	1.844	1.847	1.849
3d-Br	2.008	2.013	2.015
3d-I	2.261	2.266	2.269
4-Cl	1.855	1.865	1.869
4-Br	2.017	2.025	2.029
4-I	2.278	2.287	2.292

**here, 1a-Br = BSI-3, 2a-Br = BSI-34, 3a-Br = BSI-33 and 4-Br = EBiB*

4.3.2.2 Homolytic Bond Dissociation Enthalpies and Free Energies

The bond dissociation enthalpy (BDE) data for the studied compounds is displayed in **Table 4.3**. They are in the ranges 304.25 kJ mol⁻¹ to 170.64 kJ mol⁻¹ for series **1**, 263.26 kJ mol⁻¹ to 127.72 kJ mol⁻¹ for series **2**, 250.70 kJ mol⁻¹ to 108.96 kJ mol⁻¹ for series **3**, and 257.07 kJ mol⁻¹ to 115.16 kJ mol⁻¹ for the series **4** alkyl halides in gas phase. The R–X homolytic BDEs of alkyl chlorides are found to be higher than the corresponding alkyl bromides, which are in turn higher than their iodide counterparts. This variation is parallel to the decreasing ionic character of halides, Cl > Br > I. The decrease in BDEs are about 3–22 kJ mol⁻¹ from Cl to Br, but about 110–140 kJ mol⁻¹ from Br to I, for a given series. For a given halide, the trend in BDEs is **3** ≈ **4** < **2** < **1**, which is nearly according to the stability of the corresponding alkyl free radical generated. The increase is more as we go from series **2** to series **1** than going from **3** to **2** series. For a given series of alkyl halides, the BDEs decrease while the corresponding R–X bond distance increase (**Table 4.2**) as we go from X = Cl to X = I. The BDEs correlates well with the R–X bond lengths; as the R–X bond length increase, BDEs decrease (**Figure 4.13**). Solvent polarity has different effect for 1° (series **1**) alkyl halides than those of others (2° and 3°) alkyl halides. The trends are gas phase > anisole > acetonitrile for **2**, **3** and **4**

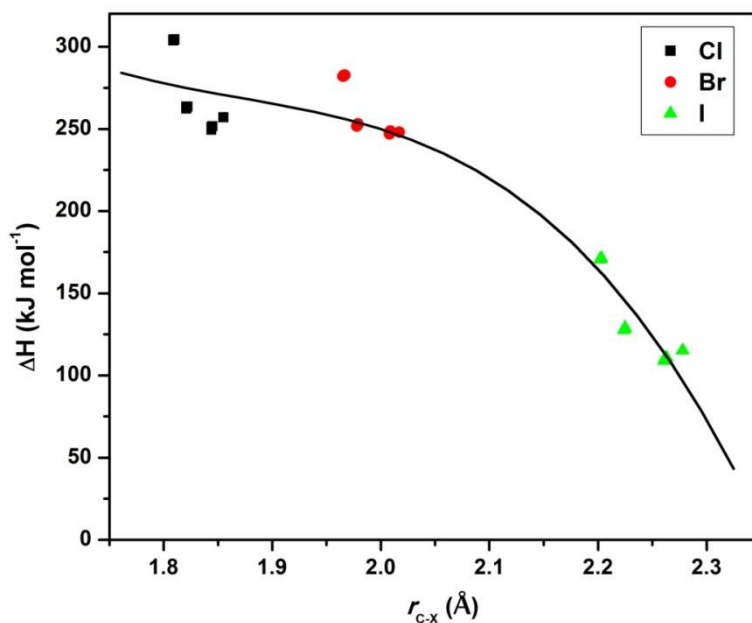


Figure 4.13: Correlation plot of bond dissociation enthalpies with R–X bond distances (Å) of the studied alkyl halides.

Table 4.3: Enthalpy and free energy for R–X homolytic cleavage of studied alkyl halides in gas phase and solution phase at 25 °C.

R-X	ΔH (kJ mol ⁻¹)			ΔG (kJ mol ⁻¹)		
	Gas	Anisole	Acetonitrile	Gas	Anisole	Acetonitrile
1a-Cl	304.25	309.03	312.42	262.30	267.55	270.73
1a-Br	282.14	285.92	289.09	240.78	243.14	247.92
1a-I	171.1	173.88	176.37	130.99	132.72	135.14
1b-Cl	304.29	306.67	312.67	262.92	273.03	271.26
1b-Br	282.54	284.00	289.42	244.74	254.1	248.66
1c-Cl	304.51	309.27	312.75	263.29	266.56	266.54
1c-Br	282.65	286.18	289.48	241.11	242.47	243.93
1c-I	171.31	174.16	176.77	131.45	133.45	133.62
1d-Cl	303.79	323.71	312.62	262.23	278.44	272.18
1d-Br	281.88	285.78	289.21	240.34	243.22	246.32
1d-I	170.64	173.72	176.46	130.64	134.26	135.03
2a-Cl	263.26	261.18	260.68	223.23	221.16	220.06
2a-Br	252.48	249.94	249.11	212.67	210.36	209.71
2a-I	128.76	126.04	125.23	89.49	87.24	86.62
2b-Cl	263.55	-	260.93	223.58	-	216.27
2b-Br	253.05	-	251.99	211.54	-	200.68
2c-Cl	263.56	261.67	261.14	223.80	222.49	219.97
2c-Br	252.86	250.51	249.56	213.15	212.15	209.36
2c-I	129.05	126.47	125.8	89.70	87.43	87.31
2d-Cl	262.22	260.06	259.76	222.29	220.69	223.86
2d-Br	251.6	248.79	248.34	211.83	208.9	208.93
2d-I	127.72	125.24	124.59	88.14	86.13	85.24
3a-Cl	250.7	247.39	245.92	208.66	204.27	202.69
3a-Br	247.88	243.71	242.06	205.12	199.94	198.21
3a-I	110.61	106.07	104.31	68.86	64.63	64.28
3b-Cl	251.07	247.62	246.46	208.01	204.38	203.10
3b-Br	248.42	244.18	242.59	206.26	199.30	197.32
3c-Cl	251.48	248.16	246.66	209.61	207.29	203.48
3c-Br	248.7	245.02	243.04	205.76	201.86	196.88
3c-I	110.83	106.47	104.8	69.54	64.95	63.82
3d-Cl	249.42	245.81	244.9	207.07	202.72	203.66
3d-Br	246.95	242.58	241.26	204.06	198.95	197.71
3d-I	108.96	104.45	102.84	67.58	62.81	62.26
4-Cl	257.07	255.98	255.53	209.90	208.81	205.31
4-Br	247.87	246.44	245.9	200.87	199.29	195.68
4-I	115.16	112.71	111.66	69.30	66.64	62.98

*here, **1a-Br** = BSI-3, **2a-Br** = BSI-34, **3a-Br** = BSI-33 and **4-Br** = EBiB

#Reported calculated values of ΔH for the compounds **4-Cl**, **4-Br**, and **4-I** are 279.91 kJ mol⁻¹, 246.44 kJ mol⁻¹, and 141.00 kJ mol⁻¹, respectively. Similarly, reported calculated values of ΔG for the compounds **4-Cl**, **4-Br**, and **4-I** are 240.16 kJ mol⁻¹, 206.69 kJ mol⁻¹ and 78.08 kJ mol⁻¹. This values were calculated using B3P86/6-31G(dp)/LANL2DZdp method in gas phase at 25 °C [57].

series while it is gas phase < anisole < acetonitrile, for series **1** alkyl halides. Thus with increasing polarity of the medium, the relatively-stable radicals (**2**, **3** and **4** series) become more unstable, while the less stable radicals **1** become more stable.

The free energies for the studied alkyl halides (**Table 4.3**) are nearly a constant difference with the enthalpy data (about 42 kJ mol⁻¹ for series **1**, **2**, **3** and about 48 kJ mol⁻¹ for series **4**). This means that the entropy factor contributing for the series **1**, **2** and **3** alkyl halides (and similarly for the series **4**) is nearly same. This is understandable from the structural similarities among alkyl halides of series **1**, **2** and **3**, (and similarly series **4**). The free energies vary according to $4 \approx 3 < 2 < 1$ for a given X and follows the trends Cl > Br > I for a given series. The free energies, like BDEs, increases with decreasing R–X bond lengths. This is obvious from the correlation plot (**Figure 4.14**) between the free energies and enthalpies. In presence of polar solvents, the variation of free energies follow the trends, gas phase > anisole > acetonitrile for **2**, **3** and **4** series, while it is gas phase < anisole < acetonitrile, for series **1** alkyl halides. This trend is similar to the trends found in BDEs.

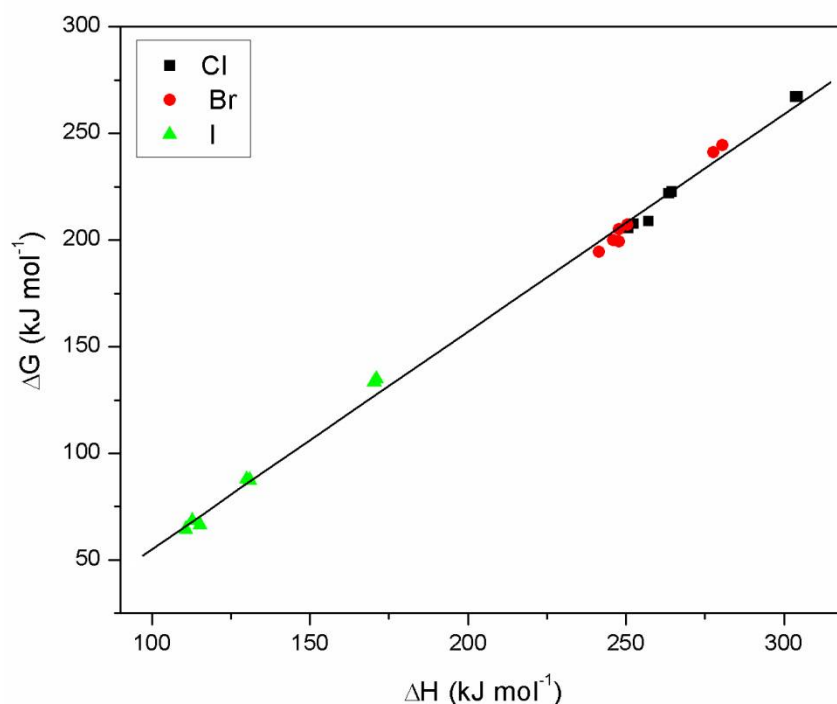


Figure 4.14: Variation of enthalpies with the free energies for the R–X bond dissociation process for the studied alkyl halides.

4.3.2.3 Relative Equilibrium Constants (K_{ATRP})

The overall equilibrium constant (K_{ATRP}) can be given as product of two equilibrium constants K_{RX} and K_{X} , the later depends on catalytic system and halogen radical. Thus, for a given catalytic system and a given X, K_{X} will be a constant, and relative value of K_{ATRP} can be obtained from knowledge of K_{RX} . The K_{RX} values of the alkyl halides from their free energy were calculated using standard text book formula [264]. The estimated $K_{\text{X}} = (K_{\text{ATRP}} / K_{\text{RX}})$ values for the series 4 alkyl halides from their literature K_{ATRP} values (1.50×10^{-6} for 4-Cl [24], 3.93×10^{-9} for 4-Br [53] and 2.2×10^{-8} for methyl-2-iodopropanoate [24]) and then use this K_{X} value for the rest of the compounds of a given X. [We could have used the K_{ATRP} value of 4-Br determined experimentally in this work. However, for chlorides and iodides we need to use the literature values only. So we decided to use the literature values for all the studied alkyl halides]. The values of K_{ATRP} , so obtained, are displayed in **Table 4.4**. A quick glance at **Table 4.4** shows that the values of K_{ATRP} for the studied alkyl halides differ in orders of magnitude 10^{-4} to 10^{-16} for gas phase at 25 °C. All the alkyl halides of series 3 and many from series 2 (2a-Cl, 2b-Cl, 2c-Cl, 2d-Cl, 2a-I, 2b-I, 2c-I, 2d-I) have comparable K_{ATRP} with those of corresponding commercial initiators (series 4). However, the alkyl halides of series 1 have K_{ATRP} values much smaller than those of series 4 alkyl halides. The K_{ATRP} data follows trends $4 \approx 3 > 2 \gg 1$ for a given X and $\text{Cl} < \text{Br} < \text{I}$ for a given series. With increasing temperature from 25 °C to 80 °C, there is order of magnitude increases (10^3 to 10^9) in the values of K_{ATRP} . Different substituents in phenyl ring at *para* position has no significant effect on bond lengths, bond dissociation enthalpy (BDEs), free energy and K_{ATRP} of 1, 2, and 3 series of alkyl halides. The trends of K_{ATRP} in changing medium of the system is gas phase > anisole > acetonitrile for series 1 alkyl halides, and gas phase < anisole < acetonitrile for the rest of alkyl halides (series 2, 3 and 4). We have obtained good correlation in the variation of K_{ATRP} and R–X bond lengths as well as variation of K_{ATRP} with BDEs. These correlation plots are displayed in **Figures 4.15** and **4.16**, respectively. **Figure 4.15** implies that as the R–X bond length increases $-\log K_{\text{ATRP}}$ decreases, viz. $\log K_{\text{ATRP}}$ increases. This is because as the R–X bond length increases (bond weakens) homolysis is easier and so K_{ATRP} increases. Thus, iodides are better initiators than bromides which in turn are better initiators than chlorides. However, for a given X, the variation of R–X bond length is very little, yet there is an order of

Table 4.4: Relative values of K_{ATRP} for R–X homolytic bond cleavage of studied alkyl halides in gas phase and in solution phase.

R-X	$K_{\text{ATRP}} (k_{\text{act}}/k_{\text{deact}})$			
	Gas, 25 °C	Gas, 80 °C	Anisole, 25 °C	Acetonitrile, 25 °C
1a-Cl	9.92×10^{-16}	2.03×10^{-07}	7.68×10^{-17}	5.19×10^{-18}
1a-Br	4.00×10^{-16}	1.86×10^{-08}	8.18×10^{-17}	2.77×10^{-18}
1a-I	1.18×10^{-15}	5.59×10^{-11}	5.30×10^{-11}	6.96×10^{-17}
1b-Cl	7.72×10^{-16}	1.58×10^{-07}	8.40×10^{-18}	4.18×10^{-18}
1b-Br	8.11×10^{-17}	4.32×10^{-09}	9.82×10^{-19}	2.06×10^{-18}
1c-Cl	6.65×10^{-16}	1.38×10^{-07}	1.14×10^{-16}	2.81×10^{-17}
1c-Br	3.50×10^{-16}	1.86×10^{-08}	1.07×10^{-16}	1.39×10^{-17}
1c-I	9.82×10^{-16}	4.71×10^{-11}	1.76×10^{-16}	1.28×10^{-16}
1d-Cl	1.02×10^{-15}	2.03×10^{-07}	9.50×10^{-19}	2.89×10^{-18}
1d-Br	4.78×10^{-16}	2.42×10^{-08}	7.92×10^{-17}	5.30×10^{-18}
1d-I	1.36×10^{-15}	6.25×10^{-11}	1.27×10^{-16}	7.26×10^{-17}
2a-Cl	6.94×10^{-09}	1.07×10^{-01}	1.03×10^{-08}	3.90×10^{-09}
2a-Br	3.36×10^{-11}	2.62×10^{-04}	4.53×10^{-11}	1.37×10^{-11}
2a-I	2.20×10^{-08}	7.21×10^{-05}	2.20×10^{-08}	2.20×10^{-08}
2b-Cl	6.02×10^{-09}	9.45×10^{-02}	-	1.80×10^{-08}
2b-Br	5.31×10^{-11}	2.01×10^{-04}	-	5.25×10^{-10}
2c-Cl	5.50×10^{-09}	8.65×10^{-02}	6.01×10^{-09}	4.04×10^{-09}
2c-Br	2.77×10^{-11}	2.22×10^{-04}	2.20×10^{-11}	1.58×10^{-11}
2c-I	2.02×10^{-08}	6.73×10^{-05}	2.04×10^{-08}	1.67×10^{-08}
2d-Cl	1.01×10^{-08}	1.46×10^{-01}	1.24×10^{-08}	8.42×10^{-10}
2d-Br	4.72×10^{-11}	3.49×10^{-04}	8.16×10^{-11}	1.88×10^{-11}
2d-I	3.79×10^{-08}	1.16×10^{-04}	3.44×10^{-08}	3.84×10^{-08}
3a-Cl	2.47×10^{-06}	$1.72 \times 10^{+01}$	9.36×10^{-06}	4.30×10^{-06}
3a-Br	7.06×10^{-10}	4.11×10^{-03}	3.03×10^{-09}	1.42×10^{-09}
3a-I	9.05×10^{-05}	9.46×10^{-02}	2.01×10^{-04}	2.00×10^{-04}
3b-Cl	3.22×10^{-06}	$2.30 \times 10^{+01}$	8.96×10^{-06}	3.65×10^{-06}
3b-Br	4.46×10^{-10}	2.64×10^{-02}	3.93×10^{-09}	2.03×10^{-09}
3c-Cl	1.68×10^{-06}	$1.23 \times 10^{+01}$	2.77×10^{-06}	3.13×10^{-06}
3c-Br	5.46×10^{-10}	3.35×10^{-03}	1.40×10^{-09}	2.42×10^{-09}
3c-I	6.89×10^{-05}	7.30×10^{-02}	1.76×10^{-04}	2.17×10^{-04}
3d-Cl	4.70×10^{-06}	$3.01 \times 10^{+01}$	1.75×10^{-05}	2.91×10^{-06}
3d-Br	1.08×10^{-09}	6.17×10^{-03}	4.52×10^{-09}	1.73×10^{-09}
3d-I	1.52×10^{-04}	1.43×10^{-01}	4.19×10^{-04}	4.07×10^{-04}
4-Cl	1.50×10^{-06}	$1.56 \times 10^{+01}$	1.50×10^{-06}	1.50×10^{-06}
4-Br	3.93×10^{-09}	2.29×10^{-02}	3.93×10^{-09}	3.93×10^{-09}
4-I	7.59×10^{-05}	1.05×10^{-01}	8.93×10^{-05}	3.05×10^{-04}

*here, **1a-Br** = BSI-3, **2a-Br** = BSI-34, **3a-Br** = BSI-33 and **4-Br** = EBiB

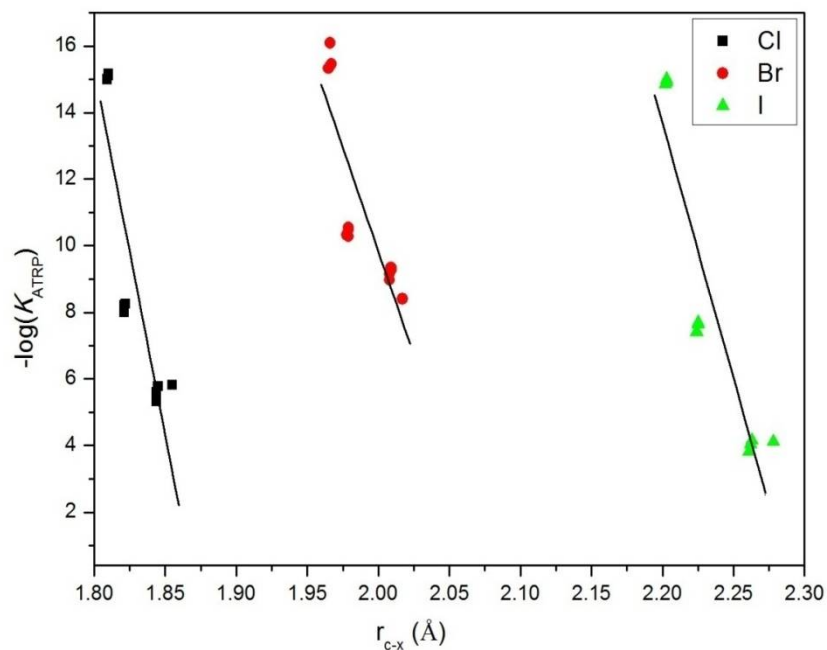


Figure 4.15: Correlation plot of relative K_{ATRP} values with R–X bond lengths for the studied alkyl halides.

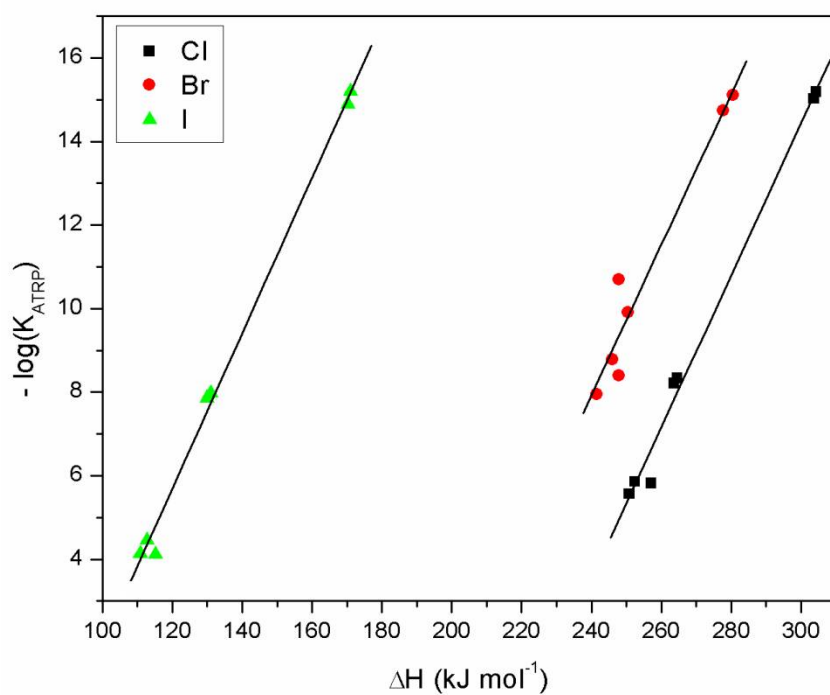


Figure 4.16: Correlation plot of relative K_{ATRP} values with R–X bond enthalpies of studied alkyl halides.

magnitude difference in K_{ATRP} . This is mainly due to the structural difference (primary, secondary and tertiary) of alkyl halides. A similar explanation holds for the correlations between BDEs and K_{ATRP} of **Figure 4.16**.

4.3.3 Comparison of Experimentally Determined and DFT Calculated K_{ATRP} Values

The experimentally determined and theoretically calculated values of K_{ATRP} for the studied alkyl bromides are found to be comparable (**Table 4.5**). The reported experimental K_{ATRP} value for EBiB is 3.39×10^{-09} [53], which is quite comparable with our experimentally determined value viz. 1.29×10^{-09} . Our theoretically (DFT) calculated K_{ATRP} values in acetonitrile at 25 °C for BSI-3, BSI-34 and BSI-33 are having good agreement with our experimentally determined K_{ATRP} values.

Table 4.5: The K_{ATRP} values for R–X homolytic bond cleavage of studied alkyl bromides.

R-X	K_{ATRP} values ($k_{\text{act}}/k_{\text{deact}}$)	
	Experimental	DFT calculated
EBiB	1.29×10^{-09}	3.93×10^{-09}
BSI-3	1.14×10^{-18}	2.77×10^{-18}
BSI-34	1.18×10^{-11}	1.37×10^{-11}
BSI-33	1.40×10^{-09}	1.42×10^{-09}

4.3.4 AGET-ATRP of PI and MMA using BSI-33 as Initiator

The copolymerization of the monomers PI and MMA was carried out using the mole fraction ratio of 2:8 in presence of $\text{CuBr}_2/\text{Bpy}/\text{Sn}(\text{EH})_2$ in anisole at 80 °C using BSI-33 as initiator (**Scheme 4.1**). The percent conversion of monomer was calculated gravimetrically by pouring the reaction mixture after 5 h, 10 h, 15 h, 20 h, 25 h, 30 h, 35 h, 45 h and 50 h in methanol. The copolymers, which precipitated out, were washed with hot methanol, dried and weighed. The molecular weights of the copolymers were determined using GPC. The details of the percent conversion of monomers, PDI and molecular weights are given in **Table 4.6**. A typical linear variation in the plots of % conversion of monomers with time (**Figure 4.17**) is observed. This is the characteristic of controlled radical polymerization. Molecular weight of copolymer also increases

linearly with % conversion of monomers (**Figure 4.18**). The concentration of the unreacted monomer (PI) in the reaction mixture was determined by $^1\text{H-NMR}$ spectra of the reaction mixture recorded at various time intervals in presence of the known amount of the standard 1,1,2,2-tetrachloroethane. For the concentration determination of PI, the intensity of the peaks at $\delta = 6.5 \pm 0.1$ ppm were compared with the peaks for the standard at $\delta = 5.9 \pm 0.1$ ppm. A linear plot (**Figure 4.19**) is observed for $\ln \{[I]_0/[I]_t\}$ vs time (here $[I]_0$ = concentration of PI at zero time and $[I]_t$ = concentration of PI at time 't'), further confirming that the polymerization is occurring under controlled radical polymerization condition. The $^1\text{H-NMR}$ spectra of the reaction mixture for copolymerization of PI and MMA in CDCl_3 , at various time intervals are given in **Figure 4.20**. The PDI of the copolymer of PI and MMA was found to be 1.3 with 98% of monomer conversion.

Table 4.6: The variation of total conversion (in percent) of monomers with time, \bar{M}_n and PDI of poly(PI-*ran*-MMA)^s copolymers.

S. No.	Time (h)	Yield (%)	Total conversion (%)	\bar{M}_n ($1 \times 10^4 \text{ g mol}^{-1}$)	PDI
1	5	17	17	0.32	1.3
2	10	25	25	0.43	1.5
3	15	34	35	0.49	1.5
4	20	43	43	0.51	1.3
5	25	55	54	0.68	1.3
6	30	64	65	0.72	1.3
7	35	73	73	0.82	1.4
8	40	80	80	1.05	1.3
9	45	90	90	1.23	1.3
10	50	98	98	1.32	1.3

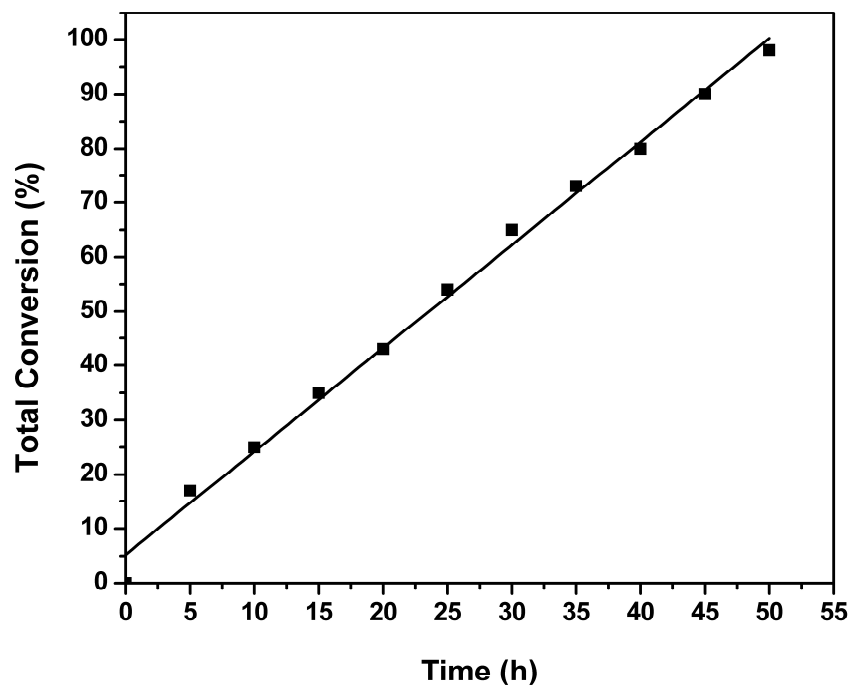


Figure 4.17: Plot of total conversion (in percent) of monomer with time for AGET-ATRP of PI and MMA.

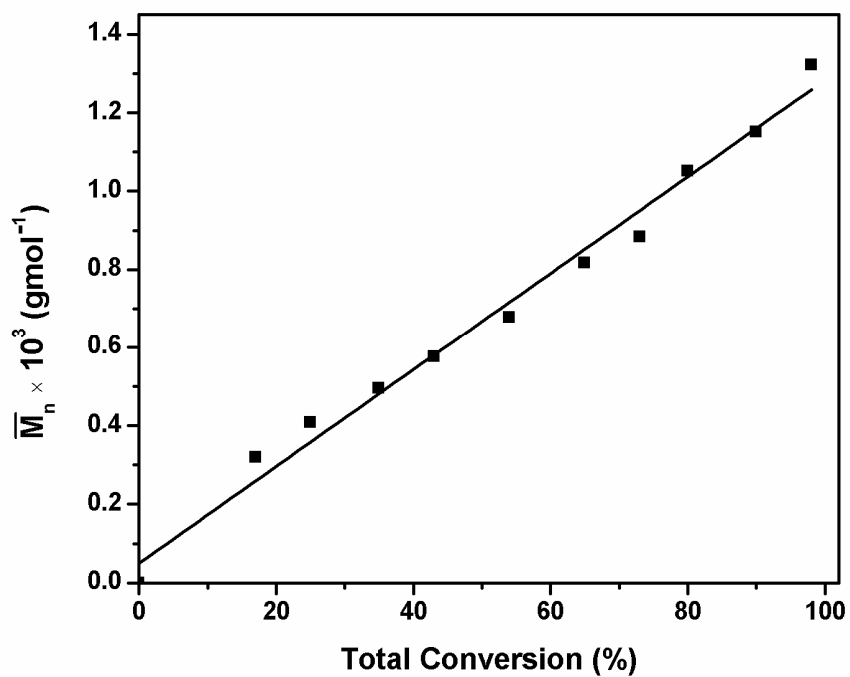


Figure 4.18: Plot of \bar{M}_n of copolymer with total conversion (in percentage) of monomer for AGET-ATRP of PI and MMA.

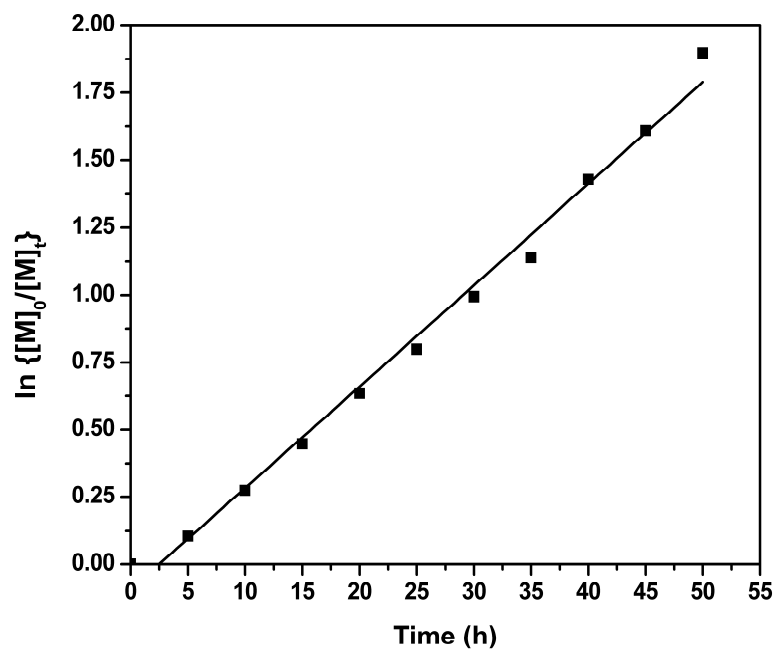


Figure 4.19: Plot of $\ln \{[M]_0/[M]_t\}$ with time for AGET-ATRP of PI and MMA.

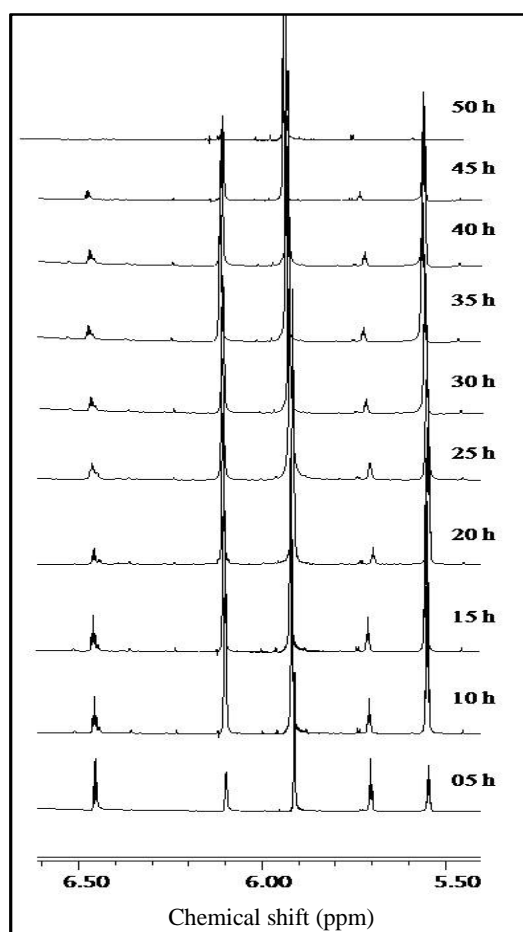


Figure 4.20: $^1\text{H-NMR}$ spectra of the reaction mixture for copolymerization of PI and MMA in CDCl_3 at various time intervals.

The various poly(NAI-*ran*-MMA)[§] (viz. poly(PI-*ran*-MMA)[§], poly(MPI-*ran*-MMA)[§], poly(MOPI-*ran*-MMA)[§] and poly(CPI-*ran*-MMA)[§]) copolymers have been synthesized using laboratory synthesized initiator viz. BSI-33 (**Scheme 4.1**) and their properties were compared with the copolymers synthesized using EBiB i.e. [poly(NAI-*ran*-MMA)[#]] (Chapter III, Section 3.3.3).

4.3.5 Characterization of Poly(NAI-*ran*-MMA)[§] Copolymers

The peak assignments for IR and ¹H-NMR spectra of the poly(NAI-*ran*-MMA)[§] copolymers were compared with the respective IR and ¹H-NMR spectra of NAI monomers discussed in Chapter II, Section 2.3.2.

4.3.5.1 IR Analysis

The IR spectra of poly(NAI-*ran*-MMA)[§] copolymers are given in **Figure 4.21**. The asymmetric and symmetric stretches for –CH₃ of MMA were observed in the regions 2940-2922 cm⁻¹ and 2853-2845 cm⁻¹, respectively. The >C=O of NAI showed two characteristics bands in the regions 1794-1784 cm⁻¹ and 1744-1724 cm⁻¹, respectively. The >C=O of MMA merged with carbonyl peak of NAI in the region 1744-1724 cm⁻¹. The characteristic three bands of >C=C< stretch for aromatic ring were observed in the regions 1612-1598 cm⁻¹, 1525-1502 cm⁻¹ and 1494-1542 cm⁻¹, respectively. The peaks observed in the region 540-525 cm⁻¹ were assigned to C-Br stretch.

4.3.5.2 ¹H-NMR Analysis

In the ¹H-NMR spectra of poly(NAI-*ran*-MMA)[§] copolymers (**Figure 4.22**), the characteristic peaks of aromatic protons of NAI was observed in the region $\delta = 7.5-7.2$ ppm. The peaks of –OCH₃ and –CH₂ (adjacent to the carbonyl group) of the side chain were observed, at $\delta = 3.6 \pm 0.10$ ppm and $\delta = 3.6 \pm 0.12$ ppm, respectively. The peaks of –CH₂ and –CH₃ of the copolymer backbone were observed in the region $\delta = 2.8-1.7$ ppm and $\delta = 1.4-0.8$ ppm, respectively. For poly(MPI-*ran*-MMA)[§] and poly(MOPI-*ran*-MMA)[§] peaks for –CH₃ and –OCH₃ attached to the aromatic ring were observed at $\delta = 2.4$ ppm and $\delta = 3.8$ ppm, respectively.

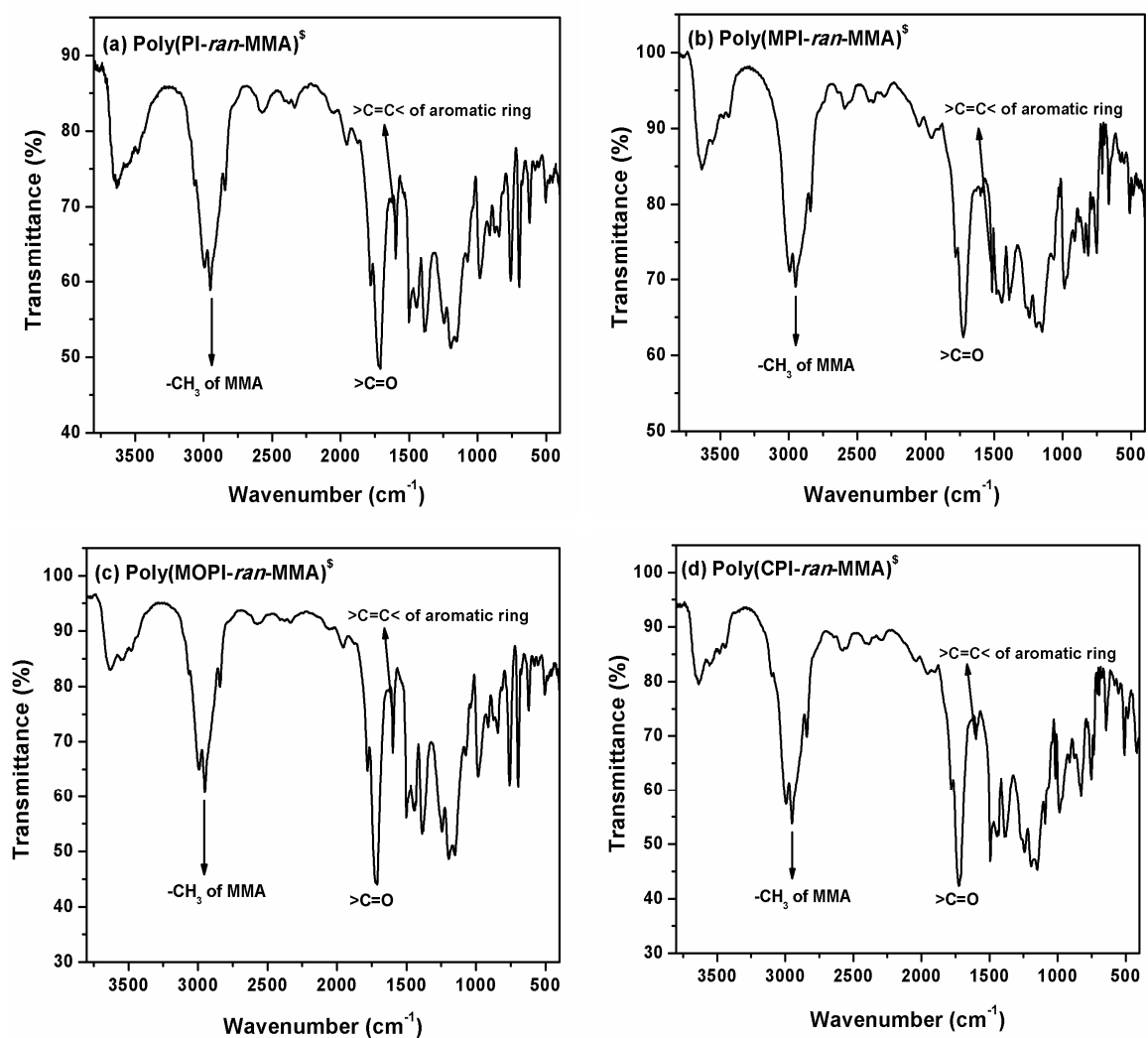


Figure 4.21: IR spectra of poly(NAI-ran-MMA)^s copolymers.

4.3.5.3 Effect of Initiator Structure on Copolymer Composition

The elemental analysis of the copolymers shows the presence of carbon, hydrogen, oxygen, nitrogen and bromine. The mole fractions of monomers in copolymers were calculated from (%N) using equations (given in chapter III, **Section 3.3.4**). Also, the mole fraction of monomers (MMA and NAI) in copolymers synthesized via n-ATRP and AGET-ATRP were calculated from the ¹H-NMR spectra of the copolymers (**Figure 4.22**). The mole fraction of monomers was determined by taking the ratio of the intensity of signals attributed to methoxy protons ($-\text{OCH}_3$) of MMA and aromatic protons of NAI. The results of copolymer composition are given in **Table 4.7**. A good correlation was

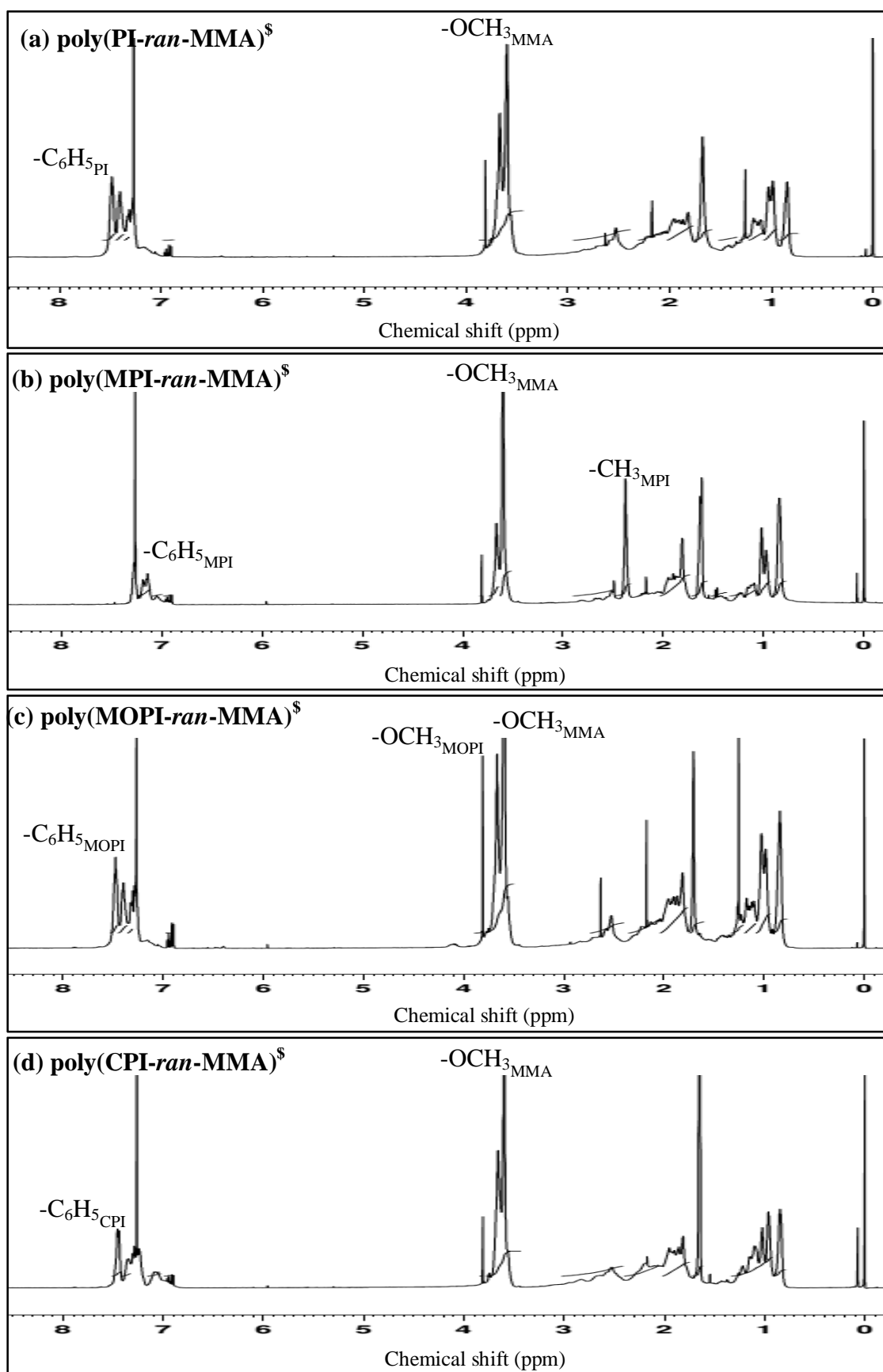


Figure 4.22: ¹H-NMR spectra of poly(NAI-ran-MMA)^s copolymers.

obtained between the mole fractions calculated from %N and calculated from the ¹H-NMR spectra of the copolymers.

When compared with the feed composition (which was maintained 2:8::NAI:MMA for all the copolymerization reactions), an enhanced incorporation (~ 5-15%) of monomers NAI and MMA in the copolymer backbone was observed (**Table 4.7**) for the copolymers synthesized using BSI-33 initiator as compared to the copolymers synthesized using EBiB (Chapter III, **Table 3.2**).

Table 4.7: Elemental analysis and copolymer composition for poly(NAI-*ran*-MMA)[§] copolymers. Experimental conditions: [NAI]/ [MMA]/ [BSI-33]/ [CuBr₂]/ [Bpy]/ [Sn(EH)₂] = 20/ 80/ 1/ 1/ 3/ 0.25, in anisole at 80 °C.

Copolymer designation	C (%)	H (%)	N (%)	O (%)	Br (%)	Mole fraction (from %N)		Mole fraction (from ¹ H-NMR)	
						NAI	MMA	NAI	MMA
poly(PI- <i>ran</i> -MMA) [§]	63.49	7.05	4.52	22.52	8.89	0.45	0.60	0.46	0.61
poly(MPI- <i>ran</i> -MMA) [§]	61.13	6.58	4.24	23.03	11.21	0.51	0.53	0.50	0.52
poly(MOPI- <i>ran</i> -MMA) [§]	60.57	6.04	5.90	24.90	11.76	0.57	0.47	0.56	0.46
poly(CPI- <i>ran</i> -MMA) [§]	57.5	6.75	3.39	21.17	8.04	0.41	0.63	0.41	0.64

4.3.5.4 Effect of Initiator Structure on Molecular Weights of Copolymers

As the incorporation of NAI and MMA monomers in copolymer backbone is more when BSI-33 was used as initiator, the molecular weights of the poly(PI-*ran*-MMA)[§], poly(MPI-*ran*-MMA)[§], poly(MOPI-*ran*-MMA)[§] and poly(CPI-*ran*-MMA)[§] was found in (g mol⁻¹) as 2.1×10⁴, 2.5×10⁴, 3.5×10⁴ and 1.8×10⁴, respectively. Which were observed to be two times greater as compared to poly(NAI-*ran*-MMA)[#] copolymers (Chapter III, **Table 3.3**). The PDI were obtained in the range of 1.2-1.3. The molecular weights of poly(NAI-*ran*-MMA)[§] copolymers was observed to increase in the order, poly(CPI-*ran*-MMA)[§] < poly(PI-*ran*-MMA)[§] < poly(MPI-*ran*-MMA)[§] < poly(MOPI-*ran*-MMA)[§], which is in accordance with the reactivity of the NAI comonomers.

4.3.5.5 Effect of Initiator Structure on Thermal Properties of Copolymers

The DSC of poly(NAI-*ran*-MMA)[§] copolymers are shown in **Figure 4.23**. The shift in the base line corresponding to the T_g of the copolymer was observed in all the samples. The T_g of the copolymers was determined by extrapolation of the two linear regions, before (onset temperature) and after (offset temperature) the T_g and the middle of the incline was considered as exact T_g of the copolymer [21]. The T_g was observed in the range of 218-240 °C for the poly(NAI-*ran*-MMA)[§] copolymers and details of the T_g are given in the **Table 4.8**. Whereas, T_g was obtained in the range of 198-217 °C for the Poly(NAI-*ran*-MMA)[#] (Chapter III, **Section 3.3.6.1, Table 3.4**). An increased in the T_g (~ 20-25%) was observed for all the poly(NAI-*ran*-MMA)[§] copolymers.

The TG/ DTG curves of the poly(NAI-*ran*-MMA)[§] copolymers are given in **Figure 4.24**. The poly(NAI-*ran*-MMA)[§] copolymers are stable upto 350 °C and degraded in single step with char yield 21-33% at 600 °C. However, poly(NAI-*ran*-MMA)[#] copolymers synthesized using EBiB initiator are stable upto 330 °C with char yield 10-13% at 600 °C (Chapter III, **Section 3.3.6.2**). The order of thermal stability was observed to be, poly(CPI-*ran*-MMA)[§] < poly(PI-*ran*-MMA)[§] < poly(MPI-*ran*-MMA)[§] < poly(MOPI-*ran*-MMA)[§].

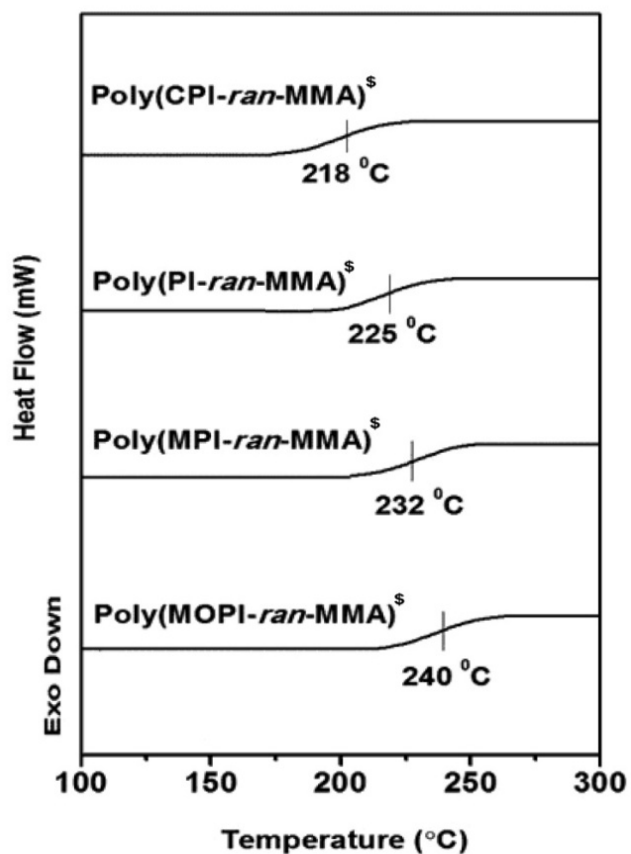


Figure 4.23: DSC of poly(NAI-*ran*-MMA)[§] copolymers.

Table 4.8: T_gs observed in the DSC of poly(NAI-*ran*-MMA)[§] copolymers.

Copolymer designation	T _o (°C)	T _g (°C)	T _e (°C)
poly(CPI- <i>ran</i> -MMA) [§]	190	218	230
poly(PI- <i>ran</i> -MMA) [§]	200	225	240
poly(MPI- <i>ran</i> -MMA) [§]	215	232	250
poly(MOPI- <i>ran</i> -MMA) [§]	220	240	260

T_o = onset temperature and *T_e* = endset temperature

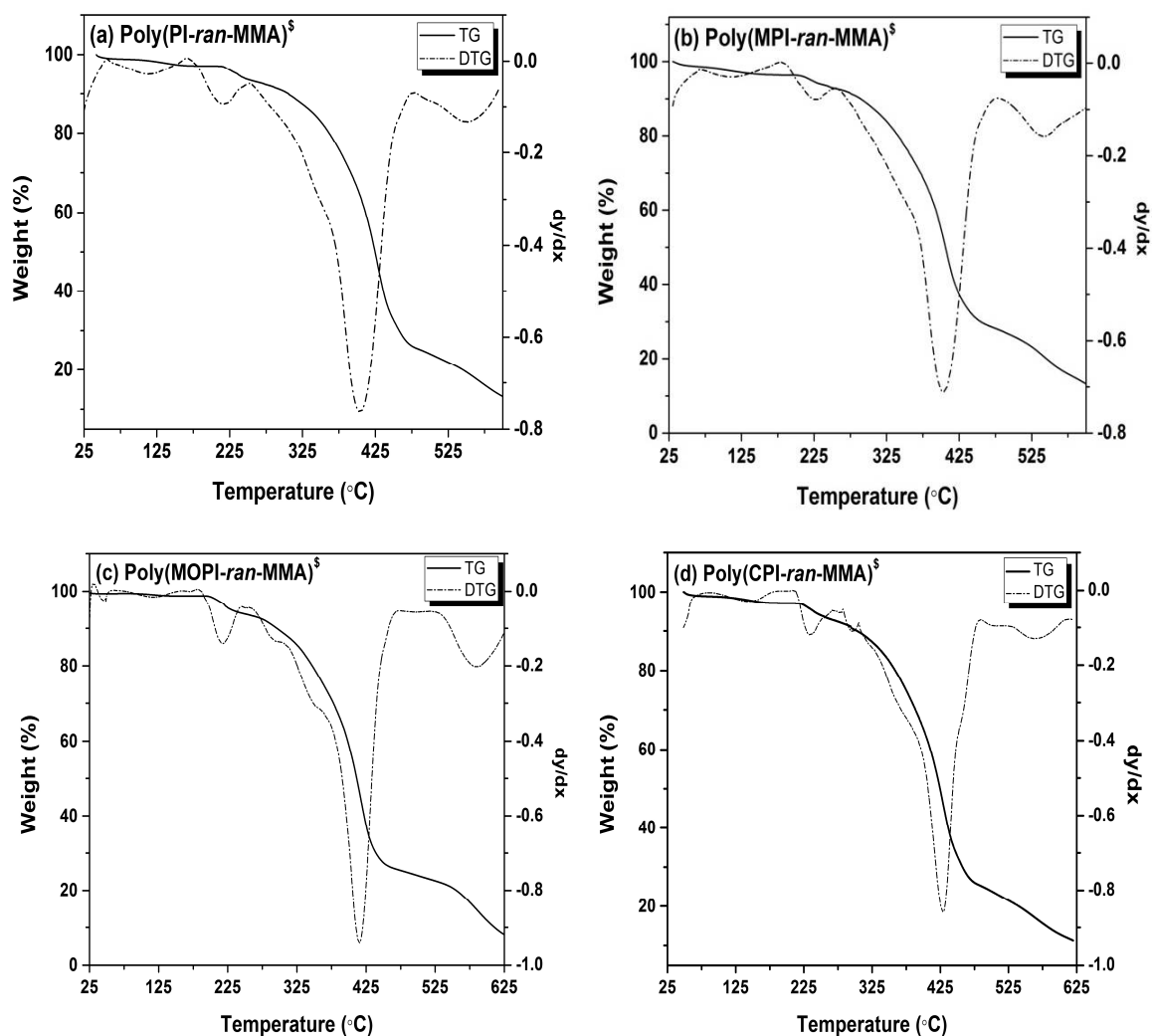


Figure 4.24: TG/ DTG scans of poly(NAI-*ran*-MMA)^s copolymers.

4.4 Conclusions

The K_{ATRP} of synthesized alkyl bromides along with a commercially available initiator (EBiB) were determined using UV-Vis-NIR spectroscopy. The k_t for the radicals were determined using DOSY-NMR spectroscopy. The relative K_{ATRP} values of synthesized alkyl bromides are extracted from the free energy values with respect to common ATRP initiators. A good agreement was obtained between the experimentally determined and theoretically calculated K_{ATRP} values of studied alkyl bromides. It is found that values of K_{ATRP} slightly decrease with increasing solvent polarity and increase significantly with increasing temperature. The copolymerization of PI and MMA was successfully carried out using synthesized alkyl bromide BSI-33 as initiator via AGET-ATRP. Kinetic

studies show that the copolymerization of PI and MMA progressed under control conditions. The obtained results shows that the synthesized BSI-33 initiator has better performance on the rate of copolymerization, molecular weight and thermal properties of the obtained copolymers as compared to the commercially available EBiB.

CHAPTER V

MECHANISTIC STUDIES OF THE COPOLYMERIZATION OF N-PHENYLITACONIMIDE AND METHYL METHACRYLATE VIA ATRP

5.1 Overview

This chapter describes the experimental and theoretical studies on the mechanistic features of the copolymerization of PI and MMA monomers using ATRP process. Experimentally, the microstructure analysis for the PI-MMA copolymer system was carried out from the triad fractions determined using the ^{13}C -NMR spectroscopy. Theoretically, the triad fractions were calculated from the propagation rate coefficients (k_p), determined using the DFT methods, treating the polymeric species as dimers and trimers. The effects of penultimate group on the structural and thermodynamic properties, such as C-X bond length, bond enthalpy, free energy and equilibrium constant have also been studied using DFT methods.

5.2 Experimental Section

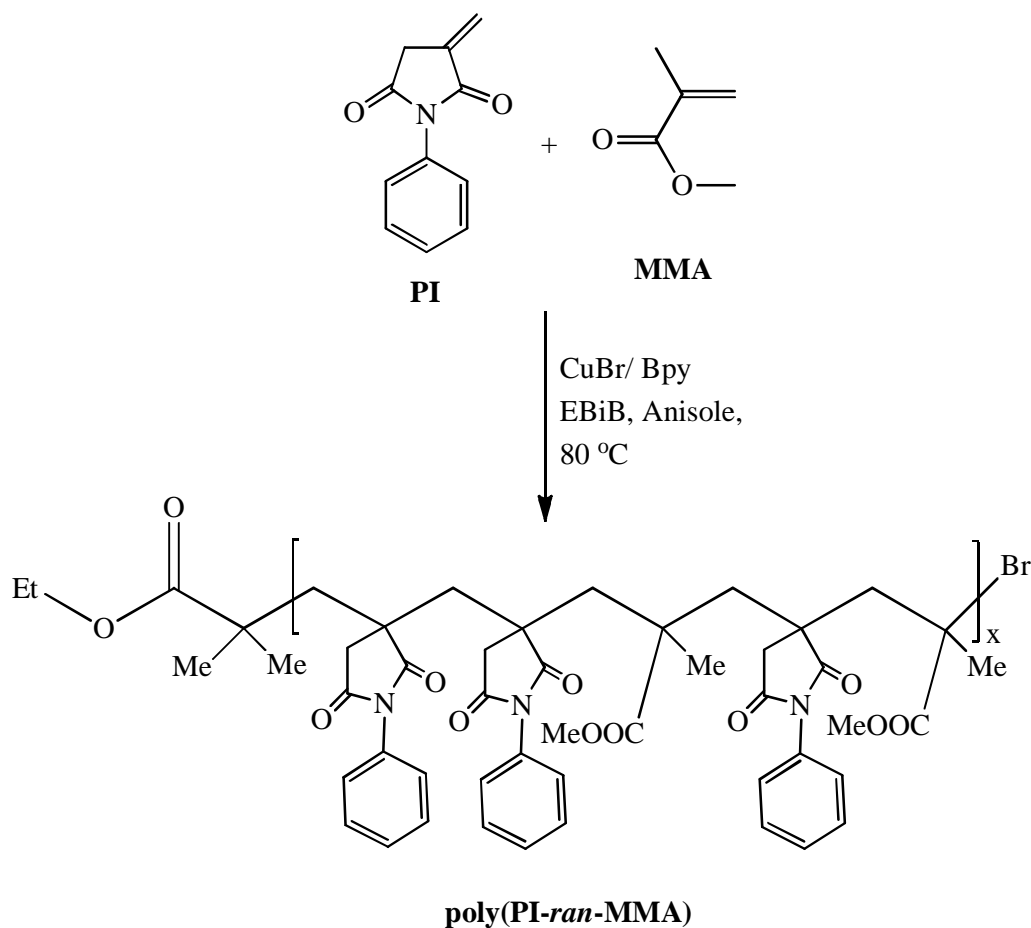
5.2.1 Materials and Methods

The ^1H decoupled ^{13}C -NMR [$^{13}\text{C}\{^1\text{H}\}$ -NMR] spectra with NOE suppression scheme of copolymers were recorded on a Bruker AV III 500 MHz with an operating frequency of 125.75 MHz, which is equipped with 5mm broadband gradient probe. The chemical shifts were reported in ppm relative to TMS in CDCl_3 . Inverse gated decoupling sequence with a relaxation delay of 3s was employed to record the spectrum.

5.2.2 Synthesis of Copolymers of PI and MMA

To the solution of PI and MMA in 10 mL of dry anisole, CuBr (0.25 mmol) and Bpy (0.75 mmol) were added. For the determination of triad fractions of PI-MMA copolymer, the monomers with varying mole fractions of PI (from 0.05-0.50) and MMA (0.95-0.50) were used for the polymerization. The reaction mixture was subjected to freeze-vacuum-

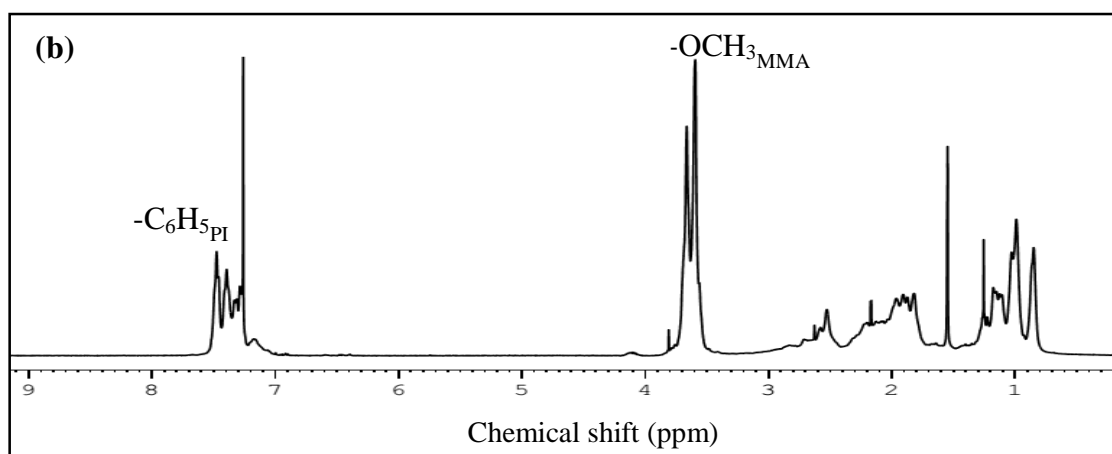
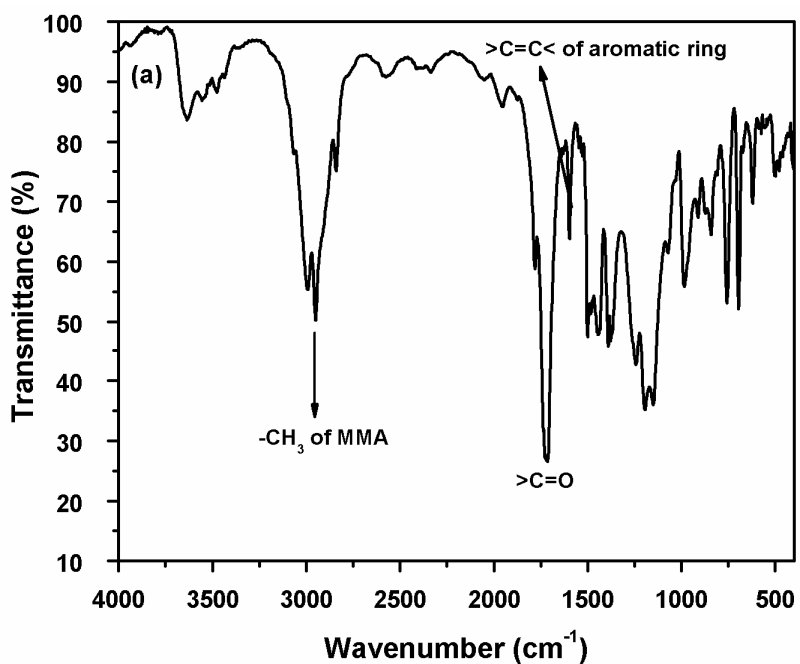
thaw cycle twice. A solution of EBiB (0.25 mmol) in 4 mL of dry anisole was degassed separately and then charged to this reaction flask through a nitrogen-purged syringe. The reaction mixture was again subjected to freeze-vacuum-thaw cycle thrice. The reaction temperature was maintained at 80 °C for 5 h. The copolymerizations were stopped at low conversions (< 15%) by adding the reaction mixture in excess of methanol. The copolymer precipitated out was filtered and washed with hot methanol to remove unreacted monomers. The obtained copolymer was dissolved in acetone and passed through the alumina bed to remove the catalyst. It was concentrated and reprecipitated with methanol, filtered and dried under vacuum. The final yield of the copolymer was obtained using the gravimetric method and was found in the range of 15-20%.



Scheme 5.1: Reaction scheme for synthesis of copolymers of PI and MMA.

5.2.3 Structural Characterization of Copolymers

The obtained poly(PI-*ran*-MMA) copolymers were characterized using IR (**Figure 5.1a**), $^1\text{H-NMR}$ (**Figure 5.1b**) and $^{13}\text{C-NMR}$ (**Figure 5.1c**) spectroscopy. The detailed analysis of the IR, $^1\text{H-NMR}$ and $^{13}\text{C-NMR}$ spectra of the poly(PI-*ran*-MMA) copolymers are given in chapter III (Section no. 3.3.1, page no. 64-65).



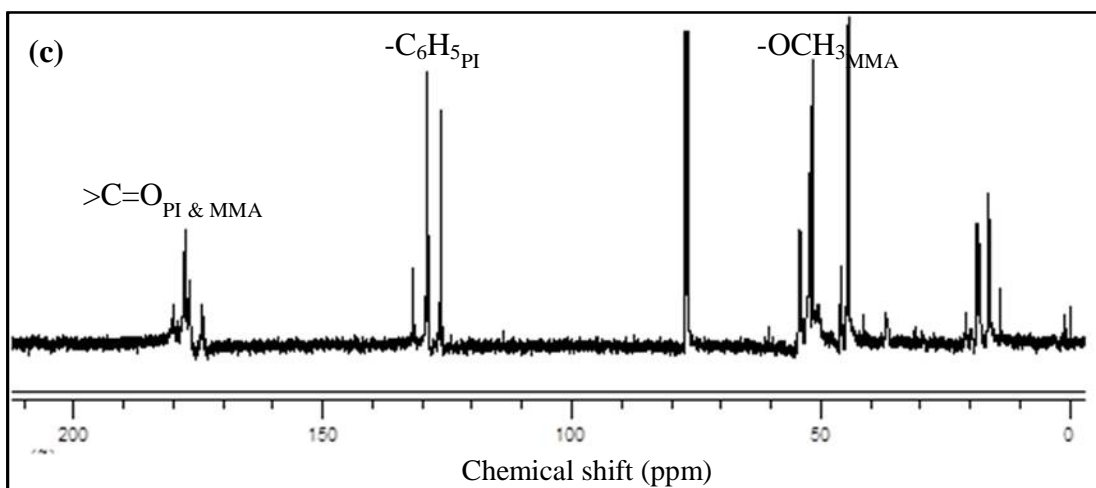


Figure 5.1: (a) IR, (b) ^1H -NMR and (c) ^{13}C -NMR of poly(PI-*ran*-MMA) copolymer.

5.2.4 Determination of Triad Fractions Using $^{13}\text{C}\{^1\text{H}\}$ -NMR Spectroscopy

Triad fraction data provides the information related to sequence distribution of monomeric units on the copolymer chain and additional information about the copolymer microstructure. The mechanism of PI-MMA copolymerization via ATRP methodology are studied using the triad fraction calculations.

To calculate the triad fractions of poly(PI-*ran*-MMA) copolymers, the copolymers were synthesized with varying mole fractions of PI in the initial feed ranging from 0.05 to 0.45 (**Scheme 5.1**). The copolymer compositions were determined from the elemental analysis (%N) data using equations given in (Chapter III, **Section 3.3.4**). Also, the mole fraction of monomers (MMA and PI) in copolymers were calculated from the ^1H -NMR spectra of the copolymers. The mole fraction of monomers was determined by taking the ratio of the intensity of signals attributed to methoxy protons ($-\text{OCH}_3$) of MMA and aromatic protons of PI. The results of copolymer composition are given in **Table 5.1**. A good correlation was obtained between the mole fractions calculated from %N and calculated from the ^1H -NMR spectra of the copolymers.

Table 5.1: Elemental analysis and copolymer compositions of poly(PI-*ran*-MMA) for various feed ratios.

Mole fractions of monomers in feed		C (%)	H (%)	O (%)	N (%)	Br (%)	Mole fractions of monomers (from %N)		Mole fractions of monomers (from ¹ H-NMR)	
PI	MMA						PI	MMA	PI	MMA
0.05	0.95	49.11	2.38	21.39	4.70	22.42	0.18	0.82	0.18	0.81
0.10	0.90	61.72	7.17	20.37	2.62	8.12	0.29	0.71	0.30	0.29
0.15	0.85	58.73	0.09	22.49	5.17	13.52	0.36	0.64	0.35	0.65
0.20	0.80	64.79	6.64	18.25	4.32	6.10	0.53	0.47	0.52	0.46
0.25	0.75	55.76	0.12	20.27	5.47	18.40	0.67	0.33	0.66	0.34
0.30	0.70	64.81	5.69	19.21	4.80	5.51	0.60	0.40	0.61	0.39
0.35	0.65	54.68	0.10	19.63	5.88	19.70	0.58	0.42	0.58	0.41
0.40	0.60	65.91	5.49	12.26	5.41	10.90	0.77	0.23	0.76	0.23
0.45	0.55	50.39	3.97	19.04	5.36	21.20	0.87	0.13	0.88	0.11

The variation of relative intensity of the signals due to the carbonyl carbons with the variations of amount of PI and MMA in the feed is shown in the ¹³C{¹H}-NMR spectra of poly(PI-*ran*-MMA) copolymer (**Figure 5.2**). The carbonyl carbon signals of MMA (M) ($\delta = 178.2-175.6$ ppm) as well as of PI (I) ($\delta = 174.6-172.8$ ppm) shows multiplets, indicating the sensitivity to compositional and configurational sequences and hence were used for the determination of the sequence distribution of M-centered and I-centered triads. The **Figure 5.3** and **Figure 5.4** shows the M-centered and I-centered carbonyl region, respectively, in ¹³C{¹H}-NMR spectra for the series of poly(PI-*ran*-MMA) copolymers of different copolymer compositions. The MMA carbonyl region is divided into three broad envelopes (**Figure 5.3**). The carbonyl carbon resonance signals in the region $\delta = 177.3-176.1$ ppm, which decrease in intensity as the MMA content in the copolymer decreases, are assigned to the MMM triad. The intensity of the carbonyl signals in the region $\delta = 176.1-175.6$ ppm increases as the MMA content in the copolymer decreases and are therefore assigned to the IMI triad compositional sequence. The region around $\delta = 177.0-177.5$ ppm is assigned to the MMI compositional triad, which first increases and then decreases with the increase in PI content in the copolymer. Similarly the I-centered carbonyl region ($\delta = 174.6-172.8$ ppm) is also divided into three broad envelopes. The region where signal intensity increases and decreases with the increasing PI content was assigned as III ($\delta = 173.9-172.8$ ppm) and MIM ($\delta = 174.6-174.3$ ppm) compositional triad regions, respectively. The region where signal intensity increases and then decreases with increasing PI content was thus assigned as the MII ($\delta =$

174.3-173.9 ppm) compositional triad region (**Figure 5.4**). Similarly for other feed composition the triad concentrations were assigned as explained above. The concentration of various compositional triad fractions were calculated from the relative areas of the resonance signals. The relative areas of resonance signals were determined using a nonlinear least-square Lorentzian line shape deconvoluting program.

There are total eight triad fractions possible for PI-MMA copolymerization, viz. MMM, MMI+IMM, IMI, III, IIM+MII, MIM. The sum of the M-centered triad fractions (MMM, MMI+IMM and IMI) as well as I-centered triad fractions (III, IIM+MII and MIM) is unity. As a result, [MMM] and [III] were eliminated in order to avoid the issue of linear dependency [265]. The six triad fractions chosen in this study are MMI+IMM, IMI, IIM+MII, MIM, the results are displayed in **Table 5.7**.

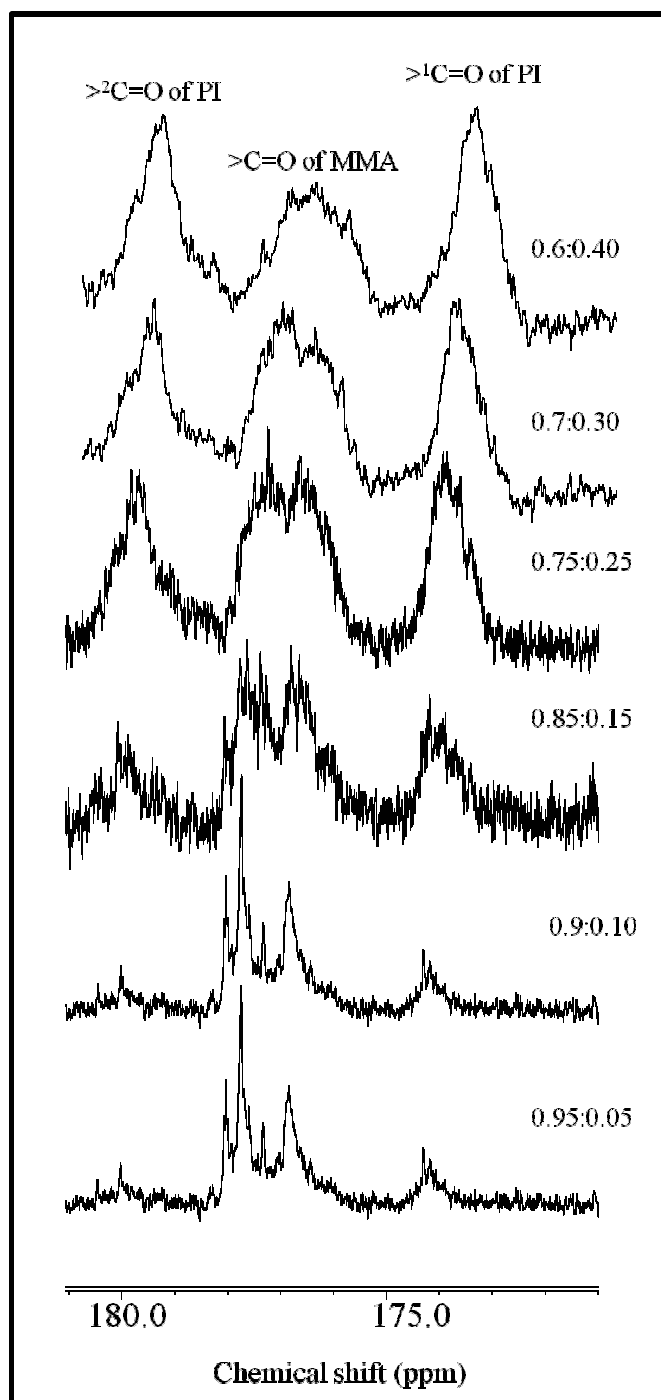


Figure 5.2: Carbonyl regions in $^{13}\text{C}\{^1\text{H}\}$ -NMR spectra for poly(PI-ran-MMA) with varied feed ratios.

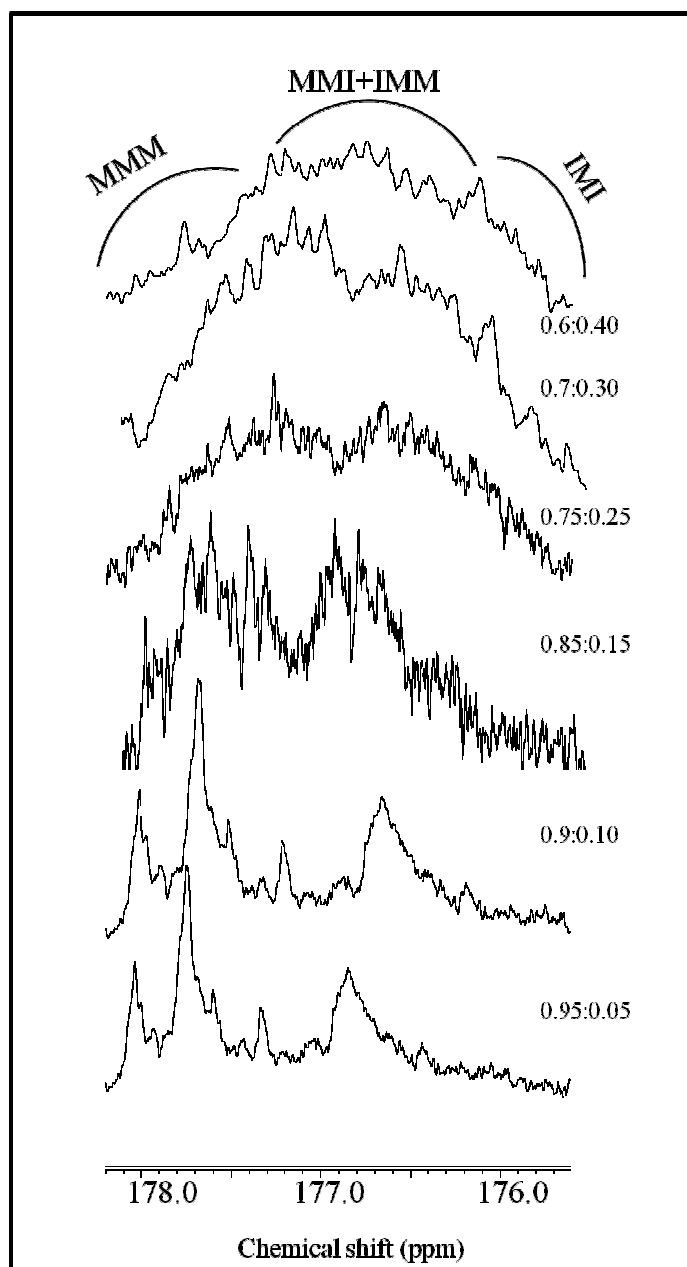


Figure 5.3: The splitting of MMA carbonyl regions in $^{13}\text{C}\{^1\text{H}\}$ -NMR spectra for poly(PI-*ran*-MMA) with varied feed ratios.

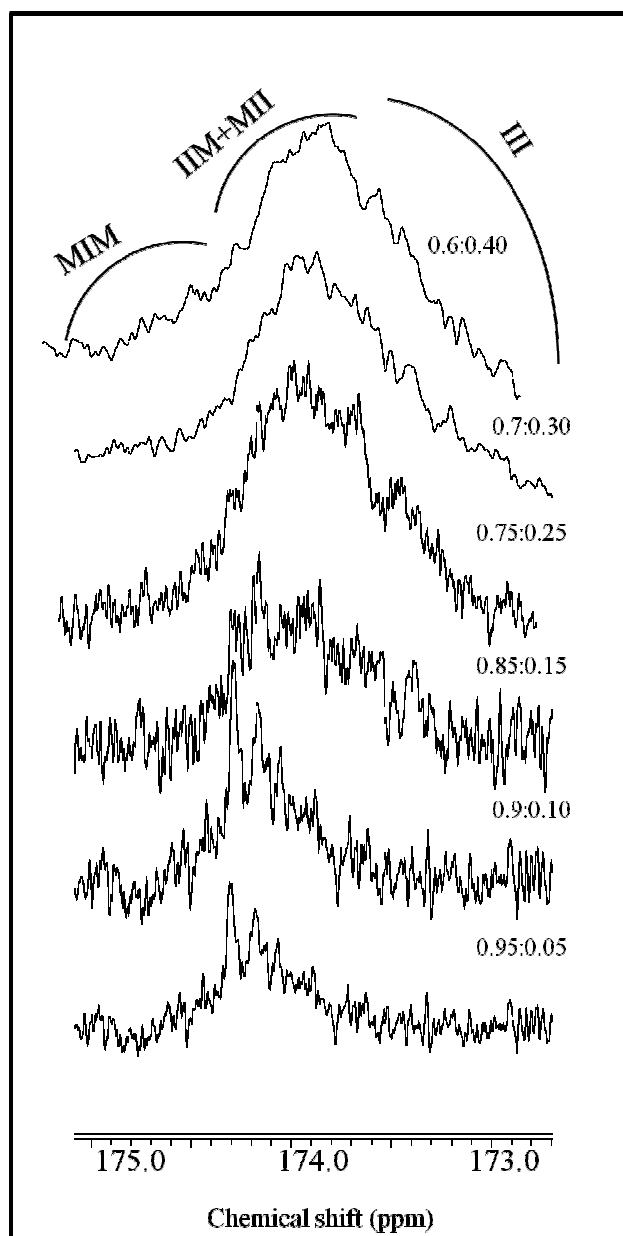


Figure 5.4: The splitting of PI carbonyl regions in $^{13}\text{C}\{^1\text{H}\}$ -NMR spectra for poly(PI-*ran*-MMA) with varied feed ratios.

5.3 Computational Details

QST3 method was used to locate the transition state structures for the formation of dimer and trimer radicals, which requires the optimized reactants, product, and an estimate of the transition state [266]. B3LYP/ 6-31+G(d) optimized geometry of the reactants and products are used to get the estimate structure of transition state. Transition states were identified as saddle points on the potential energy surface, possessing only one imaginary

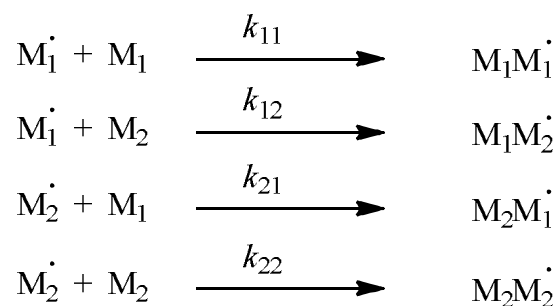
frequency. Once the transition state structures are identified, the intrinsic reaction coordinates (IRC) calculations were carried out following with a step size of 15 amu^{0.5}-Bohr. Unrestricted B3LYP/ 6-31+G(d) was used for both the QST3 and the IRC calculations. The IRC calculation is performed for the all gas phase optimized transition state structures.

The k_p values were calculated from activation energy using standard transition state theory [68]. In the transition state theory, the rate constant of a bimolecular reaction $A + B = C$ is related to the molecular properties of the reacting species and the k_p values are calculated using the following equation,

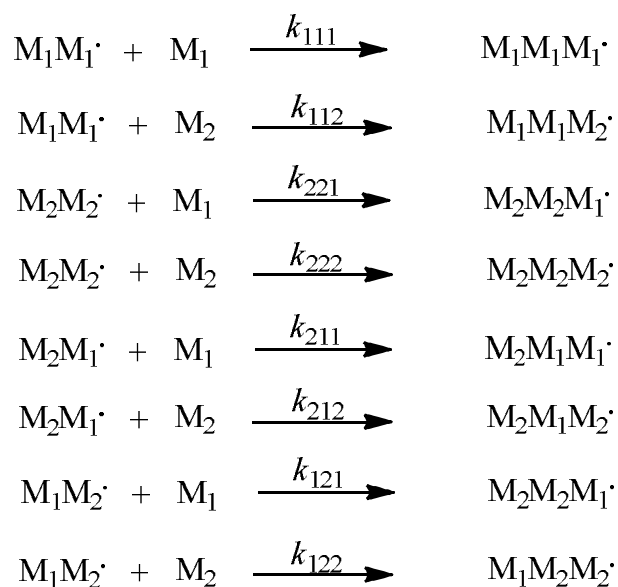
$$k(T) = \kappa(T) \frac{k_B T}{h} (c^\circ)^{1-m} e^{(-\Delta G^\ddagger/RT)} \dots\dots\dots 5.1$$

In this equation, $\kappa(T)$ = tunneling correction factor, T = absolute temperature, R = universal gas constant, k_B = Boltzmann constant, h = Planck's constant, c° ($= P/RT$) = standard unit of concentration (molL⁻¹) and m = molecularity of the reaction, ΔG^\ddagger = Gibb's free energy of activation. The value of c° depends on the standard-state concentration assumed in calculating the thermodynamic quantities, in our work, the gas phase quantities were calculated for a mole of ideal gas at 298.15 K and 1 atm pressure, and thus $c^\circ = 0.0409$ mol L⁻¹. The tunneling coefficient $\kappa(T)$ corrects for quantum effects in motion along the reaction path and can be assumed to be unity (due to the large masses of the reacting groups) in the addition of carbon-centered radicals to alkenes [267]. All the calculations are carried out in gas phase and anisole solvent at different temperature (viz. 25 °C and 80 °C). Solvent effects were studied using Tomasi's polarizable continuum model. To calculate the Arrhenius parameter the k_p calculations are carried out in the temperature range of 25 °C to 375 °C.

The chemically controlled steps in radical polymerization can be studied accurately using small model reactions in which the propagating radical or other polymeric species are replaced by dimers or trimers [68]. To study the mechanism of copolymerization of PI and MMA monomer system via ATRP, the resulting polymeric species are modeled as a dimer (for which terminal model is used) and a trimer (for which both terminal and penultimate models are used) [268]. In the proposed study, the formation of dimers from monomers using the terminal model (Chapter I, equations 1.4 to 1.7) can be written as,



Similarly, in the proposed study, the formation of trimers using the penultimate model (Chapter I, equations 1.9 to 1.16) can be written as,



where, M_1 and M_2 represents PI, MMA and NHI monomers.

To find out the reactivity ratios of PI and MMA monomers, we have selected the possible dimer radicals and trimer radicals as a propagating radicals of the chosen monomer. Apart from PI and MMA monomers, the itaconimide (NHI) monomer is also used for the modeling purpose. The structure of the monomers is given in the **Figure 5.5**.

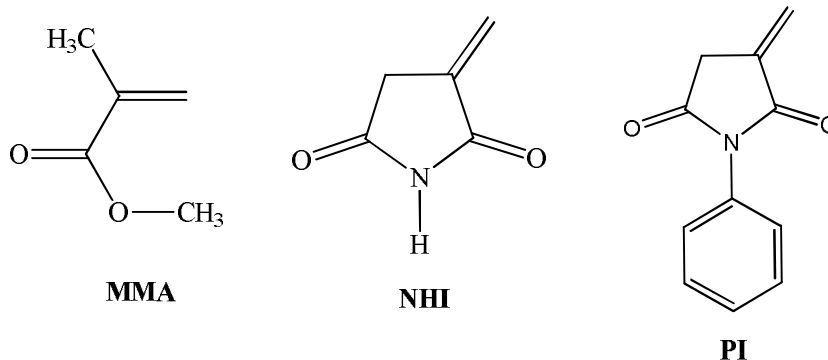


Figure 5.5: Structure of monomers MMA, NHI, and PI used for the formation of dimers and trimers.

The triad fractions of copolymers are depends on monomer reactivity ratios. The triad fractions for PI-MMA copolymerization are calculated using terminal and penultimate model expressions as given in equations 5.2-5.3 and 5.4-5.5, respectively. Terminal model expressions for M-centered triad fractions are as [21, 264],

$$[MMI] = [IMM] = \frac{r_M f_M f_I}{r_M^2 f_M^2 + 2r_M f_M f_I + f_I^2}, \text{ and } \dots\dots\dots 5.2$$

$$[IMI] = \frac{f_I^2}{r_M^2 f_M^2 + 2r_M f_M f_I + f_I^2} \dots\dots\dots 5.3$$

Penultimate model expressions for M-centered triad fractions are as [21, 264],

$$[MMI] = [IMM] = \frac{r'_M f_M f_I}{r'_M r_M f_M^2 + 2r'_M f_M f_I + f_I^2}, \text{ and } \dots\dots\dots 5.4$$

$$[IMI] = \frac{f_I^2}{r'_M r_M f_M^2 + 2r'_M f_M f_I + f_I^2} \dots\dots\dots 5.5$$

The compositions for (PI) I-centered triad are given by switching the subscripts I and M in equations 5.2-5.5.

In the above equations (5.2-5.5), r_M and r'_M = reactivity ratios of MMA, r_I and r'_I = reactivity ratios of PI, f_M = mole fraction of MMA in copolymer and f_I = mole fraction of

PI in copolymer. The values f_M and f_I are given in the **Table 5.1**. The reactivity ratios of MMA and PI monomer were calculated using DFT methods as given below:

5.4 Results and Discussion

5.4.1 Reactivity Ratios of PI and MMA Monomers via Terminal Model

We modelled the polymeric species as dimers and the reactivity ratios of PI and MMA monomers are calculated from the k_p values of dimer propagating radicals as follows:

5.4.1.1 Structure of Transition State for Dimer Formation

The optimized transition state (TS) structure for all the dimer radical obtained from unrestricted B3LYP/ 6-31+G(d) are given in **Figure 5.6**. The C=C bond length of the monomers, the C-C bond length and dihedral angle with the newly formed radical centre is mentioned on the TS structure. The TS structure of all the dimers is more similar with their product structure. In the TS, the newly formed C-C bond is longer than C-C bond of the product structure (the difference of $0.045 \text{ \AA} \pm 0.02 \text{ \AA}$), since this bond has not yet formed completely. The C=C bond length of monomer is between the single bond and double bond (the difference of $0.031 \text{ \AA} \pm 0.01 \text{ \AA}$). The dihedral angle (with respect to radical centre) in TS of dimer is increased when we compared with respective to their product structure.

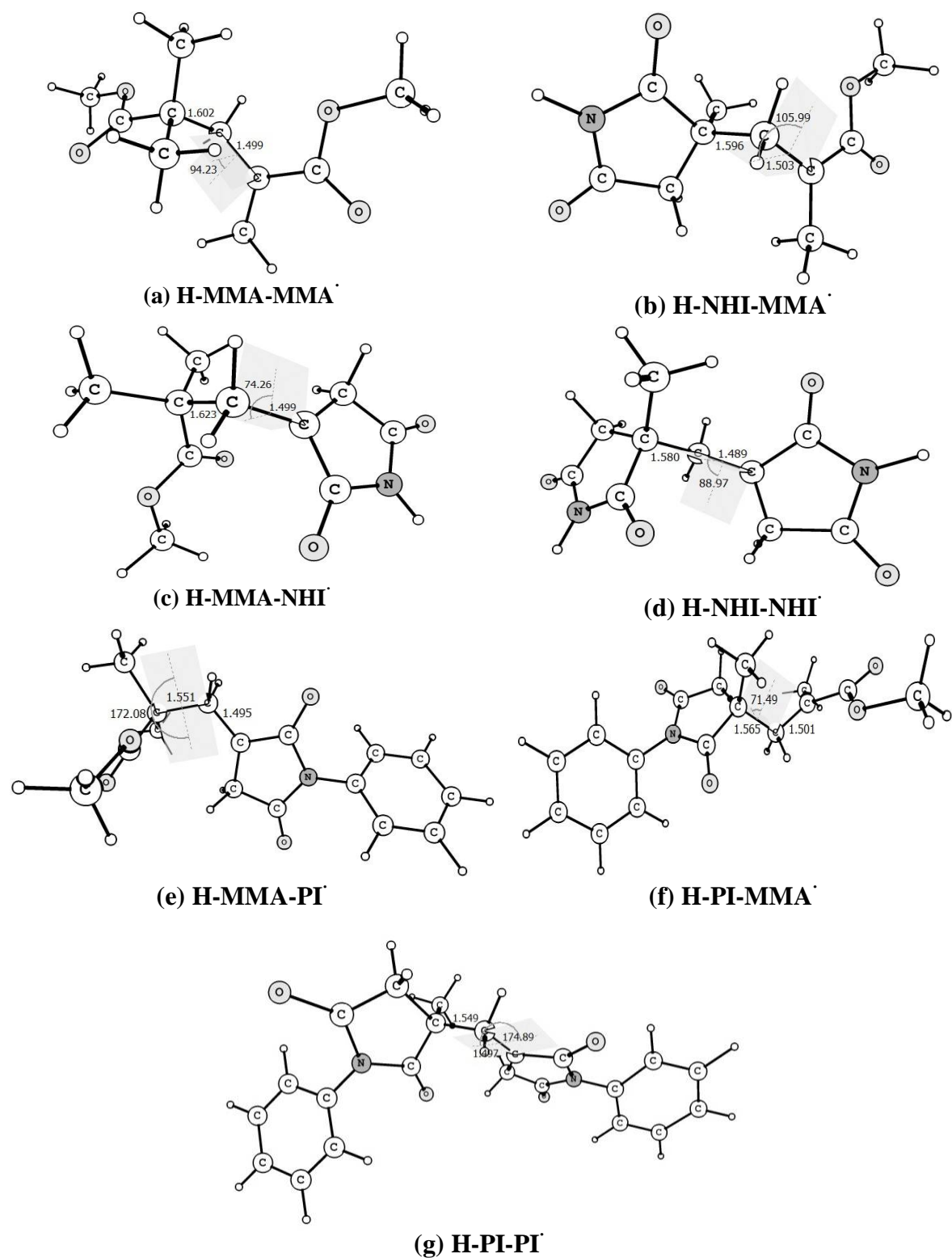


Figure 5.6: B3LYP/ 6-31+G(d) optimized gas-phase geometries of the minimum energy conformations of the transition structures for dimer radicals.

5.4.1.2 Free Energy of Activation (ΔG^\ddagger)

Free energy of activation for all dimer radicals at various temperature is calculated in gas phase (**Table 5.2**) and in anisole (**Appendix v, Table A2**). Free energy of activation is the difference between the zero point corrected free energy of reactant and zero point corrected free energy of TS structure. The free energy of TS is increases with the increase in temperature in the range 2-4 kJ mol⁻¹ in gas phase as well as in anisole. Higher values of free energy of activation are obtained for H-MMA-MMA[·] and H-PI-PI[·], than for the dimer radicals H-NHI-MMA[·] and H-PI-MMA[·]. The trends obtained for the free energy of activation of dimer radical in gas phase is, H-MMA-MMA[·] > H-PI-PI[·] > H-MMA-NHI[·] > H-MMA-PI[·] > H-PI-MMA[·] > H-NHI-NHI[·] > H-NHI-MMA[·].

Table 5.2: Free energy of activation for dimer radicals at various temperature in gas phase.

Temp. (°C)	ΔG^\ddagger (kJ mol ⁻¹)						
	H-MMA-MMA [·]	H-MMA-NHI [·]	H-NHI-MMA [·]	H-NHI-NHI [·]	H-MMA-PI [·]	H-PI-MMA [·]	H-PI-PI [·]
25	250.68	240.17	218.92	234.27	239.10	237.62	245.30
75	253.62	244.75	221.30	236.80	242.32	240.36	248.78
125	256.56	247.30	231.82	239.35	245.53	243.11	252.28
175	259.50	249.86	236.58	241.91	248.75	245.87	255.77
225	262.45	252.41	249.49	244.48	251.97	248.63	259.28
275	265.39	254.97	253.31	247.04	255.19	251.39	262.79
325	268.32	257.51	256.92	249.60	258.39	254.14	266.28
375	271.25	260.06	259.32	252.17	261.59	256.89	269.78

As we move from gas phase to solvent anisole (**Appendix v, Table A2**), an increase of 3-9 kJ mol⁻¹ in free energy of activation is observed except for H-PI-MMA[·] and H-PI-PI[·]. For H-PI-MMA[·], the free energy of activation value in anisole remains more or less constant, whereas that of H-PI-PI[·] it is decreased as compared to gas phase. The trend for free energy of activation values for dimer radicals in anisole is observed as, H-MMA-MMA[·] > H-MMA-NHI[·] > H-PI-PI[·] > H-MMA-PI[·] > H-PI-MMA[·] ~ H-NHI-NHI[·] > H-NHI-MMA[·].

5.4.1.3 Rate Constant of Propagation (k_p)

The k_p values for the studied dimer radicals are calculated using equation 5.1 at various temperature (in the range 25 °C to 375 °C) in gas phase as well as in solvent anisole (for few cases), and displayed in **Table 5.3**. At 25 °C, the k_p of the dimer H-NHI-MMA \cdot shows the highest values (6.71×10^{-25} Lmol $^{-1}$ s $^{-1}$) whereas the dimer radical H-MMA-MMA \cdot shows the lowest k_p values (1.83×10^{-30} Lmol $^{-1}$ s $^{-1}$), a difference of nearby fivefold. The overall trends for the k_p values of studied dimer radical is as, H-NHI-MMA \cdot > H-NHI-NHI \cdot > H-PI-MMA \cdot > H-MMA-PI \cdot > H-MMA-NHI \cdot > H-PI-PI \cdot > H-MMA-MMA \cdot . However, as the temperature increases, the differences in the k_p values of various dimer radicals gradually reduces and finally becomes comparable, for example at 375 °C, the highest and lowest values of k_p (in Lmol $^{-1}$ s $^{-1}$) are 3.42×10^{-6} and 9.93×10^{-8} , respectively. The trends in k_p values at this temperature is found to be, H-NHI-NHI \cdot > H-PI-MMA \cdot > H-NHI-MMA \cdot > H-MMA-NHI \cdot > H-MMA-PI \cdot > H-PI-PI \cdot > H-MMA-MMA \cdot . As we move from gas phase to solvent anisole, the k_p values for dimer radicals decreases in the range of 10^3 to 10^1 . The overall trends of k_p among the different dimer radicals are found to be similar to that of gas phase results.

Table 5.3: Rate constant of propagation for dimer radicals at different temperatures in gas phase and in anisole.

Temp. (°C)	k_p (Lmol $^{-1}$ s $^{-1}$)*						
	H-MMA-MMA \cdot	H-MMA-NHI \cdot	H-NHI-MMA \cdot	H-NHI-NHI \cdot	H-MMA-PI \cdot	H-PI-MMA \cdot	H-PI-PI \cdot
25	1.83×10^{-30} (6.44×10^{-31})	3.78×10^{-29} (1.69×10^{-29})	6.71×10^{-25} (4.29×10^{-28})	1.37×10^{-27} (3.61×10^{-29})	1.95×10^{-28} (6.84×10^{-29})	3.55×10^{-28} (3.78×10^{-28})	1.60×10^{-29} (3.12×10^{-29})
75	1.84×10^{-24}	3.92×10^{-23}	1.30×10^{-19}	6.11×10^{-22}	9.10×10^{-23}	1.79×10^{-22}	9.74×10^{-24}
80	1.84×10^{-24} (7.14×10^{-25})	3.95×10^{-23} (1.49×10^{-23})	1.32×10^{-19} (2.30×10^{-22})	6.13×10^{-22} (2.78×10^{-23})	9.14×10^{-23} (3.58×10^{-23})	1.80×10^{-22} (1.86×10^{-22})	9.76×10^{-24} (2.03×10^{-23})
125	5.93×10^{-20}	9.72×10^{-19}	1.04×10^{-16}	1.07×10^{-17}	1.66×10^{-18}	3.44×10^{-18}	2.16×10^{-19}
175	1.95×10^{-16}	2.59×10^{-15}	9.14×10^{-14}	2.19×10^{-14}	3.49×10^{-15}	7.57×10^{-15}	5.30×10^{-16}
225	1.29×10^{-13}	1.45×10^{-12}	2.94×10^{-12}	9.84×10^{-12}	1.61×10^{-12}	3.61×10^{-12}	2.76×10^{-13}
275	2.64×10^{-11}	2.60×10^{-10}	3.74×10^{-10}	1.48×10^{-9}	2.48×10^{-10}	5.70×10^{-10}	4.67×10^{-11}
325	2.27×10^{-9}	1.99×10^{-8}	2.24×10^{-8}	9.77×10^{-8}	1.67×10^{-8}	3.93×10^{-8}	3.42×10^{-9}
375	9.93×10^{-8}	7.92×10^{-7}	9.08×10^{-7}	3.42×10^{-6}	5.95×10^{-7}	1.43×10^{-6}	1.30×10^{-7}

* values in bracket are in anisole solvent and remaining are in gas phase

5.4.1.4 Activation Energy and Frequency Factor for Dimers

The activation energy (E_a) and frequency factor (A) for all dimer radicals are calculated from k_p values (over a temperature range of 25 °C to 375 °C) using the Arrhenius equation 5.6,

$$\ln k_p = \ln A - \frac{E_a}{RT} \dots\dots\dots 5.6$$

The graph of $\ln k_p$ vs $1/T$ for dimer radicals in gas phase is given in **Figure 5.7**. Similarly, the graph of $\ln k_p$ vs $1/T$ for dimer radicals in anisole is given in (**Appendix v, Figure A1**). From these graphs E_a and A are calculated from the slope and intercept values, respectively and it is given in **Table 5.4**.

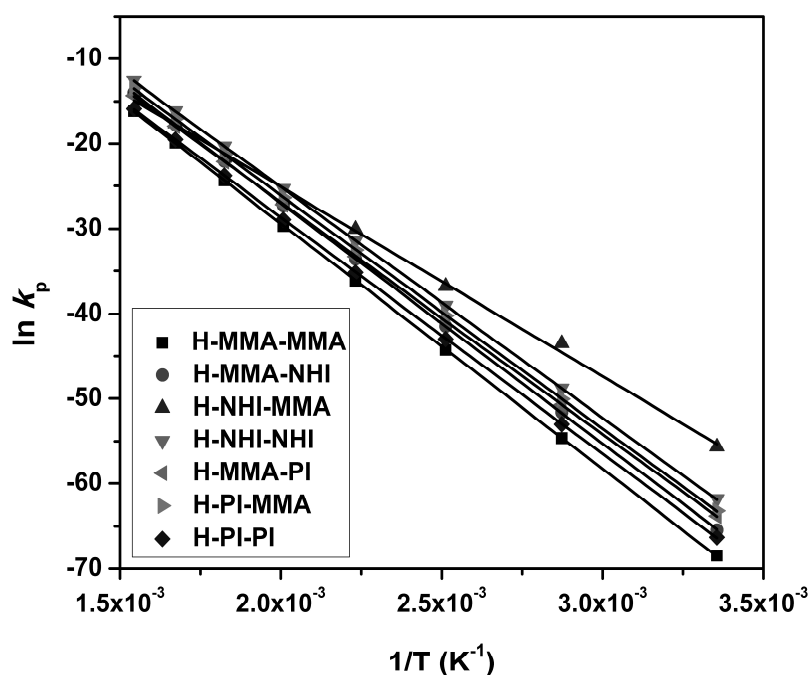


Figure 5.7: Plot of $\ln k_p$ vs $1/T$ for various dimer radical in gas phase.

The estimated activation energies for the studied dimer radicals in gas phase (and in anisole) ranges between ≈ 20 - 24 kJ mol^{-1} and frequency factor ranges between 10^{11} - $10^{12} \text{ Lmol}^{-1}\text{s}^{-1}$. Roughly, the trends for the E_a and A value in gas phase and in anisole is, $\text{H-NHI-MMA} \cdot < \text{H-PI-MMA} \cdot < \text{H-NHI-NHI} \cdot < \text{H-MMA-PI} \cdot < \text{H-PI-PI} \cdot < \text{H-MMA-NHI} \cdot < \text{H-MMA-MMA} \cdot$. Our calculated value of E_a ($24.01 \text{ kJ mol}^{-1}$) for $\text{H-MMA-MMA} \cdot$ is

comparable with the reported experimental value (using the pulse laser polymerization method) [269], but the frequency factor ($2.07 \times 10^{12} \text{ Lmol}^{-1}\text{s}^{-1}$) is orders of magnitude (10^6) different from the experimentally reported value [66, 268]. Also, for H-PI-PI \cdot dimer radical the calculated E_a and A are very different from the experimentally reported value (determined from homopolymerization of PI) given in the **Table 5.4**. These results indicates that the dimer model used for the present study may not be adequate to describe the mechanism of copolymerization of PI-MMA system.

Table 5.4: Activation energy and frequency factor for studied dimers in gas phase and in anisole.

Dimer radicals	E_a (kJ mol $^{-1}$)		A (Lmol $^{-1}$ s $^{-1}$)	
	Gas	Anisole	Gas	Anisole
H-MMA-MMA \cdot	24.01	24.18	2.07×10^{12}	3.25×10^{12}
	*(22.40) [268]		*(2.67×10^6) [66, 268]	
H-MMA-NHI \cdot	23.53	23.79	7.09×10^{12}	7.76×10^{12}
H-NHI-MMA \cdot	18.55	18.67	1.10×10^{12}	3.38×10^{12}
H-NHI-NHI \cdot	22.60	22.92	5.20×10^{12}	5.87×10^{12}
H-MMA-PI \cdot	22.69	22.89	2.06×10^{12}	8.34×10^{12}
H-PI-MMA \cdot	20.82	20.28	3.25×10^{12}	7.10×10^{12}
H-PI-PI \cdot	23.14	23.26	5.43×10^{11}	8.41×10^{11}
	*(52.20) [156]		*(9.9×10^9) [6]	

**experimentally determined values*

5.4.1.5 Reactivity Ratios of Monomers

The obtained k_p values are used for the calculation of reactivity ratios of the monomers using equation 1.8 (Chapter I, **Section 1.10.1**) and the results are displayed in **Table 5.5**. A quick glance at **Table 5.5** shows that, till 175 °C PI is more reactive as compared to the MMA, at temperature 225 °C both the monomers behaves equally but at higher temperature 275 °C to 375 °C MMA is more reactive than PI monomer. With the rise of 50 °C temperature there is a slight increase in the reactivity ratios. The increase is more in r_M values as compared to the r_I values. On comparing the gas phase values of reactivity ratios with reactivity ratios values in anisole the values are increase but with the only one decimal point (10^1 in magnitude).

Table 5.5: Reactivity ratios of various monomers (r_I and r_M) calculated from the k_p values using the terminal model. The k_p values are calculated at the B3LYP/ 6-31+G(d) level.

Temperature (°C)	From the dimers of NHI and MMA		From the dimers of PI and MMA	
	r_I (NHI)	r_M (MMA)	r_I (PI)	r_M (MMA)
25	0.002	0.048	0.045 *(0.082)	0.009 *(0.009)
75	0.004	0.056	0.054	0.020
80	-	-	0.054 *(0.109)	0.020 *(0.019)
125	0.102	0.061	0.062	0.035
175	0.239	0.075	0.070	0.055
225	0.248	0.088	0.076	0.079
275	0.252	0.101	0.082	0.106
325	0.259	0.113	0.087	0.135
375	0.265	0.125	0.091	0.166

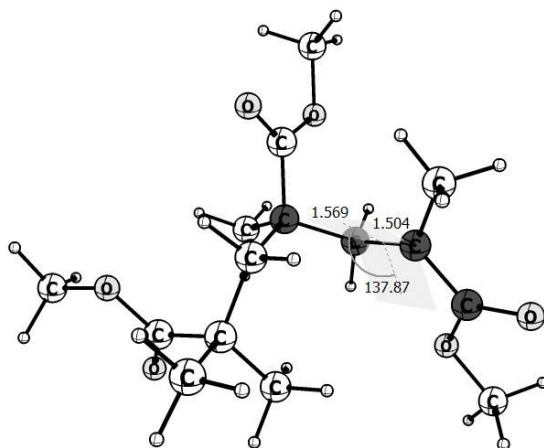
**reactivity ratios in anisole solvent*

5.4.2 Reactivity Ratios of PI and MMA Monomers via Penultimate Model

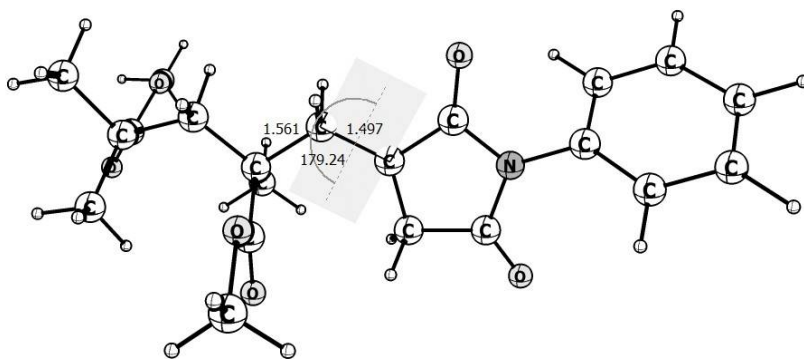
It has been describe in the **Section 5.4.1.4**, the terminal model is inadequate in predicting the kinetic parameters of PI-MMA copolymerization process. This motivates to model the polymeric species as trimer and apply the penultimate model. In the following sections the calculation of k_p for PI-MMA copolymerization using trimer model is discussed. To calculate the reactivity ratios for PI and MMA monomers using penultimate model, the values k_{111} , k_{112} , k_{221} , k_{222} , k_{211} , k_{212} , k_{121} , k_{122} are required according to the equations 1.9-1.16 given in (Chapter I, **Section 1.10.2**), which are calculated as follows.

5.4.2.1 Structure of Transition State for Trimer Formation

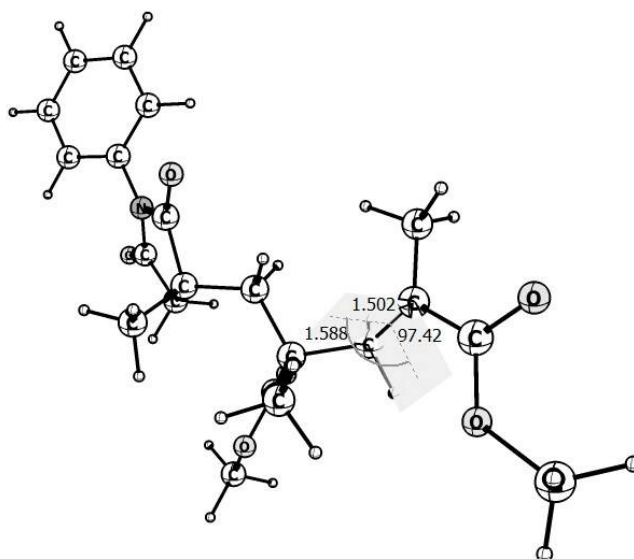
The optimized TS structure for all the trimer radicals were obtained from unrestricted B3LYP/ 6-31+G(d) in gas phase at 25 °C and it is given in the **Figure 5.8**.



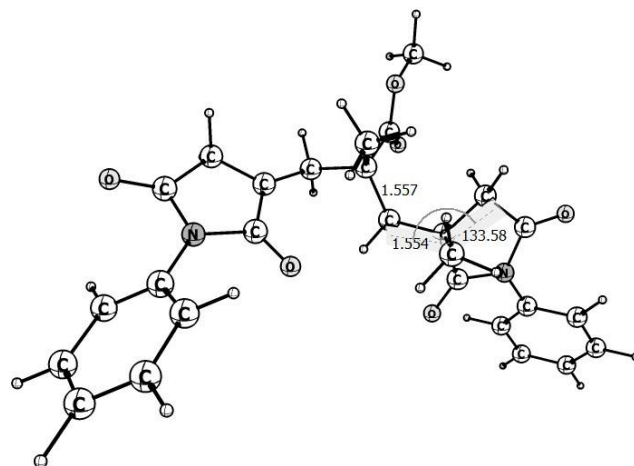
(a) H-MMA-MMA-MMA'



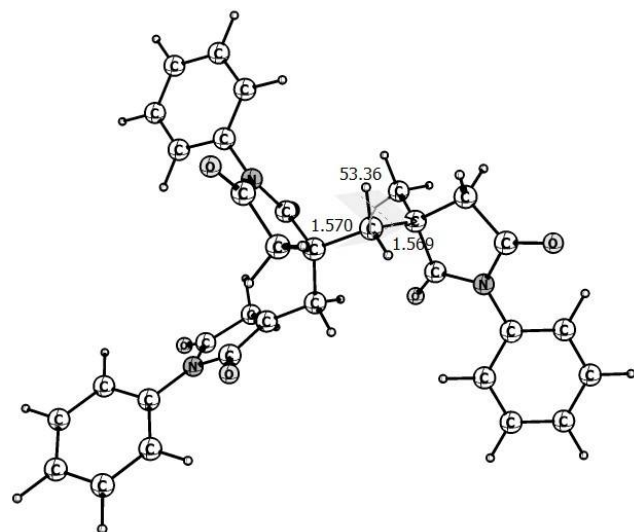
(b) H-MMA-MMA-PI'



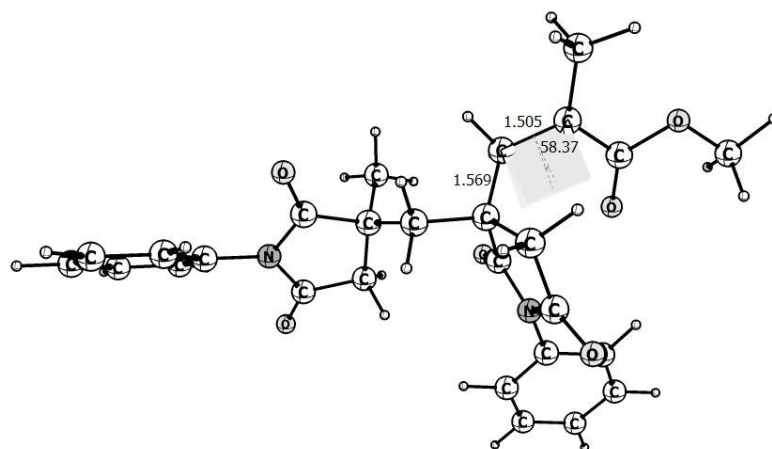
(c) H-PI-MMA-MMA'



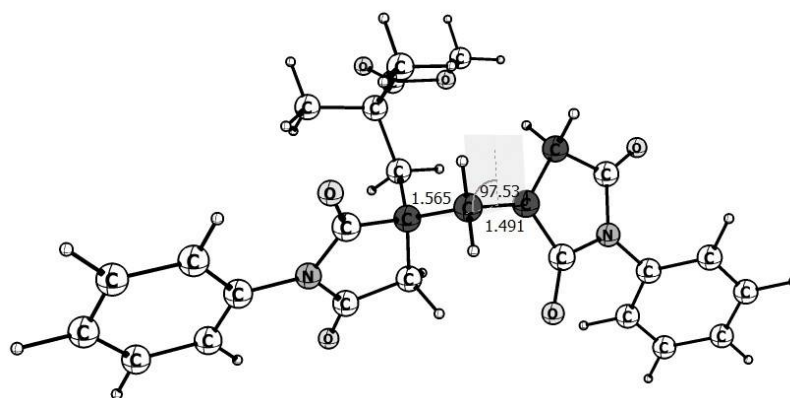
(d) H-PI-MMA-PI⁻



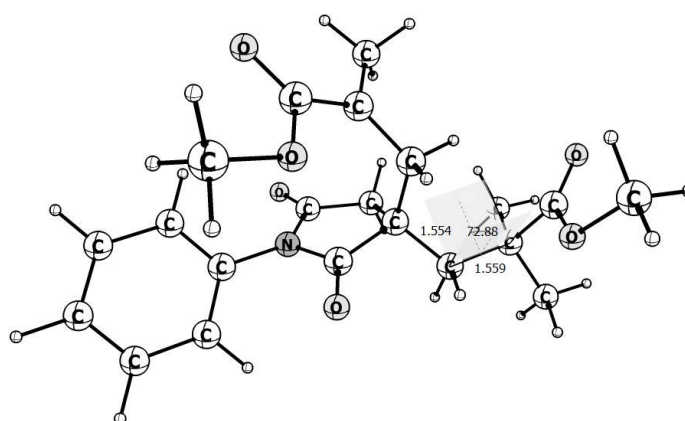
(e) H-PI-PI-PI⁻



(f) H-PI-PI-MMA⁻



(g) H-MMA-PI-PI[·]



(h) H-MMA-PI-MMA[·]

Figure 5.8: B3LYP/ 6-31+G(d) optimized gas-phase geometries of the minimum energy conformations of the transition structures of trimer radicals.

5.4.2.2 Free Energy of Activation, Rate Constant of Propagation and Reactivity Ratios

The free energy of activation (ΔG^\ddagger) and k_p values (calculated using equation 5.1) for all the studied trimer propagating radicals in gas phase at 25 °C is given in **Table 5.6**. The free energy of activation and k_p values of trimer radicals are obtained in the range of 70.48-97.74 kJ mol⁻¹ and 4.71×10^{-4} - 6.14×10^{-1} Lmol⁻¹s⁻¹, respectively. The highest value of free energy of activation for trimer radical is obtained for H-PI-PI-PI[·] and smallest value for H-MMA-PI-MMA[·]. The trend for free energy of activation values of trimer is obtained as, H-PI-PI-PI[·] > H-PI-PI-MMA[·] > H-MMA-MMA-PI[·] > H-MMA-MMA-MMA[·] > H-PI-MMA-PI[·] > H-MMA-PI-PI[·] > H-PI-MMA-MMA > H-MMA-PI-MMA[·]. Similarly, the trend for k_p value of trimer radicals is obtained as, H-PI-PI-PI[·] < H-PI-PI-

MMA \cdot < H-MMA-MMA-PI \cdot < H-MMA-MMA-MMA \cdot < H-PI-MMA-PI \cdot < H-MMA-PI-PI \cdot < H-PI-MMA-MMA < H-MMA-PI-MMA \cdot . The free energy of activation of trimer propagating radicals are about 150-155 kJ mol⁻¹ smaller than those of dimer results. Similarly, the k_p values of trimer radicals are higher as compared to the dimer radicals (with magnitude 10²⁶-10²⁷). The calculated k_p value of H-MMA-MMA-MMA \cdot and H-PI-PI-PI \cdot trimer radicals is close to the experimentally reported k_p value for homopolymerization of MMA and PI, respectively (**Table 5.6**).

Table 5.6: Free energy of activation and rate constant of propagation of trimer radicals in gas phase at 25 °C.

Trimer radicals	ΔG^\ddagger (kJ mol ⁻¹)	k_p (Lmol ⁻¹ s ⁻¹)
H-MMA-MMA-MMA \cdot	83.11	1.23×10 ⁻⁰² *(6.50×10 ²) [66]
H-MMA-MMA-PI \cdot	86.92	5.44×10 ⁻⁰²
H-PI-MMA-MMA \cdot	71.45	2.44×10 ⁻⁰¹
H-PI-MMA-PI \cdot	80.12	1.68×10 ⁻⁰¹
H-PI-PI-PI \cdot	97.74	4.71×10 ⁻⁰⁴ *(1.58×10 ⁻³) [6]
H-PI-PI-MMA \cdot	91.83	5.43×10 ⁻⁰³
H-MMA-PI-PI \cdot	75.51	6.14×10 ⁻⁰¹
H-MMA-PI-MMA \cdot	70.48	1.65×10 ⁻⁰¹

**experimentally reported value*

The reactivity ratios of PI and MMA monomer for penultimate model are calculated putting k_p value of trimer radicals (**Table 5. 6**) in the equation 1.17 (Chapter I, **Section 1.10.2**). The values of reactivity ratios for PI and MMA monomer are obtained as, $r_M = 0.23$, $r'_M = 1.46$, $r_I = 8.68$, $r'_I = 3.72$. The equations of penultimate model (Chapter I, **Section 1.10.2**) includes eight reactions, which can be used to simulate both the penultimate model as well as the terminal model, if the reactivity ratios are calculated as the average values of those for radicals with the same end unit but different penultimate units [267]. The average values of reactivity ratios (from penultimate model) of PI and MMA monomer for terminal model are obtained as, $r_{Mavg} = 0.85$ and $r_{Iavg} = 6.20$.

5.4.2.3 Triad Fractions of PI-MMA Copolymerization

The obtained values of reactivity ratios of PI and MMA monomer are used for the calculations of triad fractions. The triad fractions are calculated for both terminal (equations 5.2 and 5.3) and penultimate model (equations 5.4 and 5.5) using the respective reactivity ratios of PI and MMA monomer. The comparative experimental and theoretical results of triad fractions are given in the **Table 5.7**. The triad fractions are calculated using terminal model in gas phase at 25 °C are similar to the triad fractions calculated in anisole at 80 °C. The obtained results of calculated triad fractions based on the average values of reactivity ratios from penultimate model are also shows variation with the experimentally calculated triad fractions. Hence, from the results of triad fractions analysis we can say that the experimentally determined (using $^{13}\text{C}\{^1\text{H}\}$ -NMR spectroscopy) triad fractions agreed well with the theoretical penultimate model predictions. This shows that the copolymerization of PI and MMA monomer via ATRP proceeds with the penultimate group effect and follows penultimate model.

Table 5.7: The experimentally determined and theoretically calculated triad fractions based on terminal and penultimate model for PI-MMA copolymer system.

Mole fraction of monomer in feed		Triad fractions	Experimental ¹³ C-NMR	Dimers		Trimers	
				Terminal model (gas phase, 25 °C)	Terminal model (anisole, 80 °C)	*Terminal model	Penultimate model (gas phase 25 °C)
PI	MMA						
0.05	0.95	MMI+IMM	0.430	0.023	0.027	0.163	0.433
		IMI	0.008	0.032	0.036	0.042	0.007
		IIM+MII	0.267	0.066	0.068	0.244	0.266
		MIM	0.656	0.025	0.025	0.179	0.658
0.10	0.90	MMI+IMM	0.494	0.096	0.092	0.220	0.494
		IMI	0.019	0.070	0.076	0.106	0.020
		IIM+MII	0.388	0.041	0.044	0.203	0.389
		MIM	0.450	0.022	0.026	0.080	0.452
0.15	0.85	MMI+IMM	0.595	0.043	0.042	0.240	0.595
		IMI	0.037	0.044	0.048	0.160	0.036
		IIM+MII	0.391	0.048	0.041	0.173	0.392
		MIM	0.300	0.082	0.086	0.050	0.299
0.20	0.80	MMI+IMM	0.656	0.025	0.029	0.245	0.656
		IMI	0.057	0.012	0.016	0.327	0.057
		IIM+MII	0.330	0.058	0.060	0.109	0.332
		MIM	0.084	0.069	0.072	0.016	0.085
0.25	0.75	MMI+IMM	0.693	0.061	0.065	0.208	0.693
		IMI	0.080	0.081	0.085	0.498	0.080
		IIM+MII	0.383	0.045	0.043	0.068	0.385
		MIM	0.116	0.051	0.052	0.005	0.117
0.30	0.70	MMI+IMM	0.713	0.054	0.058	0.230	0.713
		IMI	0.105	0.040	0.046	0.409	0.105
		IIM+MII	0.330	0.016	0.018	0.088	0.314
		MIM	0.084	0.000	0.004	0.009	0.097
0.35	0.65	MMI+IMM	0.720	0.031	0.035	0.236	0.720
		IMI	0.134	0.005	0.009	0.385	0.133
		IIM+MII	0.273	0.097	0.099	0.094	0.277
		MIM	0.065	0.073	0.077	0.011	0.069
0.40	0.60	MMI+IMM	0.718	0.016	0.016	0.161	0.718
		IMI	0.165	0.068	0.069	0.638	0.164
		IIM+MII	0.239	0.077	0.079	0.044	0.243
		MIM	0.070	0.053	0.057	0.002	0.068
0.45	0.55	MMI+IMM	0.117	0.027	0.028	0.182	0.118
		IMI	0.146	0.086	0.085	0.783	0.149
		IIM+MII	0.182	0.052	0.055	0.056	0.180
		MIM	0.227	0.035	0.037	0.005	0.300

*the reactivity ratios were used as the average values of (r_M and r'_M) as well as (r_I and r'_I).

5.4.3 Effect of Neighboring and Penultimate Unit on Structural and Thermodynamic Parameters

In addition to the above obtained results we have further studied the effect of terminal and penultimate unit on the thermodynamic parameters participating in the atom transfer radical copolymerization of PI and MMA monomer. To perform this study the dimers and trimers of the chosen monomers are considered which is given in the **Figure 5.5**.

5.4.3.1 Structural Features of Dimers and Trimers

The geometries of the dimers and trimers are fully optimized using the B3LYP/ 6-31+G(d)/ LanL2DZ method. The representative optimized geometry of dimer (H-PI-MMA-Br) and trimer (H-PI-PI-MMA-Br) along with its radical is shown in **Figure 5.9** and **Figure 5.10**, respectively. Similarly, the optimized geometry of all studied dimers (H-M₂-M₁-Br) and trimers (H-M₃-M₂-M₁-Br) with their possible radicals (H-M₂-M₁[·] and H-M₃-M₂-M₁[·]) is given in (**Appendix v, Table A3 and Table A4**, respectively).

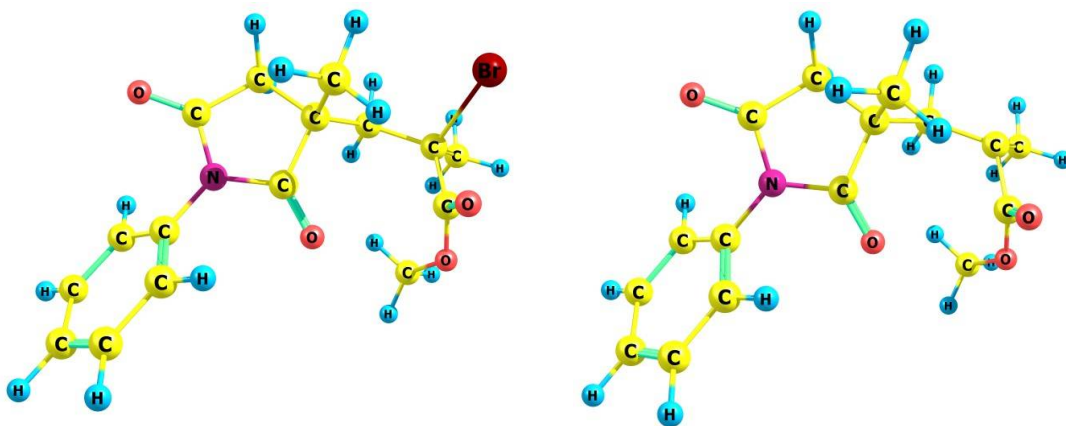


Figure 5.9: B3LYP/ 6-31+G(d) optimized geometry of H-PI-MMA-Br and H-PI-MMA[·].

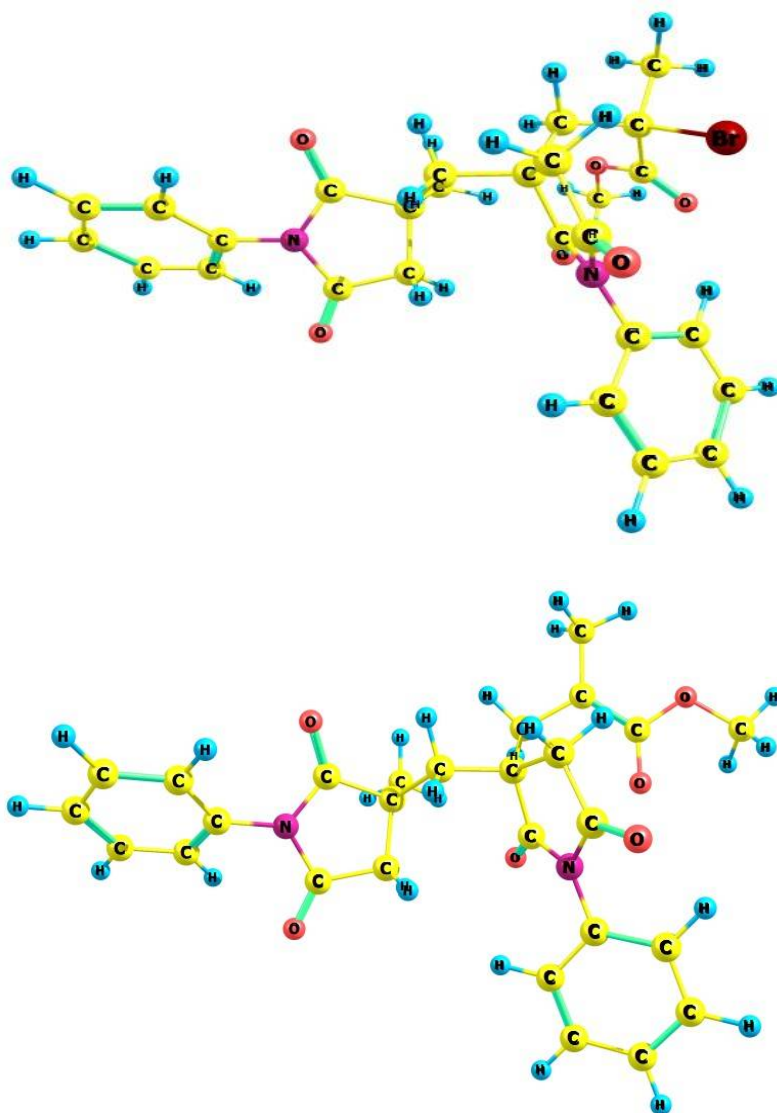


Figure 5.10: B3LYP/ 6-31+G(d) optimized geometry of H-PI-PI-MMA-Br and H-PI-PI-MMA:

The C–X bond lengths (r_{C-X}) for the studied dimers in gas phase at 25 °C are given in **Table 5.8**. They are between the ranges 1.835 Å to 1.860 Å for X = Cl, 2.004 Å to 2.027 Å. A quick glance at **Table 5.8**, shows the C–X bond length of dimers with X = Cl is smaller as compared to the dimers with X = Br which is again smaller as compared to the dimers with X = I. The C–Br bond lengths for the studied trimers are given in **Table 5.9**. They are between the range of 1.986 Å to 2.033 Å.

Table 5.8: Thermodynamic parameters for the homolysis of the M_1 -X bond in $H-M_2-M_1-X$ ($M_1, M_2 = \text{MMA, NHI, and PI}$; and $H-M_1-X$, ($X = \text{Cl, Br, I}$) in gas phase at 25 °C.

R		X	r_{C-X} (Å)	ΔH (kJ mol ⁻¹)	ΔG (kJ mol ⁻¹)	K_{ATRP}	* K/K_0
M_2	M_1						
	MMA	Cl	1.855	257.07	209.90	1.50×10^{-06}	$1.00 \times 10^{+00}$
MMA	MMA	Cl	1.860	234.07	190.26	4.14×10^{-03}	$2.76 \times 10^{+03}$
NHI	MMA	Cl	1.848	167.12	120.84	$6.01 \times 10^{+09}$	$4.01 \times 10^{+10}$
PI	MMA	Cl	1.844	185.64	137.54	$7.12 \times 10^{+06}$	$4.75 \times 10^{+10}$
	NHI	Cl	1.840	250.80	208.42	2.73×10^{-06}	$1.00 \times 10^{+00}$
MMA	NHI	Cl	1.842	213.17	169.04	$2.16 \times 10^{+01}$	$7.91 \times 10^{+06}$
NHI	NHI	Cl	1.835	246.16	201.82	3.90×10^{-05}	$1.43 \times 10^{+01}$
PI	NHI	Cl	1.836	206.02	161.06	$5.39 \times 10^{+02}$	$1.97 \times 10^{+08}$
	PI	Cl	1.844	250.70	208.66	2.47×10^{-06}	$1.00 \times 10^{+00}$
MMA	PI	Cl	1.850	237.50	188.69	7.79×10^{-03}	$3.15 \times 10^{+03}$
NHI	PI	Cl	1.839	205.91	161.90	$3.85 \times 10^{+02}$	$1.56 \times 10^{+08}$
PI	PI	Cl	1.842	234.53	186.49	1.89×10^{-02}	$7.65 \times 10^{+03}$
	MMA	Br	2.017	247.87	200.87	3.93×10^{-09}	$1.00 \times 10^{+00}$
MMA	MMA	Br	2.027	232.17	186.50	1.29×10^{-06}	$3.28 \times 10^{+02}$
NHI	MMA	Br	2.009	162.15	115.81	$3.13 \times 10^{+06}$	$7.96 \times 10^{+10}$
PI	MMA	Br	2.010	181.73	134.81	$1.47 \times 10^{+03}$	$3.74 \times 10^{+11}$
	NHI	Br	2.007	241.53	198.29	1.11×10^{-08}	$1.00 \times 10^{+00}$
MMA	NHI	Br	2.007	211.85	167.27	3.02×10^{-03}	$2.72 \times 10^{+05}$
NHI	NHI	Br	2.011	245.57	211.39	5.03×10^{-09}	4.53×10^{-01}
PI	NHI	Br	2.005	208.00	161.23	3.46×10^{-02}	$3.12 \times 10^{+06}$
	PI	Br	2.008	247.88	205.12	7.06×10^{-10}	$1.00 \times 10^{+00}$
MMA	PI	Br	2.016	234.99	185.43	1.99×10^{-06}	$2.82 \times 10^{+03}$
NHI	PI	Br	2.004	213.82	168.63	1.75×10^{-03}	$2.48 \times 10^{+06}$
PI	PI	Br	2.008	231.31	184.40	3.02×10^{-06}	$4.28 \times 10^{+03}$
	MMA	I	2.278	115.16	69.30	7.59×10^{-05}	$1.00 \times 10^{+00}$
MMA	MMA	I	2.296	86.80	41.24	$6.25 \times 10^{+00}$	$8.23 \times 10^{+04}$
NHI	MMA	I	2.258	82.75	33.18	$1.61 \times 10^{+02}$	$2.12 \times 10^{+06}$
PI	MMA	I	2.282	47.48	07.72	$3.50 \times 10^{+07}$	$4.61 \times 10^{+10}$
	NHI	I	2.259	110.83	69.42	7.23×10^{-05}	$1.00 \times 10^{+00}$
MMA	NHI	I	2.277	143.65	101.05	2.07×10^{-10}	2.86×10^{-06}
NHI	NHI	I	2.273	88.65	48.92	2.82×10^{-01}	$3.90 \times 10^{+03}$
PI	NHI	I	2.261	53.74	11.00	$1.24 \times 10^{+06}$	$1.72 \times 10^{+10}$
	PI	I	2.262	110.61	68.86	9.05×10^{-05}	$1.00 \times 10^{+00}$
MMA	PI	I	2.277	82.87	41.89	$4.80 \times 10^{+00}$	$5.30 \times 10^{+04}$
NHI	PI	I	2.264	54.69	10.65	$1.43 \times 10^{+06}$	$1.58 \times 10^{+10}$
PI	PI	I	2.264	53.71	09.76	$2.04 \times 10^{+06}$	$2.25 \times 10^{+10}$

*here, $K = K_{ATRP}$ of dimers ($H-M_2-M_1-X$) and $K_0 = K_{ATRP}$ of unimers ($H-M_1-X$)
for X = Br and 2.258 Å to 2.296 Å for X = I.

Table 5.9: Thermodynamic parameters for the homolysis of the M₁-Br bond in H-M₃-M₂-M₁-Br (M₁, M₂, M₃ = MMA, NHI, and PI) in gas phase at 25 °C.

R			X	r_{C-X} (Å)	ΔH (kJ mol ⁻¹)	ΔG (kJ mol ⁻¹)	K_{ATRP}	$*K/K_0$
M ₃	M ₂	M ₁						
MMA	MMA	MMA	Br	2.028	242.87	198.64	9.65×10 ⁻⁰⁹	7.45×10 ⁻⁰³
NHI	MMA	MMA	Br	2.026	232.90	186.25	1.43×10 ⁻⁰⁶	1.11×10 ⁺⁰⁰
PI	MMA	MMA	Br	2.033	167.66	121.81	2.79×10 ⁺⁰⁵	2.19×10 ⁺¹¹
MMA	NHI	MMA	Br	2.029	242.13	193.75	6.93×10 ⁻⁰⁸	2.18×10 ⁻¹⁴
NHI	NHI	MMA	Br	1.989	240.66	196.44	2.34×10 ⁻⁰⁸	7.35×10 ⁻¹⁵
MMA	PI	MMA	Br	2.022	170.57	128.09	2.21×10 ⁺⁰⁴	1.51×10 ⁺⁰¹
PI	PI	MMA	Br	1.997	185.43	136.78	6.63×10 ⁺⁰²	4.52×10 ⁻⁰¹
MMA	MMA	NHI	Br	2.003	240.23	194.21	5.75×10 ⁻⁰⁸	1.90×10 ⁻⁰⁵
NHI	MMA	NHI	Br	1.986	239.23	195.65	3.23×10 ⁻⁰⁸	1.06×10 ⁻⁰⁵
PI	MMA	NHI	Br	2.024	209.23	162.32	3.46×10 ⁻⁰²	7.37×10 ⁺⁰⁰
MMA	NHI	NHI	Br	2.011	235.66	184.11	3.38×10 ⁻⁰⁶	6.05×10 ⁺⁰⁴
NHI	NHI	NHI	Br	2.013	242.98	197.97	1.26×10 ⁻⁰⁸	2.25×10 ⁺⁰²
MMA	PI	NHI	Br	2.009	213.33	167.74	2.50×10 ⁻⁰³	7.23×10 ⁻⁰²
PI	PI	NHI	Br	2.004	213.82	168.63	1.75×10 ⁻⁰³	5.04×10 ⁻⁰²
MMA	MMA	PI	Br	2.017	172.32	127.01	3.41×10 ⁺⁰⁴	1.74×10 ⁺¹⁰
NHI	MMA	PI	Br	2.019	215.01	167.98	2.36×10 ⁻⁰³	1.14×10 ⁺⁰³
PI	MMA	PI	Br	1.996	175.26	129.78	1.11×10 ⁺⁰⁴	5.69×10 ⁺⁰⁹
MMA	NHI	PI	Br	2.008	231.31	185.50	3.02×10 ⁻⁰⁶	1.10×10 ⁻⁰³
NHI	NHI	PI	Br	2.013	249.01	211.39	5.65×10 ⁻⁰⁵	3.20×10 ⁻⁰⁸
MMA	PI	PI	Br	2.017	169.03	123.45	1.44×10 ⁺⁰⁵	4.83×10 ⁺¹⁰
PI	PI	PI	Br	2.027	176.62	134.23	1.86×10 ⁺⁰³	6.23×10 ⁻⁰⁸

*here, $K = K_{ATRP}$ of trimer bromide (H-M₃-M₂-M₁-Br) and $K_0 = K_{ATRP}$ of dimer bromide (H-M₂-M₁-Br).

The C–X bond lengths of all the dimers in anisole at 25 °C are given in (**Appendix v, Table A5**). The C–X bond lengths systematically increases for all the studied dimers with increasing polarity of the medium and follow the trends anisole > gas phase, but with increase in temperature from 25 °C to 80 °C (**Appendix v, Table A6**) the bond lengths do not vary much and remain more or less constant. The dihedral angle of all the dimers and trimers for the C–X bond with respect to the ring (or with respect to C(O)OCH₃) are between 52°–98° and 51°–100°, respectively. The carbon atom bearing the unpaired electron for all the radicals are found to be planar in the sense that the sum of the three bond angles at this carbon are found to be 360° in all cases. The spin densities at this carbon vary from 0.86 to 0.98 in all dimer and trimer radicals.

The C–X bond length of dimers (H-M₂-M₁-X) with respect to their unimers (H-M₁-X) are compared and the effect of neighboring group (M₂) on C–X bond length in gas phase at 25 °C is shown in the **Figure 5.11**. The C–X bond length of dimers varies

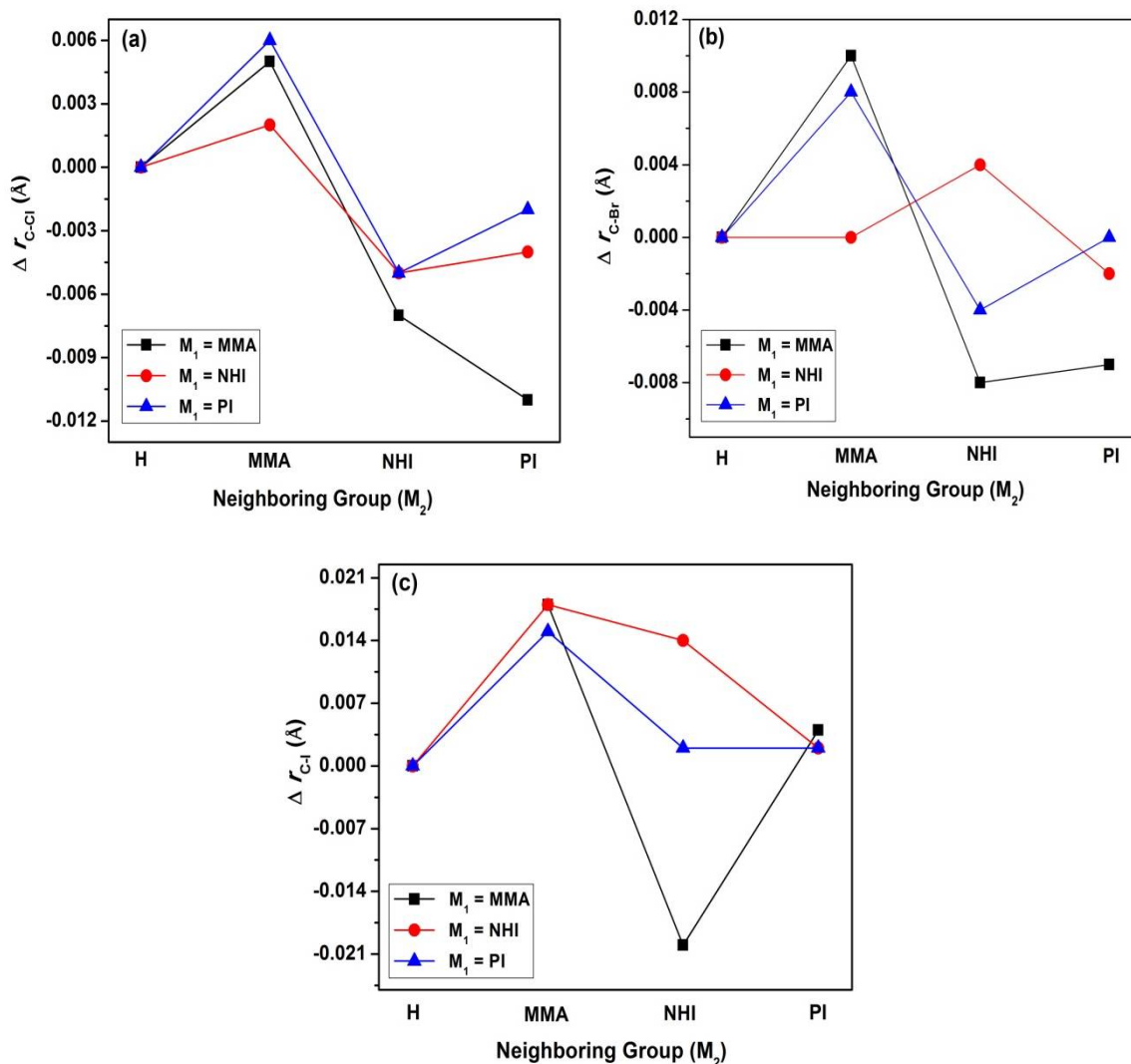


Figure 5.11: Effect of the neighboring group (M₂) on the C–X bond length (Å) of dimers (H-M₂-M₁-X) in gas phase at 25 °C (a) X = Cl, (b) X = Br and (c) X = I (here, $\Delta r_{C-X} = r_{C-X}$ of H-M₂-M₁-X – r_{C-X} of H-M₁-X).

(either increase or decrease) about 0.012 Å for X = Cl, 0.01 Å for X = Br, and 0.021 Å for X = I, as compared to the corresponding unimers. A positive deviation (an increase in C–X bond length comparing to the unimers) is obtained, when the neighbor group (M₂) = MMA for all the dimer halides. Similarly, a negative deviation (in C–X bond length comparing to the unimers) is observed for M₂ = NHI and PI for chlorides and bromides

(except for H-NHI-MMA-Br). However, for the iodides, a positive deviations are observed for H-NHI-NHI-I and H-NHI-PI-I and H-PI-MMA-I, whereas negative deviations are observed for H-NHI-MMA-I.

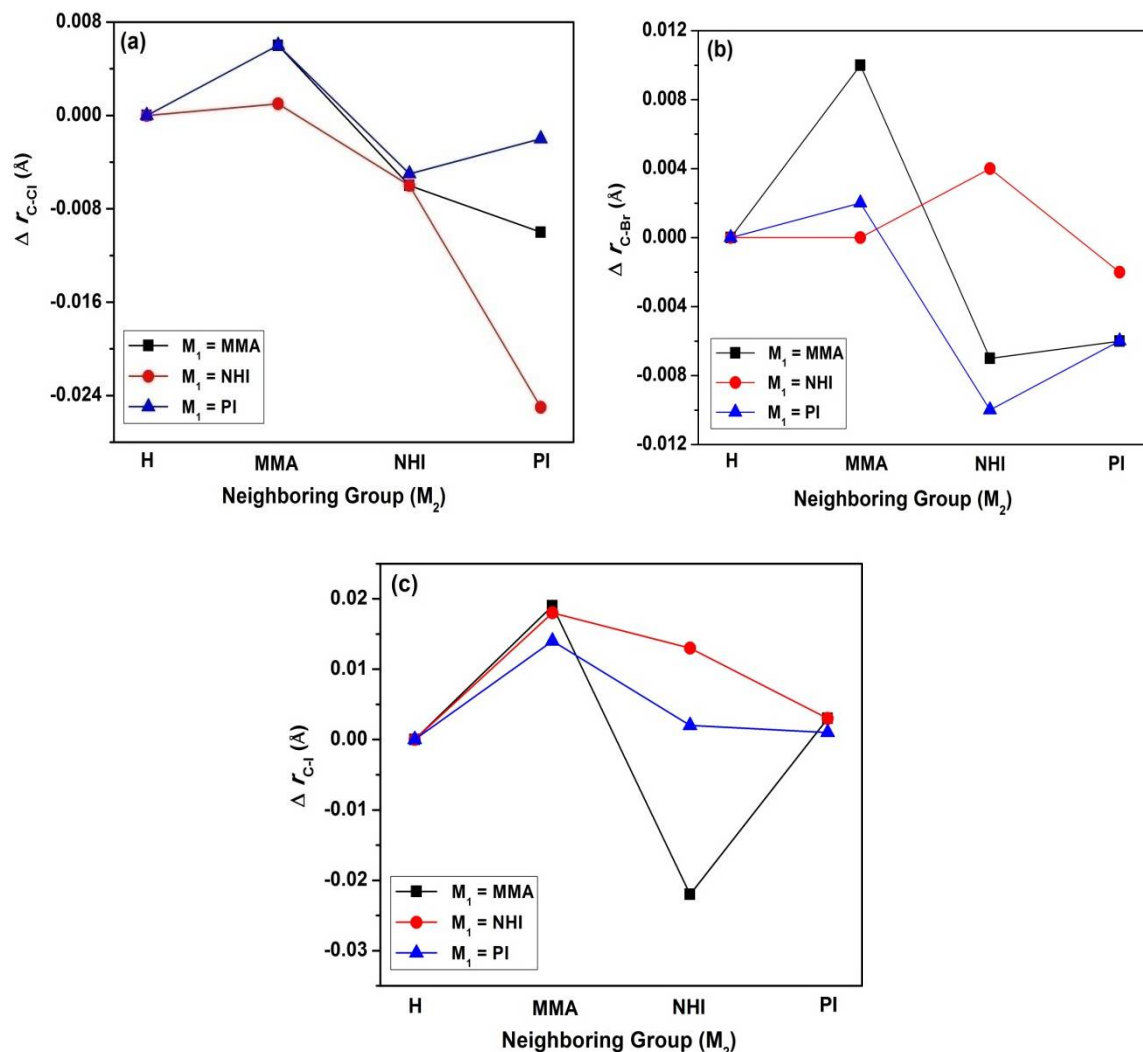


Figure 5.12: Effect of the neighboring group (M_2) on the C-X bond length (\AA) of dimers ($\text{H-M}_2\text{-M}_1\text{-X}$) in gas phase at $80\text{ }^\circ\text{C}$ (a) $\text{X} = \text{Cl}$, (b) $\text{X} = \text{Br}$ and (c) $\text{X} = \text{I}$ (here, $\Delta r_{\text{C-X}} = r_{\text{C-X}}$ of $\text{H-M}_2\text{-M}_1\text{-X} - r_{\text{C-X}}$ of $\text{H-M}_1\text{-X}$).

The variation of C-X bond lengths of dimers from the corresponding unimers at an elevated temperature (gas phase, $80\text{ }^\circ\text{C}$) and in presence of solvent (in anisole at $25\text{ }^\circ\text{C}$) are displayed in **Figure 5.12** and **Figure 5.13**, respectively. In both these cases, the trends are very similar to those of gas phase ($25\text{ }^\circ\text{C}$), though, the magnitude of variations

(from unimers) are higher (≈ 0.025 for $X = \text{Cl}$, ≈ 0.015 for $X = \text{Br}$, and ≈ 0.021 for $X = \text{I}$) as compared to the dimers.

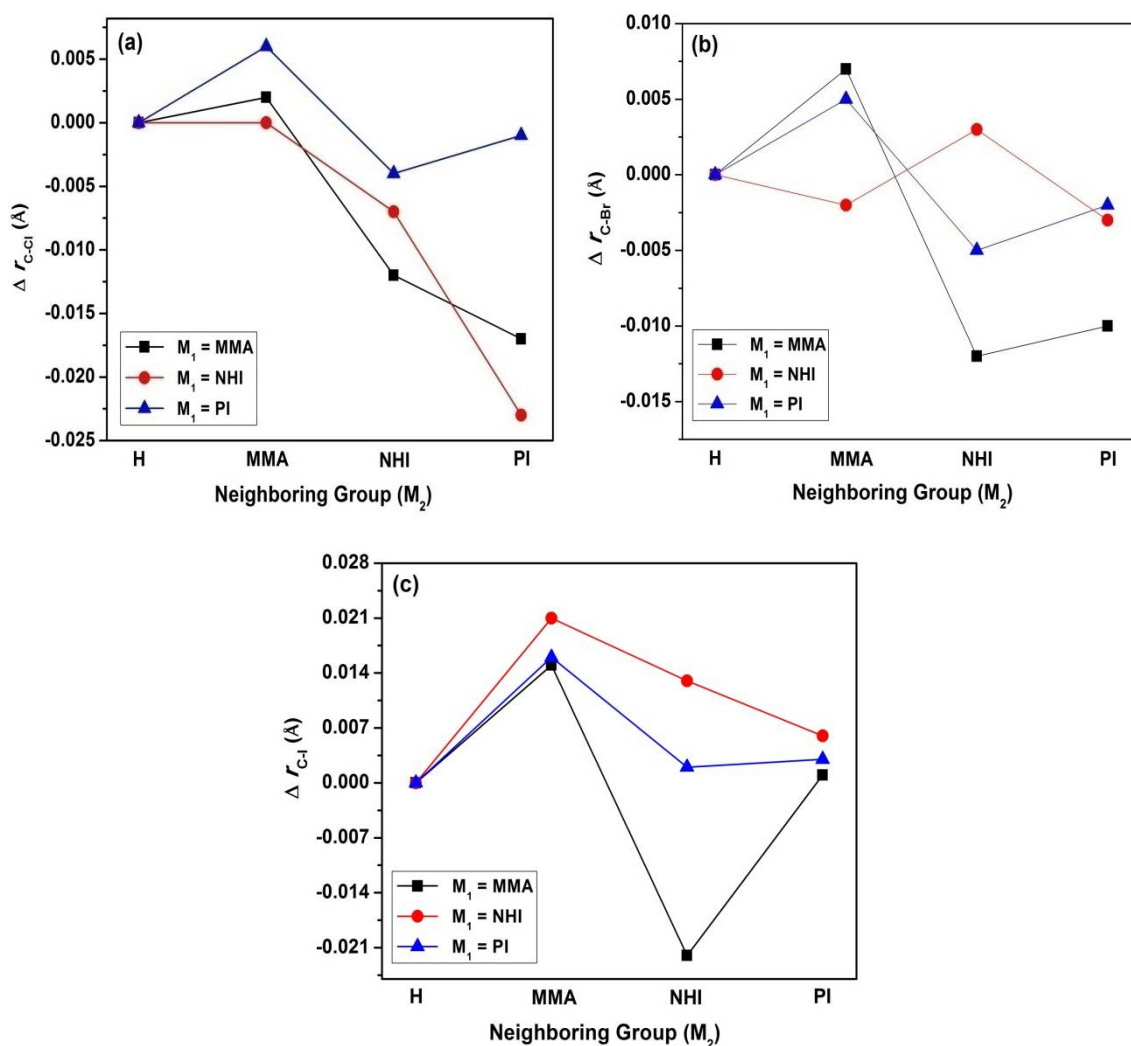


Figure 5.13: Effect of the neighboring group (M_2) on the C-X bond length (Å) of dimers ($\text{H-M}_2\text{-M}_1\text{-X}$) in anisole at 25 °C (a) $X = \text{Cl}$, (b) $X = \text{Br}$ and (c) $X = \text{I}$ (here, $\Delta r_{\text{C-X}} = r_{\text{C-X}}$ of $\text{H-M}_2\text{-M}_1\text{-X} - r_{\text{C-X}}$ of $\text{H-M}_1\text{-X}$).

The C-Br bond lengths of the trimer bromides are presented in the **Table 5.9**. A quick comparison C-Br bond lengths of the trimer bromides with the corresponding (C-Br bond lengths of) unimers indicates an increase or decrease in the values. For example, we compare the C-Br bond length of H-MMA-Br (2.017 Å) with respective to the trimers, H-MMA-MMAMMA-Br (2.028 Å), H-NHI-MMA-MMA-Br (2.026 Å), H-NHI-NHI-MMA-Br (1.989 Å), and H-NHI-Br (2.007 Å) with H-MMA-MMA-NHI-Br

(2.003 Å), H-NHI-MMA-NHI-Br (1.986 Å), H-MMA-NHI-NHI-Br (2.011 Å), H-NHI-NHI-NHI-Br (2.011 Å). The C-Br bond length in H-PI-Br is 2.008 Å and in the corresponding trimers, H-MMA-MMA-PI-Br, H-NHI-MMA-PI-Br, H-MMA-NHI-PI-Br, H-NHI-NHI-PI-Br, H-PI-MMA-PI-Br, H-MMA-PI-PI-Br and H-PI-PI-PI-Br, the C-Br bond lengths are found to be 2.017 Å, 2.019 Å, 2.008 Å, 2.013, 1.996 Å, 2.017 Å, and 2.027 Å, respectively.

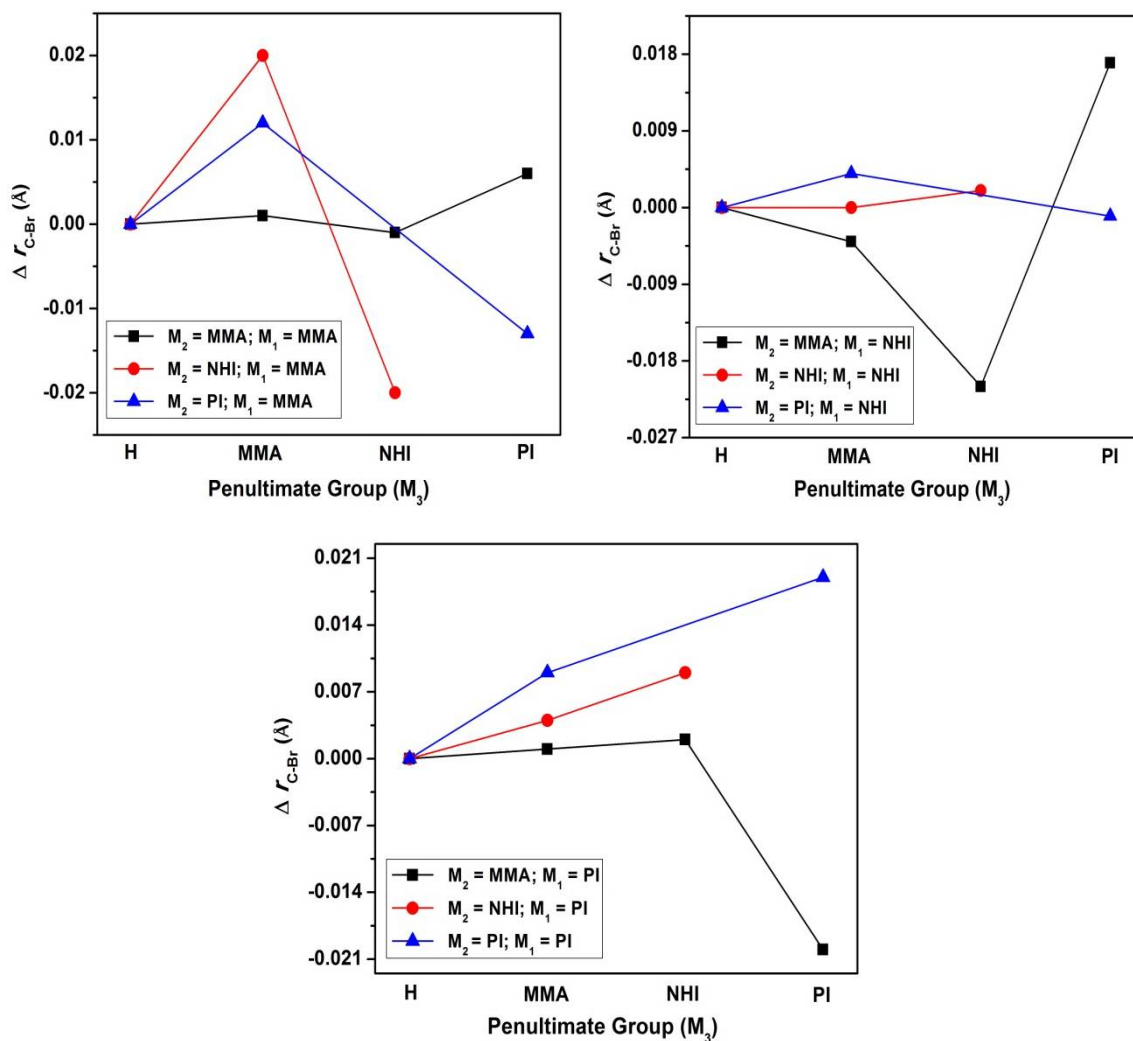


Figure 5.14: Effect of the penultimate group (M_3) on the C-Br bond length (Å) of trimers (H- M_3 - M_2 - M_1 -Br) in gas phase at 25 °C (here, $\Delta r_{C-X} = r_{C-X}$ of H- M_3 - M_2 - M_1 -Br – r_{C-X} of H- M_2 - M_1 -Br).

A comparison of C-Br bond length of trimer bromides (H-M₃-M₂-M₁-Br) with their respective dimer bromides (H-M₂-M₁-Br) (i.e. the effect of penultimate group M₃ on C-Br bond length) is shown in the **Figure 5.14**. The C-Br bond length of all the studied trimers (where MMA as penultimate group) are larger than those of the corresponding dimers (except for H-MMA-MMA-NHI-Br). However, a mixed trends are found for the trimers with penultimate group (M₃) NHI or PI. A longer C-Br bond length (as compared to the corresponding dimers) is found for trimers with M₃ = NHI and M₁ = PI, (for example H-NHI-MMA-PI-Br and H-NHI-NHI-PI-Br). Whereas, a reduction in C-Br bond lengths is found for the rest of the trimer bromides.

5.4.3.2 Homolytic Bond Dissociation Enthalpies and Free Energies of Dimers and Trimers

The homolytic C-X bond dissociation enthalpy (BDE) data for the studied dimers in gas phase at 25 °C is given in **Table 5.8**. They are in the range of 167.12 kJ mol⁻¹ to 250.80 kJ mol⁻¹ for X = Cl, 162.15 kJ mol⁻¹ to 247.88 kJ mol⁻¹ for X = Br and 53.74 kJ mol⁻¹ to 143.65 kJ mol⁻¹ for X = I. Moving from gas phase to anisole at 25 °C (**Appendix v, Table A5**), the BDEs of the dimers are observed in the range of 172.29 kJ mol⁻¹ to 247.48 kJ mol⁻¹ for X = Cl, 166.22 kJ mol⁻¹ to 243.71 kJ mol⁻¹ for X = Br and 53.92 kJ mol⁻¹ to 146.74 kJ mol⁻¹ for X = I. The BDEs of dimers remains unchanged when the temperature is increased to 80 °C (**Appendix v, Table A6**). The chloride unimers (H-M₁-X) are found to have higher BDEs than the corresponding bromides, which are in turn greater than their iodide counterparts. This variation is parallel to the decreasing ionic character of halides, Cl > Br > I. However, this trend is not same in dimers, for example, H-PI-NHI-Br and H-NHI-PI-Br show increase in BDEs as compared to its chloride counterpart in gas phase as well in anisole. All the studied dimers with X = I have smaller BDEs as compared to their chloride and bromide counterparts. For a given dimer, the decrease in BDEs are about 1-10 kJ mol⁻¹ from X = Cl to X = Br and about 70-155 kJ mol⁻¹ from X = Br to X = I. In most of the cases BDEs decrease while the corresponding R-X bond distances increase (**Table 5.8**) as we go from X = Cl to X = I. The BDEs correlates well with the R-X bond lengths. Although, the BDEs of unimers (H-M₁-X) increases in gas phase as compared to anisole, the dimers H-MMA-MMA-X and H-NHI-NHI-X (X = Cl, Br & I), show a decrease and rest all dimers show an increase in the BDEs. This increase or decrease in BDEs of dimers are about 2-12 kJ

mol⁻¹. As we increase temperature from 25 °C to 80 °C, the BDEs of dimers remains more or less constant. The obtained BDEs of H-PI-PI-X is smaller as compared to H-NHI-NHI-X (X = Cl, Br, & I). This could be due to the presence of two bulky phenyl group in the H-PI-PI-X dimer.

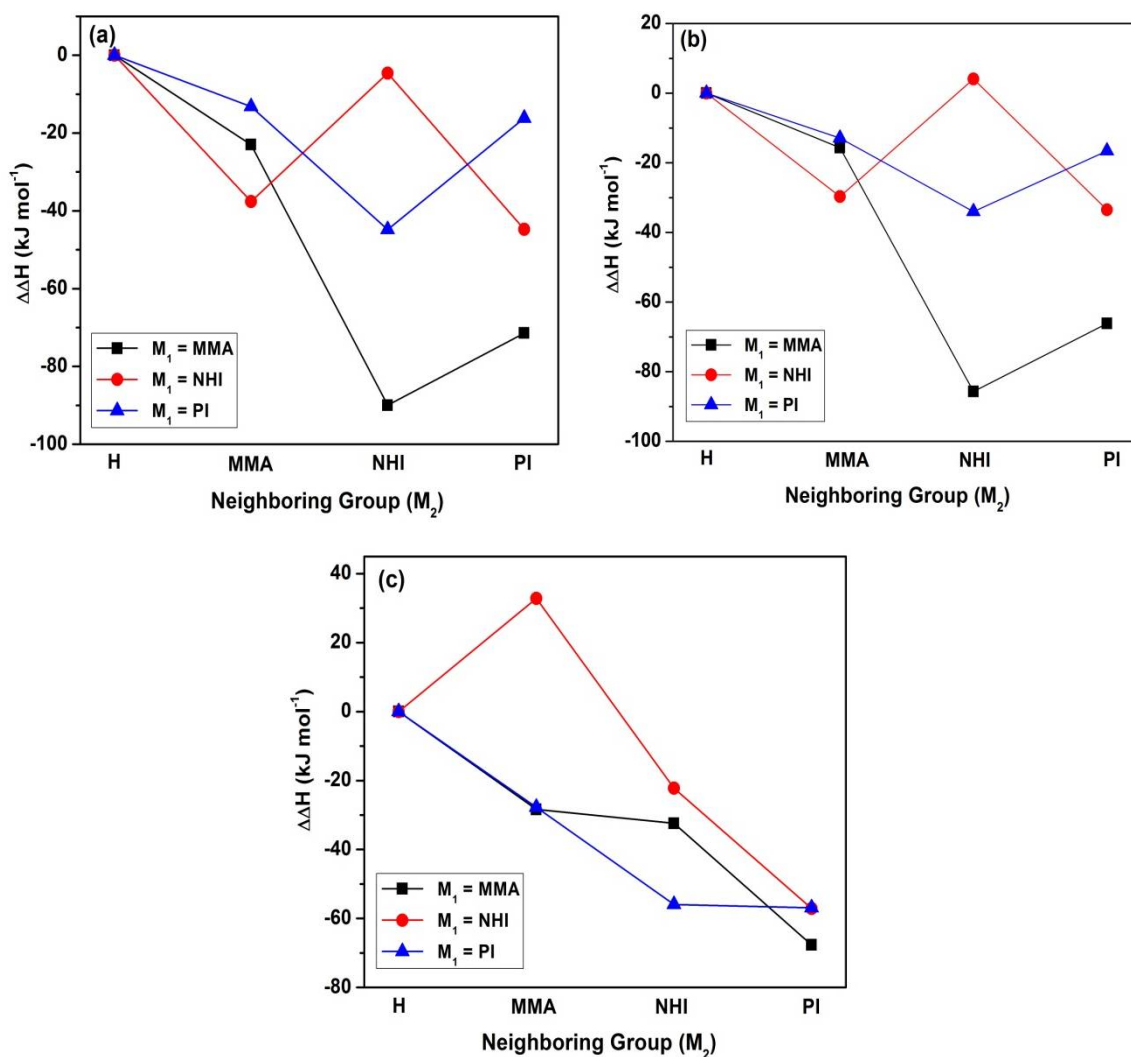


Figure 5.15: Effect of the neighboring group (M_2) on the homolytic C-X bond dissociation enthalpy (ΔH) of dimers ($H-M_2-M_1-X$) in gas phase at 25 °C (a) X = Cl, (b) X = Br and (c) X = I (here, $\Delta\Delta H = \Delta H$ of $H-M_2-M_1-X - \Delta H$ of $H-M_1-X$).

To study the effect of neighboring group (M_2) on the C-X bond dissociation enthalpy, we replace the H of the unimers ($H-M_1-X$) with a neighbor group M_2 forming the dimers. The results are displayed in **Figure 5.15** to **Figure 5.17**. In gas phase at 25 °C (**Figure 5.15**), the values of BDEs of dimers corresponding to H-MMA-Cl unimers decrease in

the range of 23-90 kJ mol⁻¹. The obtained trend for BDEs of dimers is, H-NHI-MMA-Cl < H-PI-MMA-Cl < H-MMA-MMA-Cl. Similarly, if we compare the BDEs of H-NHI-Cl with their corresponding dimers, H-MMA-NHI-Cl, H-NHI-NHI-Cl and H-PI-NHI-Cl, a decrease in BDEs is observed in the range of 4-44 kJ mol⁻¹.

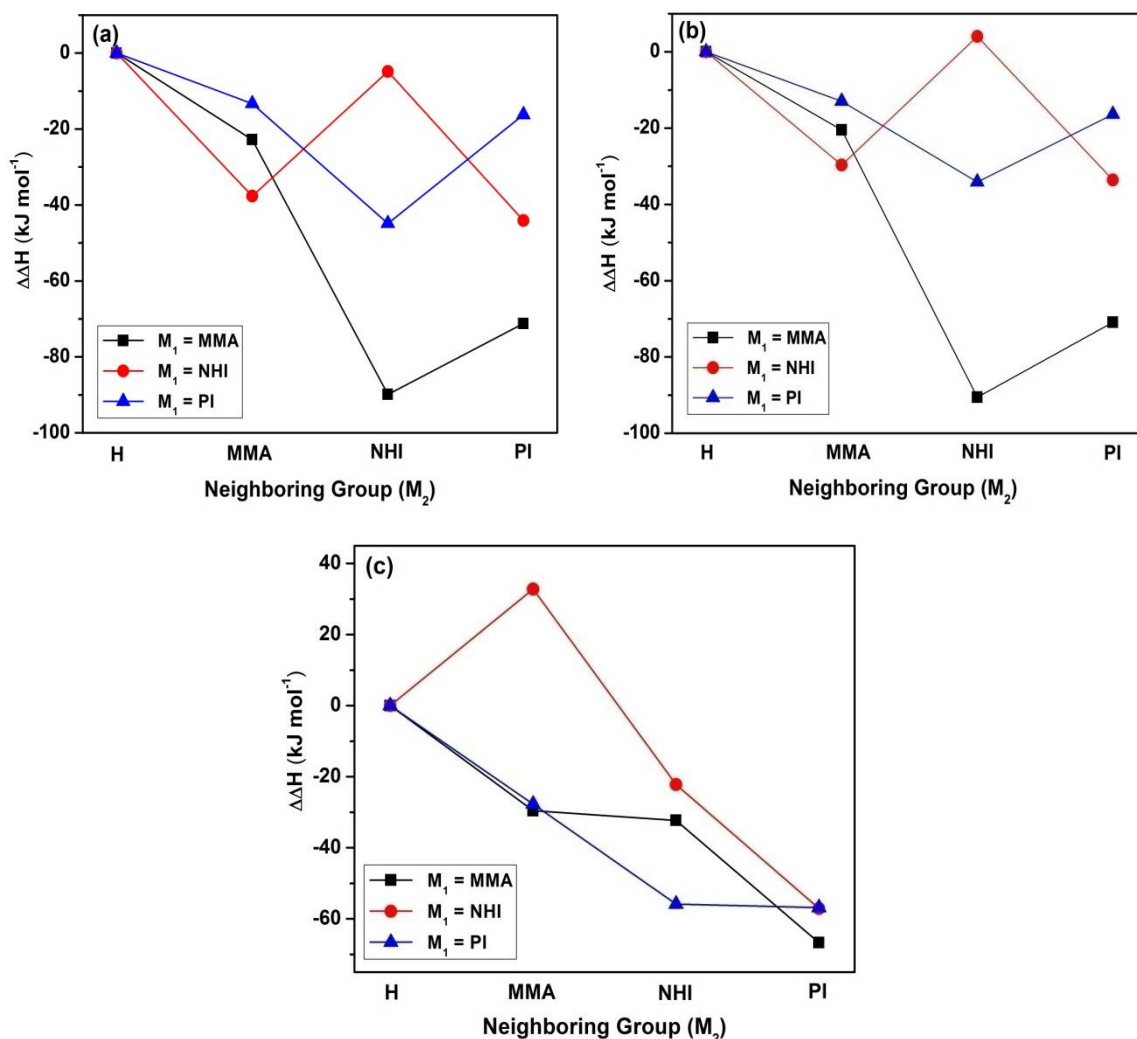


Figure 5.16: Effect of the neighboring group (M_2) on the homolytic C-X bond dissociation enthalpy (ΔH) of dimers ($H-M_2-M_1-X$) in gas phase at 80 °C (a) $X = \text{Cl}$, (b) $X = \text{Br}$ and (c) $X = \text{I}$ (here, $\Delta\Delta H = \Delta H$ of $H-M_2-M_1-X - \Delta H$ of $H-M_1-X$).

The observed trend for BDEs of the said dimers is, H-PI-NHI-Cl < H-MMA-NHI-Cl < H-NHI-NHI-Cl. Similarly, in the comparison of BDE of H-PI-Cl, with corresponding dimers H-MMA-PI-Cl, H-NHI-PI-Cl and H-PI-PI-Cl, the BDEs are decreasing in the range of 13-45 kJ mol⁻¹. The observed trend is, H-NHI-PI-Cl < H-PI-PI-Cl < H-MMA-

PI-Cl. Similar results is observed for the dimers where X = Br. If we compare the BDE of H-MMA-I and their corresponding dimers such as, H-MMA-MMA-I, H-NHI-MMA-I and H-PI-MMA-I, a decrease in the BDEs of dimers is observed. For the H-NHI-I and their corresponding dimers H-NHI-NHI-I, H-PI-NHI-I, shows the decrease but the

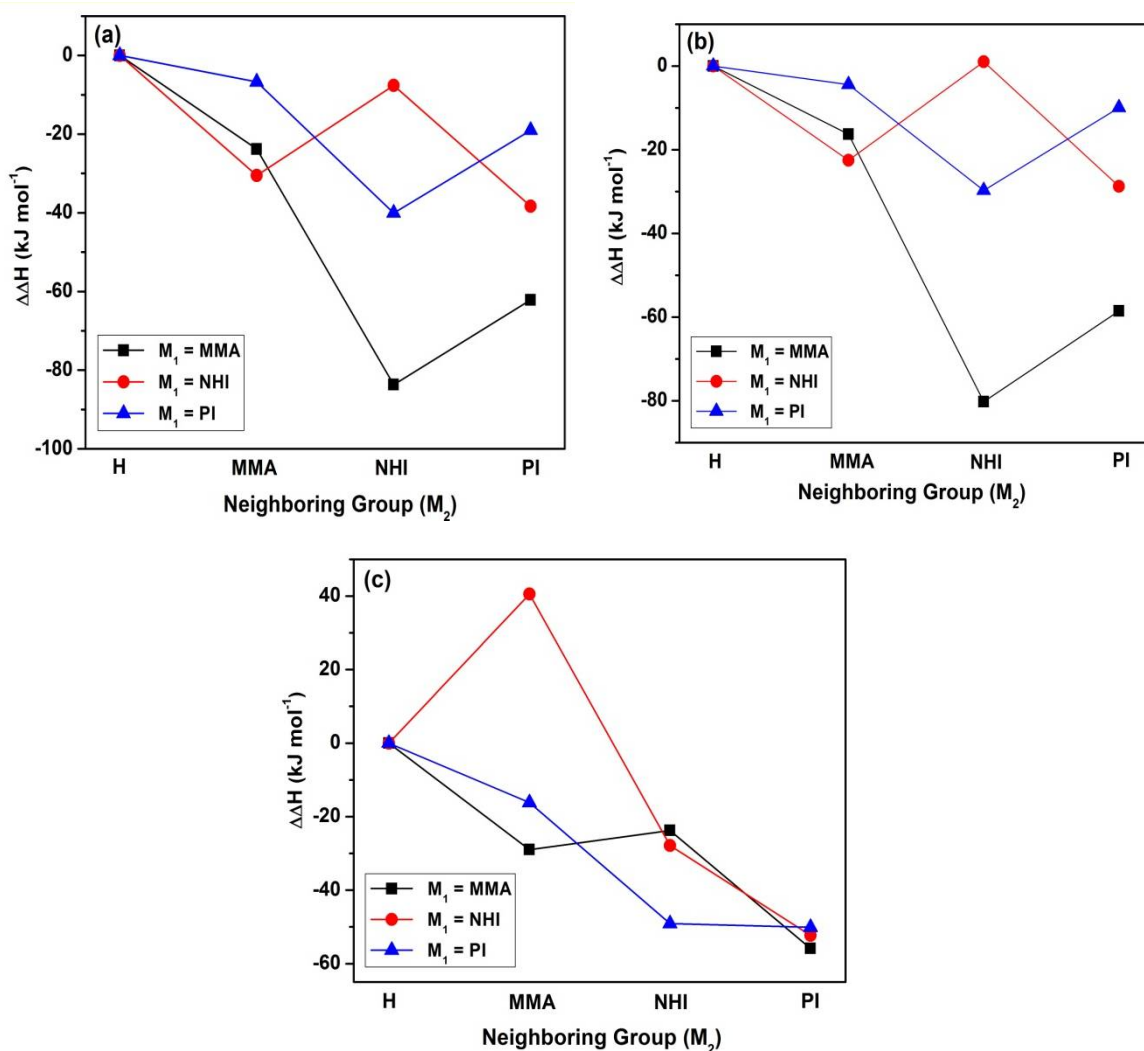


Figure 5.17: Effect of the neighboring group (M_2) on the homolytic C-X bond dissociation enthalpy (ΔH) of dimers ($H-M_2-M_1-X$) in anisole at 25 °C (a) X = Cl, (b) X = Br and (c) X = I (here, $\Delta\Delta H = \Delta H$ of $H-M_2-M_1-X - \Delta H$ of $H-M_1-X$).

dimers H-MMA-NHI-I shows increase in BDE values. For the H-PI-I and its corresponding dimers shows the decrease in BDEs and the trend is, H-PI-PI-I < H-NHI-PI-I < H-MMA-PI-I. A similar trend is observed for all studied dimers (where X = Cl, Br

and I) at elevated temperature (80 °C) and in anisole solvent which is shown in the **Figure 5.16** and **Figure 5.17**, respectively.

The BDEs of trimer bromides are found in the range of 167.66 kJ mol⁻¹ to 249.01 kJ mol⁻¹ (**Table 5.9**). The trimers having the bulky PI at the penultimate position such as H-PI-MMA-MMA-Br, H-PI-PI-MMA-Br, H-PI-MMA-NHI-Br, H-PI-MMA-PI-Br are found to have lower BDEs as compared to trimers H-MMA-MMAMMA-Br, H-MMA-MMA-NHI-Br, H-MMA-NHI-NHI-Br and H-MMA-NHI-MMA-Br, H-NHI-MMA-MMA-Br, H-NHI-NHI-MMA-Br, H-NHI-MMA-NHI-Br, H-NHI-NHI-NHI-Br. As we compare the BDE of H-MMA-Br with their corresponding trimers, H-MMA-MMA-MMA-Br, H-NHI-MMA-MMA-Br, H-NHI-NHI-MMA-Br, & H-MMA-NHI-MMA-Br, there is a decrease in the BDEs in the range of 2-15 kJ mol⁻¹. Similarly, comparing the BDE of H-NHI-Br with their corresponding trimers, H-MMA-MMA-NHI-Br, H-NHI-MMA-NHI-Br, H-MMA-NHI-NHI-Br and H-NHI-NHI-NHI-Br, there is a decrease in BDEs in the range of 1-8 kJ mol⁻¹. The BDEs of trimers, H-NHI-MMA-PI-Br, H-MMA-NHI-PI-Br, H-PI-MMA-PI-Br, H-MMA-PI-PI-Br and H-PI-PI-PI-Br are found to be smaller with compared to BDE of H-PI-Br, and it is in the range of 20-82 kJ mol⁻¹.

As we compare the BDEs of dimers and trimers such as H-MMA-MMA-Br and H-MMA-MMA-MMA-Br, H-NHI-MMA-MMA-Br, respectively, (and H-MMA-NHI-Br and H-MMA-MMA-NHI-Br, H-NHI-MMA-NHI-Br, respectively), an increase in BDEs was observed for trimers in the range of 8-29 kJ mol⁻¹. Similarly, for H-NHI-MMA-Br, H-NHI-NHI-MMA-Br, H-MMA-NHI-MMA-Br an increase in BDEs (from dimer to trimers) are observed in the range of 73-90 kJ mol⁻¹. However, for the dimers (H-NHI-NHI-Br, H-MMA-PI-Br) and its corresponding trimers (H-MMA-NHI-NHI-Br, H-NHI-NHI-NHI-Br, H-MMA-MMA-PI-Br, H-NHI-MMA-PI-Br and H-PI-MMA-PI-Br) a decrease in BDEs (in the range of 5-11 kJ mol⁻¹) is observed. The variation of BDEs of dimers and trimers are shown in the **Figure 5.18**.

The free energy values for all the studied dimers in gas phase at 25 °C are given in **Table 5.8**. They are in the range of 120.84 kJ mol⁻¹ to 208.42 kJ mol⁻¹ for X = Cl, 115.81 kJ mol⁻¹ to 211.39 kJ mol⁻¹ for X = Br, and 7.72 kJ mol⁻¹ to 101.05 kJ mol⁻¹. In anisole at 25°C (**Appendix v, Table A5**), the free energies of dimer are found between 126.11 kJ mol⁻¹ to 205.48 kJ mol⁻¹ for X = Cl, 118.85 kJ mol⁻¹ to 199.94 kJ mol⁻¹ for X = Br and 8.29 kJ mol⁻¹ to 104.66 kJ mol⁻¹ for X = I. At elevated temperature (i.e. 80 °C) the free energies of dimers (**Appendix v, Table A6**) are observed in the range of 112.29 kJ mol⁻¹ to 200.57 kJ mol⁻¹ for X = Cl, 107.23 kJ mol⁻¹ to 197.22 kJ mol⁻¹ for X = Br and

2.45 kJ mol⁻¹ to 90.68 kJ mol⁻¹ for X = I. The free energies of the dimers are having nearly constant difference with their enthalpy values (~ 40-50 kJ mol⁻¹). This means that the entropy factor contributing for all studied dimers are almost constant. The free energies of trimers are found in the range of 184.65 kJ mol⁻¹ to 198.64 kJ mol⁻¹ (Table 5.9).

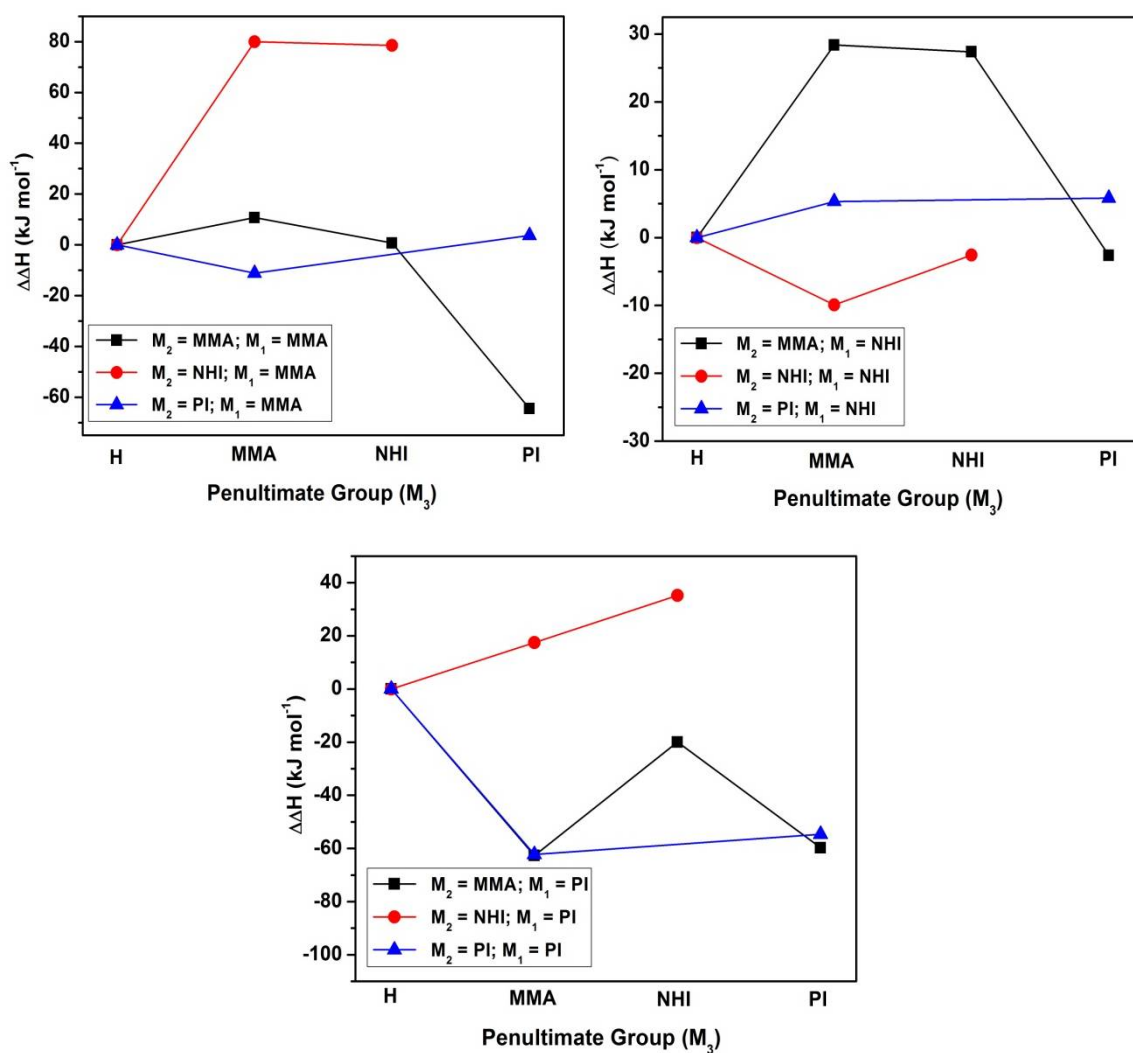


Figure 5.18: Effect of the penultimate group (M_3) on the homolytic C-Br bond dissociation enthalpy (ΔH) of trimers ($H-M_3-M_2-M_1-Br$) in gas phase at 25 °C (here, $\Delta\Delta H = \Delta H$ of $H-M_3-M_2-M_1-Br - \Delta H$ of $H-M_2-M_1-Br$).

5.4.3.3 Relative Equilibrium Constants (K_{ATRP}) of Dimers and Trimers

Following a reported procedure [270], we have calculated the ratios of equilibrium constants (K) for the C-Br bond dissociation of dimers ($H-M_2-M_1-X$), relative to the equilibrium constants (K_0) of its corresponding unimers ($H-M_1-X$). The K/K_0 ratios are presented for gas phase (25 °C) in **Table 5.8**, in anisole solvent at 25 °C (**Appendix v, Table A5**) and for gas phase at 80 °C (**Appendix v, Table A6**). A quick glance on the K/K_0 values of all studied dimers show significant change in K/K_0 values from its unimers. The variation of K/K_0 values due to change in different neighboring group (M_2) in the dimers $H-M_2-M_1-X$ (with respect to unimers $H-M_1-X$) in gas phase at 25 °C is displayed in **Figure 5.19**. The K/K_0 ratios for studied dimers (for $X = Cl$) is observed in the range of 10^0 to 10^{+10} . For the H-MMA-Cl and its related dimers the K/K_0 ratios are decreased in the order, H-NHI-MMA-Cl > H-PI-MMA-Cl > H-MMA-MMA-Cl. For the dimers corresponding to H-NHI-Cl unimer the trend of K/K_0 is, H-PI-NHI-Cl > H-MMA-NHI-Cl > H-NHI-NHI-Cl > H-NMI-NHI-Cl. For the dimers corresponding to H-PI-Cl unimer, the trend of K/K_0 ratios is, H-NHI-PI-Cl > H-NMI-PI-Cl > H-PI-PI-Cl > H-MMA-PI-Cl. For the studied dimers with $X = Br$, the values K/K_0 are found in the range of 10^{-2} to 10^{+11} . Similar results are observed for the bromide dimers, but the values K/K_0 are slightly decreases as compared to chloride dimers. For the dimers with $X = I$, the values K/K_0 are observed in the range of 10^{-6} to 10^{+10} . For the H-MMA-I and its corresponding dimers the trend of K/K_0 ratio is obtained as, H-PI-MMA-I > H-NHI-MMA-I > H-MMA-MMA-I > H-NMI-MMA-I. For the H-PI-I and its corresponding dimers (H-NHI-PI-I and H-PI-PI-I) are having similar K/K_0 value. The highest K/K_0 values are observed for the PI as the neighboring group (M_2). If we move from gas phase to anisole (**Figure 5.20**) or from 25 °C to 80 °C (**Figure 5.21**) the values of K/K_0 do not vary much and the trends remains more or less similar to those of gas phase at 25 °C cases.

To study the penultimate unit effect in the copolymerization of PI and MMA system using trimer model, we have calculated the ratios (K/K_0) of ATRP equilibrium constants (K) for the C-Br bond dissociation of trimer bromides ($H-M_3-M_2-M_1-Br$), relative to the equilibrium constants (K_0) of its corresponding dimer bromides ($H-M_2-M_1-Br$), in gas phase at 25 °C is displayed in the **Table 5.9**. The K/K_0 ratio for studied trimers are observed in the range of 10^{-5} to 10^{+15} . A significant change is observed in the K/K_0 values of the trimers as compared to the dimers. The variation of K/K_0 values due to

the change in the penultimate group (M_3) in the trimers ($H-M_3-M_2-M_1-Br$) (with respect to dimers, $H-M_2-M_1-Br$) in gas phase at 25 °C is displayed in **Figure 5.22**. The trimers, $H-MMA-NHI-MMA-Br$, $H-NHI-NHI-MMA-Br$, $H-MMA-MMA-MMA-Br$, $H-MMA-MMA-NHI-Br$, $H-NHI-MMA-NHI-Br$, $H-MMA-PI-NHI-Br$, $H-PI-PI-NHI-Br$, $H-MMA-NHI-PI-Br$ and $H-NHI-NHI-PI-Br$ shows positive deviation (an increase in K/K_0 values as compared to the dimers) from its corresponding dimer. Similarly, the trimers such as $H-MMA-PI-MMA-Br$, $H-PI-MMA-MMA-Br$, $H-MMA-NHI-NHI-Br$, $H-NHI-NHI-NHI-Br$, $H-PI-MMA-NHI-Br$, $H-MMA-MMA-PI-Br$, $H-NHI-MMA-PI-Br$, $H-PI-MMA-PI-Br$, $H-MMA-PI-PI-Br$ and $H-PI-PI-PI-Br$ shows negative deviation (decrease

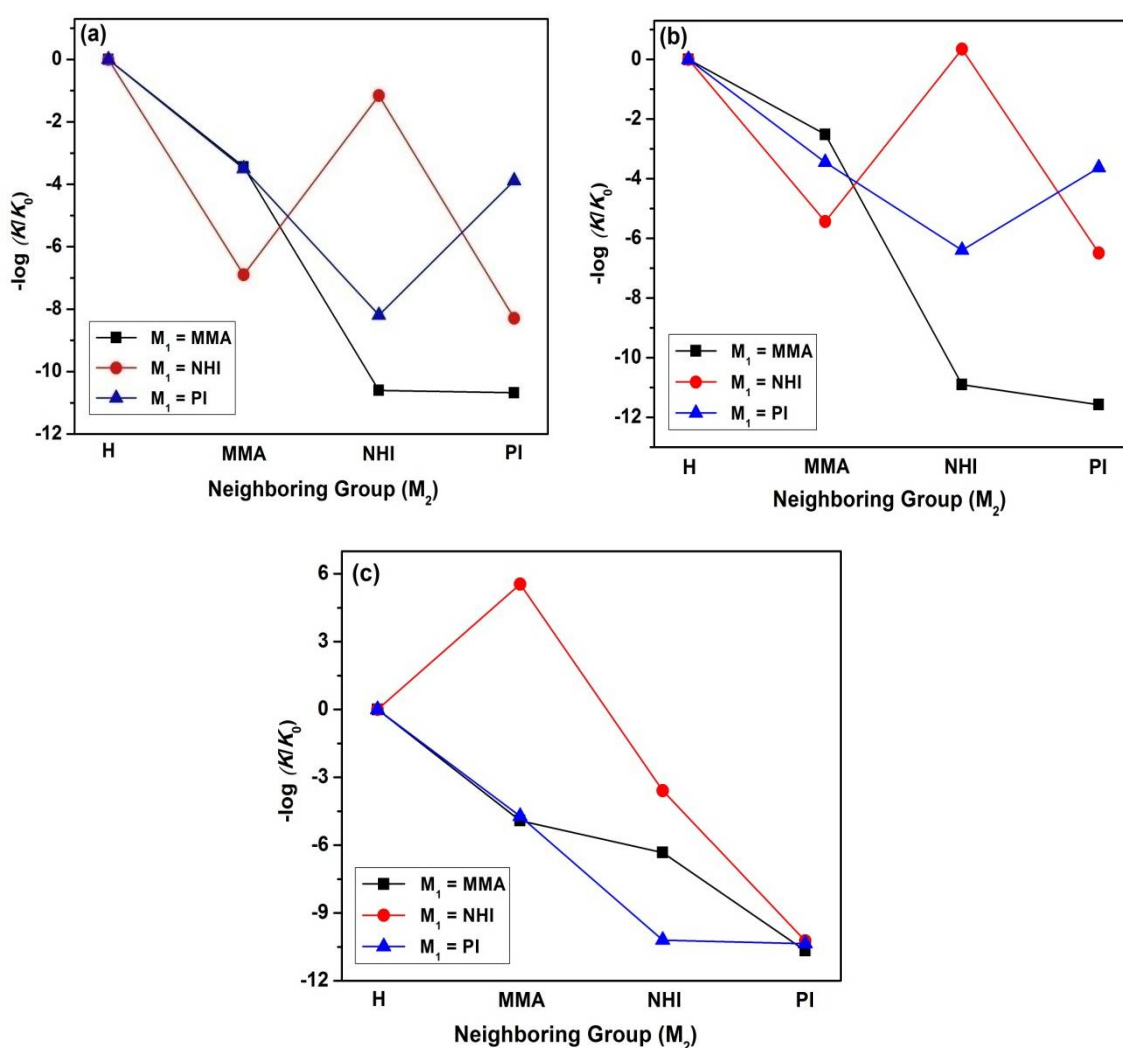


Figure 5.19: Effect of the neighboring group (M_2) on the K/K_0 ratio of dimers ($H-M_2-M_1-X$) in gas phase at 25 °C (a) $X = Cl$, (b) $X = Br$ and (c) $X = I$ (here, $K = K_{ATRP}$ of $H-M_2-M_1-X$ and $K_0 = K_{ATRP}$ of $H-M_1-X$).

in K/K_0 values as compared to the dimers) from its dimer counterpart. However, the trimers (H-NHI-MMA-MMA-Br and H-PI-PI-MMA-Br) are not showing any deviation of K/K_0 values as compared to its corresponding dimers.

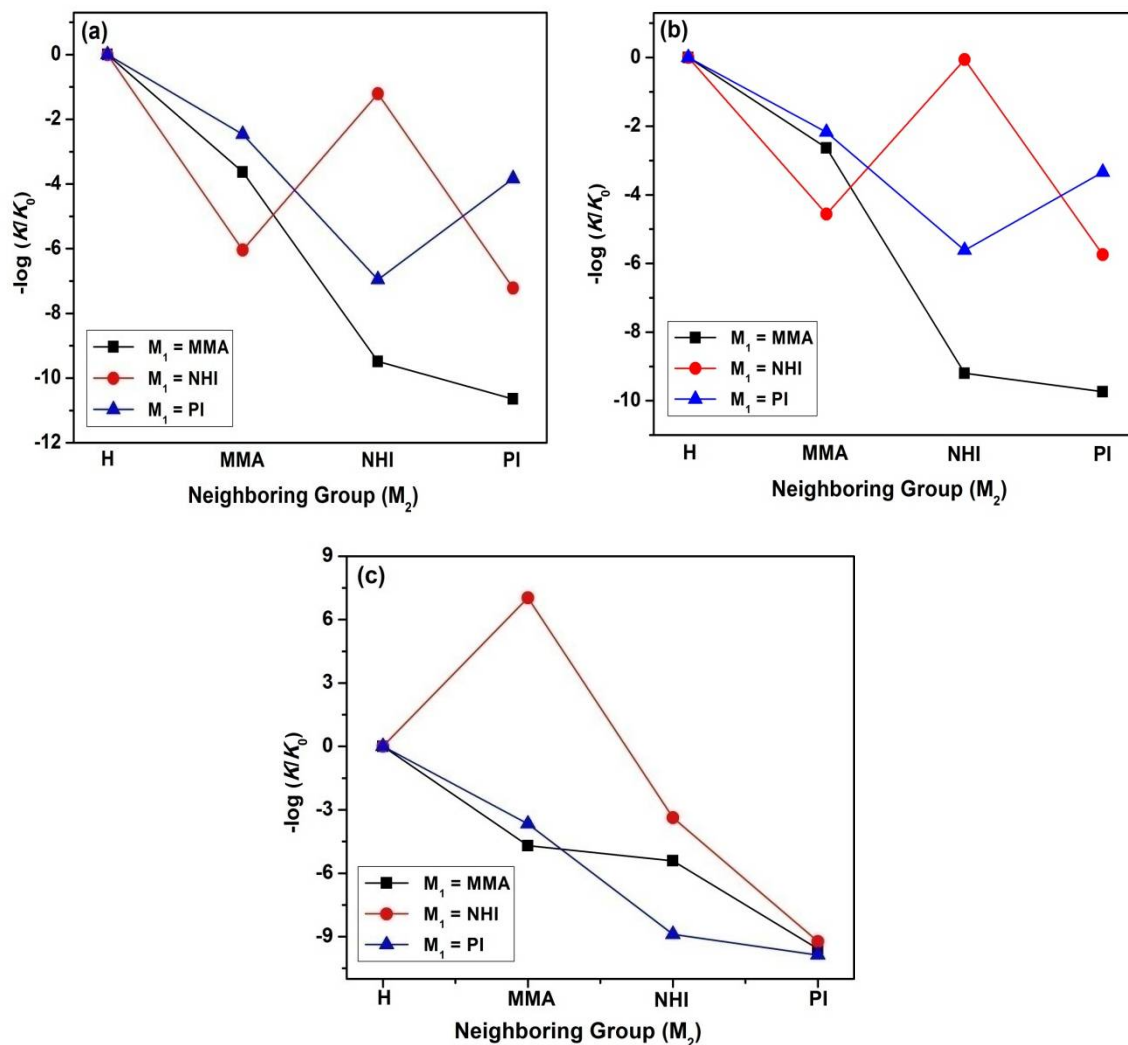


Figure 5.20: Effect of the neighboring group (M_2) on the K/K_0 ratio of dimers (H- M_2 - M_1 -X) in anisole at 25 °C (a) X = Cl, (b) X = Br and (c) X = I (here, $K = K_{\text{ATRP}}$ of H- M_2 - M_1 -X and $K_0 = K_{\text{ATRP}}$ of H- M_1 -X).

If we compare the K/K_0 values for the trimers corresponding to unimer H-MMA-Br, the trend is observed as, H-PI-MMA-MMA-Br > H-MMA-PI-MMA-Br > H-PI-PI-MMA-Br > H-NHI-MMA-MMA-Br > H-MMA-NHI-MMA-Br > H-NHI-NHI-MMA-Br > H-MMA-MMA-MMA-Br. Similarly, for the trimers corresponding to unimers H-NHI-Br, the trend of K/K_0 is, H-PI-MMA-NHI-Br > H-MMA-PI-NHI-Br > H-PI-PI-NHI-Br >

H-MMA-NHI-NHI-Br > H-MMA-MMA-NHI-Br > H-NHI-MMA-NHI-Br > H-NHI-NHI-NHI-Br. For the trimers corresponding to unimers H-PI-Br, the trend of K/K_0 is as, H-MMA-PI-PI-Br > H-MMA-MMA-PI-Br > H-PI-MMA-PI-Br > H-PI-PI-PI-Br > H-NHI-MMA-PI-Br > H-NHI-NHI-PI-Br > H-MMA-NHI-PI-Br. The observed K/K_0 values are highest for the trimers having the bulky PI group at the penultimate position.

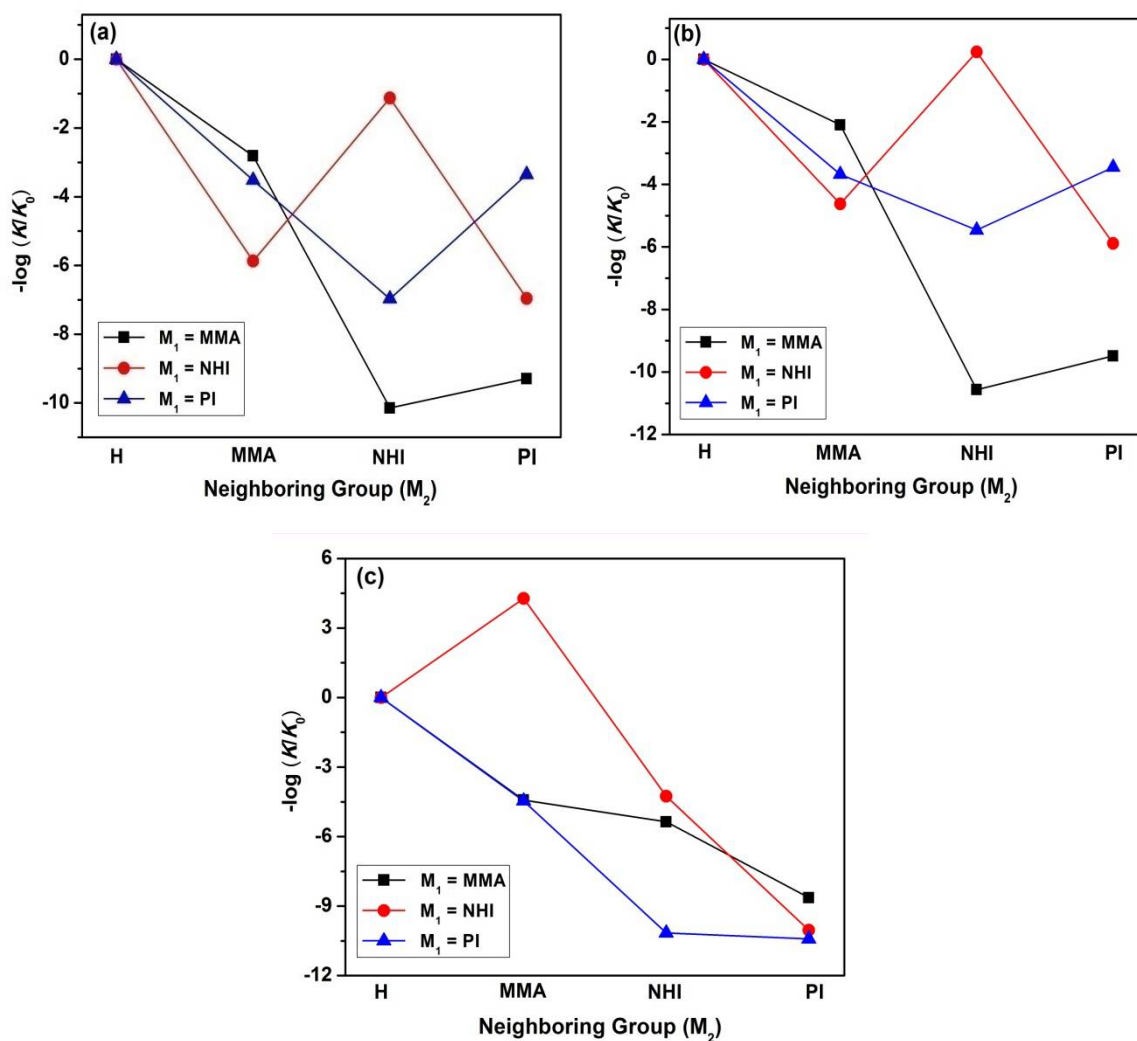


Figure 5.21: Effect of the neighboring group (M_2) on the K/K_0 ratio of dimers (H- M_2 - M_1 -X) in gas phase at 80 °C (a) X = Cl, (b) X = Br and (c) X = I (here, $K = K_{\text{ATRP}}$ of H- M_2 - M_1 -X and $K_0 = K_{\text{ATRP}}$ of H- M_1 -X).

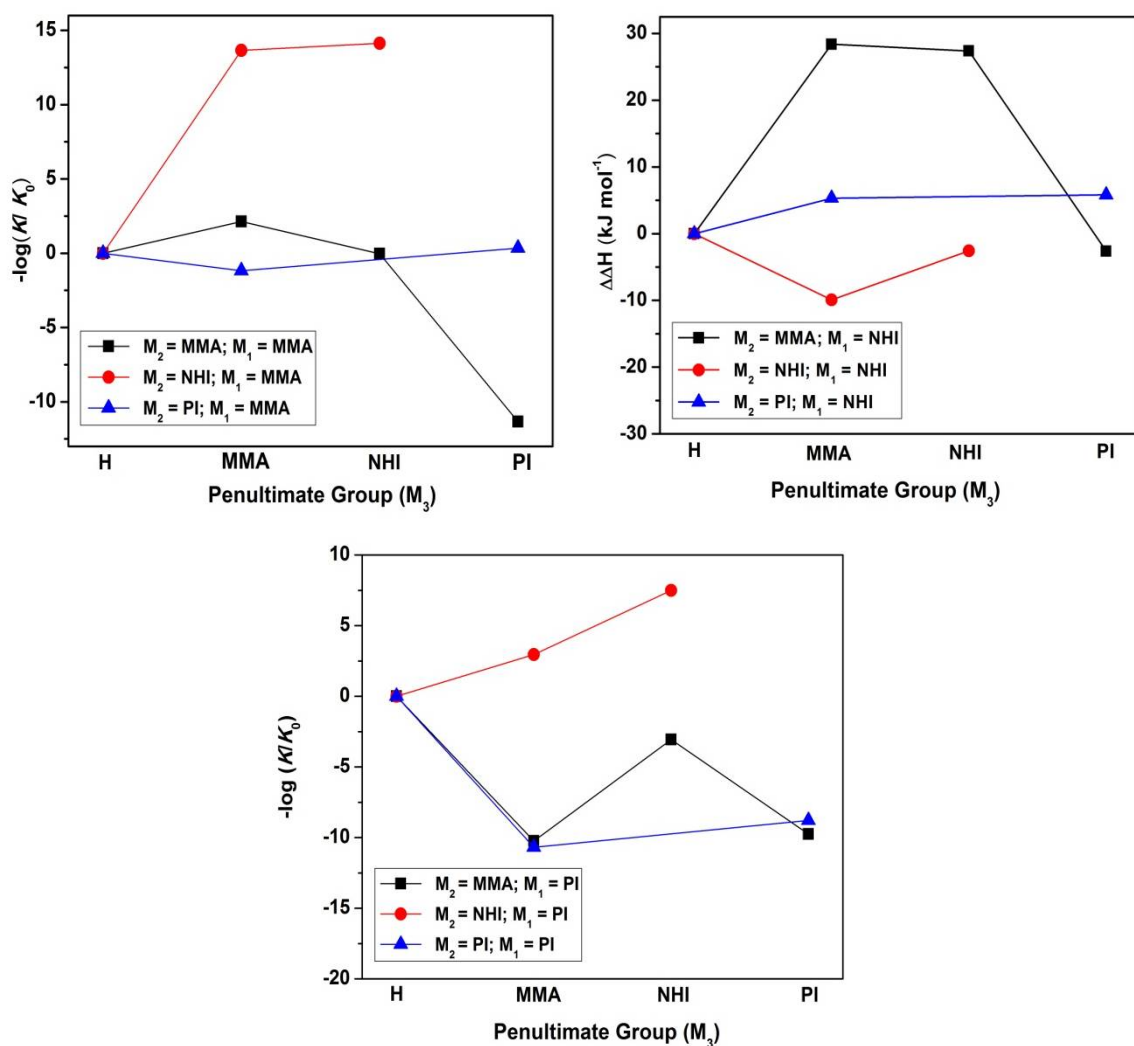


Figure 5.22: Effect of the penultimate unit on the K/K_0 ratio of trimer (H-M₃-M₂-M₁-Br) in gas phase at 25 °C (here, $K = K_{\text{ATRP}}$ of H-M₃-M₂-M₁-Br and $K_0 = K_{\text{ATRP}}$ of H-M₂-M₁-Br).

5.5 Conclusions

The mechanistic study for the copolymerization of PI and MMA monomer system was carried out both experimentally as well as theoretically. Experimentally, the triad fractions of PI-MMA copolymers are calculated using ¹³C{¹H}-NMR spectroscopy. Alternatively, the triad fractions of PI-MMA copolymers are calculated using DFT methods by treating polymeric species as dimers (with terminal model) as well as trimers (with both terminal and penultimate model). A good agreement with experimental triad fractions is obtained when the polymeric species are treated as trimer and using the

penultimate model. The results indicate substantial penultimate effect for the chosen copolymerization system and the polymeric species should be modelled at least with a trimer (and not a dimer). The effects of penultimate unit on C-X bond lengths, C-X bond dissociation enthalpy, free energy and on the relative K_{ATRP} values are investigated. A substantial penultimate effect is found in the PI-MMA copolymer system. The C-X bond length, C-X bond dissociation enthalpy and K/K_0 values of dimers are increased ≈ 0.025 Å, ≈ 90 kJ mol⁻¹ and in the range of 10^{-6} to 10^{+11} , respectively, as compared to its corresponding unimers. Similarly, the C-X bond length and C-X bond dissociation enthalpy and K/K_0 values of trimers are increased ≈ 0.021 Å, ≈ 65 kJ mol⁻¹ and in the range of 10^{-5} to 10^{+15} as compared to its corresponding dimers. It is found that the solvent anisole and elevated temperature (80 °C) having very little effect on C-X bond lengths, C-X bond dissociation enthalpy, free energy and the relative K_{ATRP} values of dimers.

CHAPTER VI

SUMMARY, CONCLUSIONS AND FUTURE SCOPE

This thesis has been focused on the experimental and theoretical studies on the atom transfer radical copolymerization of NAI and MMA monomers. The overall summary, conclusions and future scope of the thesis is given below:

6.1 Summary

➤ The copolymerization of NAI and MMA are mostly studied by using conventional free radical polymerization methods. The resultant random copolymers showed enhanced glass transition temperature and thermal stability. The conventional methods of radical polymerization offer poor control over the molecular weight. Hence, it is difficult to synthesize different architectures of the copolymers such as block. These restrictions can be removed by using RDRP methods such as ATRP, which is the robust and most commonly used RDRP technique. The *ab initio* methods such as DFT methods can be used to study the mechanism of ATRP of NAI-MMA copolymer systems.

➤ The synthesis and characterizations of NAI monomers [such as *N*-phenylitaconimide, *N*-(4-methylphenyl)itaconimide (MPI), *N*-(4-methoxyphenyl)itaconimide, *N*-(4-chlorophenyl)itaconimide (CPI)] as well as bromo derivatives of succinimides [such as *N*-phenyl(3-bromo-3-methyl)succinimide (BSI-33), *N*-phenyl(3-bromo-4-methyl)succinimide (BSI-34), *N*-phenyl(3-bromomethyl)succinimide (BSI-3)] was carried out successfully. The obtained compounds were characterized experimentally as well as using DFT methods and the results were compared.

➤ The synthesis of copolymers of NAI and MMA monomers with different architectures viz. random [poly(NAI-*ran*-MMA)] and block [poly(NAI-*ran*-MMA)-*b*-poly(MMA), poly(NAI-*ran*-MMA)-*b*-poly(NAI)] were successfully carried out using ATRP methodology. Two different architectures were obtained with '*N*-arylimide' as the pendant group. The substituent on aromatic ring of NAI varied from strongly activating

group $-\text{OCH}_3$ to weakly deactivating group $-\text{Cl}$, thus changing the polarity and rigidity of the pendant group. The structural characterization of the copolymers was carried out using IR, $^1\text{H-NMR}$, $^{13}\text{C-NMR}$ spectroscopy and elemental analysis. The molecular and thermal characterization of copolymers was carried out by using GPC and DSC/ TGA, respectively. With the increase in the electron releasing tendency of substituent on aromatic ring of the pendant group, an increase in the rate of copolymerization, \bar{M}_n and T_g of the copolymers was observed. The block architectures such as poly(NAI-*ran*-MMA)-*b*-poly(MMA) and poly(NAI-*ran*-MMA)-*b*-poly(NAI) were synthesized using poly(NAI-*ran*-MMA)* as macroinitiator via AGET-ATRP. The IR and $^1\text{H-NMR}$ analysis of the block copolymers poly(NAI-*ran*-MMA)-*b*-poly(MMA) and poly(NAI-*ran*-MMA)-*b*-poly(NAI) shows the incorporation of poly(MMA) and poly(NAI) block, respectively. The block architecture was further confirmed by the increase in the molecular weight of block copolymers as compared to the corresponding macroinitiator. The T_g corresponding to the two blocks of the copolymers, observed in DSC scans of the block copolymer. Thus, the living copolymers of NAI and MMA with two different architectures i.e. random and block were successfully synthesized and characterized. These copolymers are having 60-117% increase in softening temperature and 80-100% increase in thermal stability as compared to PMMA

➤ The potential of synthesized bromo derivatives of succinimides in absence of monomer has been investigated by determining its K_{ATRP} values. Experimentally, the K_{ATRP} values were determined using Fischer-Fukuda equation for the ‘persistent radical effect’. For determining K_{ATRP} values using Fischer-Fukuda equation the concentration of deactivating species $[\text{BrCu}^{\text{II}}\text{Bpy}]$ and k_t value of stable radical is required. The concentration of $[\text{BrCu}^{\text{II}}\text{Bpy}]$ complex were determined using UV-Vis-NIR spectroscopy. The k_t value of *N*-phenylsuccinimide (used as model compound) was obtained from the diffusion coefficient ($1.65 \times 10^{-5} \text{ cm}^2\text{s}^{-1}$) which was determined from the DOSY-NMR spectroscopy. Alternatively, these compounds along with some similar alkyl halides (R-X) are investigated using density functional theory methods for their possible chain initiation activity for the ATRP process. The B3LYP functional and 6-31+G(d)/ LanL2DZ basis set is used for the prediction of geometries and energetics associated with the homolytic R-X bond dissociation. The relative value of K_{ATRP} are calculated from the free energy values of R-X bond dissociation and its variation with system parameters (such as, substituent, temperature and solvent) is investigated. A

variation of substituent in phenyl ring at *para* position of the studied alkyl halides has very little effect on bond length, bond dissociation enthalpy (BDEs), free energy, and K_{ATRP} . It is found that values of K_{ATRP} slightly decrease with increasing solvent polarity and increase significantly with increasing temperature. The potential of synthesized initiators has been tested for the PI and MMA monomer system. For these the copolymerization of PI and MMA was carried out via AGET-ATRP using BSI-33 as initiator. The kinetics of copolymerization shows, (i) a typical linear variation in the plots of % conversion of monomers with time, (ii) linear increase of molecular weight of copolymer with % conversion of monomers, and (iii) a linear plot is observed for $\ln \{[M]_0/[M]_t\}$ vs time, confirming that the polymerization is occurring under controlled radical polymerization condition. Our experiments show that the newly synthesized initiator BSI-33 performs better than the commercially available initiator ethyl- α -bromoisobutyrate for the atom transfer radical copolymerization of PI and MMA.

➤ The NAI is a bulky with electron withdrawing substituent on double bond and it is expected that the copolymerization of NAI and MMA monomers to follow “penultimate unit effect” especially for the reaction where radical terminated with MMA. To confirm this view, the PI-MMA copolymer system was chosen as the representative system. The mechanistic study for the chosen copolymerization system was carried out experimentally as well as theoretically. For this the triad fractions of PI-MMA copolymers were used. Experimentally, the triad fractions were determined using $^{13}\text{C}\{^1\text{H}\}$ -NMR spectroscopy. For that carbonyl regions from the $^{13}\text{C}\{^1\text{H}\}$ -NMR spectra of the PI-MMA copolymers were taken under the observation. Theoretically, the triad fractions of PI-MMA copolymer are calculated using terminal and penultimate model. For this the resulting copolymers of PI-MMA are modeled as a dimer (H-M₂-M₁-X) model (based on terminal model) and trimer (H-M₃-M₂-M₁-X) model (includes both terminal and penultimate model). For the theoretical study two different temperature (viz. 25 °C and 80 °C) and two different medium (viz. gas phase and anisole solvent) were selected. Experimentally determined triad fractions were agreed well with the theoretically calculated triad fractions when the polymeric species were treated as trimer and using the penultimate model. We further studied the effect of neighboring and penultimate unit on the structural and thermodynamic properties of the dimers and trimers. For this the C-X bond length, bond dissociation enthalpy, free energy and K_{ATRP} of the dimers and trimers have been taken under consideration. The solvent anisole is not

effecting the thermodynamic parameter but the temperature is having pronounced effect on it.

6.2 Conclusions

1. The synthesized compounds (such as PI, MPI, MOPI and CPI, BSI-3, BSI-34 and BSI-33) were characterized experimentally as well as using DFT methods. A good correlation was obtained between the experimentally found and theoretically calculated vibrational frequencies and $^1\text{H-NMR}$ (δ) values of the synthesized compounds. This confirms that the selected DFT method [B3LYP/ 6-31+G(d) level] of calculation is quite appropriate for this studies.

2. The copolymerization of different NAI monomers (viz. PI, MPI, MOPI and CPI) was carried out with MMA *via* ATRP resulting in *N*-arylimide as the pendant group. The linear variation of $\ln \{([M]_t[I]_0) / ([I]_t[M]_0)\}$ vs time, indicates that the copolymerization of NAI and MMA follows second order kinetics. The rate of copolymerization, molecular weight and T_g of poly(NAI-*ran*-MMA) copolymers were found to increase with increase in the electron releasing tendency of substituent on aromatic ring of the pendant group. An increase in the molecular weight of block copolymers viz. poly(NAI-*ran*-MMA)-*b*-poly(MMA) and Poly(NAI-*ran*-MMA)-*b*-poly(NAI) as compared to the poly(NAI-*ran*-MMA)* macroinitiator, shows the “living” nature of the random copolymers. The T_g corresponding to the two blocks of the copolymers, observed in DSC scans shows the architecture of the copolymer as “block”.

3. The K_{ATRP} of synthesized bromo succinimides (viz. BSI-3, BSI-34 and BSI-33) along with a commercially available initiator (ethyl-2-bromoisobutyrate) were determined experimentally using UV-Vis-NIR spectroscopy and k_t for radicals using DOSY NMR spectroscopy. Alternatively, the structural and thermodynamic properties (bond dissociation enthalpies and free energies) of these alkyl bromides (along with some similar alkyl halides and some common ATRP initiators) has also been studied using DFT methods. A good agreement was obtained between our experimentally determined and theoretically calculated K_{ATRP} values of the synthesized bromo succinimides in acetonitrile at 25 °C. The copolymerization of PI and MMA was successfully carried out using one of our synthesized alkyl bromide (i.e. BSI-33 as an

initiator) in anisole at 80 °C via AGET-ATRP. Comparisons with the copolymerization of same systems with commercially available initiator, ethyl-2-bromoisobutyrate, shows that our newly synthesized BSI-33 has better performance over ethyl-2-bromoisobutyrate in terms of control on rate of polymerization, % conversion of monomer and PDI of obtained copolymers.

4. For studying the mechanism of copolymerization of PI-MMA copolymer system, the triad fractions were calculated experimentally as well as theoretically. A good agreement with experimental triad fractions is obtained when the polymeric species are treated as trimer and using the penultimate model. The obtained results shows that, to study the mechanism of the PI-MMA copolymerization system, the trimer model or penultimate model has to be taken under consideration (and not dimer or terminal model). The effects of penultimate group on the structural and thermodynamic properties, such as C-X bond length, bond enthalpy, free energy and equilibrium constant have also been studied using DFT methods. The observed K/K_0 values are highest for the trimers having the bulky PI group at the penultimate position.

6.3 Future Scope

1. The functionalized alkyl bromides (bromo derivatives of succinimide) based on renewable resource can be used as initiators for the synthesis of various architectures of itaconimide copolymers. These area needs to be explored further.

2. The living copolymers of NAI and MMA monomers with block architecture viz. poly(NAI-*ran*-MMA), poly(NAI-*ran*-MMA)-*b*-poly(MMA) and poly(NAI-*ran*-MMA)-*b*-poly(NAI) having high T_g and thermal stability as compared to the PMMA are potential candidates as ‘thermoplastic’ (that can be used in a higher temperature service). The other architectures and mechanical properties of these copolymers needs to be explored.

3. The DFT methods can be explored to study the mechanism and thermodynamics of copolymerization of various NAI-MMA copolymer system (the trimer model or penultimate model should be used for the calculation of reactivity ratios). Prior to the

experiments, the DFT methods can be used to design the copolymers of NAI-MMA system with different architectures.

References

- [1] Darshan, P. Sharma, P. Malhotra, A. K. Narula, *Journal of Applied Polymer Science*, **107**, 1628-1634 (2008).
- [2] T. Oishi, *Polymer Journal*, **12**, 719-727 (1980).
- [3] A. Mishra, V. Choudhary, *Journal of Applied Polymer Science*, **62**, 707-712 (1996).
- [4] R. Madan, A. Srivastava, R. C. Anand, I. K. Varma, *Progress in Polymer Science*, **23**, 621-663 (1998).
- [5] A. Solanki, V. Anand, V. Choudhary, I. K. Varma, *Journal of Macromolecular Science, Part C: Polymer Reviews*, **C41**, 253-284 (2001).
- [6] T. Oishi, *Polymer Journal*, **12**, 799-807 (1980).
- [7] T. Oishi, M. Momoi, M. Fujimoto, *Journal of Polymer Science: Polymer Chemistry Edition*, **21**, 1053-1063 (1983).
- [8] H. Watanabe, A. Matsumoto, T. Otsu, *Journal of Polymer Science: Part A: Polymer Chemistry*, **32**, 2073-2083 (1994).
- [9] R. Bharel, V. Choudhary, I. K. Varma, *Journal of Applied Polymer Science*, **54**, 2165-2170 (1994).
- [10] R. Bharel, V. Choudhary, I. K. Varma, *Journal of Applied Polymer Science*, **57**, 767-773 (1995).
- [11] H. Yamazaki, A. Matsumoto, T. Otsu, *European Polymer Journal*, **33**, 157-162 (1997).
- [12] Y. Zhao, H. Li, P. Liu, H. Liu, J. Jiang, F. Xi, *Journal of Applied Polymer Science*, **83**, 3007-3012 (2002).
- [13] C. Soykan, I. Erol, *Journal of Applied Polymer Science*, **91**, 964-970 (2004).
- [14] V. Anand, V. Choudhary, *Journal of Applied Polymer Science*, **82**, 2078-2086 (2001).
- [15] V. Anand, V. Choudhary, *Journal of Applied Polymer Science*, **89**, 1195-1202 (2003).
- [16] K. Yahiro, S. Shibata, S-R. Jia, Y. Park, M. Okabe, *Journal of Fermentation and Bioengineering*, **84**, 375-377 (1997).
- [17] C. S. K. Reddy and R. P. Singh, *Bioresource Technology*, **85**, 69-71 (2002).
- [18] X. Huang, M. Chen, X. Lu, Y. Li, X. Li, J-J. Li, *Microbial Cell Factories*, **13**, 108-118 (2014).

- [19] R. Chauhan, V. Choudhary, *Journal of Applied Polymer Science*, **98**, 1909-1915 (2005).
- [20] R. Chauhan, V. Choudhary, *Journal of Applied Polymer Science*, **109**, 987-996 (2008).
- [21] G. Odian, *Principles of Polymerization*, Wiley Interscience, Staten Island, 4th Edition, pp 464-543 (2004).
- [22] A. Goto, T. Fukuda, *Progress in Polymer Science*, **29**, 329-385 (2004).
- [23] V. Anand, S. Agarwal, A. Greiner, V. Choudhary, *Polymer International*, **54**, 823-828 (2005).
- [24] A. Mullar, K. Matyjaszewski, *Radical polymerization, Controlled and Living Polymerization*, WILEY-VCH Verlag GmbH and Co. KGaA, Weinheim, pp. 103-166 (2009).
- [25] W. A. Braunecker, K. Matyjaszewski, *Progress in Polymer Science*, **32**, 93-146 (2007).
- [26] T. Oishi, T. Kawamoto, *Polymer Journal*, **26**, 920-929 (1994).
- [27] T. Oishi, K. Nagai, T. Kawamoto, H. Tsutsumi, *Polymer*, **37**, 3131-3139 (1996).
- [28] R. Chauhan, V. Choudhary, *Journal of Applied Polymer Science*, **101**, 2391-2398, (2006).
- [29] K. Matyjaszewski, Ed. *Controlled/Living Radical Polymerization, Progress in ATRP, NMP, and RAFT; ACS Symposium Series 768*; American Chemical Society: Washington, DC, (2000).
- [30] K. Matyjaszewski, Ed. *Controlled/Living Radical Polymerization, From Synthesis to Materials; ACS Symposium Series 944*; American Chemical Society: Washington, DC, (2006).
- [31] K. Matyjaszewski, *Progress in Polymer Science*, **30**, 858-875 (2005).
- [32] A. D. Jenkins, R. G. Jones, G. Moad, *Pure and Applied Chemistry*, **82**, 483-491 (2010).
- [33] K. Matyjaszewski, *Macromolecules*, **45**, 4015-4039 (2012).
- [34] D. J. Siegwart, J. K. Oh, K. Matyjaszewski, *Progress in Polymer Science*, **37**, 18-37 (2012).
- [35] K. Matyjaszewski, J. Xia, *Chemical Reviews*, **101**, 2921-2990 (2001).
- [36] H. Fischer, *Journal of Polymer Science: Part A: Polymer Chemistry*, **37**, 1885-1901 (1999).
- [37] H. Fischer, *Chemical Reviews*, **101**, 3581-3610 (2001).

- [38] C. J. Hawker, A. W. Bosman, E. Harth, *Chemical Reviews*, **101**, 3661-3688 (2001).
- [39] C. Diehl, P. Laurino, N. Azzouz, P. H. Seeberger, *Macromolecules*, **43**, 10311-10314 (2010).
- [40] L. E. N. Allan, M. R. Perry, M. P. Shaver, *Progress in Polymer Science*, **37**, 127-156 (2012)
- [41] Jin-Shan Wang and Krzysztof Matyjaszewski, *Macromolecules*, **28**, 7901-7910 (1995).
- [42] K. Matyjaszewski, D. A. Shipp, J.-L. Wang, T. Grimaud, T. E. Patten, *Macromolecules*, **31**, 6836-6840 (1998).
- [43] K. Matyjaszewski, N. V. Tsarevsky, *The Journal of American Chemical Society*, **136**, 6513-6533 (2014).
- [44] C. Boyer, N. A. Corrigan, K. Jung, D. Nguyen, T.-K. Nguyen, M. Adnan, S. Oliver, S. Shanmugam, J. Yeow, *Chemical Reviews*, **116**, 1803-1949 (2016).
- [45] T. E. Patten, K. Matyjaszewski, *Advanced Materials*, **10**, 901-915 (1998).
- [46] T. Pintauer, K. Matyjaszewski, *Chemical Society Reviews*, **37**, 1087-1097 (2008).
- [47] K. Matyjaszewski, *Israel Journal of Chemistry*, **52**, 206-220 (2012).
- [48] V. Coessens, T. Pintauer, K. Matyjaszewski, *Progress in Polymer Science*, **26**, 337-377 (2001).
- [49] S. S. Sheiko, B. S. Sumerlin, K. Matyjaszewski, *Progress in Polymer Science*, **33**, 759-785 (2008).
- [50] J. K. Oh, R. Drumright, D. J. Siegwart, K. Matyjaszewski, *Progress in Polymer Science*, **33**, 448-477 (2008).
- [51] D. A. Shipp, K. Matyjaszewski, *Macromolecules*, **33**, 1553-1559 (2000).
- [52] W. A. Braunecker, N. V. Tsarevsky, A. Gennaro, K. Matyjaszewski, *Macromolecules*, **42**, 6348-6360 (2009).
- [53] W. Tang, N. V. Tsarevsky, K. Matyjaszewski, *The Journal of American Chemical Society*, **128**, 1598-1604 (2006).
- [54] K. Matyjaszewski, T. E. Patten, J. Xia, *The Journal of American Chemical Society*, **119**, 674-680 (1997).
- [55] K. Ohno, Y. Tsujii, T. Miyamoto, T. Fukuda, *Macromolecules*, **31**, 1064-1069 (1998).
- [56] H. Zhang, B. Klumperman, W. Ming, H. Fischer, R. Linde, *Macromolecules*, **34**, 6169-6173 (2001).

- [57] M. B. Gillies, K. Matyjaszewski, P-O. Norrby, T. Pintauer, R. Poli, P. Richard, *Macromolecules*, **36**, 8551-8559 (2003).
- [58] T. Guliashvili, V. Percec, *Journal of Polymer Science: Part A: Polymer Chemistry*, **45**, 1607-1618 (2007).
- [59] C. Y. Lin, M. L. Coote, A. Gennaro, K. Matyjaszewski, *The Journal of American Chemical Society*, **130**, 12762-12774 (2008).
- [60] C. Y. Lin, S. R. A. Marque, K. Matyjaszewski, M. L. Coote, *Macromolecules*, **44**, 7568-7583 (2011).
- [61] J-L. Wang, T. Grimaud, K. Matyjaszewski, *Macromolecules*, **30**, 6507-6512 (1997).
- [62] T. Pintauer, P. Zhou, K. Matyjaszewski, *The Journal of American Chemical Society*, **124**, 8196-8197 (2002).
- [63] D. A. Singleton, D. T. Nowlan, N. Jahed, K. Matyjaszewski, *Macromolecules*, **36**, 8609-8616 (2003).
- [64] W. Tang, Y. Kwak, W. Braunecker, N. V. Tsarevsky, M. L. Coote, K. Matyjaszewski, *The Journal of American Chemical Society*, **130**, 10702-10713 (2008).
- [65] F. Seeliger, K. Matyjaszewski, *Macromolecules*, **42**, 6050-6055 (2009).
- [66] H. P. Alexander, M. Schneider-Baumann, K. U. Hildebrandt, A. M. Misske, C. Barner-Kowollik, *Macromolecules*, **46**, 15-28 (2013).
- [67] X. Yu, J. Pfaendtner, L. J. Broadbelt, *The Journal of Physical Chemistry A*, **112**, 6772-6782 (2008).
- [68] M. L. Coote, *Macromolecular Theory and Simulations*, **18**, 388-400 (2009).
- [69] M. D. Miller, A. J. Holder, *The Journal of Physical Chemistry A*, **114**, 10988-10996 (2010).
- [70] I. Degirmenci, S. Eren, V. Aviyente, *Macromolecules*, **43**, 5602-5610 (2010).
- [71] K. Matyjaszewski, *Journal of Macromolecular Science Part A-Pure and Applied Chemistry*, **34**, 1785-1801 (1997).
- [72] K. Matyjaszewski, T. E. Patten, J. Xia, *The Journal of American Chemical Society*, **119**, 674-680 (1997).
- [73] K. Matyjaszewski, *Macromolecular Symposia*, **111**, 47-61 (1996).
- [74] A. Kajiwara, K. Matyjaszewski, *Macromolecules*, **31**, 5695-5701 (1998).
- [75] C. Barner-Kowollik, S. Beuermann, M. Buback, P. Castignolles, B. Charleux, M. L. Coote, R. A. Hutchinson, T. Junkers, I. Lacik, G.T. Russell, et al., *Polymer Chemistry*, **5**, 204-212 (2014).

- [76] V. Van Speybroeck, D. van Neck, M. Waroquier, S. Wauters, M. Saeys, G.B. Marin, *The Journal of Physical Chemistry A*, **104**, 10939-10950 (2000).
- [77] J. Qiu, K. Matyjaszewski, *Macromolecules*, **30**, 5643-5648 (1997).
- [78] J-L. Wang, T. Grimaud, D. A. Shipp, K. Matyjaszewski, *Macromolecules*, **31**, 1527-1534 (1998).
- [79] H. Mori, A. H. E. Muller, *Progress in Polymer Science*, **28**, 1403-1439 (2003).
- [80] D. Neugebauer, K. Matyjaszewski, *Macromolecules*, **36**, 2598-2603 (2003).
- [81] N. V. Tsarevsky, W. A. Braunecker, S. J. Brooks, K. Matyjaszewski, *Macromolecules*, **39**, 6817-6824 (2006).
- [82] K. Matyjaszewski, S. M. Jo, H-J. Paik, S. G. Gaynor, *Macromolecules*, **30**, 6398-6400 (1997).
- [83] H. Tang, M. Radosz, Y. Shen, *AIChE Journal*, **55**, 737-746 (2009).
- [84] V. Percec, A. V. Popov, E. Ramirez-Castillo, L. A. Hinojosa-Falcon, *Journal of Polymer Science: Part A: Polymer Chemistry*, **43**, 2276-2280 (2005).
- [85] S. Coca, C. B. Jasieczek, K. L. Beers, K. Matyjaszewski, *Journal of Polymer Science Part A: Polymer Chemistry*, **36**, 1417-1424 (1998).
- [86] A. Muhlebach, S. G. Gaynor, K. Matyjaszewski, *Macromolecules*, **31**, 6046-6052 (1998).
- [87] K. Matyjaszewski, S. Coca, C. B. Jasieczek, *Macromolecular Chemistry and Physics*, **198**, 4011-4017 (1997).
- [88] K. A. Davis, K. Matyjaszewski, *Macromolecules*, **33**, 4039-4047 (2000).
- [89] J. Queffelec, S. G. Gaynor, K. Matyjaszewski, *Macromolecules*, **33**, 8629-8639 (2000).
- [90] T. Ando, M. Kamigaito, M. Sawamoto, *Tetrahedron*, **53**, 15445-15457 (1997).
- [91] M. Destarac, K. Matyjaszewski, B. Boutevin, *Macromolecular Chemistry and Physics*, **201**, 265-272 (2000).
- [92] W. Tang, K. Matyjaszewski, *Macromolecules*, **40**, 1858-1863 (2007).
- [93] T-L. Wang, Y-Z. Liu, B-C. Jeng, Y-C. Cai, *Journal of Polymer Research* **12**, 67-75 (2005).
- [94] J. Parvole, G. Laruelle, C. Guimon, J. Francois, L. Billon, *Macromolecular Rapid Communication*, **24**, 1074-1078 (2003).
- [95] M. Kato, M. Kamigaito, M. Sawamoto, T. Higashimura, *Macromolecules*, **28**, 1721-1723 (1996).

- [96] J.-S. Wang, K. Matyjaszewski, *The Journal of American Chemical Society*, **117**, 5614-5615 (1995).
- [97] T. Nishikawa, M. Kamigaito, M. Sawamoto, *Macromolecules*, **32**, 2204-2209 (1999).
- [98] A. Neumann, H. Keul, H. Hocker, *Macromolecular Chemistry and Physics*, **201**, 980-984 (2000).
- [99] H. Takahashi, T. Ando, M. Kamigaito, M. Sawamoto, *Macromolecules*, **32**, 3820-3823 (1999).
- [100] K. Min, H. Gao, K. Matyjaszewski, **127**, 3825-3830 (2005).
- [101] M. A. Nájera, L. E. Elizalde, Y. Vázquez, G. Santos, *Macromolecular Symposia*, **283-284**, 51-55 (2009).
- [102] Y. Zhang, Y. Wang, C. Peng, M. Zhong, W. Zhu, D. Konkolewicz, K. Matyjaszewski, *Macromolecules*, **45**, 78-86 (2012).
- [103] J. Mosnacek, M. Ilčíková, *Macromolecules*, **45**, 5859-5865 (2012).
- [104] T. Nishikawa, T. Ando, M. Kamigaito, M. Sawamoto, *Macromolecules*, **30**, 2244-2248 (1997).
- [105] T. Ando, M. Kato, M. Kamigaito, M. Sawamoto, *Macromolecules*, **29**, 1070-1072 (1996).
- [106] K. Matyjaszewski, S. M. Jo, H. Paik, S. G. Gaynor, *Macromolecules*, **30**, 6398-6400 (1997).
- [107] K. Matyjaszewski, M. Wei, J. Xia, N. E. McDermott, *Macromolecules*, **30**, 8161-8164 (1997).
- [108] V. Percec, H.-J. Kim, B. Barboiu, *Macromolecules*, **30**, 8526-8528 (1997).
- [109] V. Percec, B. Barboiu, T. K. Bera, M. Sluis, R. B. Grubbs, J. M. J. Frechet, *Journal of Polymer Science: Part A: Polymer Chemistry*, **38**, 4776-4791 (2000).
- [110] K. Matyjaszewski, H. Paik, P. Zhou, S. J. Diamanti, *Macromolecules*, **34**, 5125-5131 (2001).
- [111] A. Goto, T. Fukuda, *Macromolecular Rapid Communication*, **20**, 633-636 (1999).
- [112] K. Matyjaszewski, S. Gaynor, J.-S. Wang, *Macromolecules*, **28**, 2093-2095 (1995).
- [113] T. Ostu, *Journal of Polymer Science: Part A: Polymer Chemistry*, **38**, 2121-2136 (2000).
- [114] R. Nicolay, Y. Kwak, K. Matyjaszewski, *Macromolecules*, **41**, 4585-4596 (2008).
- [115] W. Zhang, C. Wang, D. Li, Q. Song, Z. Cheng, X. Zhu, *Macromolecular Symposia*, **261**, 23-31 (2008).

- [116] J. Cao, J. Chen, K. Zhang, Q. Shen, Y. Zhang, *Applied Catalysis A: General*, **311**, 76-78 (2006).
- [117] J. Chen, J. Chu, K. Zhang, *Polymer*, **45**, 151-155 (2004).
- [118] L. Zhang, Z. Cheng, S. Shi, Q. Li, X. Zhu, *Polymer*, **49**, 3054-3059 (2008).
- [119] M. Y. Khan, Z. Xue, D. He, S. K. Noh, W. S. Lyoo, *Polymer*, **51**, 69-74 (2010).
- [120] G. Barre, D. Taton, D. Lastecoueres, J.-M. Vincent, *The Journal of American Chemical Society*, **126**, 7764-7765 (2004).
- [121] J. K. Oh, K. Matyjaszewski, *Journal of Polymer Science: Part A: Polymer Chemistry*, **44**, 3787-3796 (2006).
- [122] Z. Hu, X. Shen, H. Qiu, G. Lai, J. Wu, W. Li, *European Polymer Journal*, **45**, 2313-2318 (2009).
- [123] N. V. Tsarevsky, W. Tang, S. J. Brooks, K. Matyjaszewski, *American Chemical Society Symposium Series*, **944**, 56-70 (2006).
- [124] Y. A. Kabachii, S. Y. Kochev, L. M. Bronstein, I. B. Blagodatskikh, P. M. Valetsky, *Polymer Bulletin*, **50**, 271-278 (2003).
- [125] E. L. Grogneec, J. Claverie, R. Poli, *The Journal of American Chemical Society*, **123**, 9513-9524 (2001).
- [126] S. Maria, F. Stoffelbach, J. Mata, J.-C. Daran, P. Richard, R. Poli, *The Journal of American Chemical Society*, **127**, 5946-5956 (2005).
- [127] Y. Kotani, M. Kamigaito, M. Sawamoto, *Macromolecules*, **32**, 2420-2424 (1999).
- [128] T. Ando, M. Kamigaito, M. Sawamoto, *Macromolecules*, **30**, 4507-4510 (1997).
- [129] M. Teodorescu, S. G. Gaynor, K. Matyjaszewski, *Macromolecules*, **33**, 2335-2339 (2000).
- [130] C. Uchiike, M. Ouchi, T. Ando, M. Kamigaito, M. Sawamoto, *Journal of Polymer Science: Part A: Polymer Chemistry*, **46**, 6819-6827 (2008).
- [131] F. Simal, A. Demonceau, A. F. Noels, *Angewandte Chemie International Edition*, **38**, 538-540, (1999).
- [132] W. A. Braunecker, Y. Itami, K. Matyjaszewski, *Macromolecules*, **38**, 9402-9404 (2005).
- [133] W. A. Braunecker, W. C. Brown, B. C. Morelli, W. Tang, R. Poli, K. Matyjaszewski, *Macromolecules*, **40**, 8576-8585 (2007).
- [134] V. Percec, B. Barboiu, A. Neumann, J. C. Ronda, M. Zhao, *Macromolecules*, **29**, 3665-3668 (1996).

- [135] B. Wang, Y. Zhuang, X. Luo, S. Xu, X. Zhou, *Macromolecules*, **36**, 9684-9686 (2003).
- [136] C. Granel, Ph. Dubois, R. Jerome, Ph. Teyssie, *Macromolecules*, **29**, 8576-8582 (1996).
- [137] H. Uegaki, Y. Kotani, M. Kamigaito, M. Sawamoto, *Macromolecules*, **30**, 2249-2253 (1997).
- [138] Ph. Lecomte, I. Drapier, Ph. Dubois, Ph. Teyssie, R. Jerome, *Macromolecules*, **30**, 7631-7633 (1997).
- [139] K. Matyjaszewski, *Chemical European Journal*, **5**, 3095-3102 (1999).
- [140] T. E. Patten, *Accounts of Chemical Research*, **32**, 895-903 (1999).
- [141] J. Xia, K. Matyjaszewski, *Macromolecules*, **30**, 7697-7700 (1997).
- [142] J. Xia, S. G. Gaynor, K. Matyjaszewski, *Macromolecules*, **31**, 5958-5959 (1998).
- [143] L. Zhang, Q. Xu, J. Lu, X. Xia, L. Wang, *European Polymer Journal*, **43**, 2718-2724 (2007).
- [144] L. Zhang, Q.-F. Xu, J.-M. Lu, N.-J. Li, F. Yan, L.-H. Wang, *Polymer*, **23**, 4807-4812 (2009).
- [145] D. M. Haddleton, C. B. Jasieczek, M. J. Hannon, A. J. Shooter, *Macromolecules*, **30**, 2190-2193 (1997).
- [146] Z. Xue, N. T. B. Linh, S. K. Noh, W. S. Lyoo, *Angewandte Chemie International Edition*, **47**, 6426-6429 (2008).
- [147] Y. Kotani, M. Kamigaito, M. Sawamoto, *Macromolecules*, **32**, 6877-6880 (1999).
- [148] G. Moineau, Ph. Dubois, R. Jerome, T. Senninger, Ph. Teyssie, *Macromolecules*, **31**, 545-547 (1998).
- [149] W. Jakubowski, K. Matyjaszewski, *Macromolecules*, **38**, 4139-4146 (2005).
- [150] R. Luo, A. Sen, *Macromolecules*, **41**, 4514-4518 (2008).
- [151] K. Min, W. Jakubowski, K. Matyjaszewski, **27**, 594-598 (2006).
- [152] J. K. Oh, K. Min, K. Matyjaszewski, *Macromolecules*, **39**, 3161-3167 (2006).
- [153] Y. Gnanou, G. Hizal, *Journal of Polymer Science: Part A: Polymer Chemistry*, **42**, 351-359 (2004).
- [154] H. Mert, U. Tunca, G. Hizal, *Journal of Polymer Science: Part A: Polymer Chemistry*, **44**, 5923-5932 (2006).
- [155] H. Tang, M. Radosz, Y. Shen, *Macromolecular Rapid Communications*, **27**, 1127-1131 (2006).

- [156] T. Sato, K. Morino, H. Tanaka, T. Ota, *European Polymer Journal*, **25**, 1281-1284 (1989).
- [157] M. C. Galanti, A. V. Galanti, *The Journal of Organic Chemistry*, **47**, 1572-1574 (1982).
- [158] A. V. Galanti, *Journal of Polymer Science: Polymer Chemistry Edition*, **19**, 2243-2253 (1981).
- [159] A. V. Galanti, *Journal of Polymer Science: Polymer Chemistry Edition*, **19**, 451-475 (1981).
- [160] A. V. Galanti, F. Iotta, B. T. Keen, D. Scole, *Journal of Polymer Science: Polymer Chemistry Edition*, **20**, 233-239 (1982).
- [161] T. M. Pyriadi, M. Fraih, *Journal of Macromolecular Science: Part A-Chemistry: Pure and Applied Chemistry*, **18**, 159-172 (1982).
- [162] N. A. Mohamed, W. Al-Magrihi, *Polymer Degradation and Stability*, **80**, 275-291, (2003).
- [163] A. S. Abdel-Naby, *Journal of Applied Polymer Science*, **121**, 169-175 (2011).
- [164] T. Oishi, T. Kawamoto, *Polymer Journal*, **26**, 920-929 (1994).
- [165] T. Oishi, K. Nagai, T. Kawamoto, H. Tsutsumi, *Polymer*, **37**, 3131-3139 (1996).
- [166] N. A. Mohamed, W. Al-Magrihi, *Polymer Degradation and Stability*, **78**, 149-165 (2002).
- [167] R. Chauhan, V. Choudhary, *Journal of Applied Polymer Science*, **112**, 1088-1095 (2009).
- [168] J. M. G. Cowie, V. M. C. Reid, I. J. McEwen, *British Polymer Journal*, **23**, 353-357 (1990).
- [169] A. Matsumoto, S. Umehara, H. Watanabe, T. Otsu, *Journal of Polymer Science Part B: Polymer Physics*, **31**, 505-618 (1993).
- [170] N. A. Mohamed, W. Al-Magrihi, *Polymer Degradation and Stability*, **82**, 421-433, (2003).
- [171] V. Anand, R. Kumar, V. Choudhary, *Journal of Applied Polymer Science*, **91**, 2016-2027 (2004).
- [172] M. Grigoras, G. Colotin, N. C. Antonoaia, *Polymer International*, **53**, 1321-1326 (2004).
- [173] T. Sato, A. Takarada, H. Tanaka, T. Ota, *Die Makromolekulare Chemie*, **192**, 2231-2241 (1991).

- [174] R. Chauhan, V. Choudhary, *Journal of Applied Polymer Science*, **101**, 2391-2398, (2006).
- [175] B. B. Noble, M. L. Coote, *International Reviews in Physical Chemistry*, **32**, 467-513 (2013).
- [176] D. J. Hill, J. H. O'Donnell, P. W. O'Sullivan, *Polymer*, **25**, 569-573 (1984).
- [177] A. L. Burke, T. A. Duever, Alexander Penlidis, *Industrial & Engineering Chemistry Research*, **36**, 1016-1035 (1997).
- [178] A. L. Burke, T. A. Duever, Alexander Penlidis, *Macromolecules*, **27**, 386-399 (1994).
- [179] A. Kaim, P. Oracz, *Polymer*, **38**, 2221-2228 (1997).
- [180] A. Kaim, P. Oracz, *e-Polymers*, **23**, 1-10 (2003).
- [181] P. C. Deb, *Polymer*, **46**, 6235-6242 (2005).
- [182] A. Bulai, M. L. Jimeno, J. S. Roman, *Macromolecules*, **28**, 7363-7369 (1995).
- [183] A. S. Brar, M. Malhotra, *Journal of Applied Polymer Science*, **67**, 417-426 (1998).
- [184] E. A. Tonelli, F. C., Schilling, *Accounts of Chemical Research*, **14**, 233-238 (1981).
- [185] M. D. Bruch, *Macromolecules*, **21**, 2707-2713 (1988).
- [186] M. D. Bruch, F. A. Bovey, R. E. Cais, *Macromolecules*, **17**, 2547-2551 (1984).
- [187] A. S. Brar, K. Dutta, G. S. Kapur, *Macromolecules*, **28**, 8735-8741 (1995).
- [188] A. S. Brar, M. Malhotra, *Macromolecules*, **29**, 7470-7476 (1996).
- [189] C. Hijangos, D. Lopez, *Macromolecules*, **28**, 1364-1369 (1995).
- [190] M. Dube, R. A. Sanyer, A. Penlidis, K. F. O'Driscoll, P. M. Reilley, *Journal of Polymer Science: Part A: Polymer Chemistry*, **29**, 703-708 (1991).
- [191] R. Chauhan, V. Choudhary, *Journal of Applied Polymer Science*, **115**, 491-497 (2010).
- [192] B. Gacal, H. Durmaz, M. A. Tasdelen, G. Hizal, U. Tunca, Y. Yagci, A. L. Demirel, *Macromolecules*, **39**, 5330-5336 (2006).
- [193] S. Butz, H. Baethge, G. Schmidt-Naake, *Macromolecular Chemistry and Physics*, **16**, 2143-2151 (2000).
- [194] Q. Liu, Y. Chen, *Macromolecular Chemistry and Physics*, **208**, 2455-2462 (2007).
- [195] J. Weiss, A. Li, E. Wischerhoff, A. Laschewsky, *Polymer Chemistry*, **3**, 352-361 (2012).
- [196] J. Wei, Z. Zhu, J. Huang, *Journal of Applied Polymer Science*, **94**, 2376-2382 (2004).

- [197] J. Weiss, A. Laschewsky, *Macromolecules*, **45**, 4158-4165 (2012).
- [198] K. Satoh, M. Matsuda, K. Nagai, M. Kamigaito, *The Journal of American Chemical Society*, **132**, 10003-10005 (2010).
- [199] P. Yang, L. P. D. Ratcliffe, S. P. Armes, *Macromolecules*, **46**, 8545-8556 (2013).
- [200] M. P. Robin, S. A. M. Osborne, Z. Pikramenou, J. E. Raymond, R. K. O'Reilly, *Macromolecules*, **49**, 653-662 (2016).
- [201] M.-A. Berthet, Z. Zarafshani, S. Pfeifer, J.-F. Lutz, *Macromolecules*, **43**, 44-50 (2010).
- [202] J.-F. Lutz, B. V. K. J. Schmidt, S. Pfeifer, *Macromolecular Rapid Communication*, **32**, 127-135 (2011).
- [203] G.-Q. Chen, Z.-Q. Wu, J.-R. Wu, Z.-C. Li, F.-M. Li, *Macromolecules*, **33**, 232-234 (2000).
- [204] T. Cakir, I. E. Serhatli, A. Onen, *Journal of Applied Polymer Science*, **99**, 1993-2001 (2006).
- [205] Y. Cao, Y. Hong, G. Zhai, D. Zhang, Y. Song, Q. Yu, Q. Ren, B. Jiang, *Polymer International*, **57**, 1090-1100 (2008).
- [206] R. Qiang, G. Fanghong, J. Bibiao, Z. Dongliang, F. Jianbo, G. Fudi, *Polymer*, **47**, 3382-3389 (2006).
- [207] X. Jiang, D. Yan, Y. Zhong, W. Liu, Q. Chen, *Polymer International*, **49**, 893-897 (2000).
- [208] G. Mantovani, F. Lecolley, L. Tao, D. M. Haddleton, J. Clerx, J. J. L. M. Cornelissen, K. Velonia, *The Journal of American Chemical Society*, **127**, 2966-2973 (2010).
- [209] G. C Pizarro, O. G Marambio, M. Jeria-Orell, D. T Valdesa, K. E Geckelerb, *Polymer International*, **62**, 1528-1538 (2013).
- [210] T. Hagiwara, K. Isono, S.-I. Imamura, S. Toyama, H. Hamana, T. Narita, *Macromolecules*, **29**, 4473-4477 (1996).
- [211] A. Matsumoto, S. Umehara, H. Watanabe, T. Otsu, *Journal of Polymer Science Part B: Polymer Physics*, **31**, 527-535 (1993).
- [212] T. Oishi, K. Onimura, W. Sumida, T. Koyanagi, H. Tsutsumi, *Polymer Bulletin*, **48**, 317-325 (2002).
- [213] K. Satoh, D.-H. Lee, K. Nagai, M. Kamigaito, *Macromolecular Rapid Communications*, **35**, 161-167 (2014).

- [214] H. Fischer, L. Radom, *Angewandte Chemie International Edition*, **40**, 1340-1371 (2001).
- [215] E. Mavroudakis, D. Cuccato, D. Moscatelli, *Polymers*, **7**, 1789-1819 (2015).
- [216] B. M. Rosen, V. Percec, *Journal of Polymer Science: Part A: Polymer Chemistry*, **45**, 4950-4964 (2007).
- [217] N. H. Nguyen, B. M. Rosen, V. Percec, *Journal of Polymer Science Part A: Polymer Chemistry*, **49**, 1235-1247 (2011).
- [218] I. Degirmenci, V. Aviyente, V. V. Speybroeck, M. Waroquier, *Macromolecules*, **42**, 3033-3041 (2009).
- [219] X. Yu, J. Pfaendtner, L. J. Broadbelt, *The Journal of Physical Chemistry A*, **112**, 6772-6782 (2008).
- [220] C. Y. Lin, E. I. Izgorodina, M. L. Coote, *Macromolecules*, **43**, 553-560 (2010).
- [221] E. Mavroudakis, K. Liang, D. Moscatelli, R. A. Hutchinson, *Macromolecular Chemistry and Physics*, **213**, 1706-1716 (2012).
- [222] M. Dossi, G. Storti, D. Moscatelli, *Macromolecular Symposia*, **302**, 16- (2011).
- [223] D. Moscatelli, M. Dossi, C. Cavallotti, G. Storti, *The Journal of Physical Chemistry A*, **115**, 52-62 (2011).
- [224] T. Junkers, S.P.S. Koo, C. Barner-Kowollik, *Polymer Chemistry*, **1**, 438-441 (2010).
- [225] D. Cuccato, M. Dossi, D. Moscatelli, G. Storti, *Macromolecular Reaction Engineering*, **6**, 330-345 (2012).
- [226] T. Fukuda, Y.-D. Ma, H. Inagaki, *Macromolecules*, **18**, 17-26 (1985).
- [227] M. C. Piton, M. A. Winnik, T. P. Davis, K. F. O'driscoll, *Journal of Polymer Science: Part A: Polymer Chemistry*, **28**, 2097-2106 (1990).
- [228] M. L. Coote, T. P. Davis, *Progress in Polymer Science*, **24**, 1217-1251 (1999).
- [229] J. P. A. Heuts, R. G. Gilbert, I. A. Maxwell, *Macromolecules*, **30**, 726-736 (1997).
- [230] G. E. Roberts, M. L. Coote, J. P. A. Heuts, L. M. Morris, T. P. Davis, *Macromolecules*, **32**, 1332-1340 (1999).
- [231] J. Tomasi, B. Mennucci, and R. Cammi, *Chemical Reviews*, **105**, 2999-3093 (2005).
- [232] C. J. Cramer, *Essentials of Computational Chemistry: Theories and Models*, John Wiley and Sons Ltd. England, 2nd Edition, (2004).
- [233] B. Ensing, M. de Vivo, Z. Liu, P. Moore, M. L. Klein, *Accounts of Chemical Research*, **39**, 73-81 (2006).

- [234] R. Arnaud, R. Subra, V. Barone, F. Lelj, S. Olivella, A. Sole, N. Russo, *Journal of the Chemical Society, Perkin Transactions 2*, **2**, 1517-1524 (1986).
- [235] J. J. P. Stewart, *Journal of Computational Chemistry*, **2**, 209-220 (1989).
- [236] S. Mohr, L. E. Ratcliff, P. Boulanger, L. Genovese, D. Caliste, T. Deutsch, S. Goedecker, *The Journal of Chemical Physics*, **140**, 204110-16 (2014).
- [237] P. Hohenberg, W. Kohn, *Physical Review*, **136**, B864-871 (1964).
- [238] E. Lewars, *Computational Chemistry*, Kluwer Academic Publishers, Boston, United States, Chapter 7, pp. 385-399 (2003).
- [239] W. Kohn, L. J. Shan, *Physical Review*, **140**, A1133 (1965).
- [240] D. R. Yarkony (editor), *Modern Electronic Structure Theory, Part I & II*, World Scientific Publishing Co. Pte. Ltd. pp. 725-1022 (1995).
- [241] R. O. Jones, *Reviews of Modern Physics*, **87**, 897-923 (2015).
- [242] L. A. Montero, L.A. Diaz, R. Bader (eds.), *Introduction to Advanced Topics of Computational Chemistry*, Editorial de la Universidad de La Habana, Havana, chapter 3, pp. 41-70 (2003).
- [243] S. Huzinaga, J. Andzelm, E. Radzio-Andzelm, Y. Sakai, H. Tatewaki, M. Klobukowski, *Gaussian Basis Sets for Molecular Calculations, Volume 16*, 1st Edition, Elsevier Science (1983).
- [244] C. C. Price, E. C. Coyner, *Journal of the American Chemical Society*, **62**, 1306-1306 (1940).
- [245] O. Cakmak, I. Kahveci, I. Demirtas, T. Hökelek, K. Smith, *Collection of Czechoslovak Chemical Communications*, **65**, 1791-1804 (2000).
- [246] Gaussian 09, Revision B.01, M. J. Frisch, G. W. Trucks, H. B. Schlegel, G. E. Scuseria, M. A. Robb, J. R. Cheeseman, G. Scalmani, V. Barone, B. Mennucci, G. A. Petersson, H. Nakatsuji, M. Caricato, X. Li, H. P. Hratchian, A. F. Izmaylov, J. Bloino, G. Zheng, J. L. Sonnenberg, M. Hada, M. Ehara, K. Toyota, R. Fukuda, J. Hasegawa, M. Ishida, T. Nakajima, Y. Honda, O. Kitao, H. Nakai, T. Vreven, J. A. Montgomery, Jr., J. E. Peralta, F. Ogliaro, M. Bearpark, J. J. Heyd, E. Brothers, K. N. Kudin, V. N. Staroverov, T. Keith, R. Kobayashi, J. Normand, K. Raghavachari, A. Rendell, J. C. Burant, S. S. Iyengar, J. Tomasi, M. Cossi, N. Rega, J. M. Millam, M. Klene, J. E. Knox, J. B. Cross, V. Bakken, C. Adamo, J. Jaramillo, R. Gomperts, R. E. Stratmann, O. Yazyev, A. J. Austin, R. Cammi, C. Pomelli, J. W. Ochterski, R. L. Martin, K. Morokuma, V. G. Zakrzewski, G. A. Voth, P. Salvador, J. J. Dannenberg, S. Dapprich,

- A. D. Daniels, O. Farkas, J. B. Foresman, J. V. Ortiz, J. Cioslowski and D. J. Fox, Gaussian, Inc., Wallingford CT, (2010).
- [247] I. N. Levine, Physical Chemistry, Tata McGraw-Hill Companies, Inc. New York, 6th Edition, Chapter-16, pp 515-579 (2011).
- [248] F. W. Billmeyer, Textbook of Polymer Science, John Wiley and Sons (Asia) Pte. Ltd. Singapore, 3rd Edition, Chapter-5, pp-101-125 (2008).
- [249] P. Król, P. Chmielarz, eXPRESS Polymer Letters, **7**, 249-260 (2013).
- [250] U. Ali, K. J. Karim, N. A. Buang, Polymer Reviews, **55**, 678-705 (2015).
- [251] P. Galka, J. Kowalonek, H. Kaczmarek, The Journal of Thermal Analysis and Calorimetry, **115**, 1387-1394 (2014).
- [252] O. Altintas, T. Josse, M. Abbasi, J. De Winter, V. Trouillet, P. Gerbaux, M. Wilhelm, C. Barner-Kowollik, Polymer Chemistry, **6**, 2854-2868 (2015).
- [253] R. Katiyar, D. S. Bag, I. Nigam, Thermochemica Acta, **557**, 55-60 (2013).
- [254] E. O. Stejskal, J. E. Tanner, The Journal of Chemical Physics, **42**, 288-292 (1965).
- [255] D. Wu, A. Chen, C.S. Johnson Jr., Journal of Magnetic Resonance, Series A, **115**, 123-126 (1995).
- [256] C.S. Johnson Jr., Progress in Nuclear Magnetic Resonance Spectroscopy, **34**, 203-256, (1999).
- [257] H. H. Schuh, H. Fischer, Helvetica Chimica Acta, **61**, 2130-2164 (1978).
- [258] J. H. Gorrell, J. T. Dubois, Transactions of the Faraday Society, **63**, 347-354 (1967).
- [259] In-C. Yeh, G. Hummer, The Journal of Physical Chemistry B, **108**, 15873-15879 (2004).
- [260] P. S. Pregosin, P. G. Anil Kumar, I. Fernandez, Chemical Reviews, **105**, 2977-2998 (2005).
- [261] J. B. Foresman, A. Frisch, Exploring chemistry with electronics structure methods, Gaussian, Inc. Pittsburgh, 2nd edition, pp. 64 (1996).
- [262] C. E. Moore, Atomic Energy Levels, US Government Printing Office, Washington, DC, Vols. I-III, (1952).
- [263] S. Miertus, E. Scrocco, J. Tomasi, Chemical Physics, **55** 117-129 (1981).
- [264] P. Atkins, J. de Paula, Physical Chemistry, W. H. Freeman and Company, United States, 9th Edition, pp. 217 (2010).
- [265] A. L. Burke, T. A. Duever, A. Penlidis, Macromolecular Theory and Simulations, **3**, 1005-1031 (1994).

- [266] C. Peng, P. Y. Ayala, H. B. Schlegel, *Journal of Computational Chemistry*, **17**, 49-56 (1996).
- [267] A. Fernandez-Ramos, J. A. Miller, S. J. Klippenstein, *Chemical Reviews*, **106**, 4518-4584 (2006).
- [268] X. Yu, S. E. Levine, L. J. Broadbelt, *Macromolecules*, **41**, 8242-8251 (2008).
- [269] S. Beuermann, M. Buback, T. P. Davis, R. G. Gilbert, R. A. Hutchinson, A. Kajiwara, B. Klumperman, G. T. Russell, *Macromol. Chemical Physics*, **201**, 1355-1364 (2000).
- [270] C. Y. Lin, M. L. Coote, A. Petit, P. Richard, R. Poli, K. Matyjaszewski, *Macromolecules*, **40**, 5985-5994 (2007).

Appendix – i

LIST OF PUBLICATIONS

Manuscript Published/ Accepted in Peer-Reviewed Journal Counted in Thesis:

- 1) C. Deoghare, V. S. Nadkarni, R. N. Behera, R. Chauhan, “Synthesis and characterization of copolymers of methyl methacrylate with *N*-arylitaconimides via AGET-ATRP”, *Journal of Polymer Materials - An International Journal*, **34**, 455-466 (2017).
- 2) C. Deoghare, C. Baby, V. S. Nadkarni, R. N. Behera, R. Chauhan, “Synthesis, characterization, and computational study of potential itaconimide-based initiators for atom transfer radical polymerization”, *RSC Advances*, **4**, 48163-48178 (2014).

Conference Attended and Presented the Poster

- 1) C. Deoghare, V. S. Nadkarni, R. N. Behera, and R. Chauhan, “Synthesis and Characterization of Block Copolymers of *N*-arylitaconimide Monomers and Methyl Methacrylate” Royal Society of Chemistry (UK) West India Chapter Symposium on Recent Advances in Chemical Sciences and Research Scholars Meet – 2016, November 13, 2016, BITS, Pilani - K. K. Birla Goa Campus, Goa, India.
- 2) C. Deoghare, V. S. Nadkarni, R. N. Behera, and R. Chauhan, “Block Copolymers of *N*-arylitaconimide Monomers and Methyl Methacrylate” International Conference on Macromolecules: Synthesis, Morphology, Processing, Structure, Properties and Applications, May 13-15, 2016, Mahatma Gandhi University, Kottayam, Kerala, India.
- 3) C. Deoghare, V. S. Nadkarni, R. N. Behera, and R. Chauhan, “Copolymerization of *N*-(4-methoxyphenyl)itaconimide and *N*-(4-chlorophenyl)itaconimide with MMA via AGET-ATRP” National Conference on New Frontiers in Chemistry From Fundamentals to Applications, December 18-19, 2015, Department of Chemistry, BITS, Pilani - K. K. Birla Goa Campus, Goa, India.

4) C. Deoghare, C. Baby, R. N. Behera and R. Chauhan, "Effect of Structure, Solvent and Temperature on Equilibrium Constant of Atom Transfer Radical Polymerization for Bromosubstituted Succinimides" 17th CRSI National Symposium in Chemistry, February 06-08, 2015, CSIR-NCL, Pune, India.

5) C. Deoghare, R. N. Behera and R. Chauhan, "A Computational Study on the Propagation Kinetics of Atom Transfer Radical Polymerization of Itaconimide and Methyl Methacrylate", 14th Theoretical Chemistry Symposium, December 18-21, 2014, CSIR- NCL, Pune, India.

6) C. Deoghare, R. N. Behera and R. Chauhan, "A Computational Study of Homolytic Bond Dissociation Process Involved in the Initiation Process of Atom Transfer Radical Polymerization", 16th CRSI National Symposium in Chemistry, February 6-9, 2014, IIT Mumbai, India.

7) C. Deoghare, R. N. Behera and R. Chauhan, "Controlled Radical Polymerization of *N*-phenylitaconimide with Methyl Methacrylate: Experimental and Theoretical Study", 3rd FAPS Polymer Congress MACRO 2013, May 15-18, 2013, Bangalore, India.

Appendix – ii

BRIEF BIOGRAPHY OF THE CANDIDATE

Name	Chetana Anand Deoghare
Date of Birth	03-12-1984
Education	M. Sc. (Inorganic Chemistry), 2008 RTM Nagpur University, Nagpur, Maharashtra, India. B. Sc. (Chemistry, Botany, Environmental Science), 2006 Institute of Science, RTM Nagpur University, Nagpur, Maharashtra, India.
Email ID	p2010435@goa.bits-pilani.ac.in, chetskm@gmail.com

Research Experience

1. Worked as Institute Research Fellow in the Department of Chemistry, BITS, Pilani - K. K. Birla Goa Campus, Goa. Supervisor: Dr. Rashmi Chauhan (August 2016-October 2016).
2. Worked as Council of Scientific and Industrial Research-Senior Research Fellow, in the Department of Chemistry, BITS, Pilani - K. K. Birla Goa Campus, Goa. Supervisor: Dr. Rashmi Chauhan (October 2015-July 2016).
3. Worked as Institute Research Fellow in the Department of Chemistry, BITS, Pilani - K. K. Birla Goa Campus, Goa. Supervisor: Dr. Rashmi Chauhan (December 2012-September 2015).
4. Worked as Senior Research Fellow, Department of Science and Technology, India, sponsored project, in the Department of Chemistry, BITS, Pilani - K. K. Birla Goa Campus, Goa. PI: Dr. Rashmi Chauhan (July 2012-November 2012).
5. Worked as Junior Research Fellow, Department of Science and Technology, India, sponsored project, in the Department of Chemistry, BITS, Pilani - K. K. Birla Goa Campus, Goa. PI: Dr. Rashmi Chauhan (July 2010-June 2012).

No. of Publications: The list is given in *Appendix i*.

Appendix – iii

BRIEF BIOGRAPHY OF THE SUPERVISOR

Name	Dr. Rashmi Chauhan
Present Position	Assistant Professor, Department of Chemistry, BITS, Pilani - K. K. Birla Goa Campus
Address	B-315, BITS, Pilani - K. K. Birla Goa Campus NH 17B, By Pass Road, Zuarinagar, Goa – 403726, India
Email	rchauhan@goa.bits-pilani.ac.in, rashmiiitd@yahoo.co.in URL: http://universe.bits-pilani.ac.in/goa/rchauhan/profile
Education	Ph.D. (2006) in Polymer Science and Engineering, Indian Institute of Technology, Delhi, New Delhi, India. (Advisor = Prof. Veena Choudhary). M.Sc. Chemistry, (2000) Delhi University, Delhi, India. B.Sc. (Hons.) Chemistry, (1998) Delhi University, Delhi, India.

Completed Project

“Novel initiators for the controlled radical polymerization of *N*-arylitaconiamic acid/itaconimide monomers” (June 2010-November 2012).

Funding agency = Department of Science and Technology, New Delhi, India (Grant No. SR/ FT/ CS-053/ 2009).

Publications

Books

1. Rashmi Chauhan (2014), “Copolymers with Improved Thermal Stability” Publisher Scholar’s Press, ISBN-13: 978-3639664850

In Peer-Reviewed Journals

1. C. Deoghare, C. Baby, V. S. Nadkarni, R. N. Behera, R. Chauhan, Synthesis, characterization, and computational study of potential itaconimide-based initiators for atom transfer radical polymerization, *RSC Advances*, **4**, 48163-48178 (2014).
2. R. Chauhan, V. Choudhary, Microstructure determination of methyl methacrylate-*N*-arylsubstituted itaconimide copolymers by NMR spectroscopy, *Journal of Applied Polymer Science*, **115**, 491-497 (2010).
3. R. Chauhan, V. Choudhary, Thermal and mechanical properties of copolymers of methyl methacrylate with *N*-aryl Itaconimides, *Journal of Applied Polymer Science*, **112**, 1088-1095 (2009).
4. R. Chauhan, V. Choudhary, Copolymerization of MMA with *N*-(methoxyphenyl) itaconimides: Effect of position of substituent on monomer reactivity ratio and thermal behaviour, *Journal of Applied Polymer Science*, **109**, 987-996 (2008).
5. R. Chauhan, V. Choudhary. Effect of substituents on copolymerization of *N*-arylsubstituted itaconamic acid/ itaconimide with methyl methacrylate: Reactivity ratio and thermal behaviour, *Journal of Applied Polymer Science*, **101**, 2391-2398, (2006).
6. I. K. Varma, V. Choudhary, B. Gaur, B. Lochab, S. Oberoi, R. Chauhan, Curing and thermal behaviour of Poly(allyl azide) and bismaleimides, *Journal of Applied Polymer Science*, **101**, 779-786 (2006).
7. R. Chauhan, V. Choudhary, Copolymerization of *N*-(4-carboxyphenyl) itaconimide or *N*-(4-carboxyphenyl) itaconamic acid with methyl methacrylate, *Journal of Applied Polymer Science*, **98**, 1909-1915 (2005).

Appendix – iv

BRIEF BIOGRAPHY OF THE CO-SUPERVISOR

Name	Dr. R. N. Behera
Present Position	Associate professor, Department of Chemistry, BITS, Pilani - K. K. Birla Goa Campus.
Address	B-311, BITS, Pilani - K. K. Birla Goa Campus NH 17B, By Pass Road, Zuarinagar, Goa – 403726, India
Email	rbehera@goa.bits-pilani.ac.in, raghu_behera@yahoo.com
Education	Ph. D. Chemistry, IIT Kanpur, 2001, Advisor: Professor Pinaki Gupta-Bhaya. M. Sc. Chemistry, (1989) P.G. Dept. of Chemistry, Sambalpur University, India. B. Sc. (Hons. & Distinction), (1987), Sambalpur University, India.

Post-Doctoral Experience

1. Scientific coworker, University of Heidelberg, Germany (Aug 2002-Nov 2003).
2. Post-doctoral Fellow, University of California, Davis, USA (Dec 1999-Jun 2002).

Teaching & Research Interest:

Teaching interests are Physical chemistry and theoretical Inorganic chemistry. Current research includes statistical mechanics of macroionic solution, Integral equation theory of fluid, Molecular modeling & simulation, Combining Quantum-Classical Calculations in studying Enzyme function, Electronic structure calculations, Secondary Interactions, Atom-transfer radical polymerization

Completed Project

1. “Study of effective interactions in charged colloidal suspensions” Duration: 2012-2015, Funding Agency: CSIR, India.

Ongoing Sponsored Projects

1. "Computational Study of the Catalytic Mechanism of some Diaryldiselenide-based Glutathione Peroxidase Mimetics" Duration: (2017 – 2020), Funding Agency: SERB, India.
2. "Experimental and Computational Study of Boron Doped TiO₂ and ZnONanocrystals", Duration: (2017 – 2020), Funding Agency: SERB, India (with Dr. K. P. Jayadevan as PI).

Representative Publications

1. Uday Kumar Padidela and Raghu Nath Behera, Interactions in charged colloidal suspensions: A molecular dynamics simulation study, AIP Conference Proceedings, **1859**, 020111 (2017).
2. G. Anderson, R. N. Behera, R. Gomatam, "A Theoretical Approach to Engineering a New Enzyme", Journal of Physics: Conference Series, **738**, 012013 (2016).
3. C. Deoghare, C. Baby, V. S. Nadkarni, R. N. Behera, R. Chauhan, "Synthesis, characterization and computational study of potential itaconimide-based initiators for atom transfer radical polymerization", RSC Advances, **4**, 48163-48176 (2014).
4. A. Panda, R. N. Behera, Comparative study of E...N (E = Se/Te) intramolecular interactions in organochalcogen compounds using density functional theory, Journal of Hazardous Materials, **269**, 2-8 (2014).
5. R. Yogesh, R. N. Behera, Comparison of binding affinities and ADMET properties of lysine sulfonamide and cyclic urea derivatives with commercial HIV protease inhibitors for the MDR mutants, International Journal of Chemistry, **1**, 178-188 (2012).
6. D. Sengupta, R. Behera, J. C. Smith, G. M. Ullmann, "The α -helix dipole – screened Out?", Structure, **13**(6), 849-855 (2005).

7. R. Behera, On the calculation of thermodynamic properties of electrolyte solutions from Kirkwood-Buff theory, *Journal of Chemical Physics*, **108**, 3373-3374 (1998).

Appendix – v

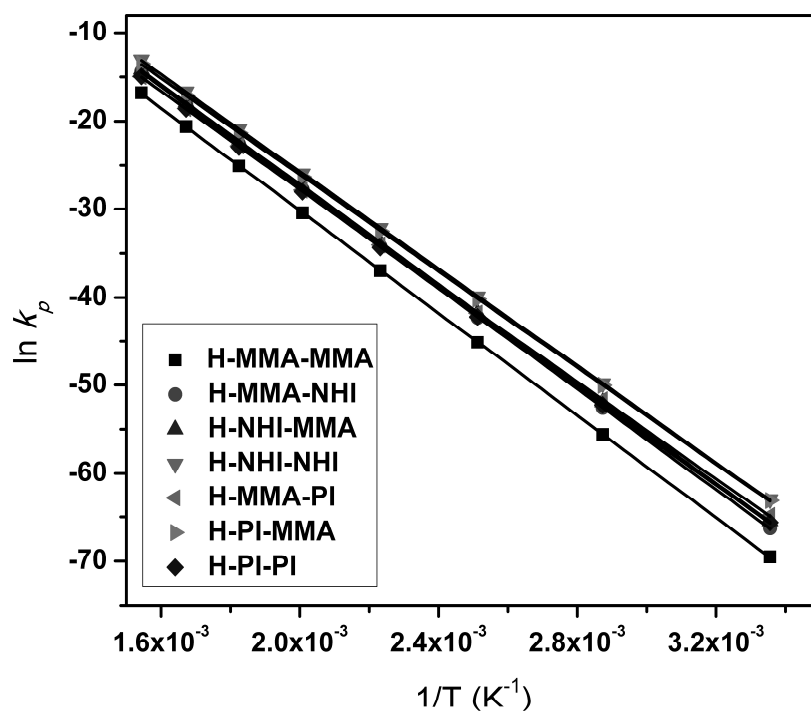
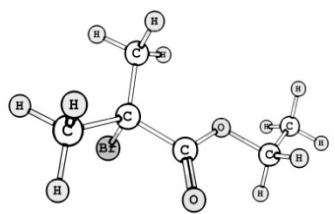
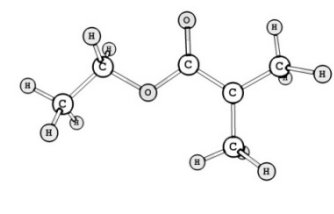
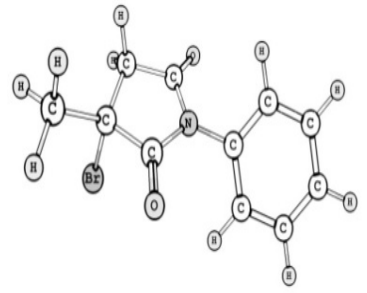
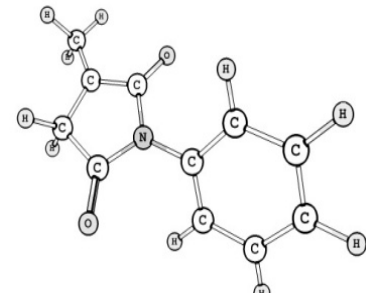
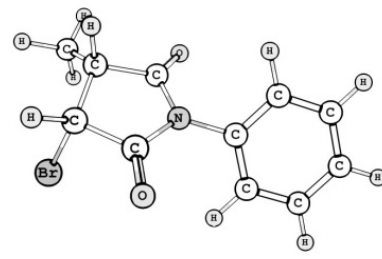
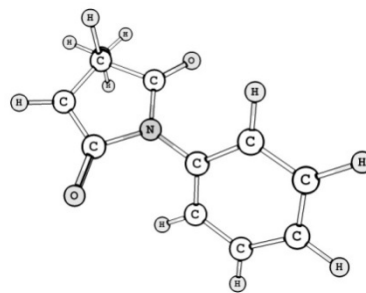
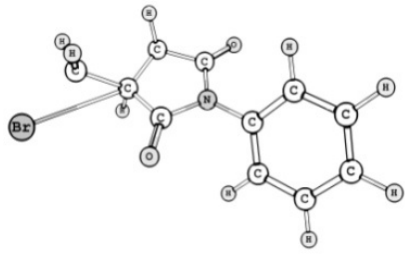
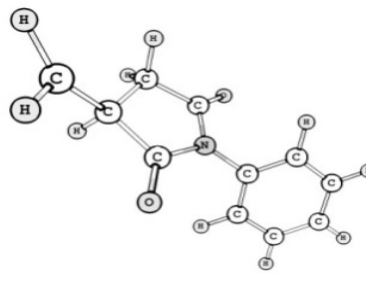
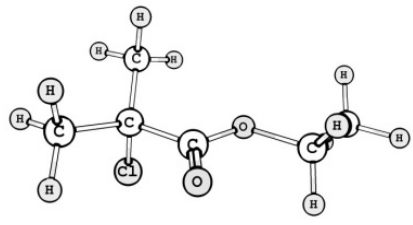
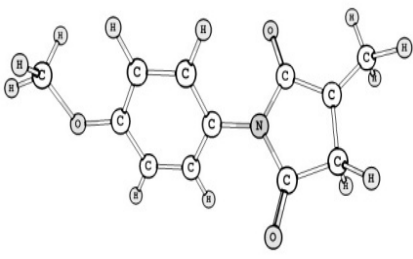
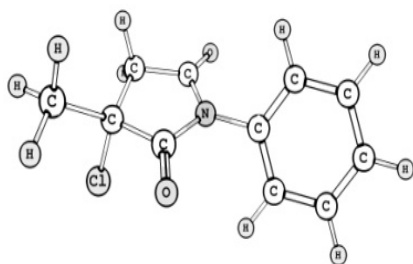


Figure A1: Plot of $\ln k_p$ vs $1/T$ for various dimer radical in anisole.

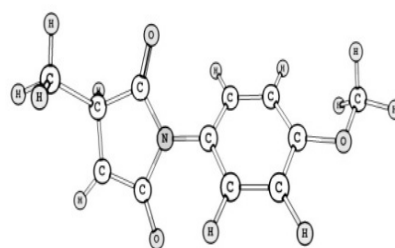
Table A1: B3LYP/ 6-31+G(d)/ LanL2DZ optimized geometries (gas phase) of studied alkyl halides (R-X) and its radicals (R \cdot) in gas phase at 25 °C.

Designation of R-X	Optimized geometry of R-X	Designation of radicals	Optimized geometry of radicals
4-Br		Rad_4	
3a-Br		Rad_3a	
2a-Br		Rad_2a	
1a-Br		Rad_1a	
4-Cl		Rad_3c	

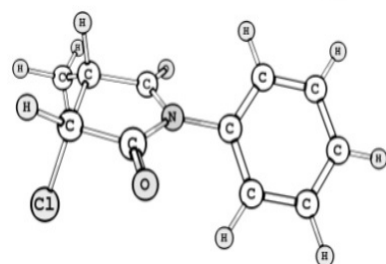
3a-Cl



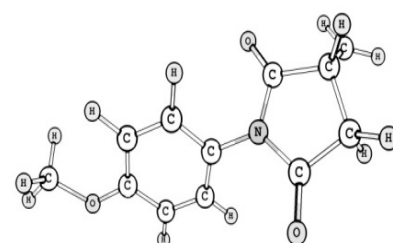
Rad_2c



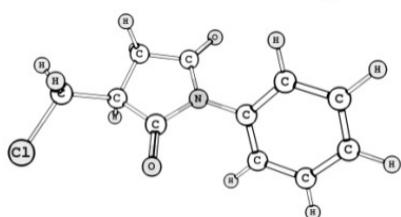
2a-Cl



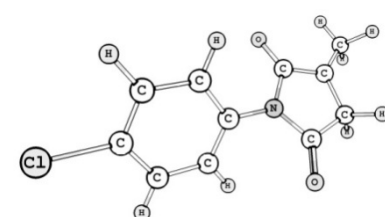
Rad_1c



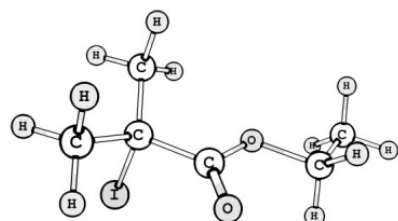
1a-Cl



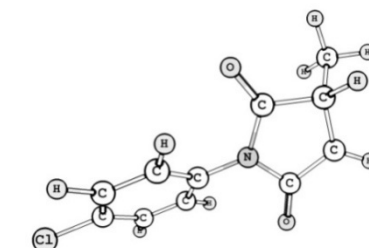
Rad_3d



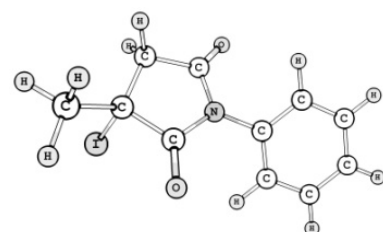
4-I



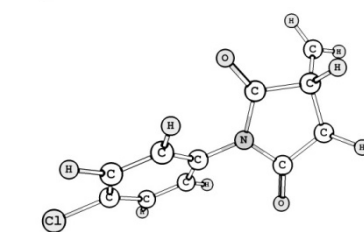
Rad_2d



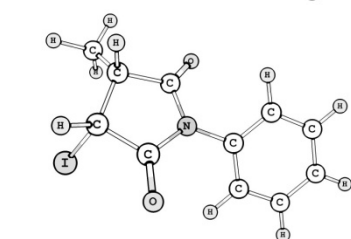
3a-I



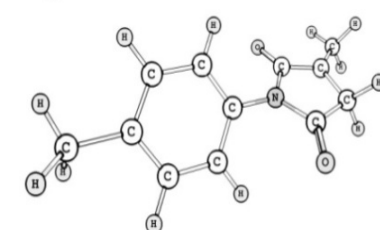
Rad_1d



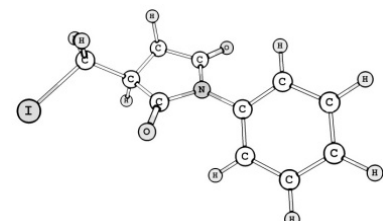
2a-I



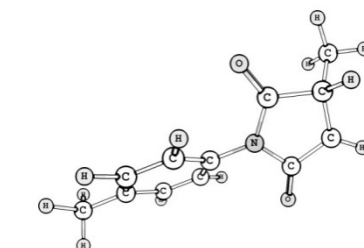
Rad_3b



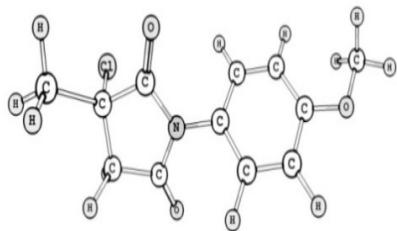
1a-I



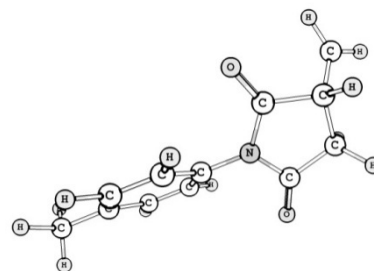
Rad_2b



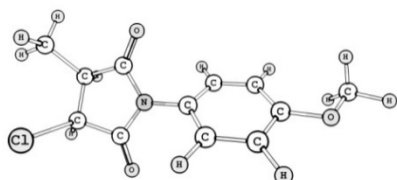
3c-Cl



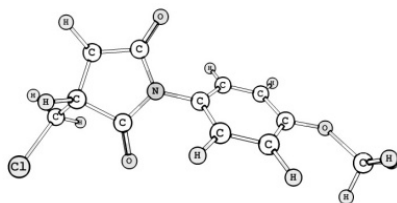
Rad_1b



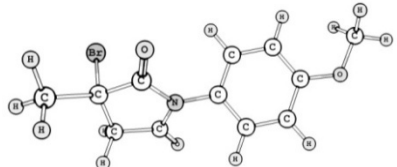
2c-Cl



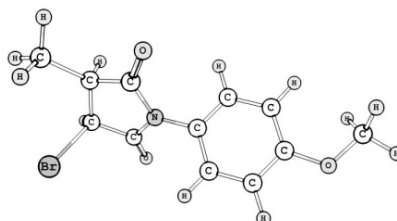
1c-Cl



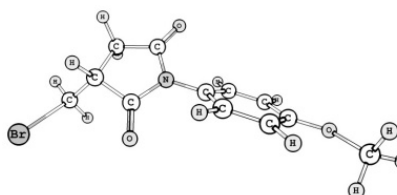
3c-Br



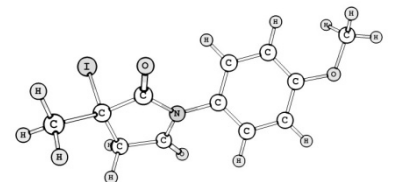
2c-Br



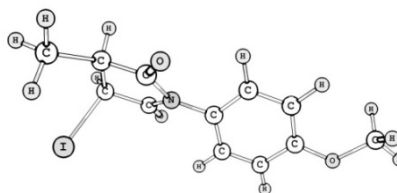
1c-Br



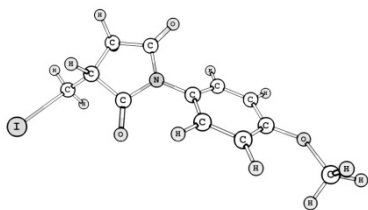
3c-I



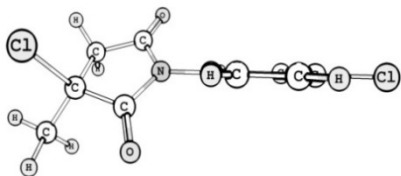
2c-I



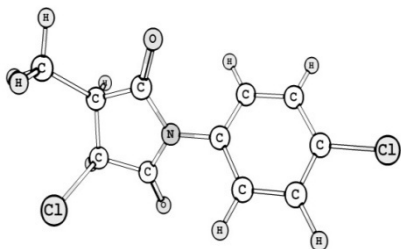
1c-I



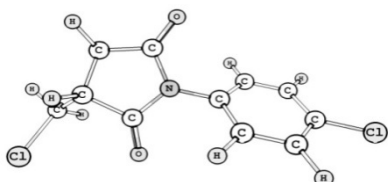
3d-Cl



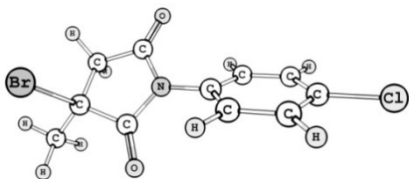
2d-Cl



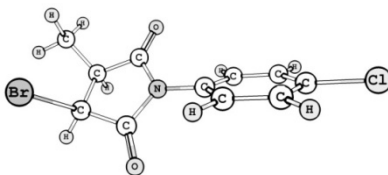
1d-Cl



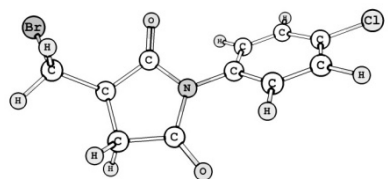
3d-Br



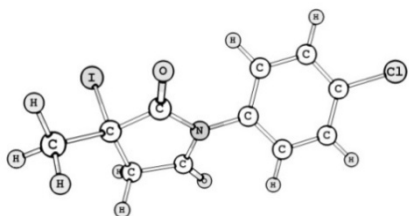
2d-Br



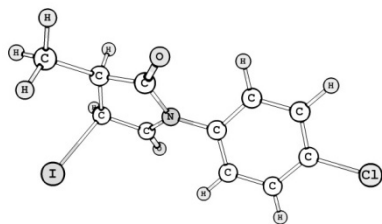
1d-Br



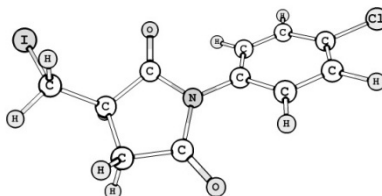
3d-I



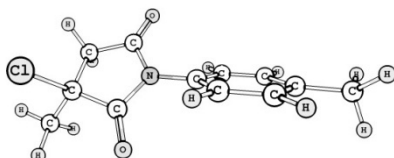
2d-I



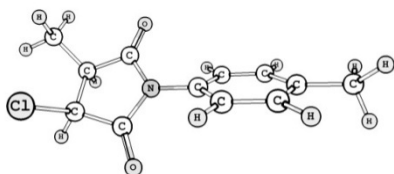
1d-I



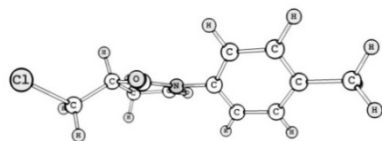
3b-Cl



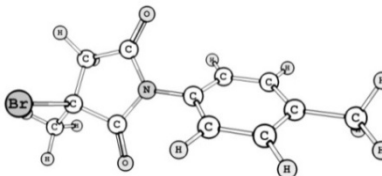
2b-Cl



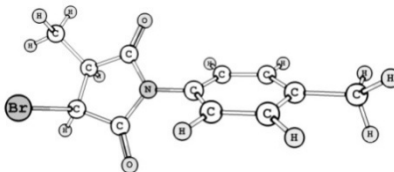
1b-Cl



3b-Br



2b-Br



1b-Br

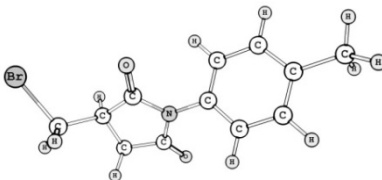
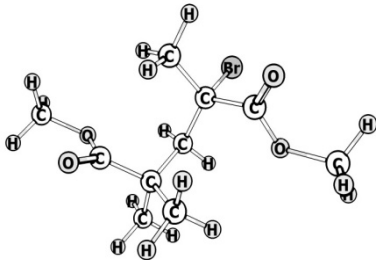
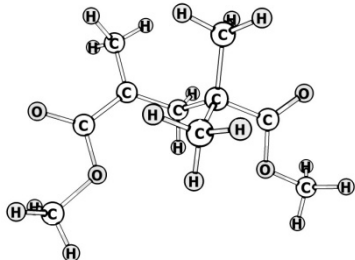
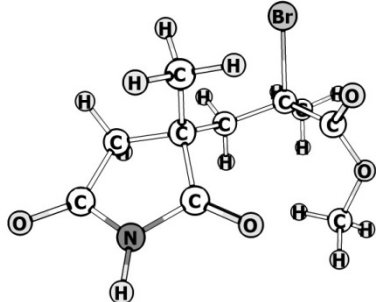
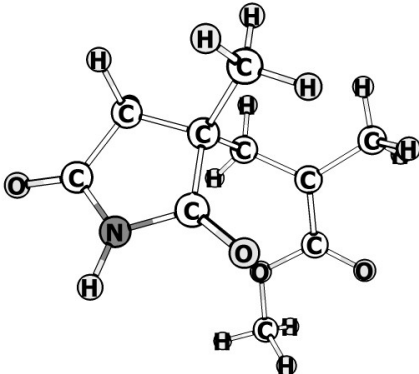


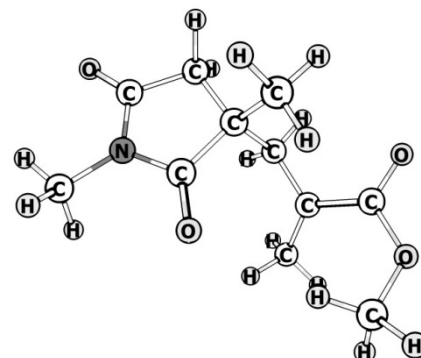
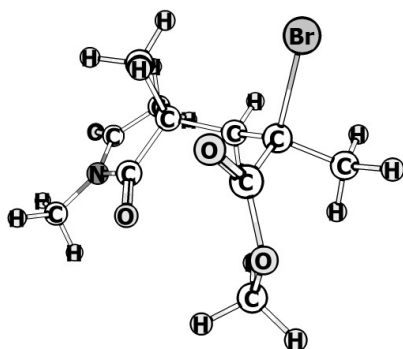
Table A2: Free energy of activation for dimer radicals at various temperature in anisole.

Temp. (°C)	ΔG^\ddagger (kJ mol ⁻¹)						
	H-MMA-MMA [·]	H-MMA-NHI [·]	H-NHI-MMA [·]	H-NHI-NHI [·]	H-MMA-PI [·]	H-PI-MMA [·]	H-PI-PI [·]
25	253.27	245.17	227.29	237.15	241.70	237.46	243.65
75	256.35	247.56	230.75	239.64	245.02	240.25	246.66
125	259.45	249.96	238.24	242.13	248.34	243.06	249.68
175	262.53	252.35	245.72	244.64	251.66	245.86	252.71
225	265.64	254.73	253.23	247.16	254.98	248.68	255.72
275	268.73	257.12	255.73	249.67	258.30	251.49	258.77
325	271.81	259.50	258.23	252.18	261.61	254.30	261.79
375	274.87	261.92	260.72	254.71	264.91	257.08	264.82

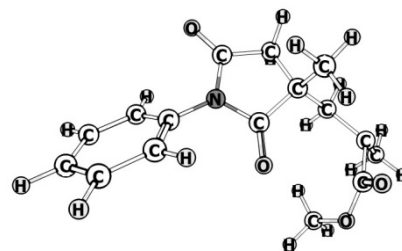
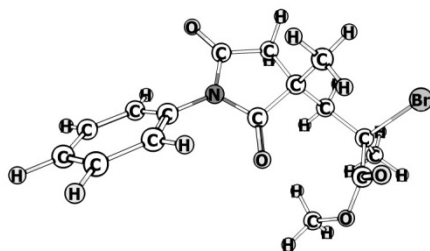
Table A3: View of the lowest energy optimized geometries for all and H-M₂-M₁-Br dimers H-M₂-M₁[·] dimer radical in gas phase at 25 °C.

Dimer designation	H-M ₂ -M ₁ -Br	H-M ₂ -M ₁ [·]
MMA-MMA-Br		
NHI-MMA-Br		

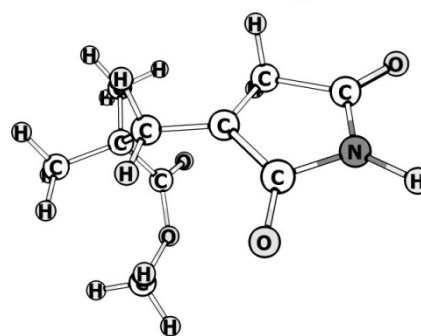
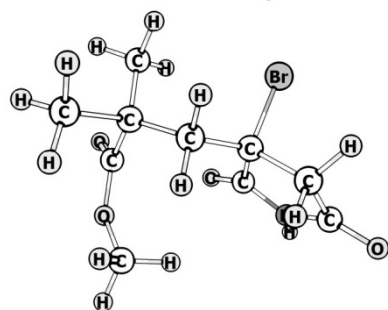
NMI-MMA-Br



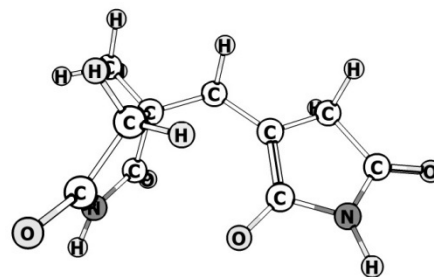
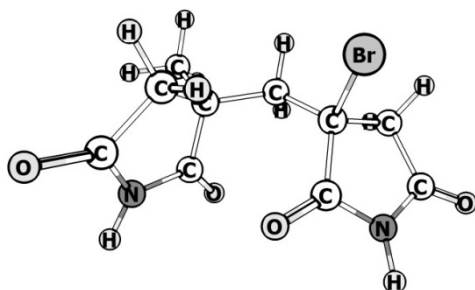
PI-MMA-Br



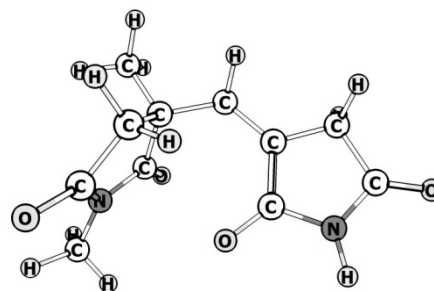
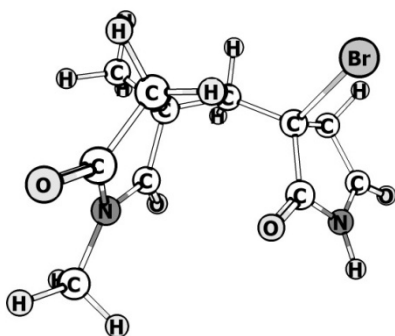
MMA-NHI-Br



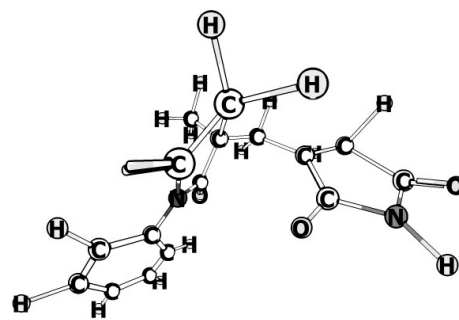
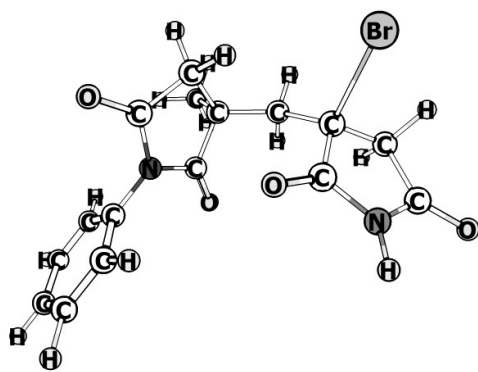
NHI-NHI-Br



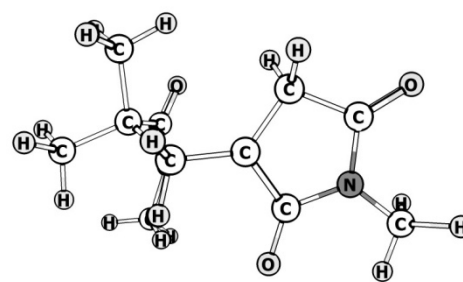
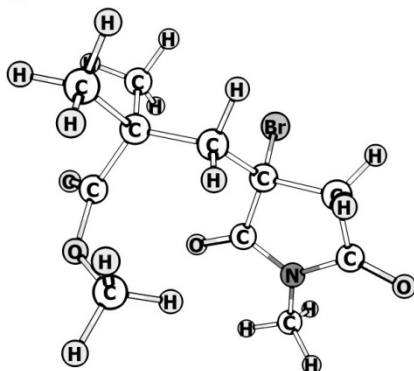
NMI-NHI-Br



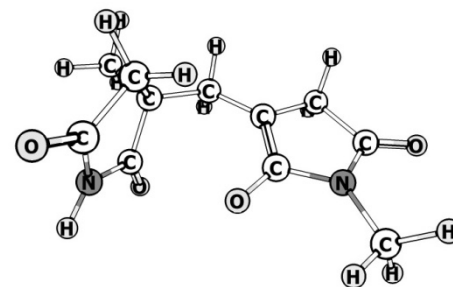
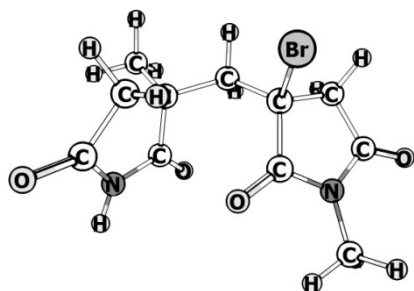
PI-NHI-Br



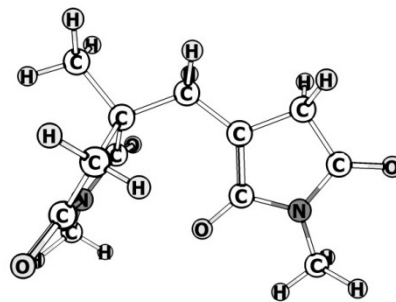
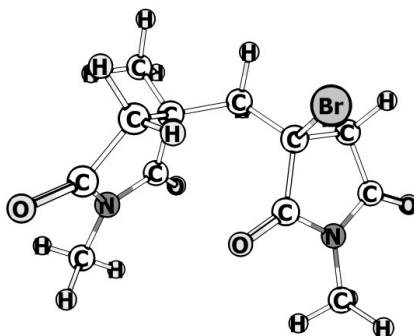
MMA-NMI-Br



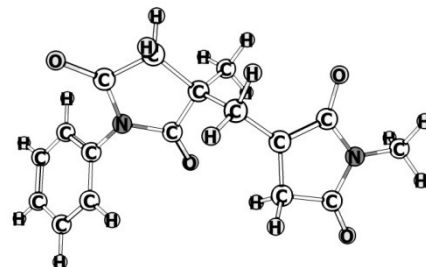
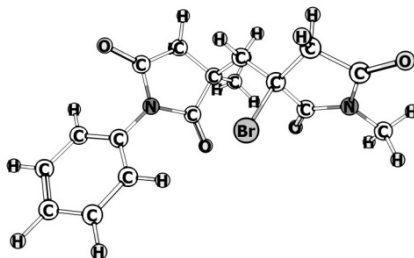
NHI-NMI-Br



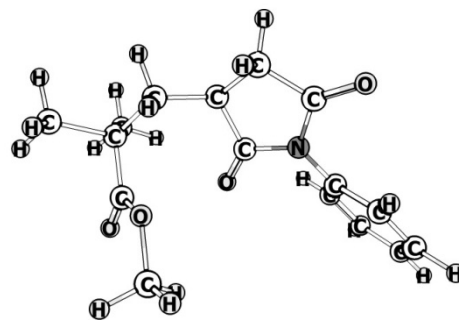
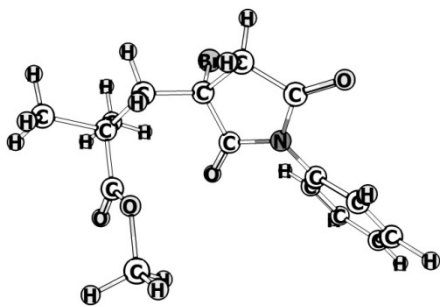
NMI-NMI-Br



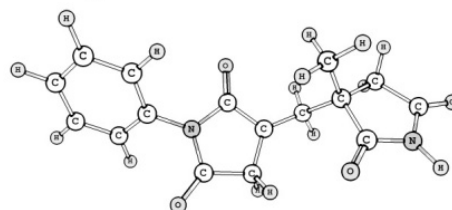
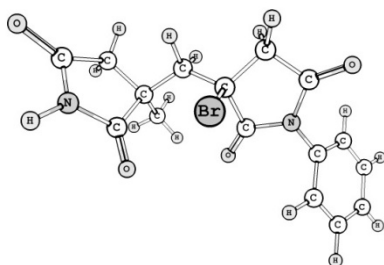
PI-NMI-Br



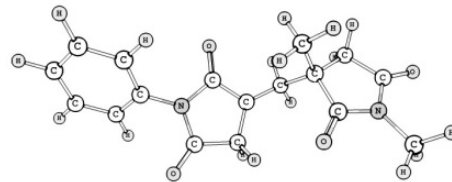
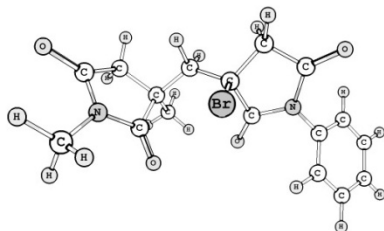
MMA-PI-Br



NHI-PI-Br



NMI-PI-Br



PI-PI-Br

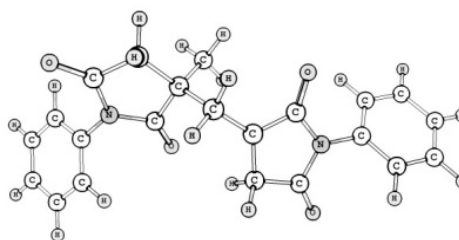
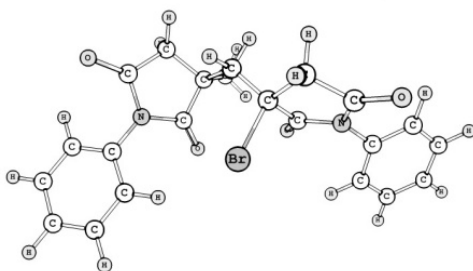
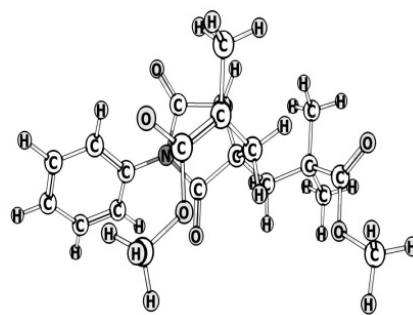
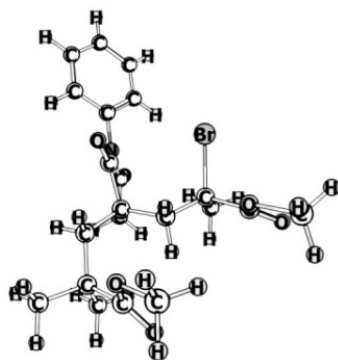


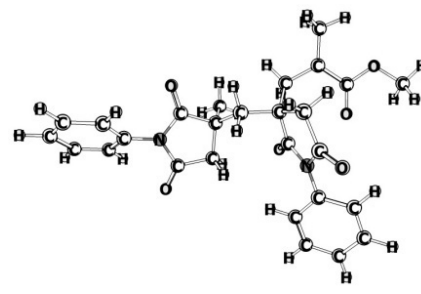
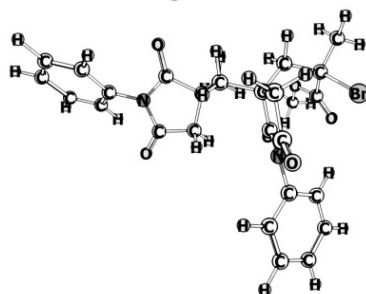
Table A4: View of the lowest energy optimized geometries for all and H-M₃-M₂-M₁-Br trimer H-M₃-M₂-M₁· trimer radical in gas phase at 25 °C.

Trimer designation	H-M ₃ -M ₂ -M ₁ -Br	H-M ₃ -M ₂ -M ₁ ·
MMM-MMA-MMA-Br		
NHI-MMA-MMA-Br		
MMA-NHI-MMA-Br		
NHI-NHI-MMA-Br		
PI-MMA-MMA-Br		

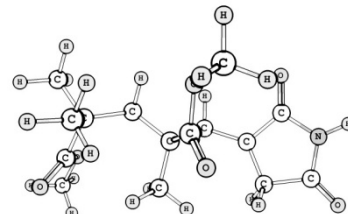
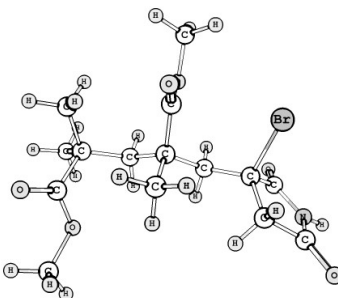
MMA-PI-MMA-Br



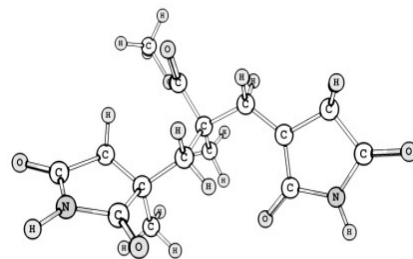
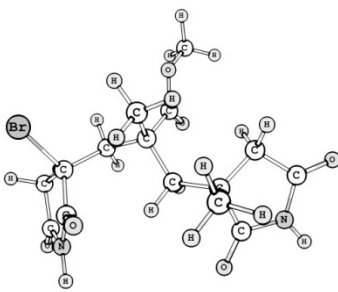
PI-PI-MMA-Br



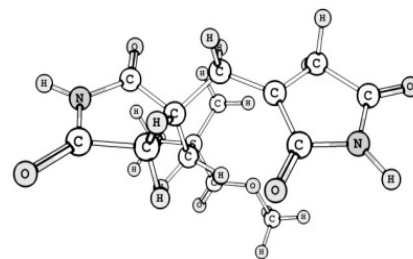
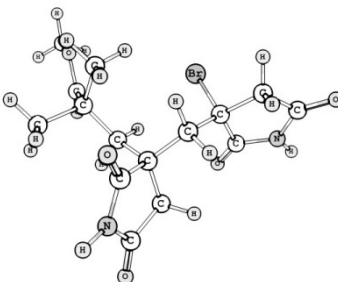
MMA-MMA-NHI-Br



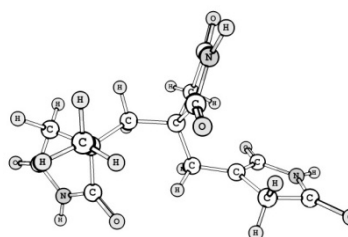
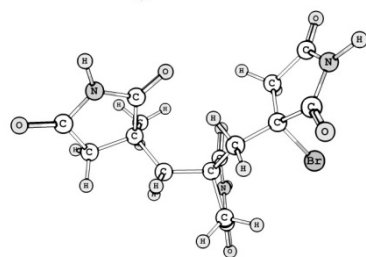
NHI-MMA-NHI-Br



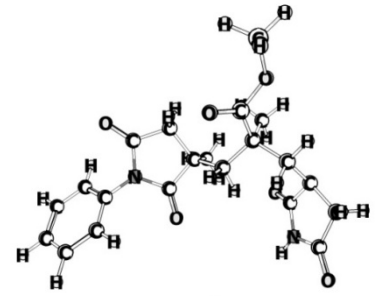
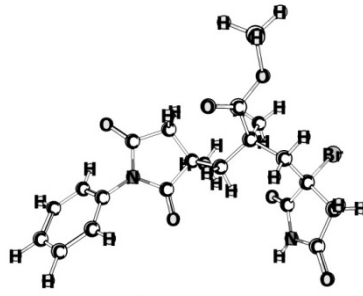
MMA-NHI-NHI-Br



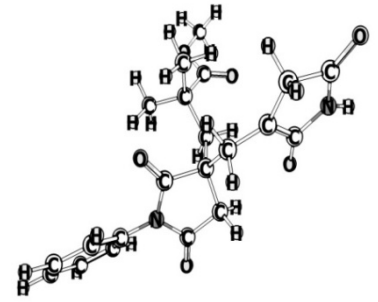
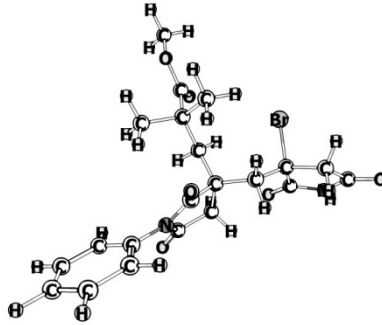
NHI-NHI-NHI-Br



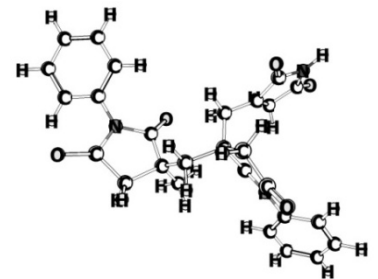
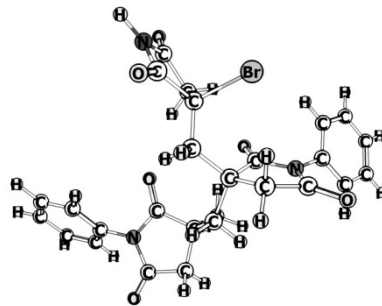
PI-MMA-NHI-Br



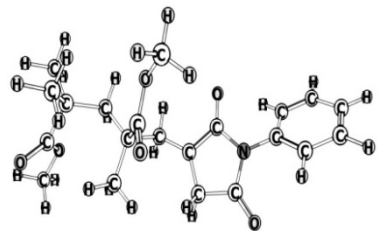
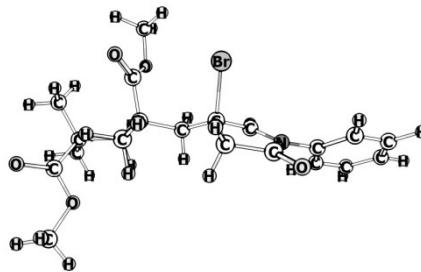
MMA-PI-NHI-Br



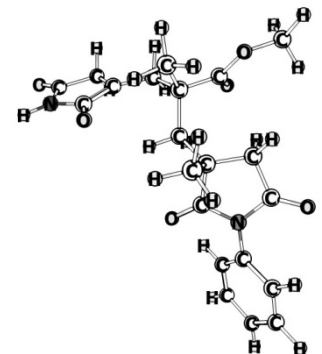
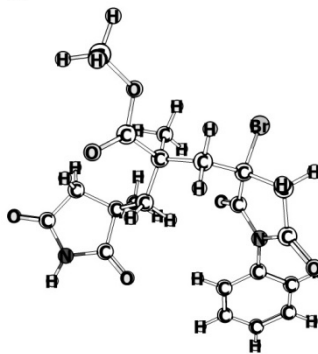
PI-PI-NHI-Br



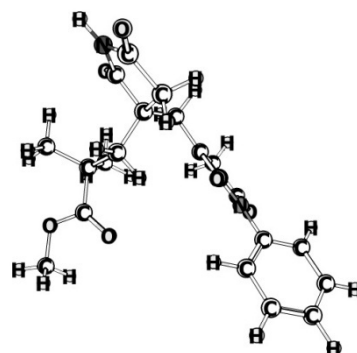
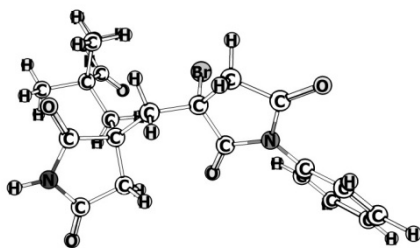
MMA-MMA-PI-Br



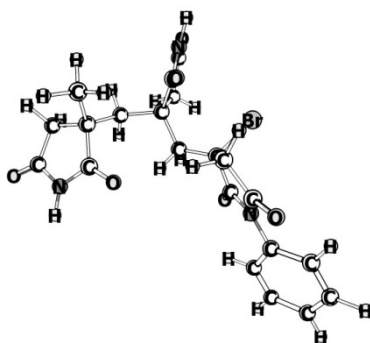
NHI-MMA-PI-Br



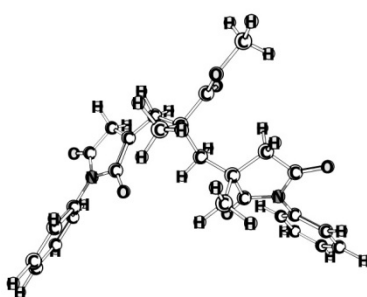
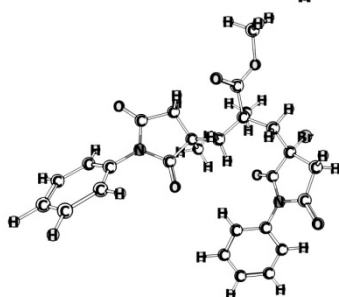
MMA-NHI-PI-Br



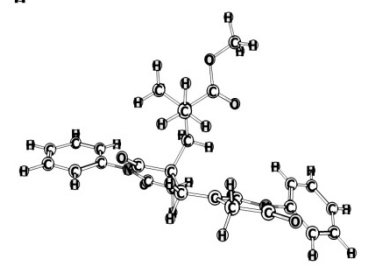
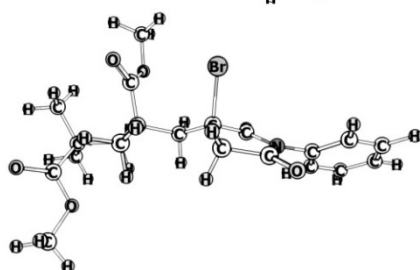
NHI-NHI-PI-Br



PI-MMA-PI-Br



MMA-PI-PI-Br



PI-PI-PI-Br

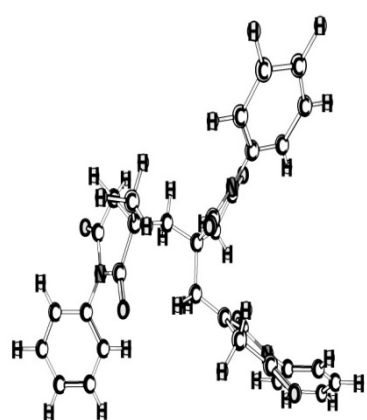
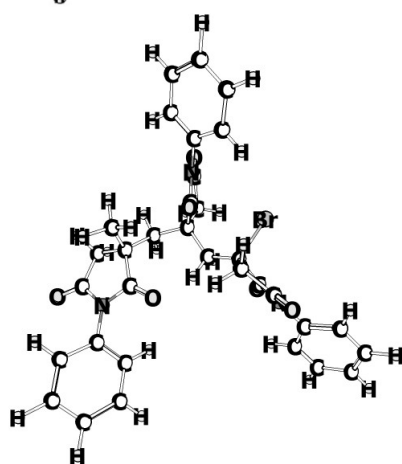


Table A5: Thermodynamic parameters for the homolysis of the M_1 -X bond in H - M_2 - M_1 -X ($M_1, M_2 = \text{MMA, NHI, and PI}$; and H - M_1 -X, ($X = \text{Cl, Br, I}$) in anisole at 25 °C.

R		X	r_{C-X} (Å)	ΔH (kJ mol ⁻¹)	ΔG (kJ mol ⁻¹)	K_{ATRP}	* K/K_0
M_2	M_1						
	MMA	Cl	1.865	255.98	208.81	1.50×10^{-06}	$1.00 \times 10^{+00}$
MMA	MMA	Cl	1.867	232.19	188.09	6.40×10^{-03}	$4.27 \times 10^{+03}$
NHI	MMA	Cl	1.853	172.29	126.11	$4.61 \times 10^{+08}$	$3.07 \times 10^{+09}$
PI	MMA	Cl	1.848	193.83	142.34	6.62×10^{-05}	$4.41 \times 10^{+10}$
	NHI	Cl	1.845	247.48	205.48	5.75×10^{-06}	$1.00 \times 10^{+00}$
MMA	NHI	Cl	1.845	216.96	171.01	$6.27 \times 10^{+00}$	$1.09 \times 10^{+06}$
NHI	NHI	Cl	1.838	239.87	198.59	9.25×10^{-05}	$1.61 \times 10^{+01}$
PI	NHI	Cl	1.822	209.17	164.27	$9.53 \times 10^{+01}$	$1.66 \times 10^{+07}$
	PI	Cl	1.848	247.39	204.27	9.36×10^{-06}	$1.00 \times 10^{+00}$
MMA	PI	Cl	1.854	240.65	190.21	2.72×10^{-03}	$2.91 \times 10^{+02}$
NHI	PI	Cl	1.844	207.33	164.58	$8.40 \times 10^{+01}$	$8.97 \times 10^{+06}$
PI	PI	Cl	1.847	238.36	182.39	6.38×10^{-02}	$6.82 \times 10^{+03}$
	MMA	Br	2.025	246.44	199.29	3.09×10^{-09}	$1.00 \times 10^{+00}$
MMA	MMA	Br	2.032	230.14	184.85	1.33×10^{-06}	$4.30 \times 10^{+02}$
NHI	MMA	Br	2.013	166.22	118.85	4.88×10^{-05}	$1.58 \times 10^{+09}$
PI	MMA	Br	2.015	187.94	138.61	$1.68 \times 10^{+02}$	$5.44 \times 10^{+09}$
	NHI	Br	2.012	237.68	194.46	2.76×10^{-08}	$1.00 \times 10^{+00}$
MMA	NHI	Br	2.010	215.19	168.45	9.98×10^{-04}	$3.62 \times 10^{+04}$
NHI	NHI	Br	2.015	238.71	194.12	3.17×10^{-08}	$1.15 \times 10^{+00}$
PI	NHI	Br	2.009	208.91	161.69	1.52×10^{-02}	$5.52 \times 10^{+05}$
	PI	Br	2.014	243.71	199.94	3.03×10^{-09}	$1.00 \times 10^{+00}$
MMA	PI	Br	2.019	239.26	187.52	4.54×10^{-07}	$1.50 \times 10^{+02}$
NHI	PI	Br	2.009	214.01	167.89	1.25×10^{-03}	$4.12 \times 10^{+05}$
PI	PI	Br	2.012	233.76	180.88	6.61×10^{-06}	$2.18 \times 10^{+03}$
	MMA	I	2.287	112.71	66.64	8.93×10^{-05}	$1.00 \times 10^{+00}$
MMA	MMA	I	2.302	83.75	39.84	$4.43 \times 10^{+00}$	$4.96 \times 10^{+04}$
NHI	MMA	I	2.265	88.95	35.76	$2.29 \times 10^{+01}$	$2.56 \times 10^{+05}$
PI	MMA	I	2.288	56.84	11.95	$3.40 \times 10^{+05}$	$3.81 \times 10^{+09}$
	NHI	I	2.266	106.19	64.54	2.08×10^{-04}	$1.00 \times 10^{+00}$
MMA	NHI	I	2.287	146.74	104.66	1.95×10^{-11}	9.38×10^{-08}
NHI	NHI	I	2.279	78.35	45.29	4.91×10^{-01}	$2.36 \times 10^{+03}$
PI	NHI	I	2.272	53.92	11.86	$3.53 \times 10^{+05}$	$1.70 \times 10^{+09}$
	PI	I	2.273	106.07	64.63	2.01×10^{-04}	$1.00 \times 10^{+00}$
MMA	PI	I	2.289	89.88	43.72	9.25×10^{-01}	$4.60 \times 10^{+03}$
NHI	PI	I	2.275	56.98	13.89	$1.56 \times 10^{+05}$	$7.76 \times 10^{+08}$
PI	PI	I	2.276	55.95	8.29	$1.49 \times 10^{+06}$	$7.41 \times 10^{+09}$

*here, $K = K_{ATRP}$ of dimers (H - M_2 - M_1 -X) and $K_0 = K_{ATRP}$ of unimers (H - M_1 -X.)

Table A6: Thermodynamic parameters for the homolysis of the M_1 -X bond in H - M_2 - M_1 -X ($M_1, M_2 = \text{MMA, NHI, and PI}$; and H - M_1 -X, ($X = \text{Cl, Br, I}$) in gas phase at 80 °C.

R		X	r_{c-x} (Å)	ΔH (kJ mol ⁻¹)	ΔG (kJ mol ⁻¹)	K_{ATRP}	$*K/K_0$
M_2	M_1						
	MMA	Cl	1.854	257.07	200.26	$1.56 \times 10^{+01}$	$1.00 \times 10^{+00}$
MMA	MMA	Cl	1.860	234.25	182.17	$1.01 \times 10^{+04}$	$6.47 \times 10^{+02}$
NHI	MMA	Cl	1.848	167.21	112.29	$2.19 \times 10^{+14}$	$1.40 \times 10^{+10}$
PI	MMA	Cl	1.844	185.84	126.59	$3.06 \times 10^{+12}$	$1.96 \times 10^{+09}$
	NHI	Cl	1.841	251.03	200.57	$1.92 \times 10^{+01}$	$1.00 \times 10^{+00}$
MMA	NHI	Cl	1.842	213.36	160.88	$1.42 \times 10^{+07}$	$7.40 \times 10^{+05}$
NHI	NHI	Cl	1.835	246.15	192.93	$2.58 \times 10^{+02}$	$1.34 \times 10^{+01}$
PI	NHI	Cl	1.816	206.91	153.53	$1.74 \times 10^{+08}$	$9.07 \times 10^{+06}$
MMA	PI	Cl	1.850	237.61	179.62	$5.65 \times 10^{+04}$	$3.28 \times 10^{+03}$
NHI	PI	Cl	1.839	206.06	153.76	$1.61 \times 10^{+08}$	$9.34 \times 10^{+06}$
PI	PI	Cl	1.842	234.69	180.73	$3.89 \times 10^{+04}$	$2.26 \times 10^{+03}$
	MMA	Br	2.016	252.75	193.56	2.29×10^{-02}	$1.00 \times 10^{+00}$
MMA	MMA	Br	2.026	232.30	178.01	$2.86 \times 10^{+00}$	$1.25 \times 10^{+02}$
NHI	MMA	Br	2.009	162.20	107.23	$8.39 \times 10^{+10}$	$3.66 \times 10^{+10}$
PI	MMA	Br	2.010	181.86	129.87	$6.99 \times 10^{+07}$	$3.05 \times 10^{+09}$
	NHI	Br	2.007	241.67	190.30	4.34×10^{-02}	$1.00 \times 10^{+00}$
MMA	NHI	Br	2.007	211.97	159.03	$1.83 \times 10^{+03}$	$4.22 \times 10^{+04}$
NHI	NHI	Br	2.011	245.69	191.88	2.53×10^{-02}	5.83×10^{-01}
PI	NHI	Br	2.005	208.12	152.60	$3.38 \times 10^{+04}$	$7.78 \times 10^{+05}$
	PI	Br	2.014	248.03	197.22	4.11×10^{-03}	$1.00 \times 10^{+00}$
MMA	PI	Br	2.016	235.05	176.79	$1.96 \times 10^{+01}$	$4.77 \times 10^{+03}$
NHI	PI	Br	2.004	213.88	160.30	$1.19 \times 10^{+03}$	$2.89 \times 10^{+05}$
PI	PI	Br	2.008	231.63	176.36	$1.16 \times 10^{+01}$	$2.82 \times 10^{+03}$
	MMA	I	2.278	115.24	60.32	1.05×10^{-01}	$1.00 \times 10^{+00}$
MMA	MMA	I	2.297	85.68	30.95	$2.77 \times 10^{+03}$	$2.64 \times 10^{+04}$
NHI	MMA	I	2.256	82.96	24.58	$2.42 \times 10^{+04}$	$2.30 \times 10^{+05}$
PI	MMA	I	2.281	48.52	2.45	$4.55 \times 10^{+07}$	$4.33 \times 10^{+08}$
	NHI	I	2.258	110.90	61.77	7.65×10^{-02}	$1.00 \times 10^{+00}$
MMA	NHI	I	2.276	143.72	90.68	4.06×10^{-06}	5.31×10^{-05}
NHI	NHI	I	2.271	88.70	39.26	$1.39 \times 10^{+03}$	$1.82 \times 10^{+04}$
PI	NHI	I	2.261	53.80	7.39	$8.46 \times 10^{+08}$	$1.11 \times 10^{+10}$
PI	NMI	I	2.263	56.21	8.63	$5.54 \times 10^{+08}$	$1.36 \times 10^{+10}$
	PI	I	2.262	110.67	61.15	9.46×10^{-02}	$1.00 \times 10^{+00}$
MMA	PI	I	2.276	82.97	30.97	$2.75 \times 10^{+03}$	$2.91 \times 10^{+04}$
NHI	PI	I	2.264	54.80	5.98	$1.37 \times 10^{+09}$	$1.45 \times 10^{+10}$
PI	PI	I	2.263	53.82	4.69	$2.46 \times 10^{+09}$	$2.60 \times 10^{+10}$

*here, $K = K_{\text{ATRP}}$ of dimers (H - M_2 - M_1 -X) and $K_0 = K_{\text{ATRP}}$ of unimers (H - M_1 -X.)